Experimental and Analytical Procedures to Characterize Mechanical Properties of Asphalt Concrete Materials for Airfield Pavement Applications

By

Mohammad Bazzaz
M.Sc., Semnan University, 2010
B.Sc., Semnan University, 2006

Submitted to the graduate degree program in Civil, Environmental and Architectural Engineering and the Graduate Faculty of the University of Kansas in partial fulfillment of the requirements for the degree of Doctor of Philosophy.

_____

Chair: Assistant Professor Masoud K. Darabi

_____

Snead Chair Professor and Regents Professor Dallas N. Little

_____

Professor Anil Misra

_____

Glenn L. Parker Professor Jie Han

_____

Associate Professor Shawn Keshmiri

_____

Dr. John F. Rushing

Date Defended: 30th August 2018

The dissertation committee for Mohammad Bazzaz certifies that this is the approved version of the following dissertation:

Experimental and Analytical Procedures to Characterize Mechanical Properties of Asphalt Concrete Materials for Airfield Pavement Applications

Chair: Assistant Professor Masoud K. Darabi

Associate Professor Shawn Keshmiri

Date Approved: 4th September 2018

Abstract

In the past two decades, the pavement mechanics community have made a significant progress in developing mechanistic-based constitutive relationships for asphalt concrete materials, flexible airfield pavements, and roadways. However, a number of factors have caused the community not to properly adopt and implement these sophisticated constitutive relationships in design and refined analysis of asphalt concrete pavements. The lack of straightforward experimental and/or analytical procedures to extract the material properties associated with these models is the main reason for the community to avoid adopting these sophisticated mechanistic-based models. Available characterization methods either are over-simplified or require extensive laboratory tests and analyses procedures to extract the material properties associated with asphalt concrete materials. Furthermore, the immergence of next generation heavy aircraft and heavy trucks require such characterization methods to design the experiments and analysis procedures to account for high tire contact stresses. This dissertation aims to develop straightforward experimental and analytical procedures to characterize coupled viscoelastic, viscoplastic, and hardening-relaxation viscoplastic properties of asphalt concrete pavements while maintaining the required level of accuracy by incorporating the important factors affecting these mechanisms. Therefore, this dissertation proposes laboratory tests and analysis procedures to systematically calibrate and validate a comprehensive constitutive material model for asphalt concrete materials. The proposed method accounts for multi-axial state of stresses; deviatoric, confinement, and shear stress levels; and time-, temperature-, and rate-dependent response of asphalt concrete when subjected to high tire pressures. Separate laboratory tests were required to measure and calibrate the individual response of asphalt concrete materials at appropriate temperatures and loading rates. The proposed characterization methods are then applied to four different asphalt mixtures used in

Federal Aviation Administration (FAA)'s National Airport Pavement and Materials Research Center (NAPMRC) test sections to evaluate the efficacy of the methods. This dissertation presents a straightforward procedure that allows for identification of nonlinear viscoelastic response of asphalt concrete. This procedure incorporates the effect of confinement and deviatoric stress levels into the analysis procedure along with a laboratory test that can be used systematically to extract nonlinear viscoelastic parameters. Furthermore, a straightforward procedure that allows for identification of viscoplastic and hardening-relaxation viscoplastic response of asphalt concrete materials were proposed. This procedure incorporates the genetic algorithms into the analysis procedure to extract viscoplastic and hardening-relaxation viscoplastic properties of asphalt concrete materials as one of many engineering optimization problems along with a laboratory test that can be used systematically to extract viscoplastic and hardening-relaxation viscoplastic response of asphalt concrete materials. The presented tests are mimicking the realistic general multi-axial state of stresses observed in a pavement structure. Moreover, rheological properties and stress-dependent behavior of modified/unmodified asphalt binders plus Evotherm–M1 additive were evaluated using multiple stress creep-recovery tests and strain controlled frequency sweep tests in different ranges of interest frequencies, temperatures and strains. The test data is analyzed to improve the Pavement Analysis using Non-linear Damage Approach – Airfield Pavements (PANDA-AP) calibration protocol and extract the material properties of asphalt concrete pavements.

Acknowledgments

I am incredibly grateful to many people who helped me to complete this strenuous journey. There are far too many, to mention all of them; but I would like to thank several here.

First and foremost, I would like to acknowledge my committee chair, Assistant Professor Masoud K. Darabi, whose guidance and support has been beyond invaluable. Without him, this work would never been accomplished. It has been an extreme pleasure learning from and working with him. He has guided my development in this research where clear paths to solutions do not exist.

I would like to express my gratitude towards my advisory committee member, Snead Chair Professor and Regents Professor Dallas N. Little, who provided me with his deep understanding on the subject. The innumerable fruitful discussions that I had with him helped set me straight whenever I got lost in the subtle twists of this difficult field. I would also like to thank Associate Professor Shawn Keshmiri, Professor Anil Misra, Glenn L. Parker Professor Jie Han, and Dr. John F. Rushing, my other advisory committee members, for their patience in reading this dissertation and their many pertinent comments.

Thanks also go to my fellow colleagues, who helped me in this research. I truly value Ms. Rashmi Kola and Mr. Atish Nadkarni's help in this research. Drs. Omid Omidi and Mohammad Karimi were supportive and very insightful. I also thank Drs. Ali Rahmati and Fazel Hadadi Far for the fruitful discussions we had during the early stages of this work.

I would like to offer special thanks to Dr. Lorena Garcia Cucalon for providing endless support on both conducting the experimental test, through a laboratory visit of Texas A&M University and Texas A&M Transportation Institute, on asphalt concretes and my understanding of the mechanical response of asphalt binders.

Finally yet importantly, I gratefully acknowledge the Federal Aviation Administration (FAA) and Kansas Department of Transportation (KDOT) for funding my research and the Civil & Environmental and Architectural Engineering (CEAE) Department of the University of Kansas (KU) for providing the require resources for my research. My sincere thanks go to Dr. Navneet Garg, FAA's Program Manager for National Airport Pavement & Materials Research Center (NAPMRC) Airport Technology R&D Branch, and Mr. Blair Heptig, Field Engineer for Kansas Department of Transportation (KDOT).

Dedication

TO MY BELOVED PARENTS, ***SIMIN & NEMAT***
Thank you for your endless patience, unconditional support, and continuous encouragement.

I cannot find enough words to express my deep and sincere gratitude to my mom. She is the one who stand by me, inspire me and help me get over all the obstacles I faced in my life. Her guiding tips were endless; she has made me who I am. I can never do anything to return her countless favors. Based on her contributions, I think "Maman Simin" deserves to be an honorary author of this dissertation.

Who can forget my dad, "Baba Nemat"? He has been the role model in my life. He is the one who planted strong perseverance in my soul, and showed me endless trust and support. He has been very generous; his lips never knew the word "no". I am grateful to have him as a father.

TO MY LOVELY BETTER HALF, ***ZAHRA***
For her endless support, encouragement, patience, and most important LOVE!

The question that poses now: what is the wife's contribution? Put simply, without Zahra there would have not been any dissertation! Zahra is graceful, patience, supportive, inspiring, and helpful. I struggled but she was with me all the way; she was the one that held my hand when I fell down and showed me the light when I was lost in the dark. Zahra's love gave me the support needed in this journey.

Table of Contents

List of Figures

List of Tables

1. Chapter 1: Statement of Research Need

1.1. Introduction

One of the largest infrastructure assets in the United States is asphalt concrete pavements (*1*). Trade industries, State Departments of Transportation, and other government organizations introduce various methods to design and analyze asphalt concrete pavements. For example, the American Concrete Pavement Association (ACPA) StreetPave, the Asphalt Institute SW-1 Asphalt Thickness Design, Washington DOT and Minnesota DOT pavement design manuals (*2*), the American Association of State Highway Transportation Officials (AASHTO) empirical 1993 (*3*) Guide and the FAA's LEDFAA methodology (*4; 5*) and Federal Aviation Administration Rigid and Flexible Iterative Elastic Layer Design (FAARFIELD) software (*6*). Yet, empirical relations still play a substantial role in design guides and manuals for asphalt concrete pavements design (*7-34*). The complex behavior of asphalt mixtures and environmental conditions during their service life, however, limit the range of application and validity of such simplified methods and empirical relationships make extremely difficult task for pavement engineers to implement sophisticated mechanistic modeling and predict the performance of asphalt concrete.

The mechanical response of asphalt concrete has been identified through different types of tests and models (*35-50*). However, most of these models are developed to predict the responses under specific test conditions or to solve a specific design problem. In addition, asphalt concrete pavements show highly nonlinear responses under different conditions. Therefore, the realistic behavior of asphalt concrete pavements under general three dimensional stress states and realistic environmental conditions, which actually happens in the field, is yet to be modeled and simulated properly.

The response of hot mix asphalt (HMA) is time-, rate-, and temperature-dependent according to experimental studies due to differences between the stiffness of the aggregate and the binder, which causes the strain localization in the binder (*47; 51-53*). Also, other factors contributing to the nonlinear behavior of asphalt concrete pavements such as rotation and slippage of aggregates and interaction between binder and aggregates during the loading (*54-59*). Severe temperature sensitivity of asphalt concrete pavements lead to substantial changes of the behavior with the temperature change (*60-64*). The combined effects of these phenomena cause the asphalt concrete pavements to show nonlinear responses even at very small strain or stress levels, which will result in evolution of the permanent deformation under the wheel path; rutting. Fatigue, evolution of micro-cracks and micro-voids, and rate-dependent viscoplastic hardening-relaxation are other major sources of nonlinearity in the thermo-mechanical response of HMA.

1.2. Background

The main objective of designing new or managing existing asphalt concrete pavement is to characterize the performance or deterioration of asphalt concrete pavements in the future and either change the design before being built or allocate the appropriate maintenance and rehabilitation funds. Obviously, performance prediction quality will impact on the quality of the corresponding service life that consider optimal timing of asphalt concrete pavement maintenance and rehabilitation activities (*65; 66*). This is a substantial concern for transportation industries and agencies. Different mechanical, thermal, and environmental effects in the asphalt concrete pavements during their life makes it necessary to develop a robust constitutive model to predict the response of asphalt mixes in the pavements. Recently, Pavement Analysis using Nonlinear Damage Approach (PANDA) was presented as a tool to predict performance of asphalt concrete

pavements (*67-77*). The constitutive model includes constitutive relationships that capture responses of asphalt concrete pavements subjected to general mechanical and environmental loading conditions. The mechanical part includes Schapery's nonlinear thermo-viscoelasticity model (*78*), Perzyna's thermo-viscoplasticity model (*79*), hardening-relaxation viscoplasticity model proposed by Darabi et al. (*71*), and thermo-viscodamage model proposed by Darabi et al. (*74*). Schapery's nonlinear viscoelastic model (*78*) was used to capture nonlinearity and temperature effects on the recoverable component of strain (*48; 80-82*). The Perzyna's theory (*79*) with extended modified Drucker-Prager yield surface (*83*) was applied to represent non-recoverable component of the strain viscoplastic response (*84*). The model contains parameters to account for the mixture frictional characteristics, hardening, and dilation (*48; 85-87*). Moreover, the constitutive model has been validated against extensive experimental measurements to ensure proper model response under complex three-dimensional stress states.

The aim of developing such a robust constitutive model is to provide a reliable tool for pavement engineers to predict the pavement performance. Yet, pavement community is reluctant to fully implement this constitutive model due to its complicity, such as large number of loading cycles (millions of loading cycles), the complex constitutive model, the complex nature of the applied loading conditions, and strain and damage localization phenomena. This raises another challenging task: how to make this tool more practical for pavement engineers? This dissertation contributes in addressing this question through presenting a clear experimental method and characterization technique to extract the material properties. The proper identification of the material properties is one of the main steps to more accurately predict the response of asphalt concrete pavements using mechanistic-based models; in this case PANDA. As mentioned in the

literature, traditional experimental methods may only partially represent the of asphalt concrete pavements (*88*). Examples of such tests are:

- Static creep test, which is application of a static load to the sample and measurement of the viscoelastic and viscoplastic deformation after removing the load, do not correlate appropriately with actual pavement rutting measurements (*89*).
- Repeated load test at a constant frequency for many repetitions and measurement of the viscoelastic and viscoplastic deformation, correlates with pavement rutting measurements better than static creep test results (*89*). As shown in the analysis of this test, asphalt concrete pavements experience primary, secondary, and tertiary deformation stages in compression, including recoverable (i.e., viscoelastic) and irrecoverable (i.e., viscoplastic) deformation with higher rate of accumulation of viscoplastic strain at early cycles compare to the preceding cycles.
- Dynamic modulus tests captures the small portion of permanent deformation, which is associated with viscous deformation, but it does not account for viscoplastic deformation.
- Hamburg wheel tracking test can correlate appropriately with pavement rutting measurements, however, this test will not provide any significant material properties.

Despite the fact that PANDA is the most sophisticated tool to analyze performance of flexible pavements using mechanistic approaches instead of the empirical methods, PANDA calibration protocol is complicated in both experimental protocol and analytical methods. This

dissertation aims to simplify the experimental procedures as well as analytical methods to make PANDA more practical for pavement community.

1.3. Literature Review

Complex states of stress, strain, and environmental conditions will result in different mechanical properties of asphalt concrete materials (*90*). The equilibrium, kinematic, compatibility, and constitutive equations are required to characterize asphalt concrete materials. These equations will describe the relationships among the various stress components; evaluate the strain components in terms of displacements; express the relationship among the several strain components; present the relationship between stress, strain, and time in terms of the material constants (*91; 92*).

1.3.1. *Asphalt Concrete Materials Properties*

1.3.1.1. Elastic Properties

Under small stresses most of materials behave approximately elastic and asphalt concrete materials are not exception. Considering a simple creep-recovery loading scenario, an immediate elastic strain response remains constant while the stress is fixed and the strain response will disappear as soon as the load is removed (*90; 93*) as shown in Figure 1-1. This emphasize on the main characteristic of elastic behavior, which is reversibility based on proportional relationship of stress and strain.

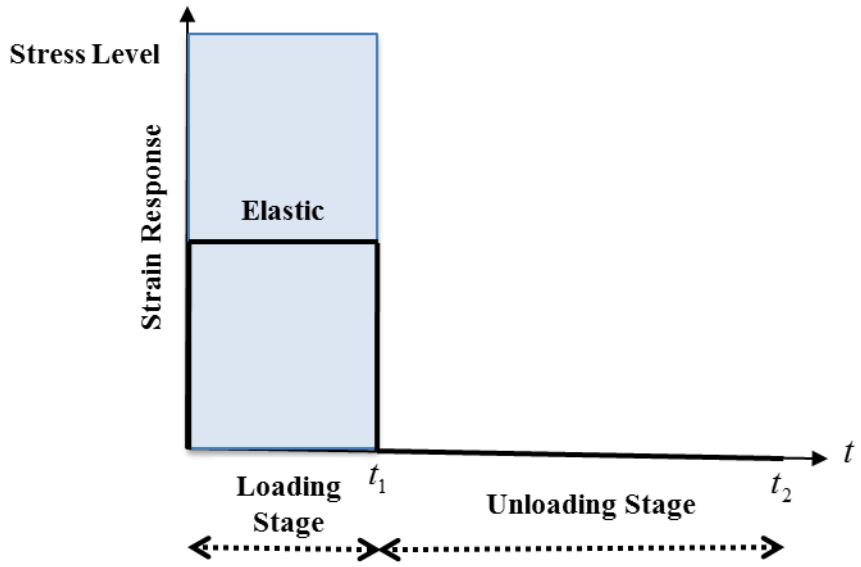

Figure 1-1: Elastic strain responses to a creep-recovery load.

1.3.1.2. Plastic Properties

To explain the plastic properties of materials, there are some concepts that need to be clarify. The first concept is elastic limit, which is the limit for stress. As soon as stress exceed the elastic limit, material are no longer elastic and strain does not disappear after removal of the stress, which is called inelastic strain (*90; 91*). For plastic materials, strain will increase for a short period of time, then it remains constant as long as the load is constant. This will result in a permanent deformation as shown in Figure 1-2. Plastic strain is time independent after unloading.

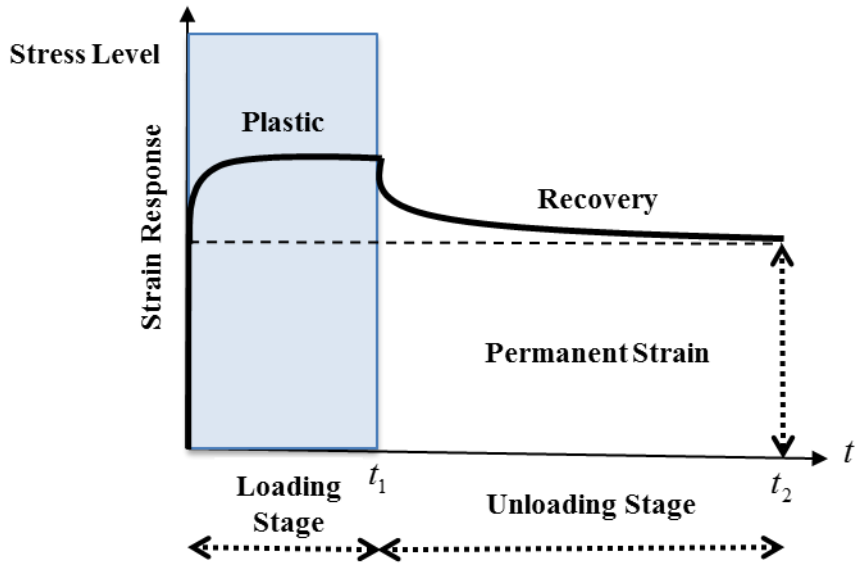

Figure 1-2: Plastic strain responses to a creep-recovery load.

1.3.1.3. Viscoelastic Properties

Viscoelastic materials are shown instantaneous elastic response under rapid enough loads, then a continuous increase of strain at a decreasing rate is expected (*91-93*). During the unloading period, instantaneous elastic recovery is expected as part of continuously decreasing strain. Viscoelastic materials are function of rate of stressing such that the higher the stress rate, the larger corresponding strain is, as shown in Figure 1-3.

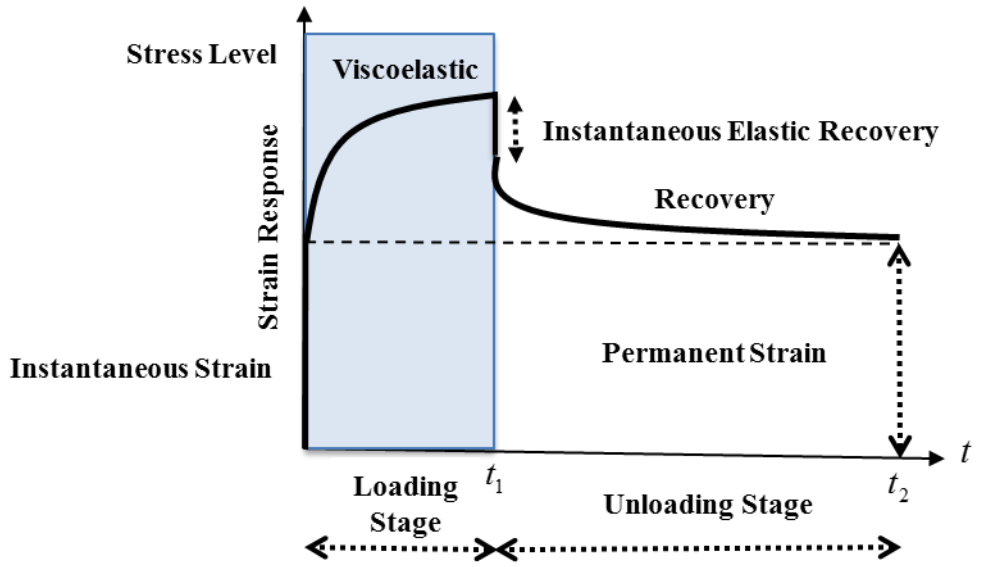

Figure 1-3: Viscoelastic strain responses to a creep-recovery load.

The asphalt mixtures are shown viscoelastic properties, which will change over the time. Therefore, asphalt mixtures are time-dependent materials that show both elasticity and viscosity. This requires a constitutive equation to account for both time and stress or strain variable. As shown in Figure 1-3, the strain response is complicated even under simple creep-recovery load. Time is not constant and could not be reversed or eliminated during an experiment. Thus, the experimental investigation of the mechanical properties of asphalt mixture is more sensitive compare to the independent materials. Quasi-static state tests such as creep-recovery, stress-relaxation, and constant rate stress/strain are used to extract the time-dependent behavior of asphalt mixture (*91*).

1.3.1.4. Creep Response

A slow continuous deformation of material under constant stress is creep (*90; 91*). Both viscoelastic and viscoplastic response may consider as creep response, which consist of three stages as presented in Figure 1-4.

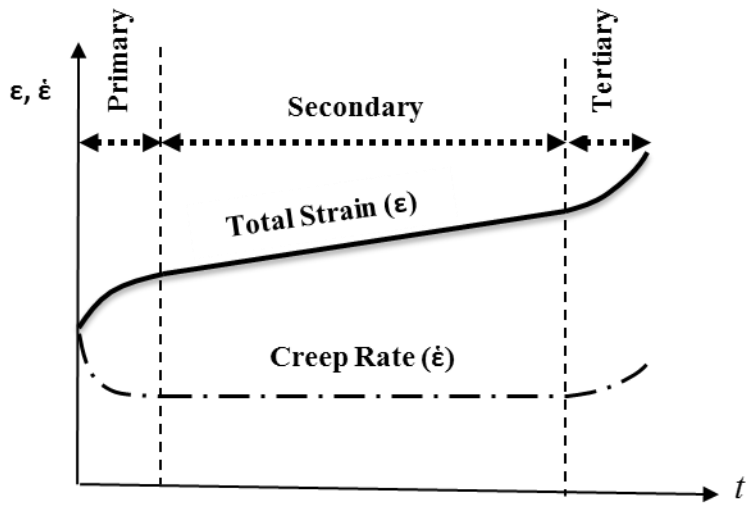

Figure 1-4: Different creep stages.

Primary creep is the first stage of creep at a decreasing rate. Then, the secondary stage at an approximately constant rate will continue. The last stage is tertiary stage at an increasing rate until fracture. Total strain (i.e., ε) could be decompose to the instantaneous elastic strain (i.e., ε^e) and the creep strain (i.e., ε^c) as shown in Equation 1-1.

Equation 1-1 $$\varepsilon = \varepsilon^e + \varepsilon^c$$

Differentiating the Equation 1-1 **Error! Reference source not found.**will result in strain rate as shown in Equation 1-2. Considering constant instantaneous elastic strain, strain rate could be presented such that:

Equation 1-2 $$\frac{d\varepsilon}{dt} = \frac{d(\varepsilon^e + \varepsilon^c)}{dt} = \frac{d\varepsilon^c}{dt} = \dot{\varepsilon}$$

1.3.1.5. Recovery Response

During the unloading time, an instantaneous elastic recovery followed by continuously decreasing rate of strain recovery is observed as recovery response (*92-94*). The time-dependent recoverable strain (i.e., strain recovery or delayed elasticity) will change depend on type of materials. For example, metals express a very small part of the time-dependent creep strain and plastics show a large portion of the time-dependent creep strain as presented in Figure 1-5. Moreover, asphalt mixtures have different portion of the time-dependent creep strain based on ambient temperature.

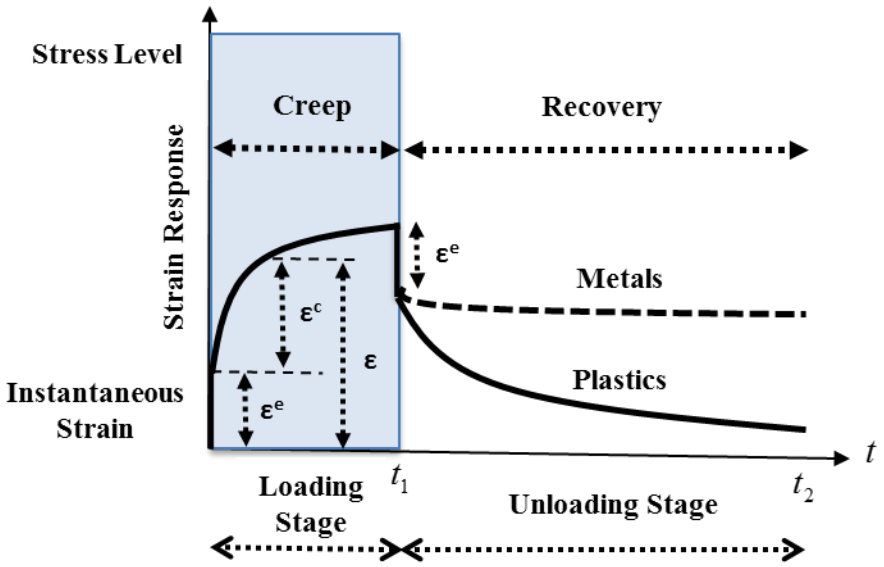

Figure 1-5: Creep and recovery of different materials.

1.3.1.6. Relaxation Response

The viscoelastic materials decrease the stress gradually at constant strain (*95; 96*) as shown in Figure 1-6. Asphalt mixtures have time-dependent responses including creep and recovery under a cyclic or random variation of the strain history.

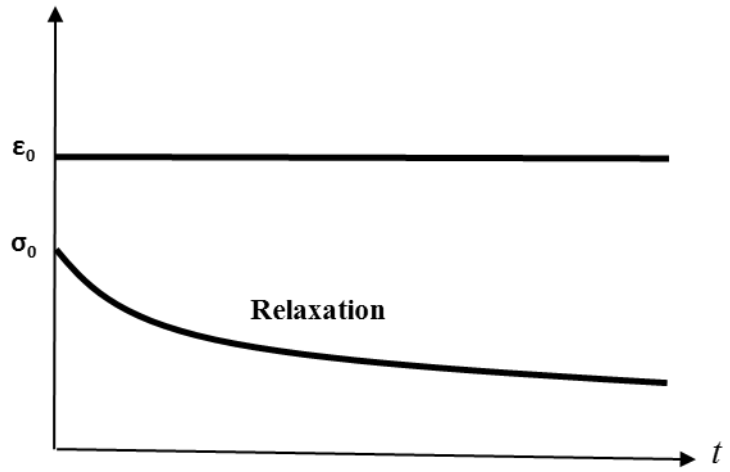

Figure 1-6: Stress relaxation at constant strain.

1.3.1.7. Linearity Response

As long as stress is proportional to strain at a given time materials will be classified as linear viscoelastic materials, where the linear superposition principle holds (*97; 98*). Asphalt mixtures as a part of materials have shown linear response, which allows application of a linear theory with enough level of accuracy under short duration of loading and small deformation. In addition, the strain during creep of asphalt mixtures might be decomposed to a time-dependent linear and a time-dependent nonlinear part under long loading time, where they experience significant level of nonlinearity.

1.3.2. Available Mechanical Models on Viscoelasticity

There are viscoelastic mechanical models to evaluate viscoelastic response of materials, which may consist of different combination of basic rheological elements. As shown in Figure 1-7, the basic rheological elements are the Hookeian element (spring) and the Newtonian element

(dashpot), which are perfectly elastic and viscous, respectively. Spring stores the applied energy as strain energy and dashpot dissipates the applied energy (*99; 100*).

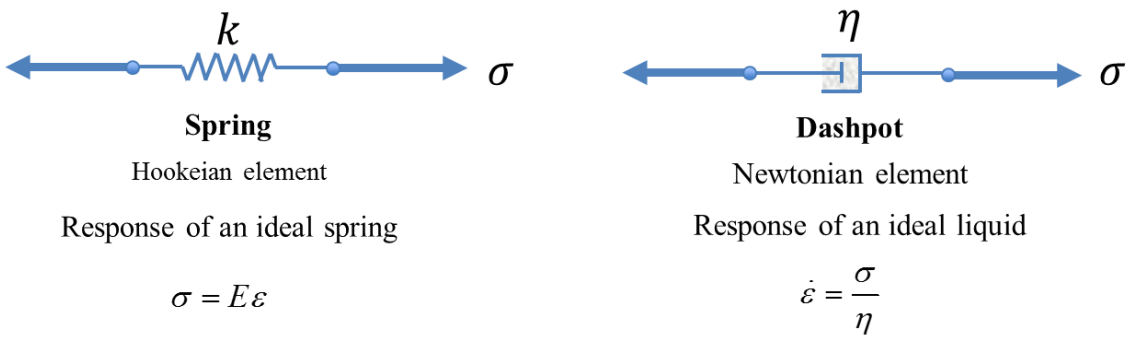

Figure 1-7: The basic rheological elements, Hookean spring (left) and Newtonian dashpot (right).

Different combination of the basic rheological elements may result in complex rheological models to evaluate the viscoelastic response of materials such as Maxwell, Kelvin, and Burger's model.

1.3.2.1. Maxwell Model

Maxwell presented a model including a spring and a dashpot in series. Based on series properties, the stress will remain constant on both elements and equal to the imposed stress but the summation of spring and dashpot's strain will result in total strain of the model (*99*). Considering a single equation for the stress-strain relationship, differentiating the strain equation and then writing the spring-dashpot strain rates in terms of the stress will result in Equation 1-3.

Equation 1-3 $$\dot{\varepsilon} = \dot{\varepsilon}_s + \dot{\varepsilon}_d = \frac{\dot{\sigma}}{k} + \frac{\sigma}{\eta}$$

Two different scenarios are valid through Maxwell model, including constant stress and constant deformation. Considering constant stress, the rate of stress is zero and rate of strain is

$\dot{\varepsilon} = \frac{\sigma}{\eta}$. The response will be an instantaneous elastic strain followed by a linearly increasing irrecoverable strain (i.e., creep response) as shown in Figure 1-8. Considering constant deformation, the rate of strain is zero and the rate of stress is a function of time an exponential stress relaxation as presented in Equation 1-4.

Equation 1-4 $$\frac{\dot{\sigma}}{E} + \frac{\sigma}{\eta} = 0 \Rightarrow \sigma = \sigma_0 e^{-Et/\eta}$$

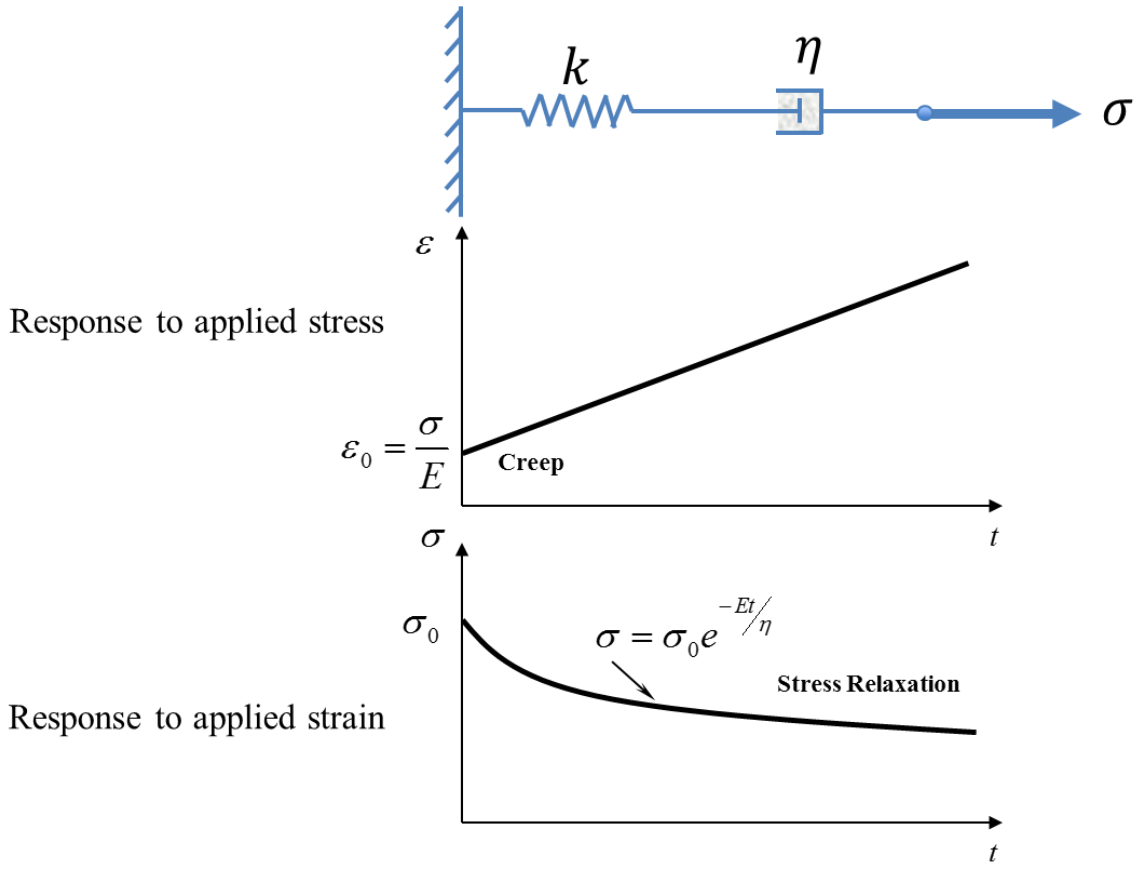

Figure 1-8: The Maxwell rheological model.

1.3.2.2. Kelvin (Voigt) Model

Kelvin presented a model including a spring and a dashpot in parallel. Based on parallel properties, the strain will remain constant on both elements but the summation of spring and dashpot's stress is equal to the imposed stress to the model (*99*). Considering a single equation for the stress response will result in Equation 1-5.

Equation 1-5 $$\sigma = \sigma_s + \sigma_d = E\varepsilon + \eta\dot{\varepsilon}$$

Considering the same scenarios, a creep response is expected for constant stress. The strain response as presented in Equation 1-6 is obtained by solving the differential equation, where an instantaneous response is observed and followed by an exponential approach.

Equation 1-6 $$\varepsilon = \frac{\sigma_0}{E}\left(1 - e^{-Et/\eta}\right)$$

Considering constant deformation, there is an exponential strain relaxation until the stress remains constant as shown in Figure 1-9. The strain response will follow the Equation 1-7.

Equation 1-7 $$\varepsilon = \varepsilon_0 e^{-Et/\eta}$$

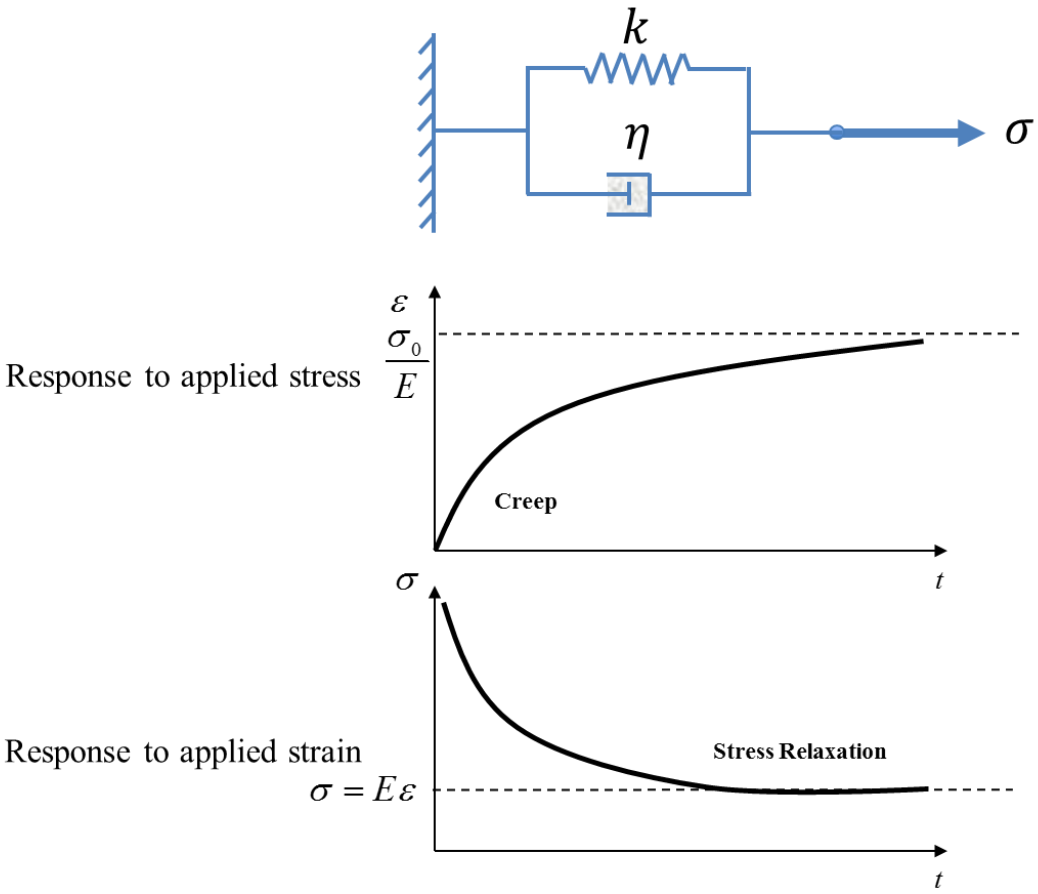

Figure 1-9: The Kelvin rheological model.

1.3.2.3. Burger's Model

Burger presented a model including Maxwell and Kelvin rheological models in series. As shown in Figure 1-10, Burger's model presents combination of three different strain response (*101*) under a constant stress, including the spring strain response (i.e., spontaneous elastic response), Kelvin element strain response (i.e., delayed elastic response), and the dashpot strain response (i.e., irreversible creep response) as shown in Equation 1-8.

Equation 1-8 $$\varepsilon = \sigma_0 \left(\frac{1}{E_1} + \frac{1}{E_2} \left(1 + e^{-E_2 t / \eta_2} \right) + \frac{t}{\eta_1} \right)$$

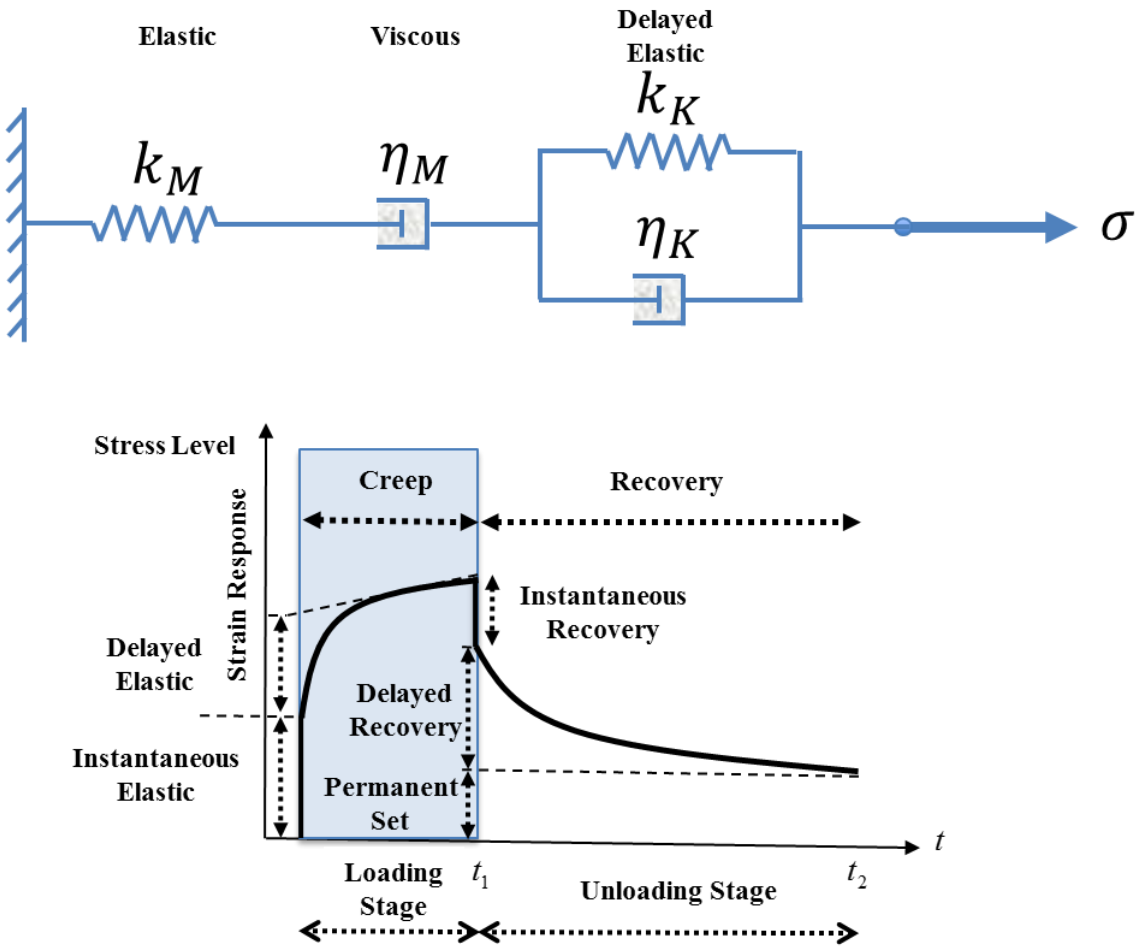

Figure 1-10: The Burger rheological model.

As explained earlier, creep response is the practical response expected from asphalt mixture as its viscoelastic response. The Burger rheological model may characterize the creep response. Usually, the mathematical formulation of experimental creep curve will be fitted to characterize the basic rheological constants for asphalt mixtures.

1.3.3. Available Mechanical Models on Plasticity

Understanding the starting point of plasticity where the elastic relationship is not valid any more is very important stage to characterize the viscoplastic behavior of asphalt mixtures,

including yield conditions and strength parameters. There are many yield surface models to evaluate the yielding criteria of an asphalt mixture, including Von Mises, Gurson, Bigoni-Piccolroaz, Mohr-Coulomb model, Drucker-Prager model, Extended Drucker-Prager model, Matsuoka-Nakai model, Hierarchical Single-Surface model, etc as shown in Figure 1-11 and Figure 1-12.

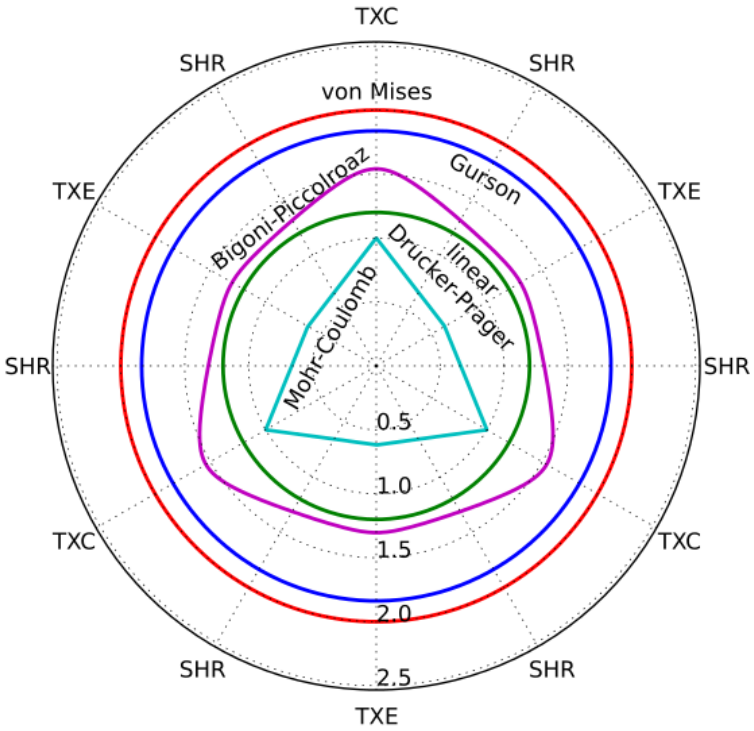

Figure 1-11: The octahedral profile of several plasticity yield surface models.

1.3.3.1. Mohr-Coulomb Model

Mohr-Coulomb model presents a yield surface following the Equation 1-9 formulation (*102*) as shown in Figure 1-12 Mohr-Coulomb yield surface is an irregular hexagon on the octahedral plane.

Equation 1-9 $\tau - \sigma \tan\phi - C = 0$

Considering τ as the yield shear stress, σ as the normal stress, C as cohesion, and ϕ as internal angle of friction for an asphalt mixture. ϕ is a function of aggregate contacts and interlocks and C is a function of temperature, strain rate, properties of the asphalt binder, and fine aggregates (*103*).

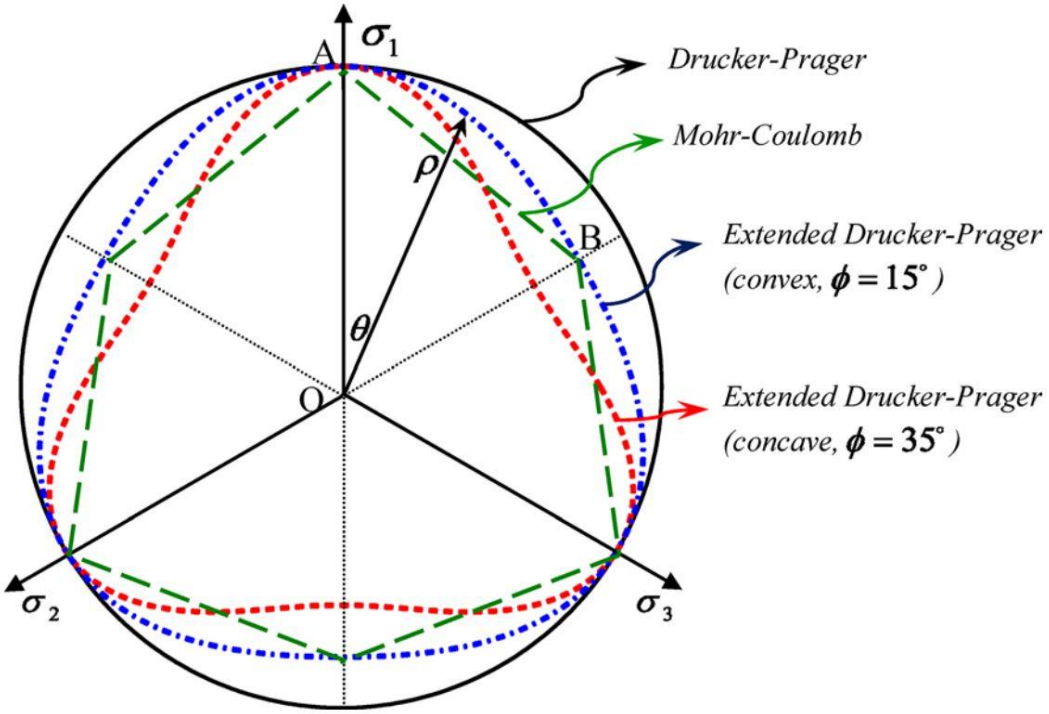

Figure 1-12: The yield surfaces on octahedral plane (*104-106*).

1.3.3.2. Drucker-Prager Model

Drucker-Prager model presents a yield surface following the Equation 1-10 formulation (*103; 107; 108*) as shown in Figure 1-12.

Equation 1-10 $$\sqrt{J_2} - \alpha I_1 - K_0 = 0$$

Considering J_2 as the second deviatoric invariant, I_1 as the first stress invariant, α as material property which is function of internal friction angle, and K_0 as material property that can

be obtained from the cohesion and internal friction angle of an asphalt mixture. Comparing the Drucker-Prager yield surface model with the external apices of the Mohr-Coulomb model α and K_0 are presented as Equation 1-11 and Equation 1-12, respectively (*87; 105*).

Equation 1-11 $$\alpha = \frac{2\sin\phi}{\sqrt{3}(3-\sin\phi)}$$

Equation 1-12 $$K_0 = \frac{6C\cos\phi}{\sqrt{3}(3-\sin\phi)}$$

1.3.3.3. Extended Drucker-Prager Model

Extended Drucker-Prager model presents a yield surface following the Equation 1-13 formulation (*48; 72; 77; 109; 110*) as shown in Figure 1-12.

Equation 1-13 $$\frac{\sqrt{3J_2}}{2}\left[1+\frac{1}{d^{vp}}+\left(1-\frac{1}{d^{vp}}\right)\frac{3J_3}{\sqrt{3J_2^3}}\right]-\alpha I_1-\kappa=0$$

Considering J_3 as the third deviatoric invariant, d^{vp} as an extension ratio which is the ratio of yield strength in extension to that of in compression, κ as the strain hardening parameter which is a function of viscoplastic strain, and K_0 as material property that can be obtained from the cohesion and internal friction angle of an asphalt mixture. d^{vp} is a function of the internal angle of friction (*111; 112*) as presented in Equation 1-14.

Equation 1-14 $$d^{vp} = \frac{3-\sin\phi}{3+\sin\phi}$$

Considering the internal angle of friction between 0 to 90 degrees, then the value of d^{vp} will be between 1 to 0.5. This is a valid statement for asphalt mixture, which specifies the yield strength in extension is lower than that of in compression. If the d^{vp} is equal to one, then the extended Drucker-Prager model is similar to the Drucker-Prager model. In order to maintain the convexity of the extended Drucker-Prager model, the value of d^{vp} is limited to 0.778 to 1, which

correlate to the internal angle of friction between 0 to 22 degrees (*85; 113; 114*) as presented in Equation (14). As shown in Figure 1-12, the extended Drucker-Prager is convex when the internal angle of friction is 15° and it is concave when the internal angle of friction is 35°.

The effect of strain hardening function and temperature on the yield surface expressed as Equation 1-15 (*115*):

Equation 1-15 $$\kappa(p) = \kappa_0 + \kappa_1\left[1 - \exp\left(-\kappa_2 p\right)\right]$$

where p is the effective viscoplastic strain as shown in Equation 1-16, κ_0, κ_1, and κ_2 are viscoplastic material parameters; κ_0 defines the initial yield strength, $\kappa_0 + \kappa_1$ determine the saturated yield stress, κ_0 defines the initial yield strength, and κ_2 is the strain hardening rate (*116; 117*).

Equation 1-16 $$\dot{p} = \left[1 + 2\left(\frac{0.5 + \beta/3}{1 - \beta/3}\right)\right]^{-0.5} \sqrt{\dot{\varepsilon}_{ij}^{vp}\,\dot{\varepsilon}_{ij}^{vp}}$$

where β is the pressure-sensitivity material parameters which is the slope of the viscoplastic potential; and $\dot{\varepsilon}_{ij}^{vp}$ is the rate of viscoplastic strain tensor.

1.3.4. Empirical Approaches for Characterization of Asphalt Concrete Materials

Pavement design and analysis started from empirical approaches. Different types of experiments have been developed to characterize asphalt concrete materials. For example, mechanistic-empirical pavement design guide (MEPDG), American Concrete Pavement Association (ACPA) StreetPave, the Asphalt Institute SW-1 Asphalt Thickness Design, Washington DOT and Minnesota DOT pavement design manuals (*2*), the American Association of State Highway Transportation Officials (AASHTO) empirical 1993 Guide (*2*), the FAA's

LEDFAA methodology (*4; 5*) and Federal Aviation Administration Rigid and Flexible Iterative Elastic Layer Design (FAARFIELD) software (*6*). Some of them will be briefly discuss as follow.

Although American Association of State Highway and Transportation Officials (AASHTO) have served well for several decades since 1950s, there are serious limitations exist in order to pursue this trend as the first priority for pavement design procedures. AASHTO design guides (*3*) are insufficient for the materials, construction techniques and traffic today. Since the empirical equations were derived from a single geographic location Road Test on around half a century ago, one type of subgrade, one Portland cement concrete (PCC) mixture, and one hot mix asphalt (HMA) mixture, two unbound base, and under slightly over one million axle load applications (*118*).

By applying newer data collected as part of the Long-Term Pavement Performance (LTPP) program researchers are interesting in Mechanistic-Empirical Pavement Design Guide (MEPDG) as the latest advances in pavement design, which had developed by the National Cooperative Highway Research Program (NCHRP) 1-37A project and published by AASHTO (*118*). The goal of the MEPDG is to recognize the physical causes of stresses in pavement structures and calibrate them with observed pavement performance. These two parts define this technique to pavement design, which “mechanistic” part stand for physical causes, and “empirical” part define by using observed performance to determine relationships. The procedure of MEPDG introduces several improvements over the current pavement design guide. Obviously, MEPDG is more complex than the AASHTO Design Guide (*3*), because it requires significantly more input parameters from the designer that influence pavement performance, including pavement structure, material properties, climate, traffic, and how to use engineering mechanics in order to predict critical pavement responses.

The Federal Aviation Administration Rigid and Flexible Iterative Elastic Layer Design (FAARFIELD) software (*6*) is a computer-based thickness design procedure for both rigid and flexible airport pavements. Regarding rigid pavements, the procedure consist of a three-dimensional finite element analysis of the rigid pavement system and a performance model based on failure criteria of full-scale traffic tests results from the National Airport Pavement Test Facility and a re-analysis of historical full-scale tests conducted by the U.S. Army Corps of Engineers prior to the 1970s. Regarding flexible pavements, FAARFIELD applies the same structural response and failure models as LEDFAA (*4; 5*). Layered elastic analysis programs such as LEDF always assume continuous, uniform layers with no interruptions (e.g., no joints). LEDFAA compensates for this with the "equivalent edge stress" approach, but this is theoretically unsatisfactory and is not extendable to new aircraft types.

1.3.5. Constitutive Models for Characterization of Asphalt Concrete Materials

Pavement design and analysis have gradually moved from empirical approaches to mechanistic principles. Different types of experiments and mechanistic-based models have been developed to characterize asphalt concrete materials. Some of them will be briefly discuss as follow.

Tashman (*119*) has developed an isotropic viscoplastic continuum damage model considering the permanent deformation of asphalt concrete materials at high temperatures. This model is based on Perzyna type viscoplasticity theory along with modified Drucker-Prager yield surface. He modified the Drucker-Prager yield surface to consider dependency of strain rate and confining level, dilation, aggregate friction, anisotropy, and damage. To validate his constitutive models he used experimental measurements from the Federal Highway Administration (FHWA)

Accelerated Loading Facility (ALF), including a comprehensive set of compressive triaxial tests with different confinement levels and strain rates.

Saadeh (*120*) has developed a damage viscoelasticity model considering the Schapery's viscoelasticity model (*78*) along with Perzyna's viscoplasticity model (*79*) for asphalt concrete materials. The recoverable response (i.e., viscoelastic) was obtained using Schapery's viscoelastic constitutive relationship and the irrecoverable response (i.e., viscoplastic) was characterized by the Perzyna's viscoplastic relationship. Using the Saadeh's anisotropic damage viscoelastic-viscoplastic model, asphalt concrete materials performance under a wide range of temperatures, loading rates, and stress states were evaluated. A set of experimental testing such as triaxial repeated creep and recovery and monotonic constant strain rate tests were conducted to quantify the recoverable and irrecoverable response.

Dessouky (*116*) has developed an elastic-viscoplastic continuum model to predict asphalt concrete materials performance considering the effects of microstructure distribution in modelling the macroscopic behavior of asphalt concrete materials. The model included a modified Drucker-Prager yield surface to capture the impact of stress path direction on material response, and material parameters, which reflect the directional distribution of aggregate and damage density in the microscale.

Researchers at North Carolina State University (*94; 121-124*) have developed a performance-related specifications based on viscoelastoplastic continuum damage (VEPCD) models to characterize asphalt concrete materials response. They believe the performance of asphalt concrete pavement is closely related to the performance of asphalt concrete. To predict the performance of asphalt concrete with reasonable accuracy, a better understanding of its deformation behavior under realistic conditions is required. Various critical phenomena such as

microcrack-induced damage that is critical in fatigue modeling, strain-rate temperature interdependence, and viscoplastic flow, which is critical for high temperature modeling. The resulting model is termed the viscoelastoplastic continuum damage model. However, they mentioned to consider the complicated nature of in-service stress states, a multidimensional model is needed. To predict the performance of the real pavement structures, it is also important to incorporate the material model in a pavement model that considers the vehicle and climatic loads as well as the boundary conditions; the in-house finite element package has been developed for this purpose.

Researchers at Texas A&M university (*69; 71-74; 77; 125; 126*) have developed an advanced mechanistic-based approach to predict rutting and fatigue damage of asphalt concrete materials subjected to multiaxial state of stresses and realistic environmental conditions that actually occur in the field. Pavement Analysis using Nonlinear Damage Approach (PANDA) was presented to implement those approaches in a user-friendly package, integrate it to stand-alone PANDA, and make it easy for an average pavement engineer to use developed characterization procedure.

1.3.5.1. Advantages of PANDA

- PANDA is a robust comprehensive mechanistic-based modeling approach, which predict the response of asphalt concrete materials subjected to multiaxial state of stresses and realistic environmental conditions that actually occur in the field. PANDA accounts for viscoelastic (VE), viscoplastic (VP), viscodamage (VD), micro-damage healing, moisture damage, and oxidative aging constitutive relationships.

- PANDA accounts for the interactions and coupling behavior of different components of constitutive relationships that enhance the model prediction of asphalt concrete materials performance.
- Evolution functions of PANDA are coupled with other components of the model to consider the effect of moisture damage and oxidative aging on performance of asphalt concrete materials. Therefore, it is able to obtain the changes in the failure mode along with the location of crack initiation due to aging effects or moisture presence.
- PANDA is capable of investigating the asphalt concrete materials constituents on performance of asphalt mixtures. An average pavement engineer will use the stand-alone PANDA to analyze and predict the performance of asphalt mixtures by checking various material combinations and selecting most cost-effective materials for a proposed project.

1.3.5.2. PANDA Research Efforts

Asphalt concrete materials have shown time- rate- and temperature-dependent performance, which is VE, VP, VD, and micro-damage healing responses. In 2008, Huang (*126*) developed a nonlinear viscoelastic-viscoplastic model to evaluate the response of asphalt concrete materials under different conditions. The model applied Schapery's nonlinear viscoelastic theory as recoverable response while used Perzyna's viscoplastic theory along with modified Drucker-Prager yield surface as irrecoverable response. Moreover, a new method to decompose the total response of the asphalt concrete materials to recoverable and irrecoverable responses was developed. The Huang's model was presented in finite element package (i.e., ABAQUS) by UMAT to evaluate fatigue and rutting distresses of asphalt concrete materials.

In 2011, Darabi (*125*) developed a thermodynamic-based framework to predict thermo-viscoelastic, thermo-viscoplastic, thermo-viscodamage, and micro-damage healing constitutive relationships of asphalt concrete materials. Moreover, a hardening-relaxation model to evaluate the viscoplastic hardening and relaxation response of asphalt concrete materials subjected to cyclic loading was developed. The proposed robust constitutive relationship is also called Pavement Analysis using Nonlinear Damage Approach (PANDA), which is validated with comprehensive experimental set of tests, including dynamic modulus, creep-recovery, constant strain rate tests in both tension and compression modes of loading. PANDA model is capable to capture time- rate- and temperature-dependent performance of asphalt concrete materials subjected to different loading conditions.

In 2012, Abu Al-Rub et al. (*127*) evaluated the effects of repeated loading patterns on performance of asphalt concrete materials by applying different finite element constitutive material modelling. These robust models consider coupling techniques of PANDA's constitutive relationships, including elasto-viscoplastic, viscoelastic-viscoplastic, and viscoelastic-viscoplastic-viscodamage to predict rutting performance of asphalt concrete materials. Moreover, different 2D and 3D modelling techniques under pulse and equivalent loading were applied to estimate and compare the rutting predictions in asphalt concrete materials.

In 2013, You (*128*) developed the 2D and 3D methods to represent the microstructure of asphalt concrete materials, considering coupled thermo-viscoelastic, thermo-viscoplastic, and thermo-viscodamage constitutive model. X-ray computed tomography images were captured to generate 2D representative volume elements based on identifying three phases of aggregate, matrix, and interfacial transmission zone (ITZ). The effect of aggregate shape, distribution, volume fraction, ITZ strength, strain rate, loading rate, loading type, and temperature on the asphalt

concrete materials were investigated by applying the 2D and 3D microstructural modelling. Moreover, the finite element nonlinear constitutive analysis and X-ray results were integrated to capture the microstructural properties and the macroscopic response of asphalt concrete materials.

In 2013, Shakiba (*129*) developed a Continuum Moisture-Mechanical Damage Mechanics (CMMDM) theory based on physical constitutive relationships, the principle of virtual power, and laws of thermodynamics to simulate the moisture degradation effect, and the induced moisture damage of asphalt concrete materials. Moreover, proposed model were implemented in PANDA to capture moisture damage effect on asphalt concrete materials performance. The microstructural response of asphalt concrete materials considering both effect of moisture diffusion and traffic loading were predicted through 2D and 3D micromechanical evaluations.

In 2015, Rahmani (*130*) evaluated oxidative aging damage based on mechanistic aging constitutive relationship on asphalt concrete materials. The thermodynamical change in mechanical and macroscopic properties of asphalt concrete materials were simulated through an evolution function based on continuum theory on oxygen content, temperature, and level of aging at a certain time. Therefore, the aging state variable was added to Schapery's viscoelastic model and implemented in PANDA.

In 2016, Awed (*88*) conducted a set of experiments to characterize the resistance of asphalt concrete materials to rutting. The experiments were conducted on Fine Aggregate Matrix (FAM), Coarse Aggregate Matrix (CAM), and dense-graded mixture (DGM). The material properties associated with the PANDA models were extracted through a wide range of experiments, including dynamic modulus (DM), repeated creep-recovery test at variable stress level (RCRT-VS), uniaxial constant strain rate in compression (UCSR-C). Moreover, the effect of different temperatures,

confinement level, air void content, aging level, and asphalt mixture type on asphalt concrete materials response were investigated.

Considering the fact that PANDA was developed based on a set of robust comprehensive mechanistic-based modeling approaches during the past decade, it still needs more effort to make PANDA practical for an average pavement engineer. Appreciating all of the efforts that TAMU researchers have put to develop the models, they have not spend enough time on the process simplification. Therefore, pavement community has been reluctant to implement these robust constitutive models. This bring an important task for us to make the PANDA more practical for an average pavement engineer to implement those models in a user-friendly package and integrate it to stand-alone PANDA.

1.4. Problem Statement

Currently, there is a rapid expansion in aviation industry and airline companies are striving to improve their operations to remain profitable. Recently, the introduction of the super-sized aircraft such as Airbus A-380 and Boeing 787 are expected to lower operating costs, which is indeed welcomed by the aviation industry. The new challenges to the airfield pavement engineers is to assess existing pavements and to design new ones that can withstand the high tire pressure of the heavy aircraft. In fact, the current method of designing airport pavements should be modified, because comparing existing aircraft to future aircraft, which will use a different landing gear configuration with significantly higher tire pressures than those in the past. To address this issue, the FAA has conducted several full-scale tests using the world's largest Heavy Vehicle Simulator (HVS), these full-scale tests are extremely expensive, time-consuming, and the results will be applicable only to the conditions at which the tests were conducted. Other than the full-scale tests,

the other available tool to design airfield pavements is FAARFIELD. FAARFIELD is based on elastic analysis and uses transfer functions to predict pavements response to aircraft tire pressures. Our research team at the University of Kansas (KU) along with our collaborators at the Texas A&M University (TAMU) have developed a constitutive relationship to predict the behavior of airfield pavements, using state-of-the-art computational tools and techniques. The developed models and computational tools will be far less expensive than actual full-scale tests and applicable to different tire pressures, gear configurations, and environmental conditions. To achieve the best results and to ensure the adoption of the model, the model calibration procedure and protocol should be simple/doable and clear. This dissertation proposes: a) a set of tests that can be conducted by airfield engineers using the conventional laboratory equipment; b) a straightforward analysis procedure that can be followed to extract the material properties as related to the desired mechanism; and c) automation of the analysis to encourage the adoption of the constitutive relationship and model, i.e. PANDA-AP.

1.5. Research Objective

The main difference between mechanistic-based pavement modelling and simplistic empirical approach is the structural response model and the material characterization procedure, which both are basic components of mechanistic-based modelling of pavements. To be more precise, the structural response model addresses the prediction of stresses and strains in the pavement, which will be used for distress and performance predictions. The material characterization, on the other hand, determines the level of accuracy of the simulated distress and performance. Initiation and evolution of pavement distress and the couplings between different distress mechanisms should be accounted for in both the model and the characterization technique.

Therefore, the material characterization model should be developed while all distresses at the material level are incorporated. The major distresses in asphalt pavement are rutting, fatigue cracking, and thermal cracking.

The overall objective of my doctoral degree in civil engineering at KU is to develop/implement straightforward algorithms to characterize material properties associated with the PANDA-AP models and the Superpave performance models system. This procedure will require the necessary models and the necessary supporting laboratory test protocols to determine the required material parameters. I conducted laboratory experiments on asphalt binders and mixtures used in FAA's NAPMRC test sections to identify and calibrate PANDA-AP parameters.

1.6. Research Approach

The overall objectives of this research are to develop experimental and analytical methods to simplify the characterization of the response of asphalt concrete pavements, determine the parameters of the PANDA models for various types of mixtures and under different loading conditions. This research may assist in the development of such an approach. It worth mentioning that this dissertation is organized following the research paper format. Chapters 3, 4, and 5 are research papers that have been or will be submitted to prominent journals in this field of study. The objectives are achieved through the following tasks:

1. Literature review and problem statement: includes a thorough literature review on the state of knowledge on the behavior of asphalt concrete, related lab experiments, developed models, and characterization techniques. Followed by the objectives, purposes, introductory discussion, and scope of this research.

2. Materials and testing procedures: Develop/propose laboratory tests that should be conducted to systematically calibrate PANDA-AP model. Different test protocols were

developed/conducted to determine the appropriate model parameters. I conduct the laboratory tests for four different mixtures used in NAPMRC test sections: I traveled to Texas A&M University to conduct the designed laboratory tests for four asphalt mixes used in FAA's NAPMRC test sections. The experimental tests were conducted in multiaxial compression/tension setup, using accurate set of equipment and tools, such as Asphalt Mixture Performance Tester (AMPT), Universal Testing Machine (UTM), Materials Testing Systems (MTS), triaxial cell, environmental chamber, and axial and radial deformations by axial and radial LVDTs.

3. Present a systematic procedure to determine nonlinear viscoelastic properties: develops a straightforward laboratory test and analysis procedure that incorporates the effect of confinement and deviatoric stress levels and allows for identification of nonlinear viscoelastic response of asphalt concrete, while mimicking the realistic stress states observed in a pavement structure.

4. Present a systematic procedure to determine viscoplastic and hardening-relaxation properties: develops a straightforward laboratory test and mechanistic-based model that incorporates the Genetic Algorithms (GAs) and allows for identification of viscoplastic and hardening-relaxation viscoplastic response of asphalt concrete pavements as one of many engineering optimization problems, while mimicking the realistic multi-axial state of stresses observed in a pavement structure.

5. Evaluate the effect of Evotherm–M1 on stress-dependent behavior and rutting resistance of modified/unmodified asphalt binders: the multiple stress creep recovery (MSCR) and strain controlled frequency sweep (FS) tests will be performed using dynamic shear rheometer (DSR), along with the extraction of master curve of all four types of asphalt binders used in FAA's NAPMRC test sections. Master curve will be extracted to characterize phenomenological behavior

of asphalt binders under dynamic shear loading in ranges of frequency, temperature and strain of interest. In addition, the non-recoverable creep compliance and the percentage recovery values were calculated at each cycle.

6. Conclusions and future work: the summary of effort, conclusions, and recommendations obtained from this research.

Table 1-1 presents the progress of the tasks.

Table 1-1: Timeline of the tasks.

Year	2015					2016												2017												2018								
Month	Aug	Sep	Oct	Nov	Dec	Jan	Feb	Mar	Apr	May	Jun	Jul	Aug	Sep	Oct	Nov	Dec	Jan	Feb	Mar	Apr	May	Jun	Jul	Aug	Sep	Oct	Nov	Dec	Jan	Feb	Mar	Apr	May	Jun	Jul	Aug	Sep
Task 1																																						
Task 2																																						
Task 3																																						
Task 4																																						
Task 5																																						
Task 6																																						

1.7. Research Summary

This research is part of a FAA's Grant awarded to our research team at KU along with our collaborators at TAMU to develop/customize a constitutive relationship that can be used to predict the response of airfield pavements using state-of-the-art computational tools and techniques. The emphasis of this dissertation is to develop/implement straightforward algorithms to systematically extract material properties associated with the PANDA-AP models, which requires laboratory tests as well as the procedure to analyze the data and identify the PANDA-AP parameters. These accurate and practical analysis procedures will result in more user-friendly evaluation and design of flexible pavements. These procedures will be thoroughly documented in this dissertation. The main conclusions that have been achieved are as follows:

- Chapter 2 of the dissertation: The designed repeated creep-recovery tests at various stress levels, rest periods, loading times, and rates can be used effectively to analyze

the response of asphalt concrete airfield pavements. These tests can be conducted with minimum training by airfield engineers.

- Chapter 3 of the dissertation:
  - The proposed procedure in chapter 3 along with the dynamic modulus and RCRT-VS tests can be used effectively to characterize nonlinear viscoelastic responses of asphalt concrete materials as well as time-temperature shift factors.
  - The nonlinear viscoelastic properties are highly correlated to the triaxiality ratio that accounts for confinement pressure, deviatoric stress level, and multi-axial stress states. The proposed triaxiality ratio can be used to simulate the nonlinear response of pavements under traffic when specific locations in pavement structures are subjected to general multi-axial state of stresses.
- Chapter 4 of the dissertation: The proposed GAs procedure in the chapter 4 along with the dynamic modulus, RCRT-VS, UCSR-C, and RCRT-CLR can be used to characterize VP and HR viscoplastic responses of the asphalt concrete materials. The proposed procedure significantly improves the accuracy of the model parameters of asphalt concrete at high temperatures subjected to cyclic-compression loading;
- Chapter 5 discusses the effect of addition of Evotherm-M1 on both types of modified (i.e., PG 76-22) and unmodified (i.e., PG 64-22) virgin binders used in FAA's NAPMRC test sections. It was shown that Evotherm-M1 will result in more HR viscoplastic strain (i.e., an increase in the rutting potential with decrease in

mixing and compaction temperatures). The result is consistent with the traffic tests results conducted by FAA on NAPMRC flexible pavement test sections (*131*);

- The asphalt binder materials used in FAA's NAPMRC test sections can be ranked with respect to their resistance to rutting as followed:
  - Polymer modified PG 76-22,
  - Polymer modified PG 76-22 plus Evotherm-M1,
  - Unmodified PG 64-22, and
  - Unmodified PG 64-22 plus Evotherm-M1.

1.8. Conclusions

Asphalt concrete materials have shown time- rate- and temperature-dependent performance, which is VE, VP, H-R, VD, and micro-damage healing responses. Moreover, complex mechanical behavior of asphalt concrete materials is observed under general traffic loading and environmental conditions. As briefly presented in this chapter, there are many research efforts, which are experimentally or mechanically evaluate the general behavior of asphalt concrete materials. Experimental efforts such as mechanistic-empirical pavement design guide (MEPDG), American Concrete Pavement Association (ACPA) StreetPave, the Asphalt Institute SW-1 Asphalt Thickness Design, Washington DOT and Minnesota DOT pavement design manuals, the American Association of State Highway Transportation Officials (AASHTO) empirical 1993 Guide, the FAA's LEDFAA methodology, and FAARFIELD software are developed using very expensive and time consuming process. The experimental methods are only applicable to the loadin and environmental conditions on which they are developed for. On the other hand, mechanistic based modeling such as performance-related specifications based on

viscoelastoplastic continuum damage (VEPCD) and Pavement Analysis using Nonlinear Damage Approach (PANDA) are developed using robust constitutive modeling process. The mechanistic based methods need more effort to make them practical for an average pavement engineer. Researchers have to spend more time on the simplification of the process to implement those methods in a user-friendly package.

PANDA is the comprehensive product of several researchers at TAMU, which is capable of analyzing the performance of asphalt concrete materials based on nonlinear damage approach. It compares the utility of several material constituent combinations to capture the effect of material components on mechanical response of asphalt concrete materials. Various environmental conditions are required to evaluate the sensitivity of model parameters. To perform these investigations, robust experimental tests and standard analytical methods are required to determine PANDA parameters and calibrate its models, which might not be practical for an average pavement engineer. This dissertation aims to simplify the experimental procedures as well as analytical methods to make PANDA more practical for pavement community. The emphasis of this dissertation is to develop/implement straightforward algorithms to systematically extract material properties associated with the PANDA models, which requires laboratory tests as well as the procedure to analyze the data and identify the PANDA parameters. These accurate and practical analysis procedures will result in more user-friendly evaluation and design of flexible pavements for an average pavement engineer.

2. Chapter 2: Materials and Testing Procedures

2.1. Abstract

This chapter proposes materials and procedures used to characterize the response of asphalt concrete materials. The simplified procedure allows for easy implementation of required tests to characterize responses of asphalt concrete materials, including specimen fabrication and instrumentation, test setup, laboratory techniques, and protocols. First, different type of materials including aggregate, binders and additives used in FAA's NAPMRC test sections is presented. Then, sample preparation procedures for five different test required to calibrate PANDA protocol are presented, including a robust experimental setup to control temperature, confinement level, loading stress, and rate of loading. Furthermore, five different test procedures including dynamic modulus tests, repeated creep-recovery tests at variable deviatoric stress levels (RCRT-VS), repeated creep-recovery tests at constant loading and rest time (RCRT-CLR), uniaxial constant strain rate in compression (UCSR-C), and uniaxial constant strain rate in tension (UCSR-T) were elaborated. It should be mentioned that dynamic modulus tests are performed according to AASHTO T342 (*132; 133*) and the rest of the test procedures were developed/simplified to characterize the response of asphalt concrete materials by the author and his collaborators. These tests mimicking the realistic conditions that may happen for any element of pavement structure under traffic. Also, the laboratory tests required to determine rheological properties and stress-dependent behavior of modified/unmodified asphalt binders including, multiple stress creep recovery (MSCR) and strain controlled frequency sweep (FS) tests by short-term aged asphalt binder samples using rolling thin film oven (RTFO) are presented.

2.2. Materials

2.2.1. Aggregates

In this study, four different asphalt mixtures used in FAA's NAPMRC test sections were investigated. The aggregate blend was the same for all four mixtures according to the job mix formula (JMF). This aggregate blend included 30% #57 stone, 26% #8 stone, 36% #10 stone, and 8% natural sand. These aggregates were used as a surface course with a nominal maximum aggregate size of 19 mm. The sieve analysis and mixture gradation were summarized in Table 2-1, Table 2-2, and Table 2-3 as well as Figure 2-1. Moreover, the Fineness Modulus of aggregates were calculated based on standard test method for sieve analysis of fine and coarse aggregates (*134; 135*).

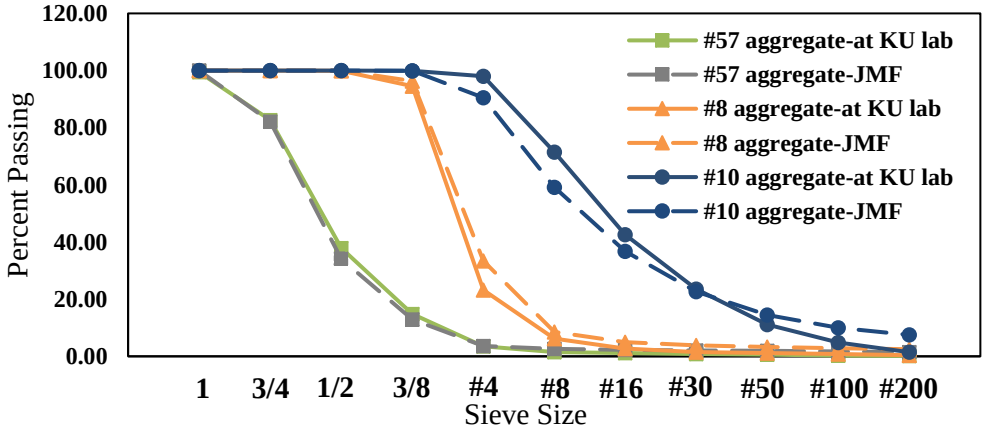

Figure 2-1: Sieve analysis for Limestone aggregate were used in NAPMRC sections based on JMF.

Table 2-1: Sieve Analysis of #57 stone based on ASTM C136/C136M (*134*) and AASHTO T 27 (*135*).

Sieve Size	#57 aggregate					JMF		%Difference Passing	%Difference Retained
	Retained (g)	%Retained	Cumulative Percent	Passing	%Passing	%Passing	%Retained		
1	40	0.55	0.55	7211	99.45	100	0	-0.55	0.55
0.75	1220	16.83	17.38	5991	82.62	82.1	17.9	0.52	-1.07
0.5	3240	44.68	62.06	2751	37.94	34.1	48	3.84	-3.32
0.375	1680	23.17	85.23	1071	14.77	12.9	21.2	1.87	1.97
#4	820	11.31	96.54	251	3.46	3.6	9.3	-0.14	2.01
#8	141	1.94	98.48	110	1.52	2.6	1	-1.08	0.94
#16	30	0.41	98.90	80	1.10	2.3	0.3	-1.20	0.11
#30	20	0.28	99.17	60	0.83	2.1	0.2	-1.27	0.08
#50	20	0.28	99.45	40	0.55	1.9	0.2	-1.35	0.08
#100	20	0.28	99.72	20	0.28	1.7	0.2	-1.42	0.08
#200	10	0.14	99.86	10	0.14	1.5	0.2	-1.36	-0.06
Pan	10	0.14	100.00	0	0.00	0	1.5	0.00	-1.36
Total	7251	Fineness Modulus	7.57	Miss	19 (g)	0.26	<0.3 OK	Sample	7270

Table 2-2: Sieve Analysis of #10 stone based on ASTM C136/C136M (*134*) and AASHTO T 27 (*135*).

Sieve Size	#10 aggregate					JMF		%Difference Passing	%Difference Retained
	Retained (g)	%Retained	Cumulative Percent	Passing	%Passing	%Passing	%Retained		
1	0	0.00	0.00	4153	100.00	100	0	0.00	0.00
0.75	0	0.00	0.00	4153	100.00	100	0	0.00	0.00
0.5	0	0.00	0.00	4153	100.00	100	0	0.00	0.00
0.375	3	0.07	0.07	4150	99.93	99.9	0.1	0.03	-0.03
#4	80	1.93	2.00	4070	98.00	90.5	9.4	7.50	-7.47
#8	1100	26.49	28.49	2970	71.51	59.2	31.3	12.31	-4.81
#16	1200	28.89	57.38	1770	42.62	36.8	22.4	5.82	6.49
#30	790	19.02	76.40	980	23.60	22.7	14.1	0.90	4.92
#50	520	12.52	88.92	460	11.08	14.5	8.2	-3.42	4.32
#100	260	6.26	95.18	200	4.82	10	4.5	-5.18	1.76
#200	140	3.37	98.56	60	1.44	7.5	2.5	-6.06	0.87
Pan	60	1.44	100.00	0	0.00	0	7.5	0.00	-6.06
Total	4153	Fineness Modulus	3.48	Miss	7 (g)	0.10	<0.3 OK	Sample	4160

Table 2-3: Sieve Analysis of #8 stone based on ASTM C136/C136M (*134*) and AASHTO T 27 (*135*).

Sieve Size	#8 aggregate					JMF		%Difference Passing	%Difference Retained
	Retained (g)	%Retained	Cumulative Percent	Passing	%Passing	%Passing	%Retained		
1	0	0.00	0.00	5204	100.00	100	0	0.00	0.00
0.75	0	0.00	0.00	5204	100.00	100	0	0.00	0.00
0.5	4	0.08	0.08	5200	99.92	100	0	-0.08	0.08
0.375	280	5.38	5.46	4920	94.54	96.3	3.7	-1.76	1.68
#4	3710	71.29	76.75	1210	23.25	33.4	62.9	-10.15	8.39
#8	890	17.10	93.85	320	6.15	8.6	24.8	-2.45	-7.70
#16	180	3.46	97.31	140	2.69	5	3.6	-2.31	-0.14
#30	60	1.15	98.46	80	1.54	3.9	1.1	-2.36	0.05
#50	20	0.38	98.85	60	1.15	3.3	0.6	-2.15	-0.22
#100	20	0.38	99.23	40	0.77	2.8	0.5	-2.03	-0.12
#200	20	0.38	99.62	20	0.38	2.5	0.3	-2.12	0.08
Pan	20	0.38	100.00	0	0.00	0	2.5	0.00	-2.12
Total	5204	Fineness Modulus	5.70	Miss	6 (g)	0.08	<0.3 OK	Sample	5210

2.2.1.1. Step by Step Guide Line for Preparing Aggregate

- Dry, sieve and store all the required aggregate.
- Determine the specific gravity and absorption of fine aggregate and coarse aggregate based on AASHTO T 84 (*136*) and T 85 (*137*), respectively.
- Conduct plastic fines in graded aggregates by use of the sand equivalent test based on AASHTO T 176 (*138*) for composite aggregate.
- Conduct standard test method for flat particles, elongated particles, or flat and elongated particles in coarse aggregate mix based on ASTM D4791 (*139*).
- Conduct uncompacted void content of fine aggregate test based on AASHTO T 304 (*140*).
- Conduct course angularity or crash bound test for determining the percentage of fractured particles in coarse aggregate based on ASTM D 5821 (*141*).

2.2.2. Binders

The binders used in this study were graded as polymer modified PG 76-22 and unmodified PG 64-22 based on AASHTO M 320 (*142*), AASHTO M 332 (*143*), and ASTM D6373 (*144*) specifications.

2.2.3. Additive

In this research, Evotherm-M1 additive were provided to study the rheological properties and stress-dependent behavior of modified/unmodified asphalt binders. In addition, two type of binders were provided such that polymer modified PG 76-22 plus 0.5% Evotherm–M1 and unmodified PG 64-22 plus 0.4% Evotherm–M1 according to JMF. Table 2-4 summarize the classification of both binders according to job mix formula (JMF) based on AASHTO M 320 (*142*) specifications using AASHTO T 228 (*145*), AASHTO T 48 (*146*), AASHTO T 316 (*147*), AASHTO T 315 (*148*), AASHTO T 240 (*149*), and AASHTO T 313 (*150*).

Table 2-4: Classification of modified/unmodified binders plus Evotherm-M1 additive.

Test type	Properties	PG 76-22 Plus 0.5% Evotherm	PG 64-22 Plus 0.4% Evotherm	unit	Description
Unaged binder					
AASHTO T228	Specific Gravity @ 77°F	1.037	1.033	°API	
	Specific Gravity @ 60°F	1.043	1.037		Calculation
	API Gravity @ 60°F	4.1	5		Calculation
	LBS/GAL	8.691	8.635		Calculation
AASHTO T48	Flash Point	293	274	°C	Min 230
AASHTO T316	Viscosity @ 135°C	1.215	0.423	Pa.s	Max 3.0
	Viscosity @ 165°C	0.303	0.123	Pa.s	Report
	Lab Mixing Temp °C, min	157	153	°C	Calculation
	Lab Mixing Temp °C, max	163	159	°C	Calculation
	Lab Compaction Temp °C, min	152	142	°C	Calculation
	Lab Compaction Temp °C, max	157	147	°C	Calculation
AASHTO T315	ODSR Test Temp	76	64	°C	
	G*/sinδ	1.2	1.49	kPa	Min 1.00
RTFO aged binder					
AASHTO T240	Mass Change	-0.224	-0.111	Wt%	Max +/-1.0
AASHTO T315	ODSR Test Temp	76	64	°C	
	G*/sinδ	2.54	3.92	kPa	Min 2.20
PAV aged binder					
AASHTO T315	PDSR Test Temp	31	25	°C	
	G*sinδ	2388	3130	kPa	Max 5000
AASHTO T313	BBR Test Temp	-12	-12	°C	
	Creep Stiffness @ 60 sec	266	180	MPa	Max 300
	m-value @ 60 sec	0.316	0.351		Min 0.300

Understanding some basic facts about Evotherm technology is important to use it successfully in asphalt concrete mixtures. Evotherm is a water-free warm mix asphalt (WMA) technology designed to allow the production and compaction of high quality asphalt concrete at temperatures 50 ºF to 90 ºF lower than conventional HMA. Evotherm WMA enables asphalt to coat aggregate at reduced temperatures while also lubricating the mix to improve workability and compaction. Evotherm improves adhesion at the asphalt-aggregate interface thereby addressing

water sensitivity issues. Any asphalt using Poly Phosphoric Acid (PPA) or any type of phosphate cross linking agent will utilize either Evotherm R1 or S1. All other asphalts will utilize J1 or M1. In this study, Evotherm-M1 provided by Ingevity were used based on JMF as shown in Figure 2-2.

2.2.3.1. Benefits of Evotherm

- Evotherm requires no equipment changes at the plant or job site. To reduce mix temperatures, the water-based Evotherm is metered into existing materials.
- Evotherm mixes have the same aggregates, volumetric and binder content as traditional hot mixes.
- Temperature and energy requirements are lower with Evotherm.
- Evotherm drops into existing HMA's JMF.
- Workability and compaction at reduced temperatures are easier than HMA, especially for coarse mixes and polymer modified asphalts.
- Traffic is returned immediately after compaction.
- Evotherm binder performance matches or surpasses the qualities found in new HMA.
- Evotherm lessens the wear and tear on HMA equipment due to its lower processing temperatures.

Figure 2-2: Evotherm-M1 from Ingevity used in NAPMRC sections based on JMF.

2.3. Mixtures

The testing was conducted on two HMA containing 6% PG 76-22 and PG 64-22 binders, and two WMA containing 6% PG 76-22 and PG 64-22 binders with 0.5% and 0.4% Evotherm-M1, respectively, as the additive in accordance with AASHTO standard T 312 (*151*). Table 2-5 lists the properties of the mixtures used in this study.

Table 2-5: Properties of asphalt mixtures used in NAPMRC test sections based on JMF.

Material	Source	Percent used in final aggregate blend	Bulk Specific Gravity (Gsb)	Maximum Specific Gravity (Gmm)
CA #57	Springhouse, Springhouse, PA	30	2.697	2.657
CA #10	Springhouse, Springhouse, PA	36	2.619	
CA #8	Springhouse, Springhouse, PA	26	2.673	
FA Nat. Sand	Hanson, Berlin, NJ	8	2.628	
Binder	PG 64-22	6	1.039	2.467
	PG 76-22		1.033	2.477

The mixing and compaction temperatures for all mixtures were illustrated in Table 2-6 based on JMF from FAA's NAPMRC test sections.

Table 2-6: Mixing and compaction temperature for the all mixtures were used in NAPMRC sections based on JMF

Mixture	Binder	Mixing temperature	Compaction temperature
HMA	PG 76-22	160°C (320°F)	152.2°C (306°F)
	PG 64-22	154.4°C (310°F)	141.1°C (286°F)
WMA	PG 76-22	135°C (275°F)	129.4°C (265°F)
	PG 64-22	135°C (275°F)	129.4°C (265°F)

2.3.1. Step by Step Guide Line for Rice or Maximum Specific Gravity AASHTO T 209 (152)

- Put the required aggregate in the oven for preconditioning.
- Using gloves and fork, carefully, pick up the exact amount of binder from the oven.
- Pick the coarse aggregate out of the oven and mix the binder with them properly, using bucket mixer. Then, add the fine aggregate to the mix.

- Make sure all particles of aggregate and binder are in the bowl and do not waste them on the equipment. Put the bucket mixer equipment in to the oven after usage.
- Place the mix in the pan and put it in the oven with compaction temperature for two hours aging. Stir the mix after 60±5 minutes to ensure uniform aging.
- Check the weight of the bowl to make sure do not wasting the material. The weight of bowl should be the same as its weight at the beginning of the experiment.
- Use binding sheet or accumulative batch, which include of the number of the aggregate and the related weight, to make an actual specimen of aggregates for maximum specific gravity test.
- Take the sample out of oven and spread it up on the surface of the table. Make sure you have all of the aggregate and binder and use gloves and fork. Leave it for at least 15 minutes.
- Break the specimen and make sure there is no big particle and no fine aggregate stock together. Some of them might still be hot. Be careful about your hands.
- Put the specimen into the pycnometer. Do not lose any of it.
- Weight it and register the weight as the dry weight of the mix.
- Put it into a water bath, controlled temperature 77 °F or 25 °C, and fill the sample of water.
- Put the sample with pycnometer on the vibrating table. Then, apply a vacuum, which stay between 25.5±2.5 mm, to it. Leave it for at least 15 minutes.

- Remove the vacuum from the sample. Then, open it very slowly in order to avoid disturbing the mix.
- Suspend it into the water on balance for ten minutes, using tachometer.
- Weight the sample and register the weight of the mix.
- Use the required calculation to achieve maximum specific gravity according to AASHTO T 209 (*152*).

After these tests, maximum specific gravity, bulk specific gravity could be calculated, which result in calculating voids in mineral aggregate (VMA) and air void (AV) of asphalt content.

2.3.2. Step by Step Guide Line for Preparing Mixtures

Having volumetric mix design in hand, follow the steps, such that:

- Pick up the exact amount of required aggregate based on volumetric mix design.
- Put the required aggregate and binder in the oven for two hours preconditioning at mixing temperature.
- One hour prior to compaction, place the mold, plates, spoon, and spatula in the oven at compaction temperature.
- Using gloves and fork, carefully, pick up the exact amount of binder from the oven.
- Pick course aggregate up and mix the binder with them, then pick the fine aggregate up and add them to the mix. Mixing will take almost 2-5 minutes and make sure aggregate does not attach to the bowl.
- Put the specimen and mold into the oven with compaction temperature for two hours cure time. Stir the mix after 60±5 minutes to ensure uniform aging.

- Make second sample for Gyratory compactor by following the same steps. (In order to reach a data point two samples are required.)
- Set the compaction pressure, angle, and gyration speed to the proper values. For ServoPac, set N_{max} to 500. Set the height to the target value.
- After cure time, use the thermometer to take the temperature of the mix. If compaction temperature is higher than 135°C, heat the mix in the oven at 12 °C higher than compaction temperature for no more than 30 minutes. Remove the mix when it reaches a temperature higher than compaction temperature by 3 or 4 degrees.
- Take gyratory specimen, mold, plates, spoon, and spatula out of the oven.
- Put a paper desk on the bottom and funnel on the top of mold.
- Try to transfer all the material in to the mold once and do not waste the material, clean all the pan and transfer the material to the mold. Whole procedure should take less than two minutes. Or once the mix has reached the compaction temperature pour half the mix into the mold and push the mix down with a spatula so that it settles and creates more room for the second half. Make sure the asphalt penetrates to the bottom of the mold. Pour second half into the mold. Using the spatula penetrate it down to the bottom to settle the mix. Also, push on the top with the spatula to further settle the mix.
- Put another paper desk on top of the mix, and the metal plate on top.
- Center the mold inside the Gyratory compactor. Next, lock the specimen. Then, lock mold in the compactor.
- Run the Superpave Gyratory Compactor (SGC).

- After compaction is complete, remove the mold from the compactor wait five minutes for the specimen to cool. Then, tack the sample off and leave it for ten minutes while a fan blowing on it.
- Remove the metal plates and mark the specimen with its ID name, top, and bottom.
- Flip the specimen onto a pan and place the specimen in front of the fan for further cooling, almost 20 min.
- Place the mold, plates, and spatula back in the oven for fabrication of other specimens.
- Weight it and register the weight as the dry weight of the specimen.
- Put it into a water bath (controlled temperature 77 °F or 25 °C) for four minutes.
- Weight it while it is in the water and register the weight of the specimen.
- Take the specimen out of the water bath and dry the surface of specimen by towel. Then, register the weight as the saturated with surface dry weight (SSD weight) of the specimen.

2.4. Sample and Specimen Preparation

2.4.1. Binder Sample Preparation

For this study, all binders were shipped from FAA's NAPMRC test sections to KU and TAMU asphalt laboratories. Evotherm-M1 additive were added to the modified/unmodified asphalt binders to prepare appropriate binders based on JMF. Obviously, viscoelastic properties of asphalt binder changes during the pavement construction and after construction, so the grading was conducted on the unaged binders as well as short-term and long-term aged binders using rolling thin film oven (RTFO) (*149; 153*) and pressure aging vessel (PAV) (*154; 155*). The RTFO

test is used to measure the effect of heat and air on a moving film of asphalt binder and to provide residue for additional testing. The effects of this treatment are determined from measurements of the properties of the asphalt binder before and after the test in accordance with the AASHTO T 240-13 (*149*) and the ASTM D2872-12 (*153*). A moving film of asphaltic material is heated in an oven for 85 min at 163°C (325°F). The effects of heat and air are determined from changes in physical test values as measured before and after the oven treatment. The residue from this test is also used for additional testing as required in the AASHTO M 320 (*142*). It yields a residue that approximates the condition of the asphalt binder immediately after the pavement is constructed. This method can also be used to determine mass change, which is a measure of asphalt binder volatility and mass changes resulting from oxidation. Two replicates were tested for each asphalt binder type with standard deviation of less than 10%, which resulted in eight acceptable tests. The chapter 6 indicate the results for the four asphalt binder types, used in FAA's NAPMRC test sections. Moreover, The low temperature stiffness of the binders was evaluated using the bending beam rheometer (BBR) (*156*).

2.4.2. Mixtures Specimen Preparation

Cylindrical specimens were prepared in the laboratory using a SGC (*157; 158*). The SGC was used to compact 15 cm diameter by 17.8 cm high specimens. These specimens were cored and cut to a 10.2 cm diameter and height of 15.2 cm to ensure uniform distribution of air voids within the specimen. The air void content of test specimens were determined in accordance with AASHTO T 269 (*159*). A tolerance of 0.5 percent from the target percent air voids was allowed. Any specimen exceeded this tolerance shall be discarded. At least two specimens shall be tested at each test condition. Figure 2-3 summarize specimen preparation steps.

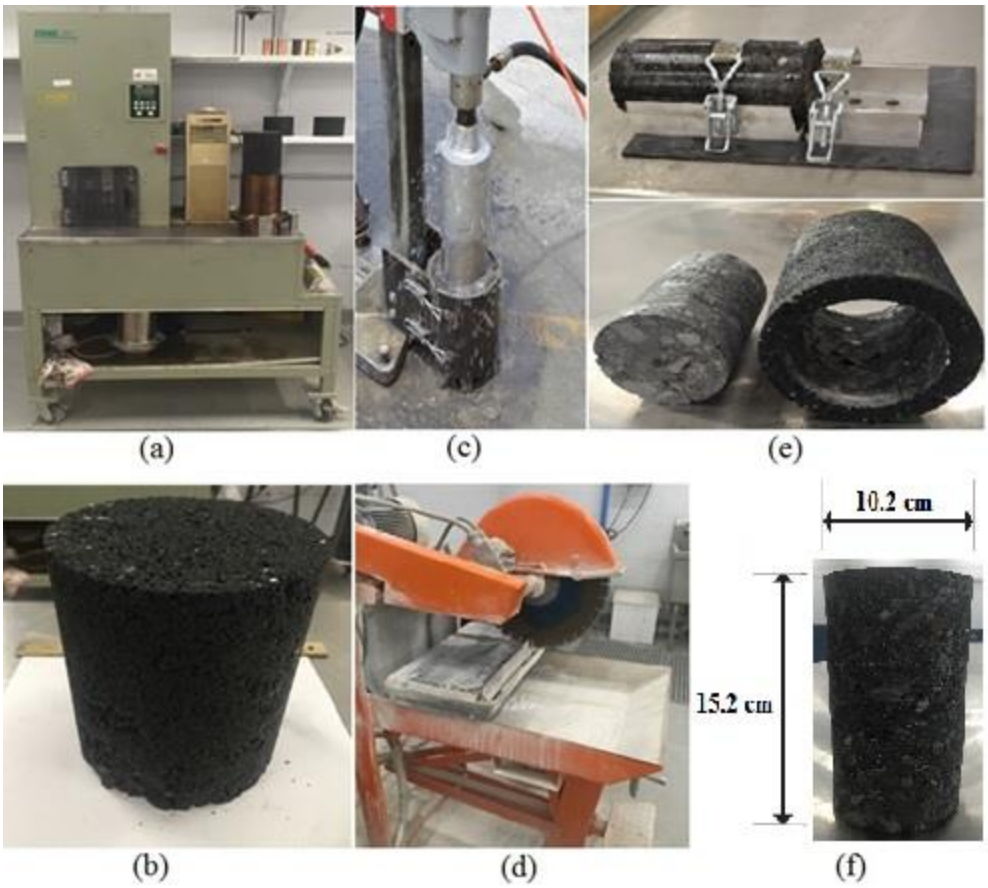

Figure 2-3: Specimen preparation steps. (a) SGC compacted the mixtures; (b) 15 cm diameter by 17.8 cm high specimens; (c) Coring the specimens to 10.2 cm diameter; (d) Cutting the specimens to 15.2 cm high; (e) Jig saw; cored and cut specimens; (f) Final specimen.

2.5. Test Procedures

This subsection briefly presents the testing matrix required for calibration of material models that will be used in predicting rutting and damage response of airfield pavements subjected to the new-generation aircraft. Table 2-7 summarizes the required tests to calibrate constitutive relationships for rutting and fatigue damage. The new HVS tests will be conducted on four different types of airfield pavement materials. These materials differ in terms of the rheology and grades of the asphalt binder used as well as the construction methodology (i.e., HMA vs WMA).

Generally, the laboratory tests listed in Table 2-7 will be conducted on the following four asphalt mixtures in my research.

- P401 HMA with PG 76-22 modified binder
- WMA (Evotherm-M1 additive) with PG 76-22 modified binder
- P401 HMA with PG 64-22 binder
- WMA (Evotherm-M1 additive) with PG 64-22 binder

Table 2-7: Required tests for calibration of the PANDA protocol to evaluate response of asphalt concrete.

Test Mode	**Total No. of Specimens**	**Test Method**	**Temperature (ºC)**	**Level**	**Loading Time/Resting Time (sec)**	**Confining Pressure (kPa)**
Compression	2	AASHTO T 342	Varies	80-110 με	N/A	0
	2	RCRT-VS	55	Varies	0.4/5	140
	6	RCRT-CLR	55	840 kPa	0.4/0.4, 1, 5	140
	4	Uniaxial Constant Strain Rate	55	0.021 mm/sec	N/A	140, 380
Tension	6	Uniaxial Constant Strain Rate	5	5×10^{-6}, 1×10^{-5}, 5×10^{-5}, 1/sec	N/A	0

2.5.1. Binder Tests

In this study, a set of experimental tests were conducted to characterize rheological properties and stress-dependent behavior of modified/unmodified asphalt binders plus Evotherm-M1 additive, such that:

2.5.1.1. Multiple Stress Creep-Recovery (MSCR) Tests

The MSCR test was performed on RTFO-aged (*149; 153*) binders according to AASHTO T 350 (*160*) and ASTM D 7405-15 (*161*) to determine percent recovery and nonrecoverable creep compliance of asphalt binders at 64 °C using DSR (*148*). The percent recovery value determines the elastic response and stress dependence of polymer modified and unmodified asphalt binders. Nonrecoverable creep compliance indicates the resistance of an asphalt binder to permanent deformation under repeated load. Ten creep and recovery cycles are tested at 0.1 kPa and 3.2 kPa stress levels. The creep portion of the test lasts for 1 s, which is followed by a 9 s recovery. Figure 2-4 shows typical binder sample for MSCR tests and Figure 2-5 presents the same sample after MSCR tests using DSR.

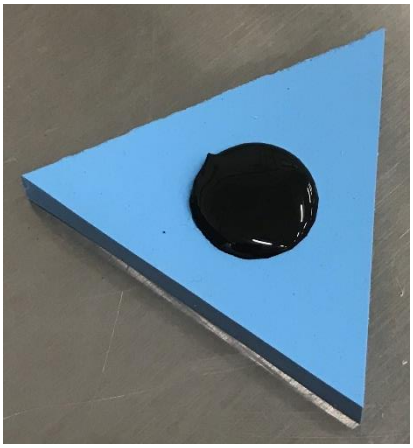

Figure 2-4: Binder sample for MSCR tests

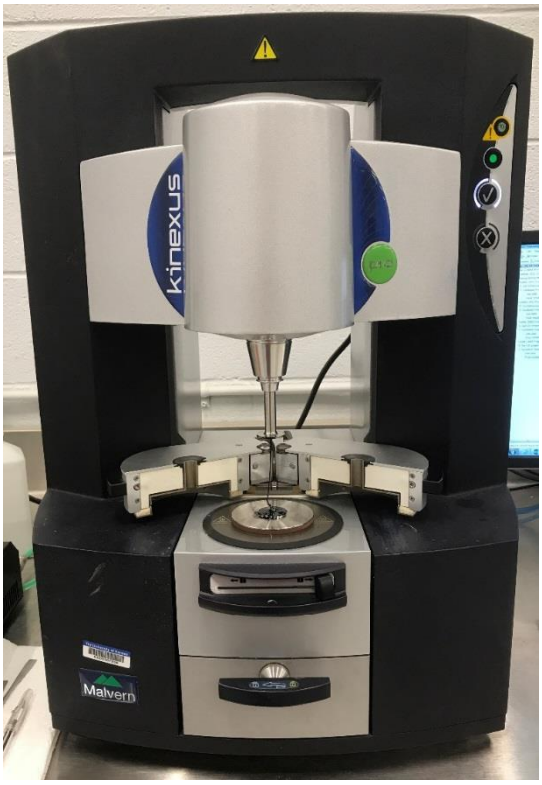

Figure 2-5: Binder sample after MSCR tests using DSR

2.5.1.2. Strain Controlled Frequency Sweep (FS) Tests

The strain controlled FS tests were conducted on the four asphalt binders to measure the dynamic shear modulus and phase angle of asphalt binder when tested in dynamic (oscillatory) shear using parallel plate test geometry and the DSR (*162*). This test method is performed to determine the master curve. This is a master curve where the time- temperature-superposition principle is combined with the similar shifting of the dynamic data at different strain levels. These tests are conducted on material aged in accordance with AASHTO T 240-13 (*149*) and ASTM D 2872-13 (*153*). The frequencies for the shear-oscillating loading were 37.5, 30, 25, 20, 15, 10, 5, 1, 0.5, and 0.1 Hz at each temperature and strain level. The temperatures were 10, 20, 30, 40, 50, 60, and 70 °C. The reference temperature was arbitrarily chosen to be 20 °C. The 8 mm parallel

plate test geometry with 2 mm working gap was used for 10, 20, and 30 °C test temperatures and the 25 mm parallel plate test geometry with 1 mm working gap was used for 40, 50, 60, and 70 °C test temperatures. Two replicates with standard deviation of less than 10% along with two samples based on the size of parallel plate test geometry were tested for each asphalt binder type, which resulted in sixteen acceptable tests. Figure 2-6 shows typical binder sample for lower than 40 °C FS tests and Figure 2-7 presents the same sample after FS tests using DSR.

Figure 2-6: Binder sample for lower than 40 °C FS tests.

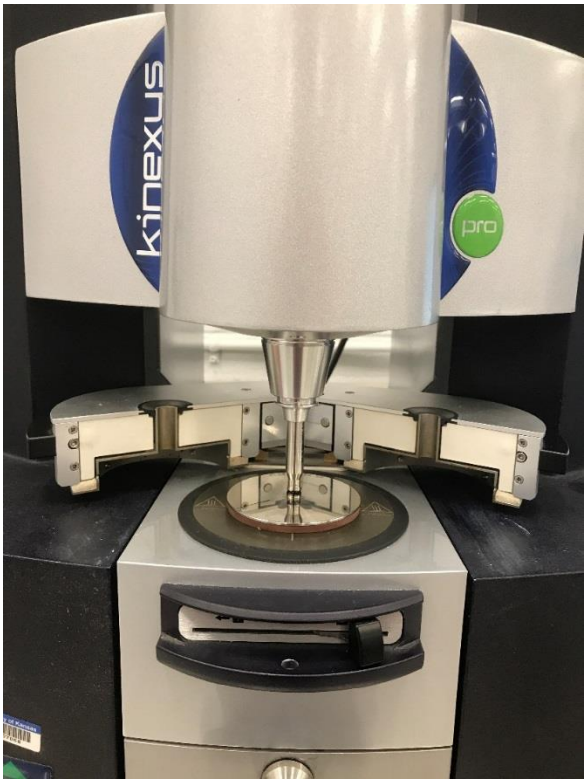

Figure 2-7: Binder sample for lower that 40 °C before FS tests using DSR

2.5.2. Mixture Tests

As mentioned in chapter 2, Table 2-7 summarize the required tests for calibration of the PANDA protocol to evaluate response of Asphalt concrete. General principles and precautions must be considered to set up experimental apparatus and executing creep and recovery experiments. In order to obtain accurate results with appropriate precision and consistency, specific apparatus parts and methods should be used. Following are detailed test procedures.

2.5.2.1. Dynamic Modulus Tests

Dynamic modulus test data were analyzed to identify LVE material properties, including Prony series coefficients and time-temperature shift factors. This test was conducted in accordance with AASHTO T342 (*132; 133*), using an AMPT as shown in Figure 2-8. Three axial linear variable differential transformers (LVDTs) were mounted radially on the specimen at 120° spacing to capture axial strain responses during testing as shown in Figure 2-9. This test was conducted in an unconfined compression mode at five different temperatures (−10 °C, 4.4 °C, 21.1 °C, 37.8 °C, and 54.4 °C) and six loading frequencies (25, 10, 5, 1, 0.5, and 0.1 Hz) at each temperature. The effect of confinement was captured through analysis of the RCRT-VS test results. The applied strain level was between 50-75 micro strains to avoid damage and to ensure the responses remained within the LVE region. Two replicates were tested for each test and the averaged values were reported.

Figure 2-8: Asphalt mixture performance tester (AMPT)

(a) (b)

Figure 2-9: Experimental testing setup on AMPT: (a) Gauge point fixing jig set up to mount axial LVDTs; (b) View of test specimen with mounted axial LVDTs before running the test.

2.5.2.2. Repeated Creep-Recovery Test at Variable Stress Levels (RCRT-VS)

A repeated creep-recovery test protocol over a range of stress levels was developed to identify the nonlinear viscoelastic and viscoplastic responses of the asphalt concrete materials. A MTS with a triaxial cell and environmental chamber, as shown in Figure 2-10, was used to conduct this test in compression at 55 °C and 140 kPa initial confinement pressure. The MTS should be capable of providing controlled load in both compression and tension. It should be equipped with ±22 kN (5,000 lb) load cell. The load cell shall be calibrated in accordance with ASTM E 4 (*163*). The system should be computer controlled and capable of measuring and recording the time, load, deformation, and confining pressure. Specimen need to be prepared according to Figure 2-11 before two hours conditioning time at desired temperature and confinement pressure. A test temperature of 55 °C was selected to minimize the contribution of fatigue cracking in the test results. Each loading block consisted of eight creep-recovery cycles with increasing applied deviatoric stress level. The initial confinement level of 140 kPa was determined to mimic the confinement level that a specific point may experience in a pavement structure under the realistic loads (i.e., 137 to 275 kPa). The loading time of 0.4 sec with an unloading time of 30 sec remained constant throughout the entire test for each loading cycle. The loading time of 0.4 sec represents slow speed of traffic. The unloading time of 30 sec ensures full recovery of the viscoelastic strain during the rest time. Figure 2-12 shows the test setup during RCRT-VS.

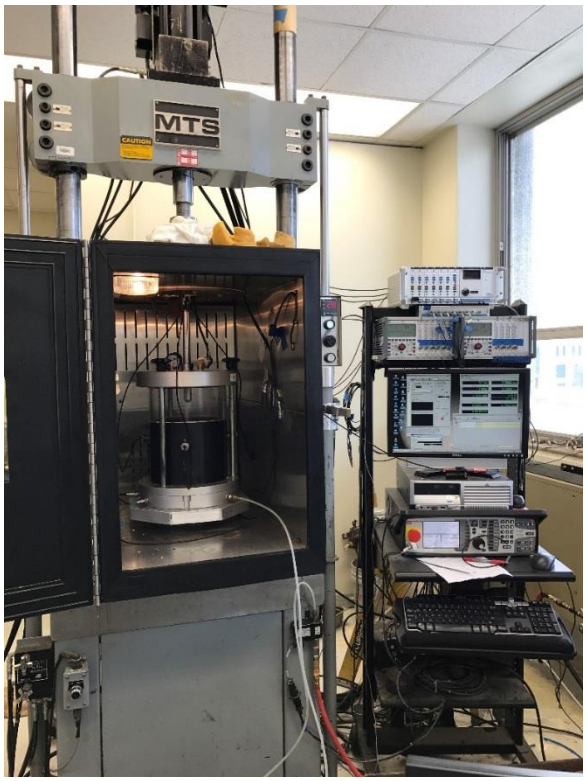

Figure 2-10: Material Testing System (MTS) with a triaxial cell and environmental chamber

(a)


ATTACH
IPC global
GAUGE POINT FIXING JIG
www.ipcglobal.com.au
VACUUM
OFF

(b)

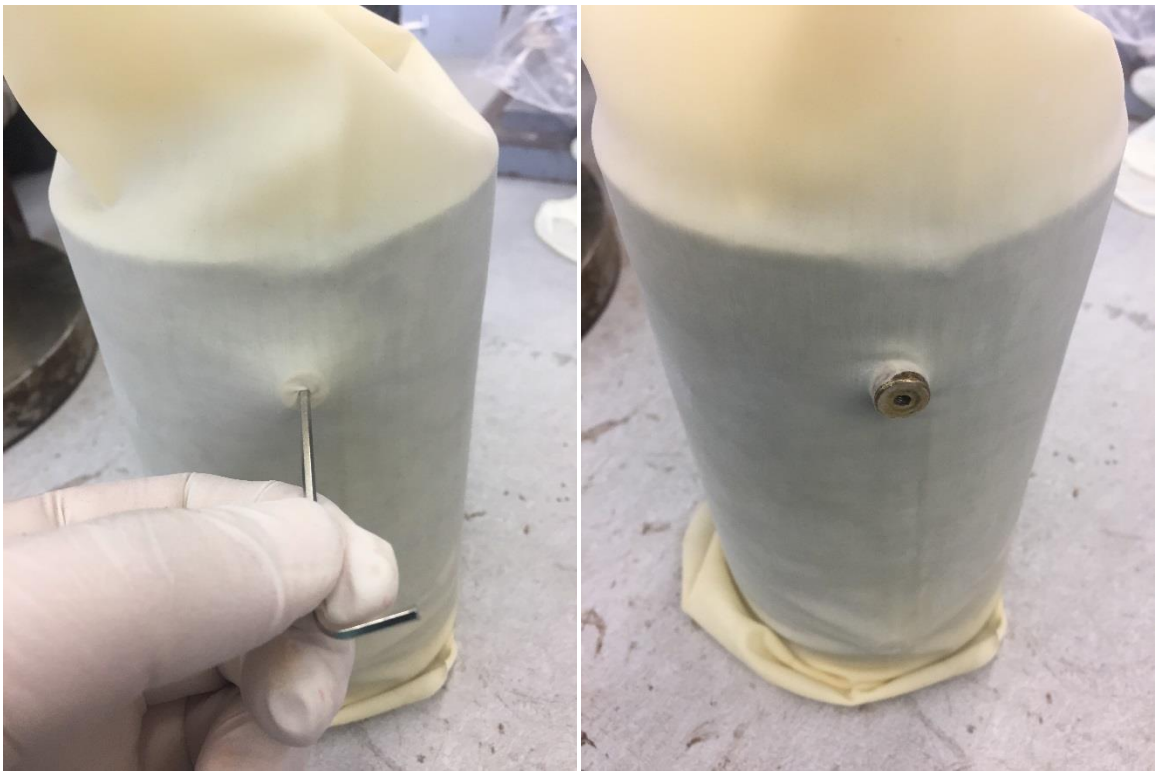

(c)

(d)

(e)

(f)

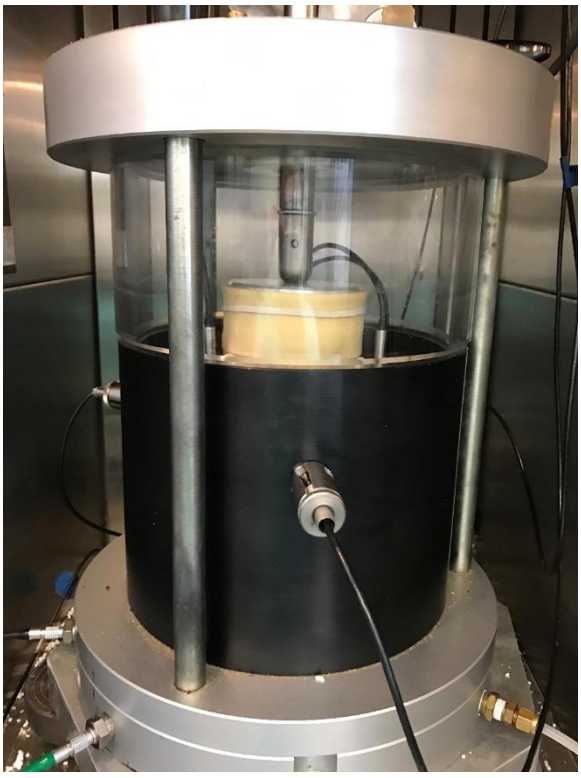

(g)

(h)

Figure 2-11: Specimen preparation before two hours conditioning time at desired temperature and confinement pressure for RCRT-VS, RCRT-CLR, and UCSR-C: (a) J-B WELD steel reinforced epoxy preparation; (b) Gauge point fixing jig to attach required studs for axial LVDTs; (c) Rubber membrane to cover the specimen; (d) Stencil to attach required studs for radial LVDTs; (e) Attaching holders for axial LVDTs and seal the top and bottom plates using rubber bands; (f) Install axial LVDTs and pressure hose inside of triaxial cell; (g) Lower down the triaxial cell and adjust load rod and radial LVDTs; (h) Set the pressure and close the environmental chamber.

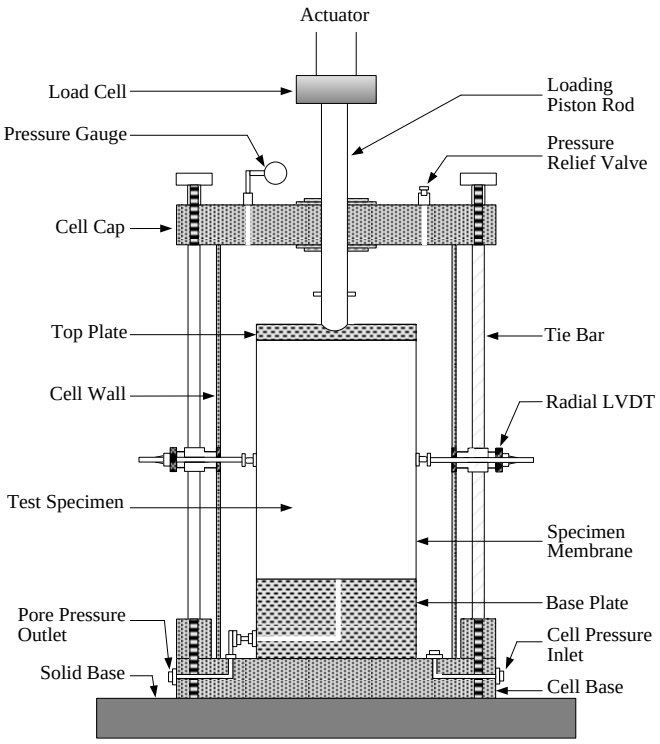
Actuator
Load Cell
Loading
Piston Rod
Pressure Gauge
Pressure
Relief Valve
Cell Cap
Top Plate
Tie Bar
Cell Wall
Radial LVDT
Test Specimen
Specimen
Membrane
Base Plate
Pore Pressure
Outlet
Cell Pressure
Inlet
Solid Base
Cell Base

(a)

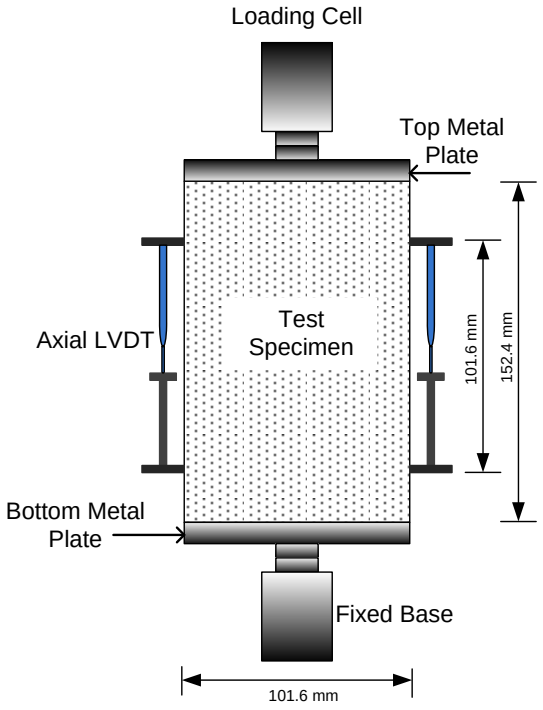
Loading Cell
Top Metal
Plate
Axial LVDT
Test
Specimen
101.6 mm
152.4 mm
Bottom Metal
Plate
Fixed Base
101.6 mm

(b)

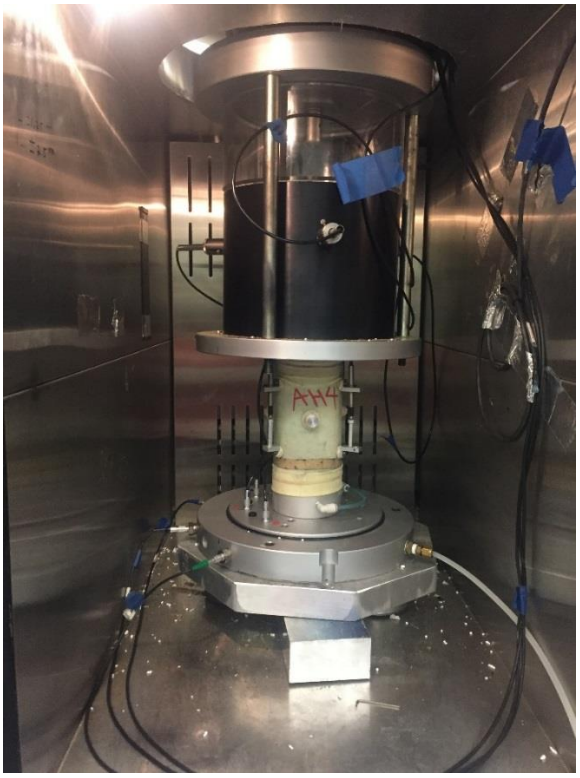

(c)

Figure 2-12: Experimental test setup for RCRT-VS: (a) Schematic view of typical triaxial cell with through-the-wall radial LVDTs; (b) Schematic view of test specimen with mounted axial LVDTs; (c) Tri-axial cell equipped with radial LVDTs inside environmental chamber.

Specimens were pre-conditioned for two hours under the confining pressure until the strain response reached a constant value. After two hours, the cyclic creep and recovery loading history was applied. Figure 2-13 shows the applied deviatoric stresses in the loading blocks of the RCRT-VS. The deviatoric stress started from 140 kPa and increased by a factor of $1.2^{(n-1)}$ for eight loading cycle (i.e., first loading block) to gradually increase the deviatoric stress level to provide data on nonlinear response of the material over a wide range of stress levels. The first deviatoric stress of the subsequent loading blocks was chosen to be equal to the third stress level in the preceding loading block, and increased by the same factor of $1.2^{(n-1)}$ for the loading cycles within that block. The test was conducted on two replicates and the averaged values were reported.

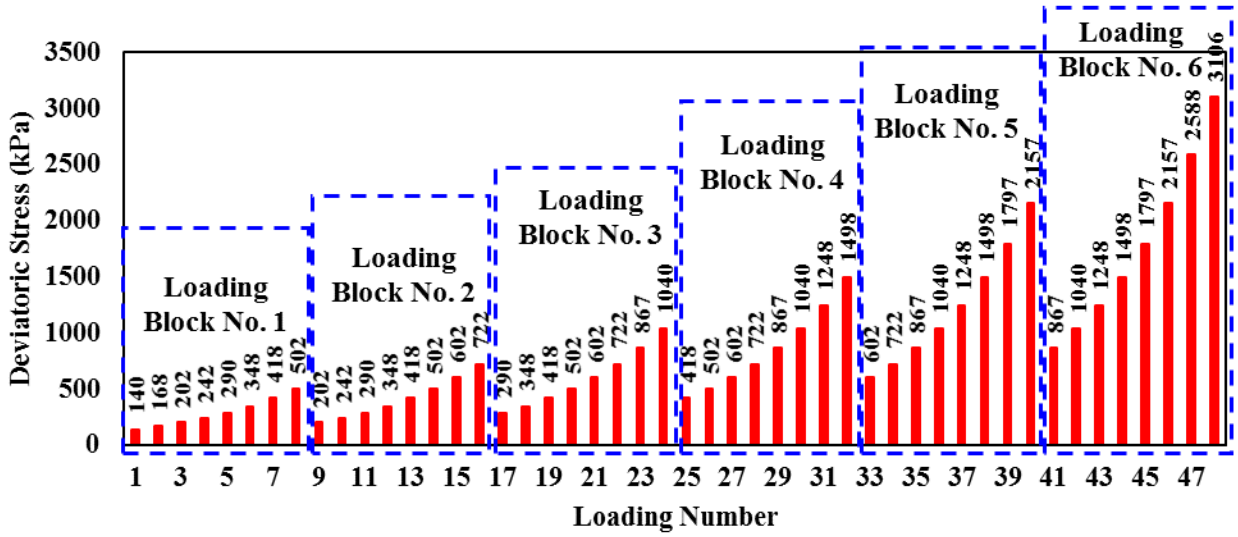

Figure 2-13: Applied deviatoric stresses in the loading blocks of the RCRT-VS.

2.5.2.3. Repeated Creep-Recovery tests at Constant Loading and Rest Time (RCRT-CLR)

The creep-recovery test at constant loading and rest times (RCRT-CLR) is developed and performed to identify the HR viscoplastic parameters. The RCRT-CLR consists of repeated creep-recovery loading cycles. Mimicking realistic situation of asphalt concrete materials, a MTS with a triaxial cell and environmental chamber was used to apply confinement and deviatoric stresses in the RCRT-CLR, 140 kPa and 840 kPa respectively at 55 °C. Confining pressures were applied to the specimen for two hours until the strain response reached a constant value. A test temperature of 55 °C was selected to minimize the contribution of fatigue cracking in the test results. The loading time and rest period of all loading cycles are maintained constant throughout the test. A loading time of 0.4 sec and rest periods of 0.4, 1, and 5 sec are used. The loading time of 0.4 sec represents the slow speed vehicle as more likely loads to happen on pavements. The test was conducted on two replicates at each rest period and the averaged values were reported. Figure 2-14 illustrates a schematic loading scenario for the RCRT-CLR. Specimen need to be prepared

according to Figure 2-11 before two hours conditioning time at desired temperature and confinement pressure. Figure 2-12 shows the test setup during RCRT-CLR.

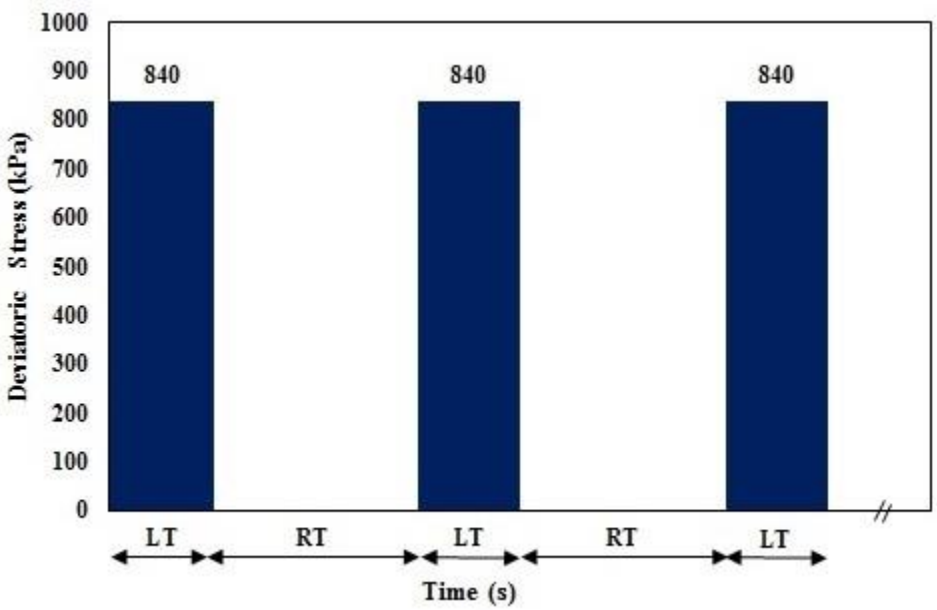

Figure 2-14: Schematic loading cycles of RCRT-CLR, where LT is loading time and RT is rest time.

2.5.2.4. Uniaxial Constant Strain Rate in Compression (UCSR-C)

A constant uniaxial strain rate of 0.021 mm/sec is applied on test specimens in compression until failure to identify the saturated yield stress of all asphalt concrete mixtures of FAA's NAPMRC test sections. A MTS with a triaxial cell and environmental chamber was used to conduct this test in compression at 55 °C and two levels of confining pressure; 140 kPa and 380 kPa are required to mimic realistic state of stresses, confining pressures were applied to the specimen for two hours before running the tests where the strain response reached a constant value. Two specimens are tested at each confining level and the average saturated yield stress is reported for each asphalt concrete mixture. Specimen need to be prepared according to Figure 2-11 before two hours conditioning time at desired temperature and confinement pressure. Figure 2-12 shows the test setup during UCSR-C.

2.5.2.5. Uniaxial Constant Strain Rate in Tension (UCSR-T)

The UCSR-T is conducted in tension at 5 ^{o}C to evaluate the viscodamage parameters. These tests are performed without confining pressure at three different constant strain rates of 5×10^{-6}, 1×10^{-5}, and 5×10^{-5} mm/sec until failure. Two specimens are tested at each strain rate as given in Table 2-7. The UCSR-T can be performed without using the triaxial cell since no confining pressure is required. In these tests the test specimen must be glued to the top and bottom plates. The used glue shall be able to withstand force applied to the sample by a machine and must bond well to the test specimen and loading platens. The J-B WELD steel reinforced epoxy is found to provide satisfied adhesion between specimen surface and end plates, and it stands the tensile force. A schematic of the test specimen for the uniaxial constant strain rate in tension is illustrated in Figure 2-15. Specimen need to be prepared according to Figure 2-16 before two hours conditioning time at desired temperature. Figure 2-17 shows the test setup during UCSR-T.

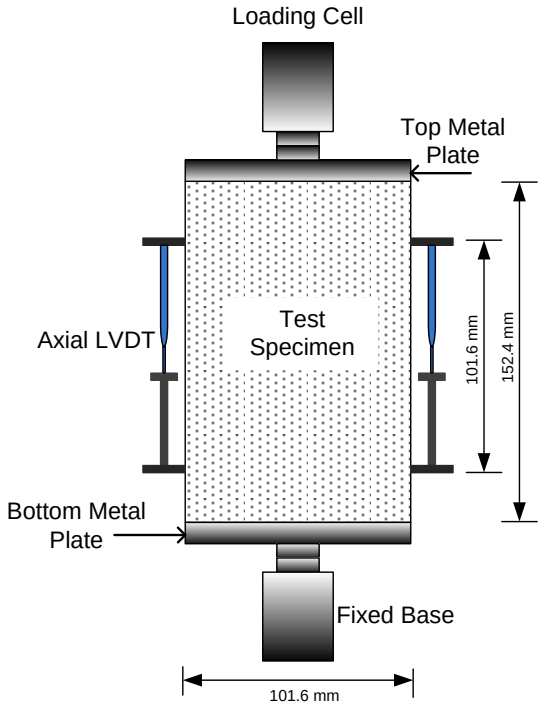

Figure 2-15: Schematic view of test setup with mounted axial LVDTs.

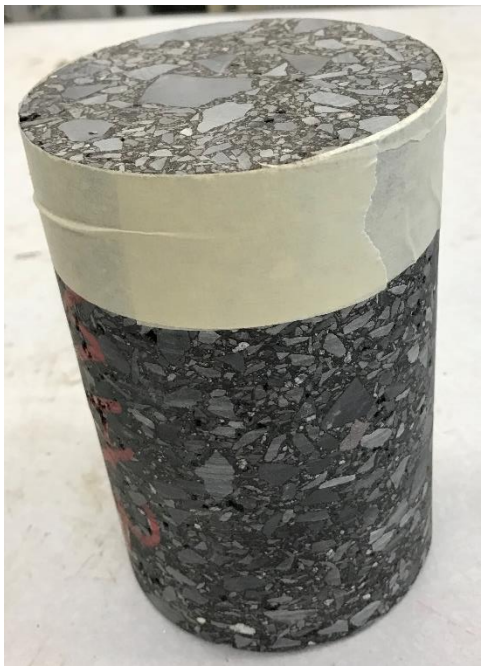

(a)

(b)

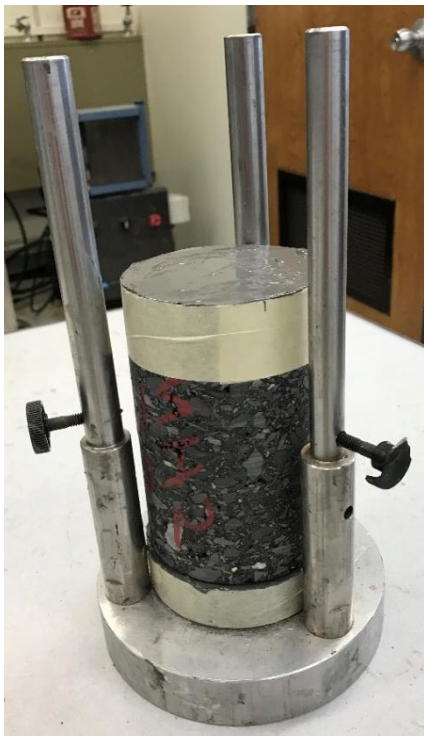

(c)

(d)

(e)

(f)

Figure 2-16: Specimen preparation for UCSR-T before two hours conditioning time at 5 ^{o}C temperature: (a) Use tape to avoid leaking of glue on top of the specimen and the bottom loading plate; (b) J-B WELD steel reinforced epoxy preparation; (c) Apply the glue on top of the bottom plate and top of the specimen; (d) Add the top plate and appropriate weight on top of the specimen, then fix the specimen using the pointer and leave it for at least 24 hr; (e) Gauge point fixing jig to attach required studs for axial LVDTs; (f) Attach holders for axial LVDTs and put it in environmental chamber for 2 hr condition at 5 ^{o}C.

Figure 2-17: Experimental test setup for UCSR-T.

2.6. Conclusions

This chapter presents experimental procedures to characterize sophisticated constitutive relationship of asphalt concrete materials in a user friendly manner. The proposed procedures were applied to extract linear and nonlinear viscoelastic, viscoplastic, and hardening-relaxation viscoplastic properties of asphalt mixtures used in FAA's NAPMRC test sections. These properties extracted based on PANDA protocol which developed by the author collaborators and simplified by the author. The experimental studies presented in this chapter based on developed theoretical models, and data analysis presented in this following chapters lead to predict the response of asphalt concrete materials. The following conclusions can summarize findings of this chapter:

- PANDA incorporates several material constitutive relationships that define the behavior of asphalt mixtures at a wide range of stress and temperature levels;

- The dynamic modulus and RCRT-VS tests can be used effectively to characterize linear and nonlinear viscoelastic responses of asphalt concrete materials as well as time-temperature shift factors;
- The dynamic modulus, RCRT-VS, UCSR-C, and RCRT-CLR can be used effectively to characterize VP and HR viscoplastic responses of asphalt concrete materials.

3. Chapter 3: A Straightforward Procedure to Characterize Nonlinear Viscoelastic Response of Asphalt Concrete at High Temperatures

3.1. Abstract

This chapter proposes a straightforward procedure to characterize the nonlinear viscoelastic response of asphalt concrete materials. Furthermore, a model is proposed to estimate the nonlinear viscoelastic parameters as a function of the triaxiality ratio, which accounts for both confinement and deviatoric stress levels. The simplified procedure allows for easy characterization of linear viscoelastic (LVE) and nonlinear viscoelastic (NVE) responses. First, Schapery's nonlinear viscoelastic model is used to represent the viscoelastic behavior. Dynamic modulus tests are performed to calibrate LVE properties. Repeated creep-recovery tests at variable deviatoric stress levels (RCRT-VS) were designed and conducted to calibrate the nonlinear viscoelastic properties of four types of mixtures used in the FAA's NAPMRC test sections. The RCRT-VS were conducted at 55 °C, 140 kPa initial confinement pressure, and wide range of deviatoric stress levels; mimicking the stress levels induced in a pavement structure under traffic. Once calibrated, the model was validated by comparing the model predictions and experimental measurements at different deviatoric stress levels. The predictions indicate that the proposed method is capable of characterizing NVE response of asphalt concrete materials.

3.2. Introduction

Rutting and fatigue damage are two major forms of distress that cause the most concern in asphalt concrete pavements as they affect both serviceability and safety over the performance life of asphalt pavements. Rutting, permanent deformation under the wheels' path, is more dominant at high temperatures while fatigue damage, evolution of micro-cracks and micro-voids, generally

is more problematic at low and intermediate temperatures (*86; 164-168*). Several prominent studies have been conducted regarding constitutive modeling of rutting and fatigue damage mechanisms resulting in proposed (visco-)plastic and (visco-)damage constitutive relationships (*42; 48; 72; 79; 169-174*). These mechanisms result because of the temperature-dependency of asphalt binders, the complex composite microstructure of asphalt concrete, and localization of strain in the binder phase due to significant differences between the moduli of the asphalt binder and the aggregate phases (*47; 175; 176*). However, the nonlinear viscoelastic response of asphalt concrete (i.e., the mechanism responsible for recoverable strain response) plays a pivotal role in the evolution rate and magnitude of distress induced in asphalt pavements. Therefore, prediction of these fatigue damage and rutting require accurate characterization of NVE responses. Schapery's (*78*) nonlinear viscoelastic model has been widely used to represent the viscoelastic response of asphalt concrete materials and structures (*45; 50; 75; 80; 81; 177-185*).

While significant progress has been made during the past several years in mechanistic-based constitutive modeling of different mechanisms of asphalt concrete, the pavement community has been reluctant to fully implement and use these sophisticated constitutive relationships in design and refined analysis of asphalt concrete pavements and structures. One of the main obstacles that prevents the pavement engineers from using these models is the lack of straightforward and simple procedures to extract the material properties associated with these models. Available characterization methods either are over-simplified or require extensive laboratory tests and complex analyses procedures to extract the material properties associated with viscoelastic as well as distress mechanisms observed in pavements. This paper aims to provide a straightforward procedure to extract nonlinear viscoelastic parameters of asphalt concrete

materials while maintaining the required level of accuracy by incorporating the important factors affecting this mechanism.

Accurate estimation of NVE responses of asphalt concrete materials requires precise characterization of complex mechanical responses. Deviatoric, confinement, and shear stress levels are factors affecting the nonlinear viscoelastic response and significantly contribute to the level of induced distress. Furthermore, a location within the pavement structure experiences a multi-axial state of stress under the traffic loading. To mimic realistic stress states in pavement structures under traffic, a repeated creep-recovery test at variable deviatoric stress levels (RCRT-VS) was designed and used in this study to identify NVE response of asphalt mixtures. The proposed characterization method was then applied to four different asphalt mixtures used in FAA's NAPMRC test sections to evaluate the efficacy of the method. The first stress invariant and von Mises equivalent stress were considered as surrogates to confinement level and level of deviatoric stress, respectively. We have shown that the nonlinear viscoelastic parameters strongly correlate with the triaxiality ratio that accounts for both confinement level, deviatoric stress level, and multi-axial states of stress. Finally, we propose a model by which to relate NVE parameters to the level of triaxiality.

3.3. Objectives

The primary objectives of the study presented in this chapter are to:

- Develop a straightforward procedure that allows for identification of NVE response of asphalt concrete;
- Incorporate the effect of confinement and deviatoric stress levels into the proposed procedure;

- Introduce a laboratory test that can be used systematically to extract NVE parameters while mimicking the realistic stress states observed in a pavement structure;
- Apply the proposed method to extract NVE parameters associated with asphalt mixtures used in FAA's NAPMRC test sections;
- Propose a mechanistic-based model for NVE parameters of asphalt concrete when subjected to general multi-axial state of stresses.

3.4. Analysis Approaches and Results

The total strain is decomposed into viscoelastic and viscoplastic components as shown in Equation 3-1:

Equation 3-1 $$\boldsymbol{\varepsilon}^{total} = \boldsymbol{\varepsilon}^{rec(ve)} + \boldsymbol{\varepsilon}^{irrec(vp)}$$

where $\boldsymbol{\varepsilon}^{total}$, $\boldsymbol{\varepsilon}^{rec(ve)}$, and $\boldsymbol{\varepsilon}^{irrec(vp)}$ are total, viscoelastic, and viscoplastic strain tensors, respectively. Schapery's (*78*) nonlinear viscoelastic constitutive relationship was used to represent the nonlinear recoverable strain as shown in Equation 3-2:

Equation 3-2 $$\varepsilon^{rec(ve)}(t) = g_0^{\sigma_t} D_0 \sigma^t + g_1^{\sigma_t} \int_0^t \Delta D\left(\psi^t - \psi^\tau\right) \frac{d\left(g_2^{\sigma_\tau}\sigma^\tau\right)}{d\tau} d\tau$$

where superscripts t and τ designate responses at a specific time over the history of loading; D_0 and ΔD are the instantaneous and transient creep compliances; g_0, g_1, and g_2 are nonlinear viscoelastic parameters, which are a function of the stress level. The parameters g_0 and g_1 capture the effect of stress level on instantaneous and transient compliances, respectively, while g_2

incorporates the nonlinearity due to the rate of loading. The term $\psi^t = \int_0^t \frac{d\xi}{a_T}$ is the reduced time, where a_T is the time-temperature shift factor. The transient compliance is expressed in terms of the Prony series as shown in Equation 3-3:

Equation 3-3 $$\Delta D(t) = \sum_{n=1}^{N} D_n \left[1 - \exp\left(-\lambda_n \psi^t\right)\right]$$

where D_n and λ_n are the nth compliance and retardation time, respectively, and N is the number of Prony series components.

3.5. Identification of Linear and Nonlinear Viscoelastic Properties

3.5.1. Identification of Linear Viscoelastic Properties

The dynamic modulus master curve at the reference temperature of 20 ^{o}C was produced by analyzing complex dynamic modulus (i.e., $E^*(\omega)$) and phase angle (i.e., δ) at different frequencies and temperatures. In this study, a sigmoidal-type function proposed by Pellinen (*186*) was used to construct the dynamic modulus master curve. The nonlinear generalized reduced gradient method (*187*) was used to minimize the error between the experimental measurements and model predictions of the storage and loss moduli (i.e, $E'_{Exp}(\omega) = \left|E^*(\omega)\right|\cos\delta$ and $E''_{Exp}(\omega) = \left|E^*(\omega)\right|\sin\delta$, respectively) from which the Prony series coefficients were obtained.

3.5.2. Identification of Nonlinear Viscoelastic Properties

To provide data over a wide range of deviatoric stresses, RCRT-VS was conducted and analyzed to extract nonlinear viscoelastic properties. Figure 3-1 schematically represents one cycle of the RCRT-VS.

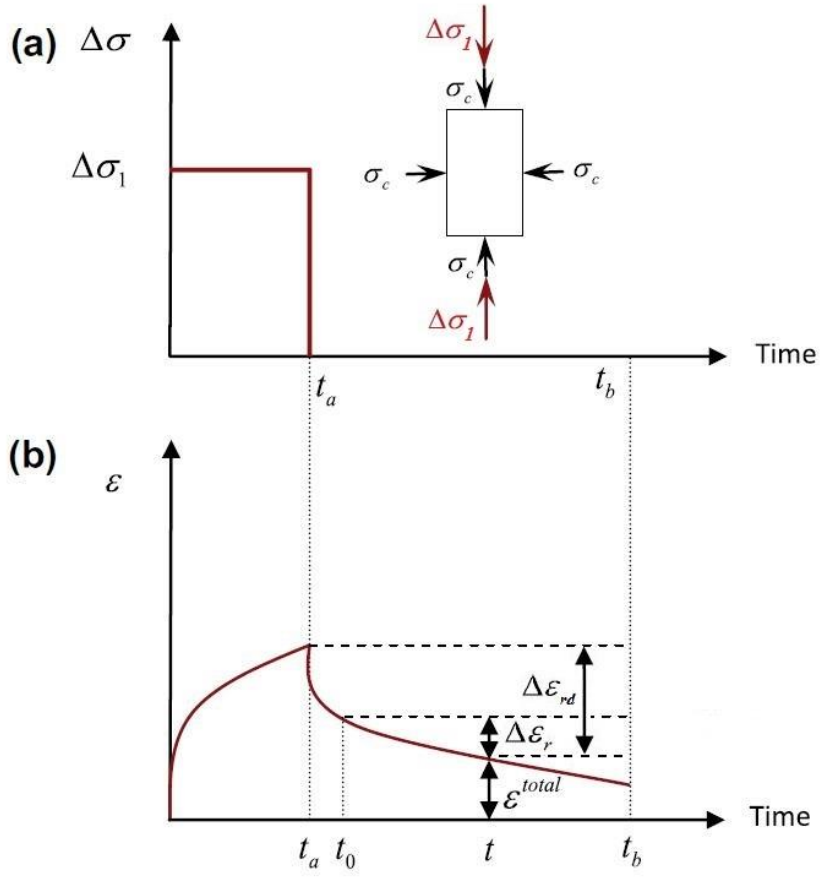

Figure 3-1: Schematic representation of the strain response during a cycle of RCRT-VS test.

The components of the stress tensor during the RCRT-VS test are expressed as shown in Equation 3-4:

Equation 3-4 $$\sigma_{11} = \sigma_c + \Delta\sigma_1; \qquad \sigma_{22} = \sigma_{33} = \sigma_c; \qquad \sigma_{12} = \sigma_{23} = \sigma_{13} = 0$$

where σ_c is the initial confinement pressure and $\Delta\sigma_1$ is the additional applied axial stress. Although initial confinement pressure is constant (i.e., σ_c), the mean pressure (i.e., $\frac{I_1}{3} = \sigma_c + \frac{\Delta\sigma_1}{3}$) during each loading cycle changes, which means that the mean pressure varies as the additional applied axial stress changes. The deviatoric stress tensor and the mean pressure (i.e., averaged volumetric stress during RCRT-VS can be calculated as shown in Equation 3-5:

Equation 3-5 $$\frac{1}{3}\sigma_{kk}\delta_{ij} = \left(\sigma_c + \frac{\Delta\sigma_1}{3}\right)\delta_{ij}; \qquad S_{ij} = \begin{bmatrix} \frac{2}{3}\Delta\sigma_1 & 0 & 0 \\ 0 & -\frac{1}{3}\Delta\sigma_1 & 0 \\ 0 & 0 & -\frac{1}{3}\Delta\sigma_1 \end{bmatrix}$$

The experimental measurements for the viscoelastic recovery strain response $\Delta\varepsilon_r^{Exp}$ between times t_0 and an arbitrary time t during the rest period can be calculated as shown in Equation 3-6:

Equation 3-6 $$\Delta\varepsilon_r^{Exp} = \varepsilon_{11}^{total}(t_0) - \varepsilon_{11}^{total}(t); \qquad t_o \le t \le t_b$$

It should be noted that the viscoelastic recovery strain $\Delta\varepsilon_r$ which is the difference between total strains at two points during the rest period (e.g., between times t_0 and t such that $t_0 - t_a$ is $\frac{1}{40}$ of the rest period as shown in Figure 3-1), is analyzed to characterize the nonlinear viscoelastic properties. The viscoelastic recovery strain, Equation 3-6, can be simplified as shown in Equation 3-7:

Equation 3-7 $$\Delta\varepsilon_r = \left[\varepsilon_{11}^{NVE}(t_0) + \varepsilon_{11}^{vp}(t_0)\right] - \left[\varepsilon_{11}^{NVE}(t) + \varepsilon_{11}^{vp}(t)\right]$$

It is argued that the permanent deformation and viscoplastic strain do not evolve during the rest period and therefore $\varepsilon_{11}^{vp}(t_0) = \varepsilon_{11}^{vp}(t)$, such that $\Delta\varepsilon_r$ can be expressed as shown in Equation 3-8 using Schapery's nonlinear viscoelasticity yields:

Equation 3-8
$$\Delta\varepsilon_r = \varepsilon_{11}^{NVE}(t_0) - \varepsilon_{11}^{NVE}(t) = g_2\left[\Delta D\left(\psi^{t_0}\right) - \Delta D\left(\psi^{t_0} - \psi^{t_a}\right)\right]\Delta\sigma_1 - g_2\left[\Delta D\left(\psi^{t}\right) - \Delta D\left(\psi^{t} - \psi^{t_a}\right)\right]\Delta\sigma_1; \quad t_o \le t \le t_b$$

where g_2 is the nonlinear parameter which is a function of the stress level at the end of the loading time. The parameter g_2 is the only unknown in Eq. Equation 3-8 and can be identified by minimizing the error between experimental measurements and model predictions for viscoelastic recovery strain (i.e., $\Delta\varepsilon_r^{Exp}$ and $\Delta\varepsilon_r$, respectively). Once g_2 is identified, the total recovered viscoelastic strain $\Delta\varepsilon_{rd}^{Exp}$ at any time t during the rest period can be calculated by subtracting the total strain at time t from the total strain at the end of the creep (i.e., $\varepsilon_{11}^{total}\left(t_a^-\right)$), as shown in Equation 3-9:

Equation 3-9
$$\Delta\varepsilon_{rd}^{Exp} = \varepsilon_{11}^{total}\left(t_a^-\right) - \varepsilon_{11}^{total}(t); \qquad t_a \le t \le t_b$$

Similarly, the viscoplastic strain during the rest time remains equal to the viscoplastic strain at the end of the creep loading, such that one can use nonlinear Schapery's viscoelastic model to calculate Equation 3-9, as shown in Equation 3-10:

Equation 3-10
$$\Delta\varepsilon_{rd} = \varepsilon_{11}^{NVE}\left(t_a^-\right) - \varepsilon_{11}^{NVE}(t) = \left[\left(D_0 + g_1 g_2 \Delta D\left(\psi^{t_a}\right)\right)\Delta\sigma_1\right] - \left[g_2\left(\Delta D\left(\psi^{t}\right) - \Delta D\left(\psi^{t} - \psi^{t_a}\right)\right)\Delta\sigma_1\right]; \qquad t_a \le t \le t_b$$

Having the parameter g_2 in hand, the parameter g_1 can be identified by minimizing the error between experimental measurements for total recovered strain $\Delta\varepsilon_{rd}^{Exp}$ and model

representation of the same measure $\Delta\varepsilon_{rd}^{NVE}$. This analysis procedure was repeated for each loading cycle of RCRT-VS test. The nonlinear parameter g_0 was assumed to be one from our previous studies (*81*) based on the fact that: (1) it is difficult and in some cases impractical to accurately measure instantaneous response during recovery; and (2) instantaneous strain response at high temperatures is negligible as compared to the total viscoelastic strain. Therefore, viscoelastic nonlinearity was captured through the parameters g_1 and g_2 (*75*). The nonlinear parameter g_1 controls the nonlinearity in the transient compliance term, which affects the viscoelastic nonlinearity mostly during the loading stages. The nonlinear parameter g_2 affects both loading and recovery strain responses.

The confinement level and deviatoric stress levels change during each loading cycle of the RCRT-VS test as the additional axial stress increases. To incorporate the effect of confinement level and deviatoric stress level, the identified nonlinear parameters were plotted as a function of the triaxiality ratio (*75*), η. The parameter η is the ratio of the first stress invariant to the second deviatoric stress invariant (the ratio of hydrostatic pressure over the von Mises equivalent stress), as shown in Equation 3-11:

Equation 3-11 $$\eta = \frac{I_1/3}{\sqrt{3J_2}}$$

where I_1 is the first stress invariant and J_2 is the second deviatoric stress invariant. The sign of the triaxiality ratio is the same as the sign of the first stress invariant, such that negative triaxiality ratio indicates compressive mean pressure and positive triaxiality ratio indicates tensile mean pressure. For ductile materials, the triaxiality ratio strongly affects the level of permanent strain and this ratio increases as the confinement level dominants the Mises equivalent stress. Therefore,

high confinement levels or low values of the Misses equivalent stress result in higher values of η . In case of RCRT-VS test, triaxiality ratio η is the confinement pressure over the deviatoric applied stressas shown in Equation 3-12:

Equation 3-12 $$\eta = \frac{\sigma_c + \Delta\sigma/3}{\Delta\sigma} = \frac{\sigma_c}{\Delta\sigma} + \frac{1}{3}$$

As shown in the next section, the analysis results indicate that the nonlinear parameters are strong functions of the triaxiality ratio.

3.6. Results and Discussions

3.6.1. Linear Viscoelastic Properties

Figure 3-2 shows the constructed master curve at the reference temperature of 20 ^{o}C for the four types of asphalt mixtures used in the NAPMRC test sections with 4.5% air void content for PG 76-22 and 3.5% air void content for PG 64-22 cored specimens. The Prony series coefficients, shown in Equation 3-3, were determined by interconversion relationships (*188*) between the Prony series coefficients and the loss and storage dynamic compliances. Table 3-1 lists the identified Prony series coefficients and time-temperature shift factors.

As shown in Figure 3-2, Evotherm causes a decrease in moduli at different frequencies except for PG 76-22 at high frequencies. Furthermore, PG 76-22 resulted in higher moduli as compared to moduli for PG 64-22, as expected. As it will be shown, the impact of Evotherm on nonlinear viscoelastic parameters is much more pronounced than its impact on linear viscoelastic parameters.

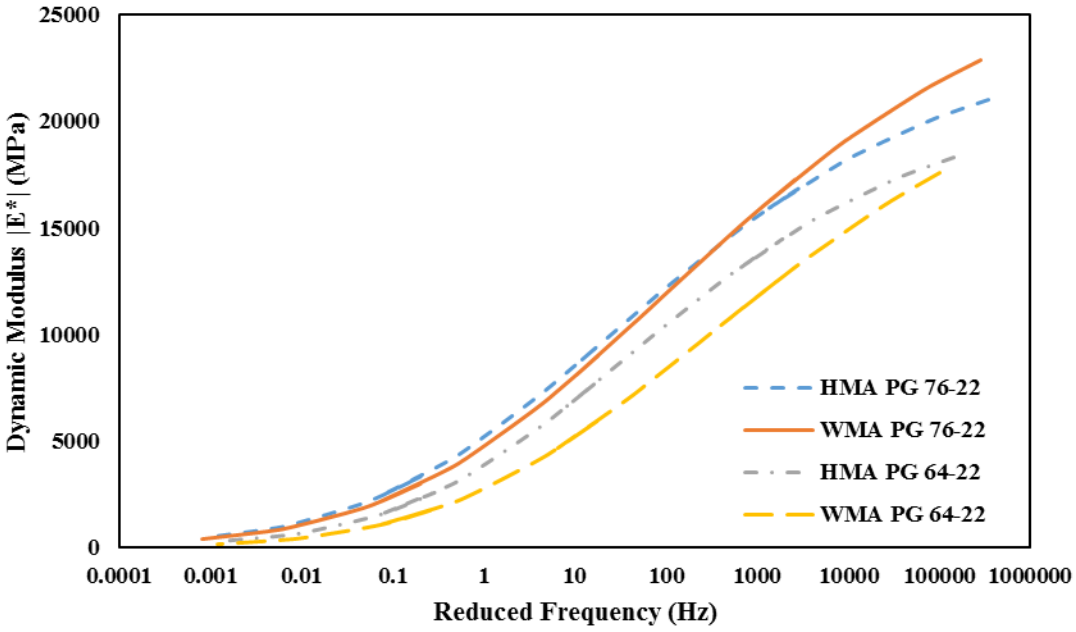

Figure 3-2: Master curve according to AASHTO T342 (*133*) and ASTM D3497-79 (*132*) for the dynamic modulus, E^*, using the sigmoidal fitting function in log–log scale.

Table 3-1: Identified Prony series coefficients.

	HMA PG 76-22		WMA PG 76-22		HMA PG 64-22		WMA PG 64-22	
n	D_n (MPa^{-1})	λ_n (1/s)	D_n (MPa^{-1})	λ_n (1/s)	D_n (MPa^{-1})	λ_n (1/s)	D_n (MPa^{-1})	λ_n (1/s)
0	5.58×10^{-5}	-	5.63×10^{-5}	-	6.20×10^{-5}	-	3.85×10^{-5}	-
1	2.54×10^{-5}	4.35×10^{3}	2.37×10^{-5}	4.21×10^{3}	3.70×10^{-5}	1.65×10^{3}	3.54×10^{-5}	7.47×10^{4}
2	2.73×10^{-5}	4.01×10^{2}	2.40×10^{-5}	3.93×10^{2}	3.89×10^{-5}	1.78×10^{2}	4.33×10^{-5}	5.95×10^{3}
3	7.23×10^{-5}	3.69×10	6.23×10^{-5}	3.67×10	1.00×10^{-4}	1.92×10	6.91×10^{-5}	4.73×10^{2}
4	1.45×10^{-4}	3.40	1.23×10^{-4}	3.42	2.08×10^{-4}	2.07	1.52×10^{-4}	3.76×10
5	4.14×10^{-4}	3.13×10^{-1}	3.43×10^{-4}	3.19×10^{-1}	6.39×10^{-4}	2.24×10^{-1}	3.82×10^{-4}	2.99
6	9.94×10^{-4}	2.88×10^{-2}	8.12×10^{-4}	2.98×10^{-2}	1.26×10^{-3}	2.41×10^{-2}	1.13×10^{-3}	2.38×10^{-1}
7	2.94×10^{-3}	2.65×10^{-3}	2.41×10^{-3}	2.78×10^{-3}	4.97×10^{-3}	2.60×10^{-3}	3.61×10^{-3}	1.89×10^{-2}
8	5.96×10^{-3}	2.44×10^{-4}	4.23×10^{-3}	2.59×10^{-4}	8.35×10^{-3}	2.81×10^{-4}	1.77×10^{-2}	1.51×10^{-3}
9	2.07×10^{-2}	2.25×10^{-5}	1.50×10^{-2}	2.42×10^{-5}	2.44×10^{-2}	3.03×10^{-5}	2.39×10^{-2}	1.20×10^{-4}

3.6.2. Nonlinear Viscoelastic Properties

Figure 3-3 and Figure 3-4 present the extracted nonlinear viscoelastic parameters. According to these figures, g_1 increases as the deviatoric stress level increases while g_2 decreases as the deviatoric stress level increases. The product of g_1 by g_2 (i.e., $g_1 \times g_2$) controls the nonlinearity of the strain response during the loading stages while g_2 dominates the nonlinearity of the strain response during the recovery. As shown in Figure 3-3 and Figure 3-4, both $g_1 \times g_2$ and g_2 values decrease as the deviatoric stress level increases. This observation is physically sound since higher deviatoric stress levels cause permanent rotation and sliding of the aggregates to form a stiffer microstructure, which builds up more resistant against the applied load. According to Equation 3-2, reduction in the value of $g_1 \times g_2$ leads to a drop in the effective transient compliance (i.e., $g_1 \times g_2 \Delta D$). Therefore, as the deviatoric stress level increases, the effective transient compliance decreases.

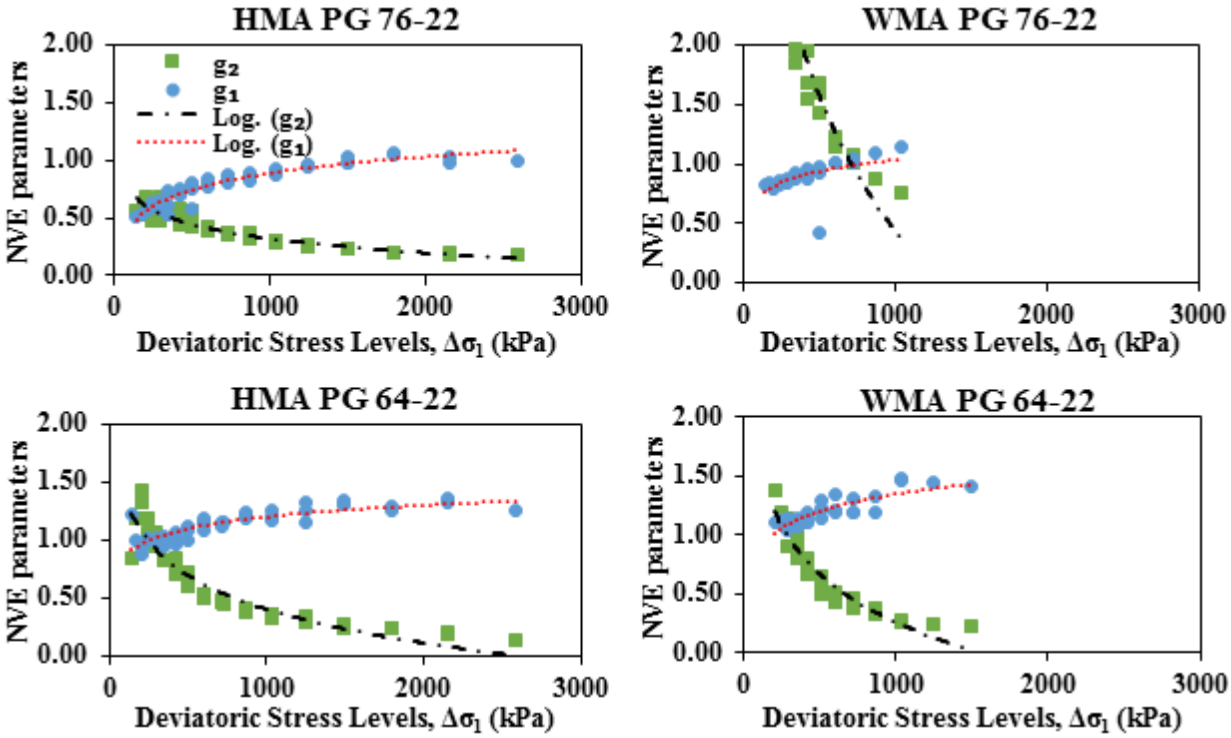

Figure 3-3: Variation of nonlinear parameters g_1 and g_2 with respect to the level of deviatoric stress level.

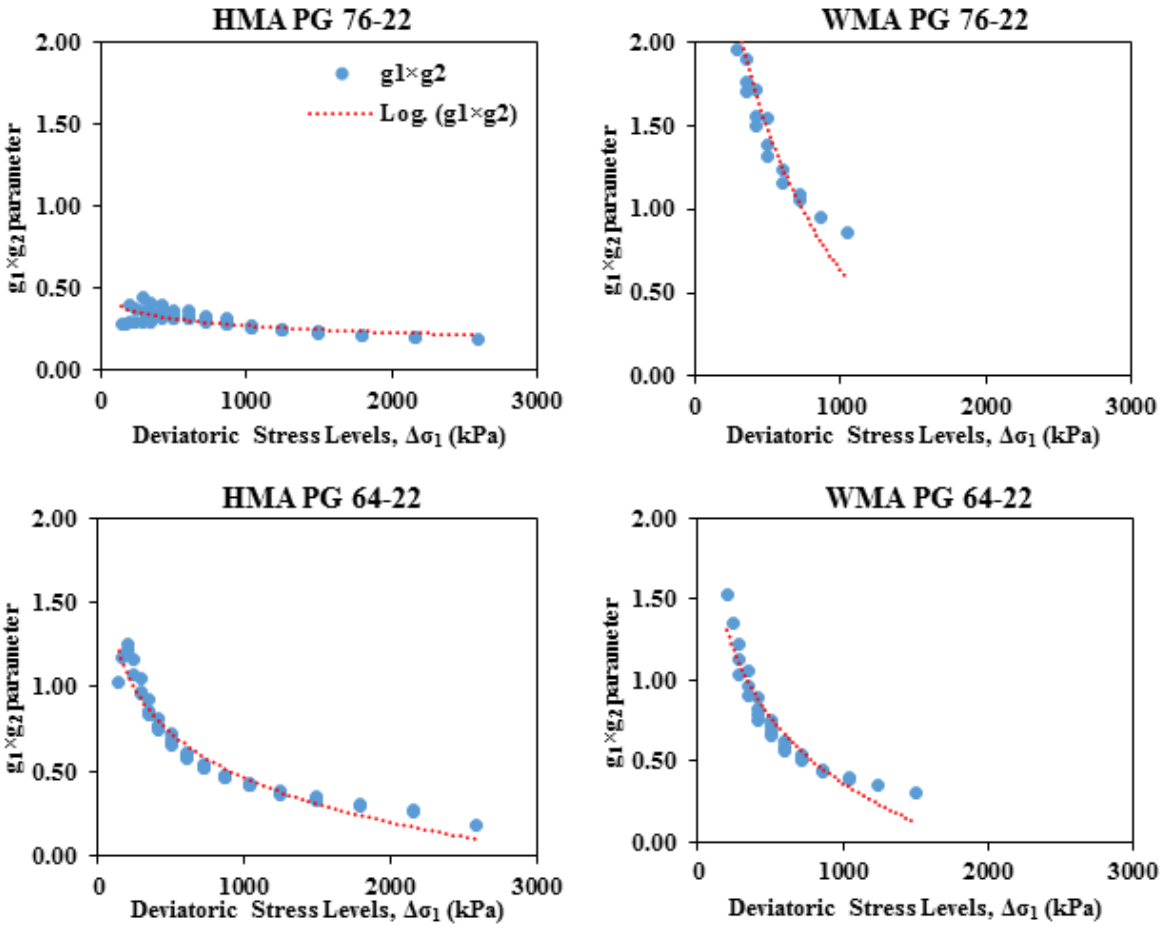

Figure 3-4: Variation of the nonlinear parameter $g_1 \times g_2$ with respect to the level of deviatoric stress level.

Figure 3-5 compares the experimental measurements and the calibrated nonlinear viscoelastic model predictions for recovered strain. As shown in Figure 3-5, the predictions of the calibrated NVE model agree well with experimental measurements. It is observed that HMA PG76-22 yields the lowest level of recovered strain. This could be due to high viscosity of modified PG 76-22 which results in higher values of the dynamic modulus E^*. For the same stress level, as the dynamic modulus increases the induced NVE strain and therefore the recovered strain decreases.

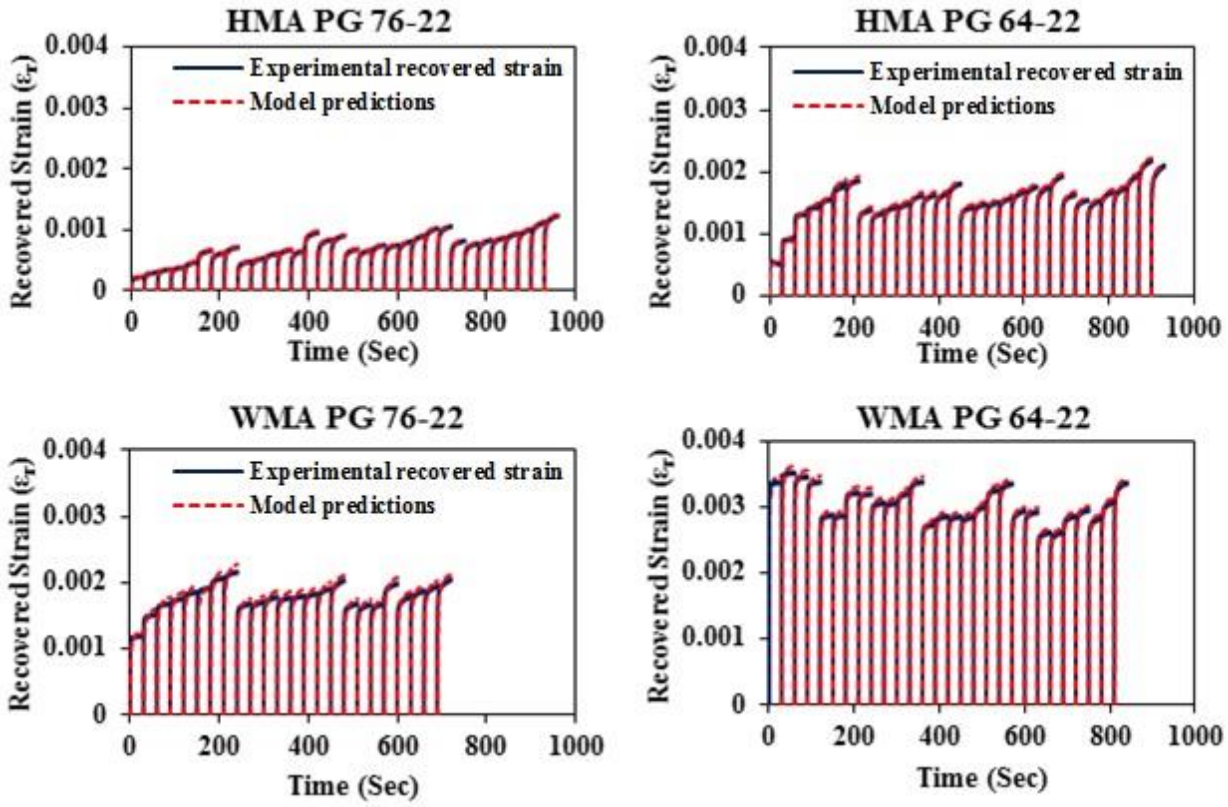

Figure 3-5: Comparison of the experimental measurements and the model predictions for the recovered strain response.

Figure 3-3 and Figure 3-4 show the variation of the nonlinear viscoelastic parameters with respect to the deviatoric stress. However, as mentioned, both confinement and deviatoric stress levels affect the nonlinear viscoelastic response of asphalt concrete. Figure 3-6 and Figure 3-7 illustrate the variation of nonlinear viscoelastic parameters with respect to the triaxiality ratio. The triaxiality ratio, η, accounts for the combined effects of confinement pressure, deviatoric stress level, and multi-axial state of stresses within a single scalar parameter. Figure 3-6 and Figure 3-7 clearly show that the nonlinear parameters are highly correlated to the level of the triaxiality ratio and can be represented as a power law function of this parameter. Therefore, the following model is proposed for the nonlinear viscoelastic properties, as shown in Equation 3-13:

Equation 3-13 $$g_i(\eta) = a_i \eta^{b_i}, \quad i = 1,2; \quad g_1 g_2 = \alpha \eta^{\beta}$$

where a_i , b_i , α , and β are model parameters. Figure 3-6 and Figure 3-7 clearly show that as the triaxiality ratio increases, the variation of the nonlinear parameters decreases. A high triaxiality ratio indicates a high level of confining pressure or low level of deviatoric stresses. Obviously, asphalt concrete demonstrates less variation in deformation at high confining pressures and low deviatoric stress levels. Moreover, as the confinement pressure increases, the same level of the deviatoric stress has a lesser effect on the nonlinear response of asphalt concrete materials. Therefore, asphalt concrete materials show less time-dependent response at high confinement levels.

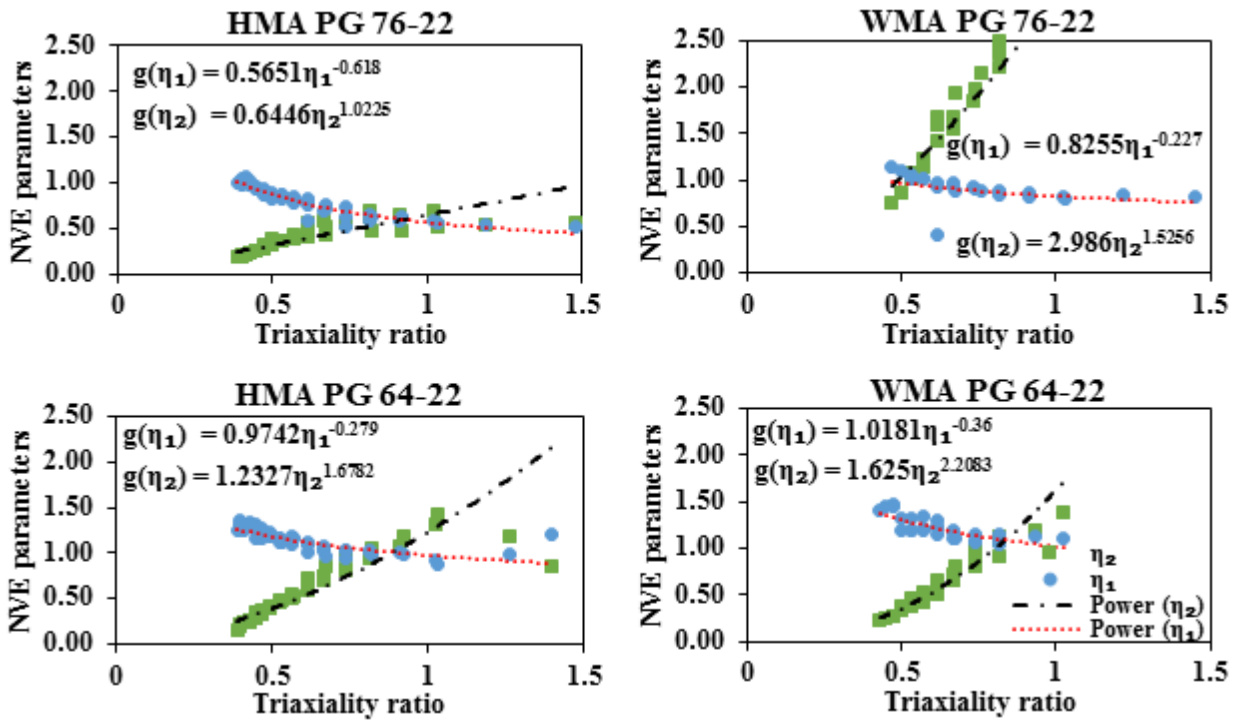

Figure 3-6: Variation of the nonlinear viscoelastic parameters g_1 and g_2 with respect to the triaxiality ratio.

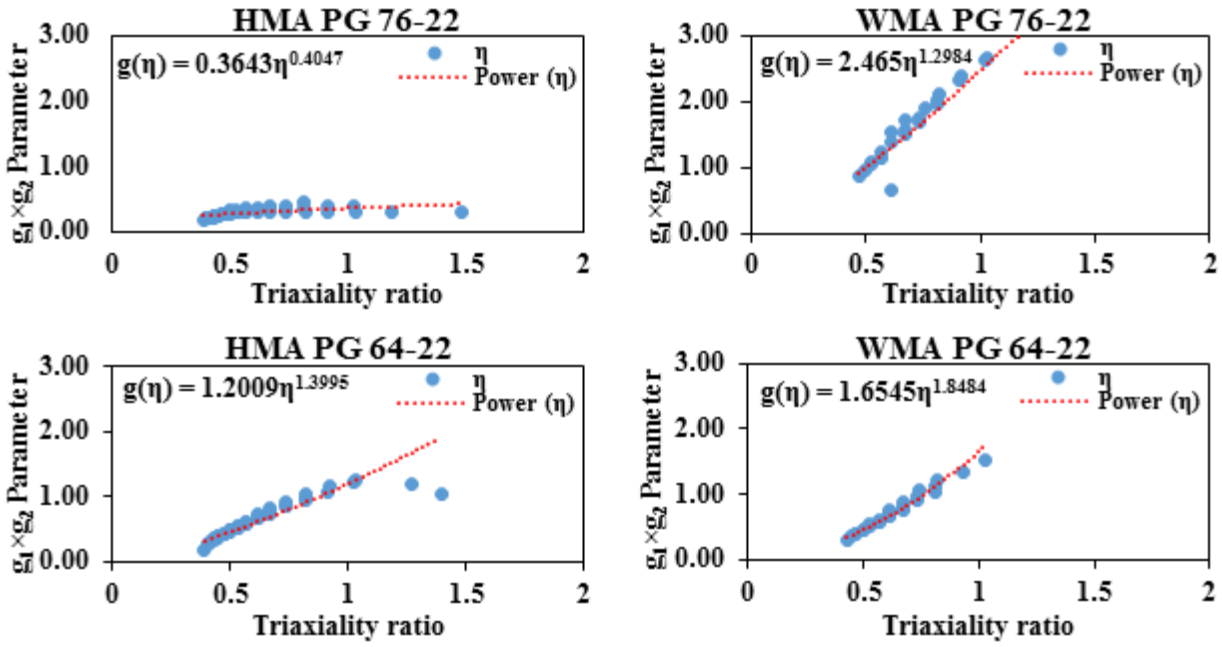

Figure 3-7: Variation of the nonlinear viscoelastic parameter $g_1 \times g_2$ with respect to the triaxiality ratio.

The results presented in this study agrees with the results reported by pervious researchers (*75; 189*). In addition, expressing the NVE responses using g_1 and g_2 through the expression of triaxiality ratio will considerably simplify the implementation of the NVE response of asphalt concrete materials. Eventually, application of the triaxiality ratio enhances the Schapery's (*78*) nonlinear viscoelastic model by considering the NVE response of asphalt concrete materials and structures subjected to the multi-axial state of stresses. Utilization of the NVE response as a function of the effective von Mises stress is a common practice for implementing Schapery's nonlinear model (*78*). In addition, the effect of mode of loading under multiaxial stress states can be included in Schapery's (*78*) model. This improvement is imperative for pressure sensitive materials such as asphalt concrete, geomaterials, and polymer composites.

3.7. Conclusions

This study presents a straightforward procedure to characterize nonlinear viscoelastic response of asphalt concrete materials. The proposed procedure was applied to extract linear and nonlinear viscoelastic properties of asphalt mixtures used in FAA's NAPMRC test sections. The nonlinear parameters were expressed in terms of the triaxiality ratio based on which a model was proposed. Finally, model predictions were compared with experimental measurements for validations purposes. The experimental studies, theoretical developments, and data analysis presented in this chapter lead to the following conclusions:

- The proposed procedure along with the dynamic modulus and RCRT-VS tests can be used effectively to characterize nonlinear viscoelastic responses of asphalt concrete materials;
- The nonlinear viscoelastic response of asphalt concrete strongly depends on confining pressure, deviatoric stress level, and multi-axial state of stresses. Therefore, uniaxial tests such as uniaxial creep-recovery tests cannot be used accurately to characterize nonlinear viscoelastic properties of asphalt concrete.
- The nonlinear viscoelastic properties are highly correlated to the triaxiality ratio that accounts for confinement pressure, deviatoric stress level, and multi-axial stress states;
- The proposed model for nonlinear viscoelastic properties as a function of triaxiality ratio can be used effectively to simulate the nonlinear response of pavements under traffic when specific locations in pavement structures are subjected to general multi-axial state of stresses.

- The nonlinear viscoelastic response of asphalt concrete materials can be effectively expressed as a function of the triaxiality ratio.
- The nonlinear parameter g_1 decreases with the increase in triaxiality ratio leading to less creep strain either as the confinement level increases or the deviatoric stress level decreases.
- The nonlinear parameter g_2 increases with the increase in triaxiality ratio leading to higher recovery of viscoelastic strain during rest period as the confinement level increases and the deviatoric stress level decreases.
- Comparisons between the characterized nonlinear viscoelastic model and experimental measurements illustrate the capabilities of the proposed model and characterization procedure in capturing nonlinear viscoelastic response of asphalt concrete materials.

4. Chapter 4: A Straightforward Procedure to Characterize Viscoplastic and Hardening-relaxation Viscoplastic Response of Asphalt Concrete at High Temperatures

4.1. Abstract

This chapter presents a straightforward procedure for determining viscoplastic (VP) and hardening-relaxation (HR) viscoplastic properties of asphalt concrete materials using Genetic Algorithms (GAs) that employs concepts of Natural Selection and Genetic Inheritance of the Darwinian principle (*190*), which inspired by the biological evolution process as a class of probabilistic optimization algorithms. The simplified procedure allows for easy characterization of VP and HR viscoplastic responses. First, dynamic modulus tests are performed to calibrate linear viscoelastic (LVE) properties. Then, Perzyna-type viscoplasticity model (*79*) is used to represent the VP behavior. Repeated creep-recovery tests at variable deviatoric stress levels (RCRT-VS) were designed and conducted to calibrate the nonlinear viscoelastic (NVE) and VP properties of four types of mixtures used in the FAA's NAPMRC test sections. Saturated yield stress of all mixtures are obtained using uniaxial constant strain rate in compression (UCSR-C) tests. Moreover, repeated creep-recovery tests at constant loading and rest time (RCRT-CLR) were designed and conducted to calibrate HR viscoplastic properties of all four types of mixtures based on the model proposed by Darabi et al. (*69; 71*). Once calibrated, the model was validated by comparing the model predictions and experimental measurements using the traffic tests results conducted by FAA on NAPMRC flexible pavement test sections (*131*). The predictions indicate that the proposed method is capable of characterizing VP and HR viscoplastic responses of asphalt concrete materials. Both of WMA and HMA PG 64-22 test were found to be the worst performing test in terms of resulting in more VP and HR viscoplastic strain, which will result in more rutting. The HMA PG 76-22 performed slightly better than the respective WMA test.

4.2. Introduction

The conventional mechanistic-based methods for characterization of the response of asphalt concrete materials require multiple experimental tests and analyses of multi-axial state of stresses. One of the main obstacles that prevents the pavement engineers from using these models is the lack of straightforward and simple procedures to extract the material properties associated with these models. However, such simplifications should maintain the accuracy of the analysis as well. This manuscript aims to contribute in simplifying these procedures while maintaining the accuracy.

Serviceability and safety over the performance life of asphalt pavements are the most concern in asphalt concrete pavements cause by two major distress, rutting and fatigue damage. Permanent deformation under the wheels' path, rutting, is more dominant at high temperatures while evolution of micro-cracks and micro-voids, fatigue damage, generally is more problematic at low and intermediate temperatures (*86; 164; 165*). Constitutive modeling of rutting and fatigue damage mechanisms have been studied through several proposed viscoplastic and viscodamage constitutive relationships (*42; 48; 72; 79; 169-174; 179; 191-193*). These mechanisms result because of the temperature-dependency of asphalt binders, the complex composite microstructure of asphalt concrete, and localization of strain in the binder phase due to significant differences between the moduli of the asphalt binder and the aggregate phases (*47; 175; 176; 194*). Schapery's (*78*) nonlinear viscoelastic model has been widely used to represent the viscoelastic response of asphalt concrete materials and structures (*45; 50; 75; 80; 81; 177-185; 195*). A straightforward procedure to extract NVE parameters of asphalt concrete materials while maintaining the required level of accuracy by incorporating the important factors affecting this mechanism is presented

recently. More information on characterization of LVE and NVE properties of asphalt concrete materials can be found in Bazzaz, et al. (*196*).

In this chapter, having LVE and NVE properties of asphalt concrete materials in hand by applying dynamic modulus and RCRT-VS tests, we used UCSR-C test to extract saturated yield stress of all mixtures of FAA's NAPMRC test sections. Accurate estimation of VP and HR responses of asphalt concrete materials requires precise characterization of complex mechanical responses. The HR viscoplastic parameters of asphalt concrete materials were extracted using RCRT-CLR and analyzing the data using optimization technics as Genetic Algorithms (GAs) for the first time by pavement community.

There are three approaches to machine intelligence including logic-based search, cultural search, and genetically or evolutionary search (*197*). These approaches developed by Turing (1948) to connect tween searches and the challenge of getting a computer to solve a problem without explicitly programming it. Logic-based search is an approach, which is a search through the space of integers representing candidate computer programs. Cultural search relies on knowledge and expertise acquired over a period of years from others. Genetically or evolutionary search by which a combination of genes is looked for, the criterion being the survival value. GAs are particularly well suited for hard problems where little is known about the underlying search space. GAs are widely-used in business, science, and engineering (*198-200*). Surprisingly, there are very few papers, which are using optimization technics on asphalt concrete (*201-204*). Moreover, just one of them presents optimization technics to extract the material properties of asphalt concrete, which used harmony search (HS) algorithm to extract viscoelastic and damage properties of HMA concrete (*203*). However, extraction of VP and HR viscoplastic properties of asphalt concrete materials are part of many engineering optimization problems, which are very

complex in nature and quite difficult to be solved using gradient-based search algorithms. Specially, when there are local optimums in the problem, the results shall depend on selected initial points, and the obtained optimal solution may not necessarily be the global optimum. This paper, for the first time, presents GAs to capture the VP and HR viscoplastic properties of asphalt concrete materials.

4.3. Objectives

The primary objectives of the study presented in this paper are to:

- Develop a straightforward procedure that allows for identification of VP and HR viscoplastic response of asphalt concrete materials;
- Incorporate the GAs into the proposed procedure to extract VP and HR viscoplastic properties of asphalt concrete materials as one of many engineering optimization problems;
- Introduce laboratory tests which can be used systematically to extract VP and HR viscoplastic parameters while mimicking the realistic stress states observed in a pavement structure;
- Apply the proposed method to extract VP and HR viscoplastic parameters associated with asphalt mixtures used in FAA's NAPMRC test sections;
- Propose a mechanistic-based model for VP and HR viscoplastic parameters of asphalt concrete when subjected to general multi-axial state of stresses.

4.4. **Analysis Approaches**

The total strain of an asphalt mixture can be decoupled into a recoverable (viscoelastic) component and an irrecoverable (visco-plastic) component with the assumption of a small strain deformation as shown in Equation 4-1:

Equation 4-1 $$\varepsilon^{total} = \varepsilon^{rec(ve)} + \varepsilon^{irrec(vp)}$$

where ε^{total} is the total strain. The terms $\varepsilon^{rec(ve)}$ and $\varepsilon^{irrec(vp)}$ are the recoverable (viscoelastic) and irrecoverable (viscoplastic) strain components, respectively. The Schapery's (*78*) non-linear visco-elastic theory to capture the recoverable (viscoelastic) components of asphalt mixture which implemented by the authors recently (*75; 196*). This study emphasis on the irrecoverable (viscoplastic) components, which were decomposed from recoverable (viscoelastic) components. More information and detailed procedure of characterization of NVE properties of asphalt concrete materials can be found in Chapter 3: A Straightforward Procedure to Characterize Nonlinear Viscoelastic Response of Asphalt Concrete at High Temperatures and Bazzaz, et al. (*196*).

4.4.1. Perzyna-type Viscoplastic Model

The classical hardening Perzyna-type VP model (*79*) has been applied frequently to model the VP response of asphalt concrete (*107; 116; 169; 205*). The classical nonassociative VP flow rule is introduced as shown in Equation 4-2:

Equation 4-2 $$\dot{\varepsilon}_{ij}^{vp} = \dot{\gamma}^{vp} \frac{\partial F}{\partial \sigma_{ij}}$$

where ε^{vp} is VP strain tensor; $\dot{\gamma}^{vp}$ and F represent the VP multiplier and the VP potential function, respectively; The $\dot{\gamma}^{vp}$ can be expressed in terms of an overstress function and a fluidity parameter (*79*) as shown in Equation 4-3:

Equation 4-3 $$\dot{\gamma}^{vp} = \Gamma^{vp} \left\langle \phi(f) \right\rangle^{N}; \qquad \phi(f) = \frac{f}{\sigma_y^0}$$

where Γ^{vp} is the VP fluidity parameter, N is the VP rate-sensitivity exponent, $\langle\ \rangle$ is the Macaulay brackets defined by $\langle\phi\rangle = (\phi + |\phi|)/2$, ϕ is the overstress function which is expressed in terms of the yield function f, σ_y^0 and is a yield stress quantity used to normalize the overstress function and can be assumed unity.

Due to the nonassociative nature of the VP response of asphalt concrete (*206*), a nonassociative viscoplasticity model is applied. A modified Drucker-Prager-type yield surface function, f, and a viscoplastic potential function, F, are defined (*116*) as shown in Equation 4-4:

Equation 4-4 $$f = \tau - \alpha I_1 - \kappa(p); \qquad F = \tau - \beta I_1; \qquad \tau = \frac{\sqrt{3J_2}}{2}\left[1 + \frac{1}{d^{vp}} + \left(1 - \frac{1}{d^{vp}}\right)\frac{3J_3}{\sqrt{3J_2^3}}\right]$$

where α and β are the pressure-sensitivity material parameters; $I_1 = \sigma_{kk}$ is the first stress invariant; τ is the deviatoric effective shear stress; $J_2 = \frac{1}{2}\bar{S}_{ij}\bar{S}_{ij}$ and $J_3 = \frac{1}{2}\bar{S}_{ij}\bar{S}_{jk}\bar{S}_{ki}$ are second and third deviatoric stress invariants, respectively; d^{vp} is the parameter that distinguishes the VP responses during extension and contraction mode of loadings; and κ is the hardening function expressed as shown in Equation 4-5:

Equation 4-5 $$\kappa(p) = \kappa_0 + \kappa_1\left[1 - \exp(-\kappa_2 p)\right]; \qquad \dot{p} = \left[1 + 2\left(\frac{0.5 + \beta/3}{1 - \beta/3}\right)\right]^{-0.5}\sqrt{\dot{\varepsilon}_{ij}^{vp}\dot{\varepsilon}_{ij}^{vp}}$$

where p is the effective VP strain, κ_0, κ_1, and κ_2 are VP material parameters; κ_0 defines the initial yield strength, $\kappa_0 + \kappa_1$ determine the saturated yield stress, and κ_2 is the strain hardening rate.

4.4.2. Hardening-relaxation Viscoplastic Model

The Hardening-relaxation constitutive relationship and its associated parameters when subjected to cyclic creep loading with rest periods between the loading cycles, the VP behavior of asphalt concrete materials changes such that the rate of accumulation of the VP strain at the beginning of a loading cycle increases comparing to that at the end of the preceding loading cycle. This phenomenon is referred to as the *hardening-relaxation* and is a key element in predicting the permanent deformation (rutting) of asphalt concrete materials. Figure 4-1 schematically presents the underlying phenomenon for the hardening relaxation mechanism and illustrates the need to modify the classical Perzyna-type viscoplastic model to incorporate this important mechanism. Consider one cycle of creep-recovery loading, as shown in Figure 4-1. During the loading cycle, aggregates reorient and confine the binder in between. At this stage, the viscoplastic strain evolves and induces a level of viscoplastic hardening in the material as shown in Figure 4-1(c). During the rest period, the induced hardening stresses redistributes the aggregates and therefore the induced hardening stresses relax. This relaxation in the internal hardening stresses changes the level of the viscoplastic hardening. This phenomenon is referred to as the hardening-relaxation (*69*).

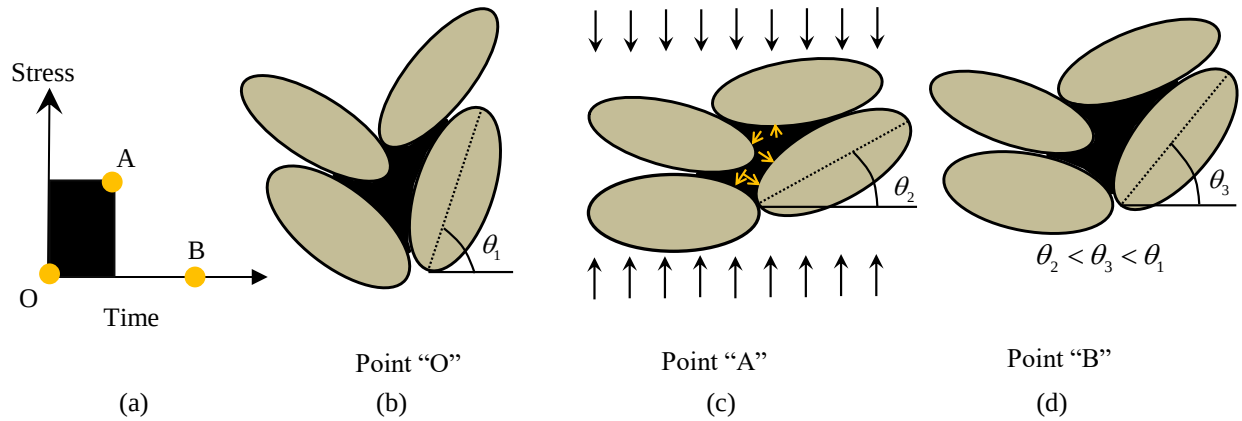

Figure 4-1: Schematic representation of the changes in the asphalt mixtures microstructure during a cyclic creep cycle. (a) Stress history; (b) initial microstructure; (c) microstructure during the loading; (d) microstructure during the rest period (*69*).

This phenomenon can also be explained from the thermodynamic point of view. During the rest period, the viscoplastic strain does not evolve and remains constant. Therefore, the force conjugate to the viscoplastic strain (i.e., the hardening level) should relax. This effect if more pronounced for time-dependent materials (e.g., asphalt mixtures) and signifies at elevated temperatures. The conventional viscoplastic theories, however, do not account for the evolution of the viscoplastic properties during the resting period and significantly underestimate the prediction of the viscoplastic strain response. Figure 4-2 shows the prediction of a calibrated Perzyna-type viscoplastic model as compared to experimental measurements. Figure 4-2 shows that the conventional Perzyna-type viscoplastic model cannot accumulates more viscoplastic strain once the viscoplastic strain saturates, such that no more viscoplastic strain accumulates during the following loading cycles. However, experimental measurements show that the material gains its capability to accumulate more viscoplastic strain during the rest period, such that the viscoplastic strain keeps accumulating during all loading cycles.

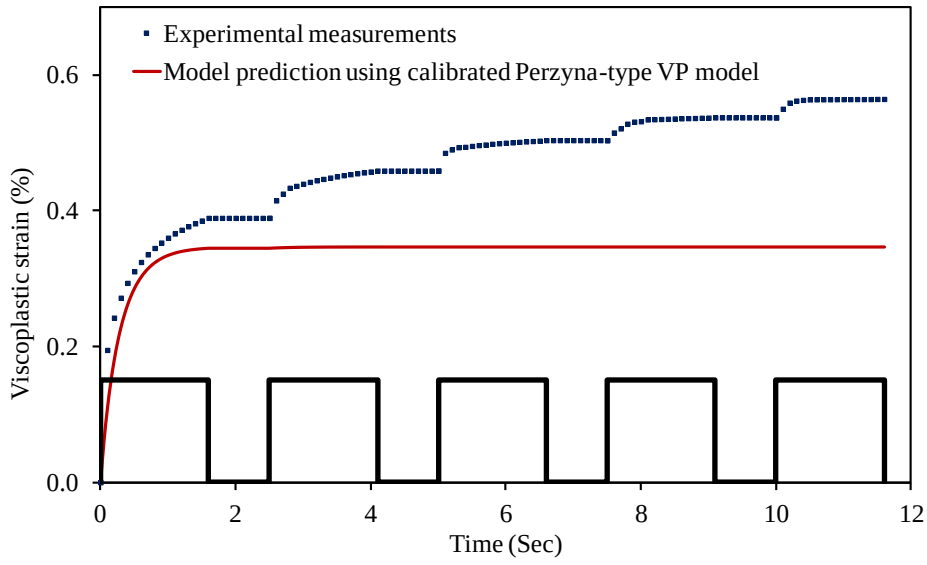

Figure 4-2: Predictions of a calibrated classical Perzyna-type viscoplastic model and experimental measurements of viscoplastic strain for a cyclic creep test (*69*).

To remedy this issue, the hardening level should be allowed to undergo relaxation during the rest period. Motivated by the experimental observations, the mechanisms at microstructural level, and thermodynamic description, a hardening-relaxation model using the HR memory concept is developed by Darabi, et al. (*68*). To model the HR, static and dynamic HR memory surfaces are defines as shown in Equation 4-6:

Equation 4-6 $$f^{h-r} = p - q^{vp} \le 0; \qquad \chi^{h-r} = p - q^{vp} - \left(\frac{\dot{q}^{vp}}{\Gamma^{h-r}} \right)^{\frac{1}{S_1}} \le 0$$

where f^{h-r} and χ^{h-r} are static and dynamic HR memory surfaces, respectively. The term q^{vp} is the HR internal state variable that memorizes the maximum experienced viscoplastic strain for which the HR has occurred while p is the effective viscoplastic strain. Parameters Γ^{h-r} and S_1 are HR parameters. The rate of relaxation in the hardening parameter is calculated as shown in Equation 4-7:

Equation 4-7 $$\dot{\kappa}_1 = -S_2 \dot{q}^{vp}$$

where S_2 is another parameter associated with the HR constitutive relationship. Table 4-1 lists the parameters associated with the HR constitutive relationship and their physical significance. Repeated creep-recovery test at constant loading and rest times (RCRT-CLR) will be used to identify the HR parameters.

Table 4-1: List of hardening-relaxation VP parameters.

Parameter	Physical meaning
Γ^{h-r}	Hardening-relaxation fluidity parameter controlling the rate of evolution of the hardening-relaxation state variable.
S_1	Hardening-relaxation exponent controlling the time-dependency of the hardening-relaxation state variable.
S_2	Hardening-relaxation parameter controlling the rate at which the hardening parameter relaxes.

Figure 4-3 demonstrates the effect of rest period in the accumulation of viscoplastic strain obtained from the proposed hardening-relaxation model coupling with Perzyna-type viscoplastic model, respectively. The result shows that as the rest period increases, the material develops more capacity to accumulate viscoplastic strain, which is in agreement with experimental observations.

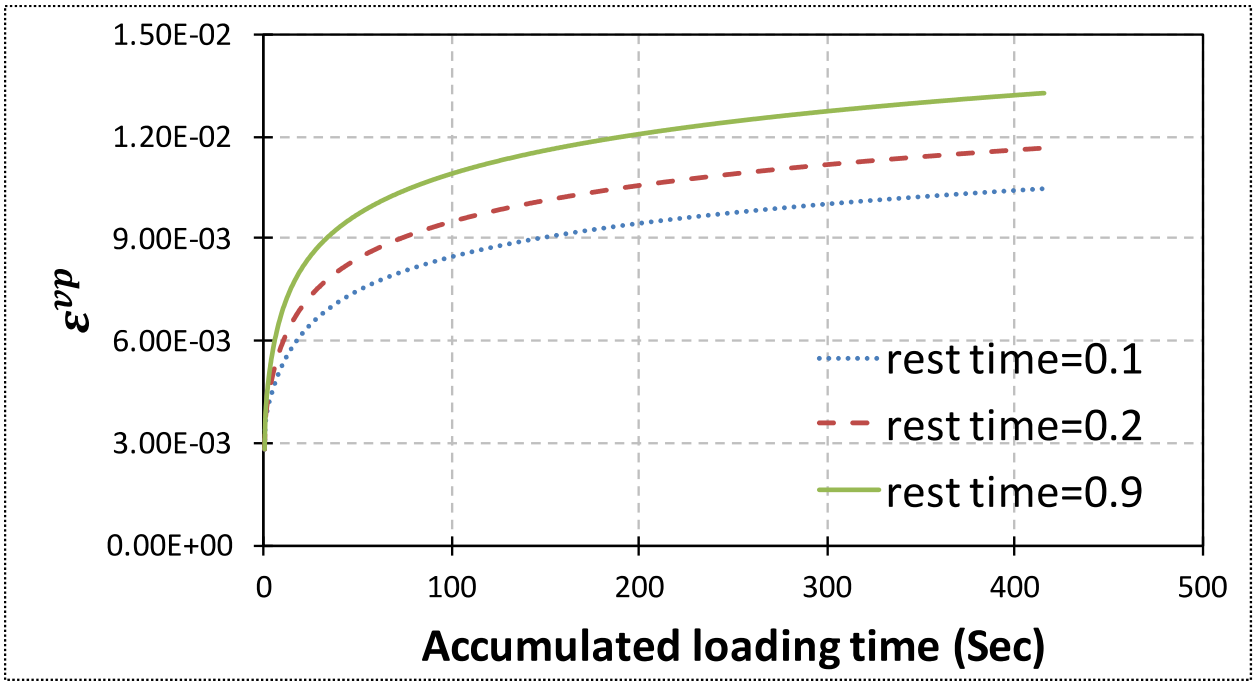

Figure 4-3: The effect of rest period in hardening-relaxation model.

4.4.3. Genetic Algorithms Analysis

The genetic algorithms (GAs) are originally developed by John Holland (*207*), which apply concepts of Natural Selection and Genetic Inheritance of the Darwinian principle (*190*). GAs are inspired by the biological evolution process as a class of probabilistic optimization algorithms. GAs iteratively transform a set (called a population) of mathematical objects (typically fixed-length binary character strings), each with an associated fitness value, into a new population of offspring objects using the Darwinian principle (*190*) of natural selection and using operations that

are patterned after naturally occurring genetic operations, such as crossover (sexual recombination) and mutation. Probabilistic steps could be illustrated such that the initial population is typically random, probabilistic selection based on fitness which means neither the best is always picked nor the worst is necessarily excluded, random picking of mutation and crossover points, and there usually is probabilistic scenario as part of the fitness measure.

Genetic programming (GP) applies the approach of the GAs to the space of possible computer programs. Computer programs are the *lingua franca* for expressing the solutions to a wide variety of problems. A wide variety of seemingly different problems from many different fields can be reformulated as a search for a computer program to solve the problem. GP is an automated invention machine which is routinely delivers high-return human-competitive machine intelligence and has delivered a progression of qualitatively more substantial results in synchrony with five approximately order-of-magnitude increases in the expenditure of computer time. High-return is the artificial-to-intelligence ratio (AI ratio) of a problem-solving method as the ratio of which is delivered by the automated operation of the artificial method to the amount of intelligence that is supplied by the human applying the method to a particular problem. A problem solving method is routine if it is general and relatively little human effort is required to get the method to successfully handle new problems within a particular domain and to successfully handle new problems from a different domain (*208*). Figure 4-4 illustrates the GP flowchart.

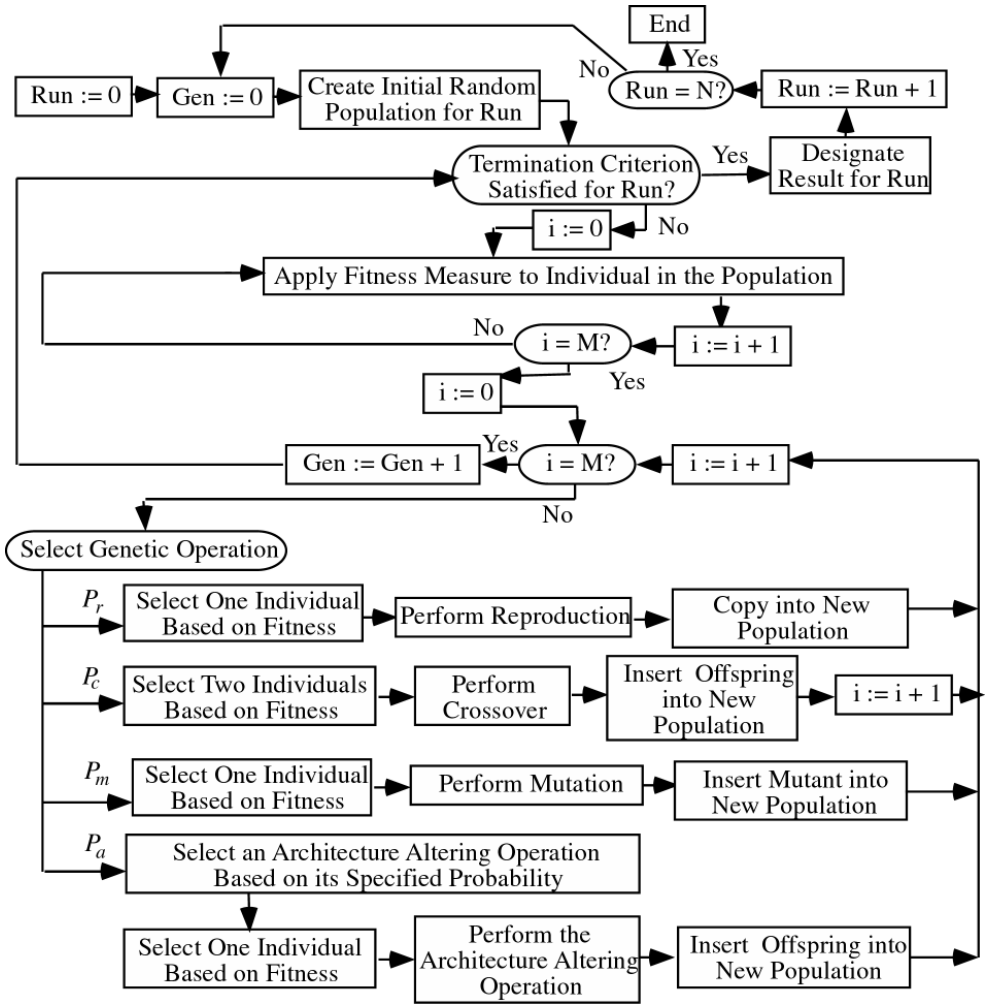

Figure 4-4: Applied GP flowchart (*208*).

4.5. Identification of Viscoplastic and Hardening-relaxation Viscoplastic Parameters

4.5.1. Assumed Viscoplastic Parameters

Some of VP parameters are assumed because they do not vary significantly from one asphalt mixture to the other and can be assumed constant with reasonable accuracy. These parameters, their physical meaning, and the recommended values are listed in Table 4-2, please refer to Huang (*126*), Abu Al-Rub et al. (*209*), and Darabi et al. (*71*) for more details on the identification of assumed VP parameters.

Table 4-2: List of VP parameters that are fixed and can be assumed.

Parameter	Recommended value	Physical significance	Assumed value
α	0.15-0.3	Related to the angle of friction of the asphalt mixtures.	0.25
β	$\alpha - 0.05$	Related to the angle of friction and the dilation characteristics of asphalt mixtures.	0.2
d^{vp}	0.778	Ratio of yield strength in tension to that in compression. Fixed for most asphalt mixes.	0.778
σ_y^0	100 kPa	Yield stress quantity	100 kPa

4.5.2. Extraction of Viscoplastic Strain During the Creep Part of RCRT-VS

Calculate the viscoelastic strain response during the loading stage of RCRT-VS, readers are referred to the recent papers published by authors and their collaborators to extract LVE and NVE parameters of asphalt concrete (*75; 210*). Once LVE and NVE parameters are identified, subtract the viscoelastic strain from the total strain to obtain the VP strain response during the creep part of RCRT-VS. Figure 4-5 illustrates the extraction of the viscoelastic and viscoplastic strain responses from the total measured strain (*69; 71*) both schematically and actually. The VP parameters will be identified by analyzing the extracted VP strain response.

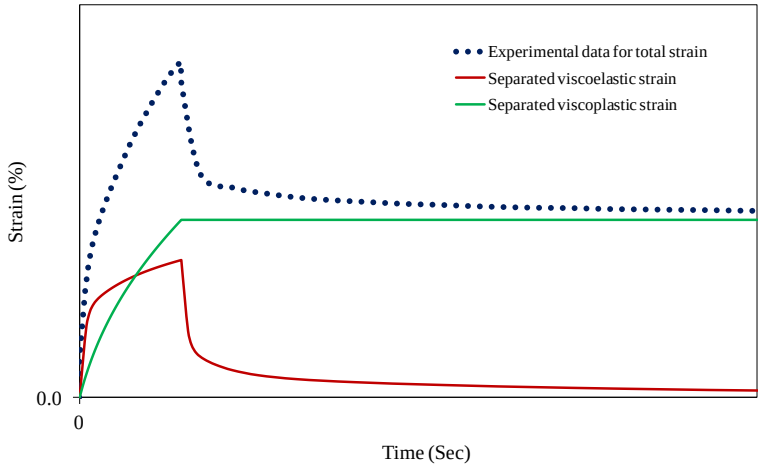

(a)

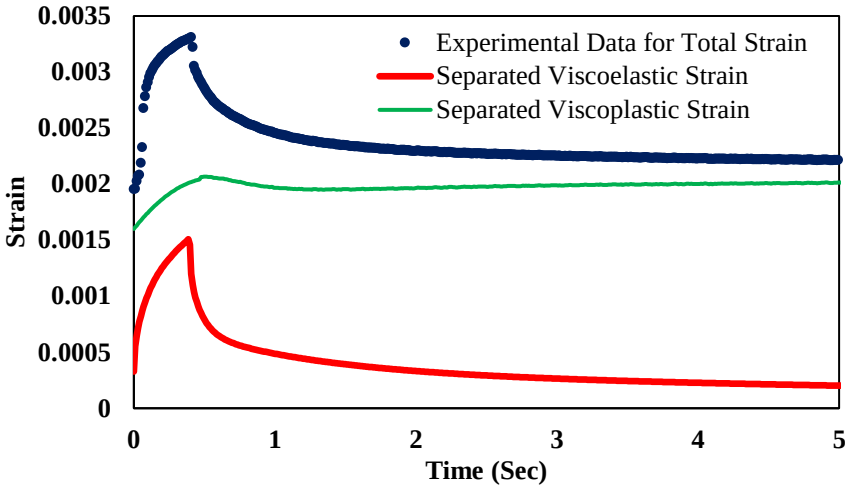

(b)

Figure 4-5: Extraction of the VP components of the strain response: (a) Schematic illustration (*70*); (b) Actual data

Calculate effective VP strain p^{Exp} using extracted a (i.e. ε_1^{vp} and ε_2^{vp}) as shown in Equation 4-8:

Equation 4-8 $$p^{Exp} = \left[1+2\left(\frac{0.5+\beta/3}{1-\beta/3}\right)\right]^{-0.5}\sqrt{\left(\varepsilon_1^{vp}\right)^2+2\left(\varepsilon_2^{vp}\right)^2}$$

Estimate radial VP strain using Equation 4-9, if radial measurements are not available.

Equation 4-9 $$\varepsilon_2^{vp} = \left(\frac{0.5+\beta/3}{1-\beta/3}\right)\varepsilon_1^{vp}$$

Manipulating Equation 4-3 and Equation 4-4 yields to Equation 4-10:

Equation 4-10 $$\frac{\Delta\gamma^{vp}}{\Delta t} = \Gamma\left[\frac{\left\{\tau-\alpha I_1-\left[\kappa_0+\kappa_1\left(1-\exp\left(-\kappa_2 p\right)\right)\right]\right\}}{\sigma_y^0}\right]^N$$

Calculate $\Delta\gamma^{vp}$ using the extracted axial VP strain $\Delta\varepsilon_1^{vp}$ as shown in Equation 4-11:

Equation 4-11 $$\Delta\gamma^{vp} = \Delta\varepsilon_1^{vp}/\left(1-\beta/3\right)$$

Figure 4-6 shows the relationship between $\Delta\gamma^{vp}$ and time for each stress level.

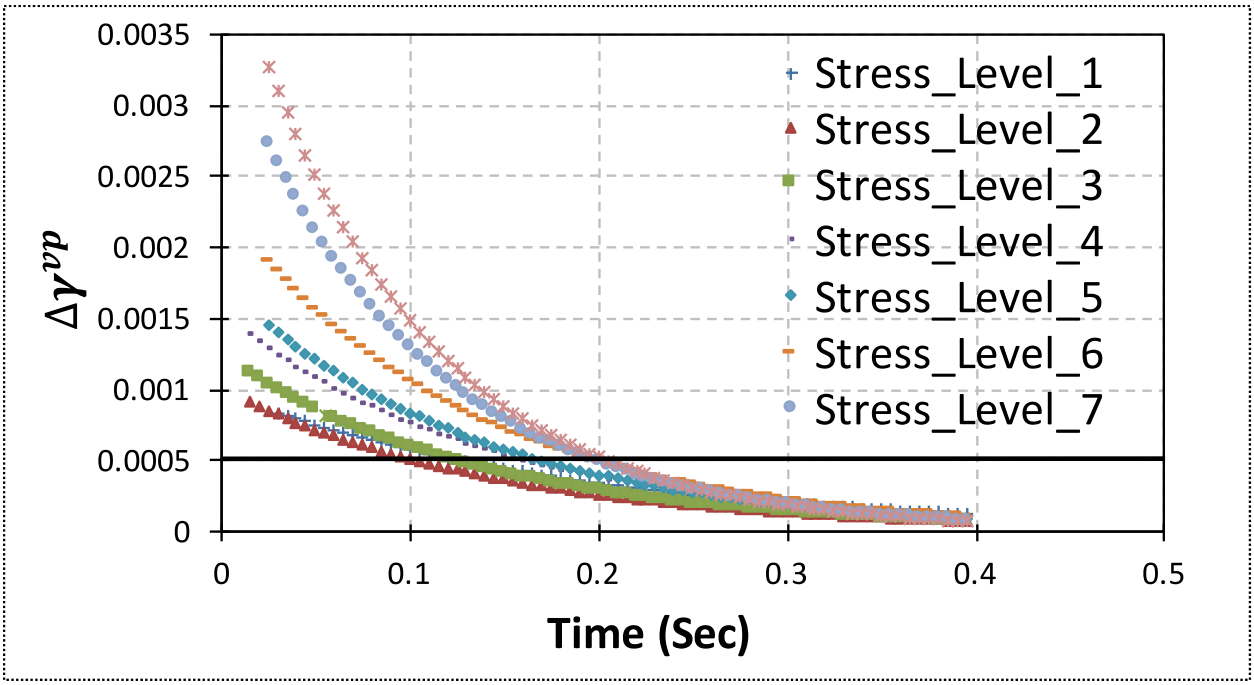

Figure 4-6: The relationship between $\Delta\gamma^{vp}$ and time for each stress level.

Pick values for $\Delta\gamma^{vp}$ at different stress levels of RCRT-VS test at constant Δt, the recommended time intervals are 0.05, 0.1, 0.15, 0.2, 0.25, 0.3, 0.35, and 0.4 second as shown in Figure 4-7.

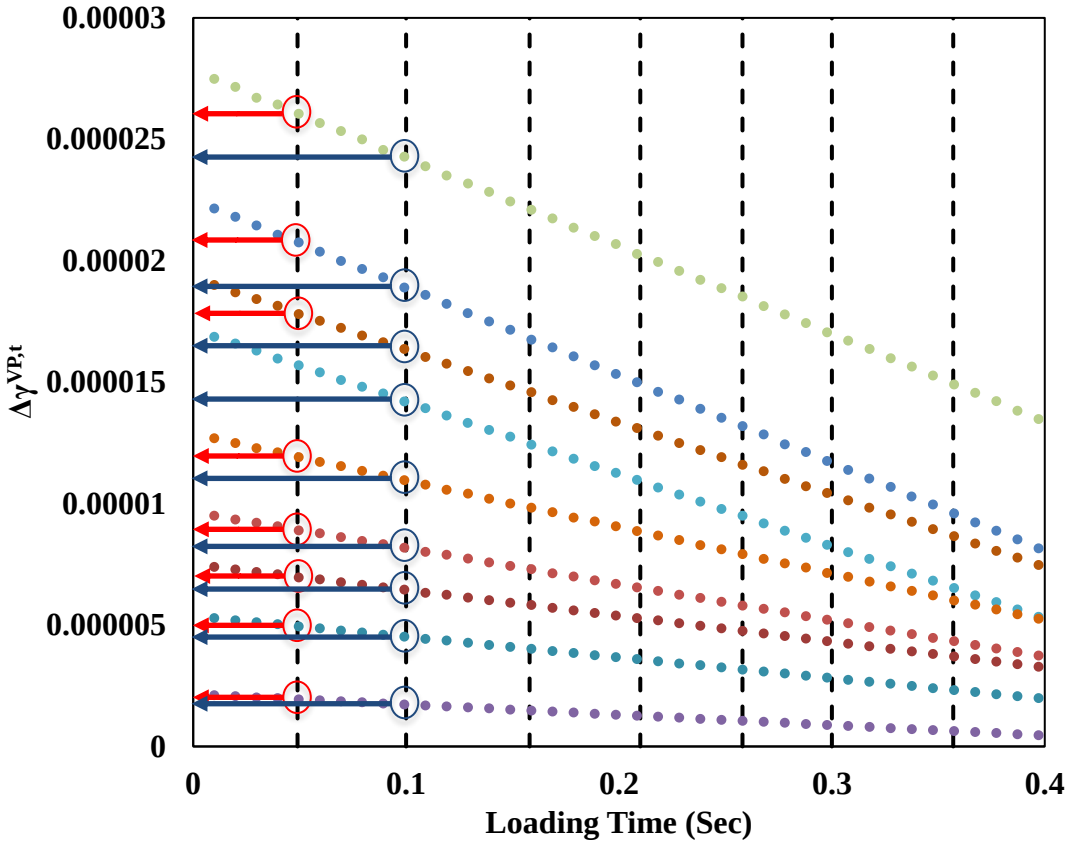

Figure 4-7: The values for $\Delta\gamma^{vp}$ at different stress levels of RCRT-VS test at constant Δt.

Rearrange Equation 4-10 to calculate p^{Model} as shown in Equation 4-12:

Equation 4-12
$$p^{Model} = -\frac{1}{\kappa_2} ln\left(1 - \frac{\tau - \alpha I_1 - \left(\sigma_y^0 \left(\frac{\Delta\gamma^{vp}}{\Gamma\Delta t}\right)^{1/N} + \kappa_0\right)}{\kappa_1}\right)$$

The parameters κ_0, κ_1, κ_2, N, and Γ are unknowns in Equation 4-12, which can be extracted by minimizing the error, i.e. Equation 4-13, between the experiments, i.e. Equation 4-8, and analysis, i.e. Equation 4-12, using GAs.

Equation 4-13 $$error = \sum_{i=1}^{K}\left[\left(\frac{p^{Model}}{p^{Exp}} - 1\right)^2\right]$$

The relationship between $\tau - \alpha I_1$ and effective VP strain can be plotted as shown in Figure 4-8.

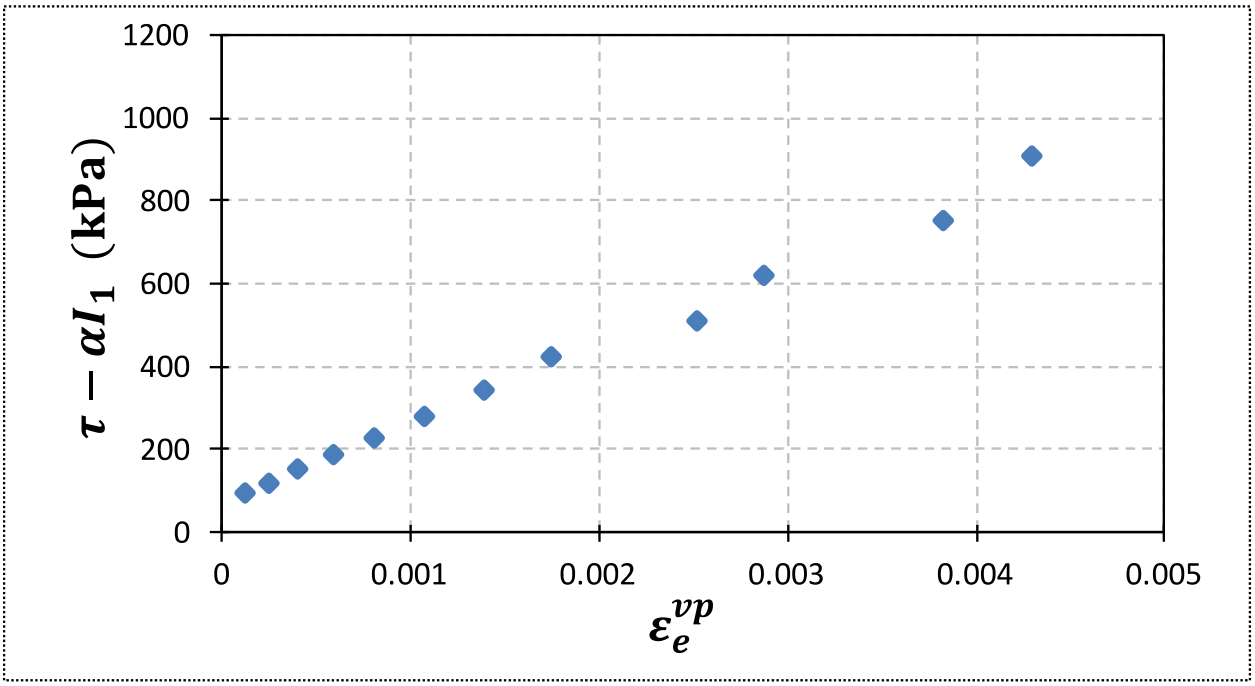

Figure 4-8: The relationship between $\tau - \alpha I_1$ and effective VP strain.

The fitting results are shown in Figure 4-9 for deviatoric stress 137.9 kPa as an example. The values of Γ remained constant for other stress levels as well.

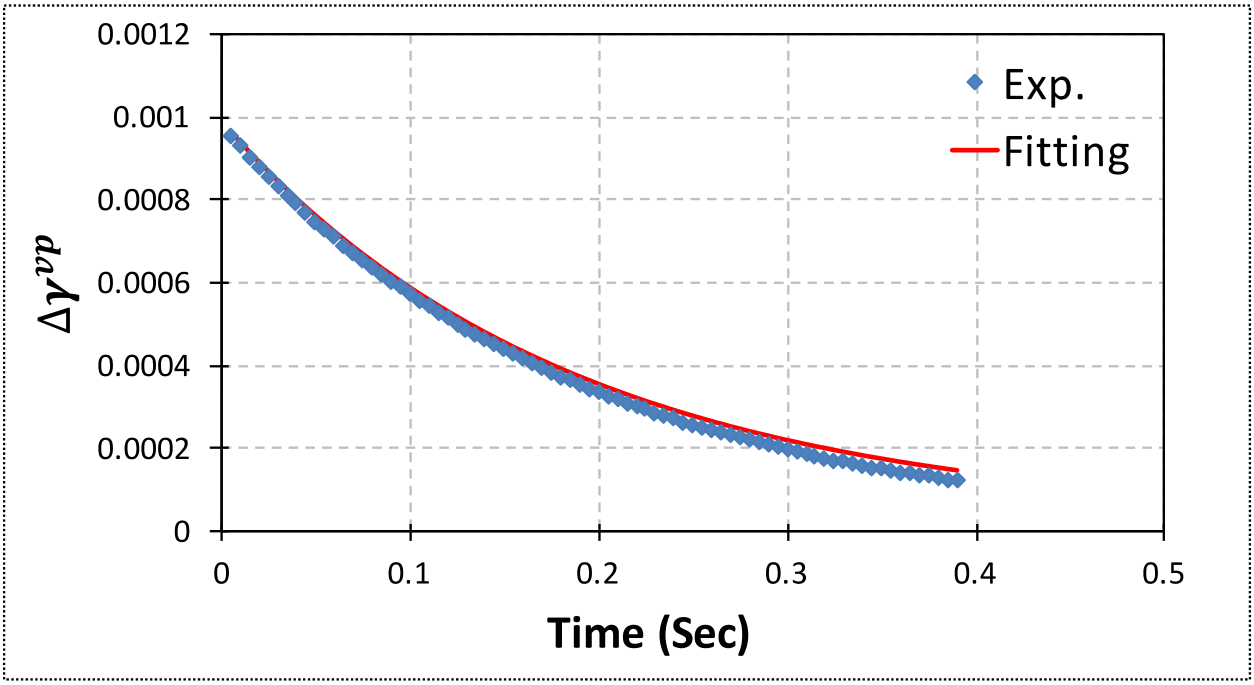

Figure 4-9: The fitting of $\Delta\gamma^{vp}$ to obtain viscoplastic parameter Γ .

4.5.3. Extraction of Hardening-relaxation Viscoplastic Parameters Using RCRT-CLR

Figure 4-10 schematically shows the evolution of the effective VP strain p and the HR state variable q^{vp} during a cycle of RCRT-CLR.

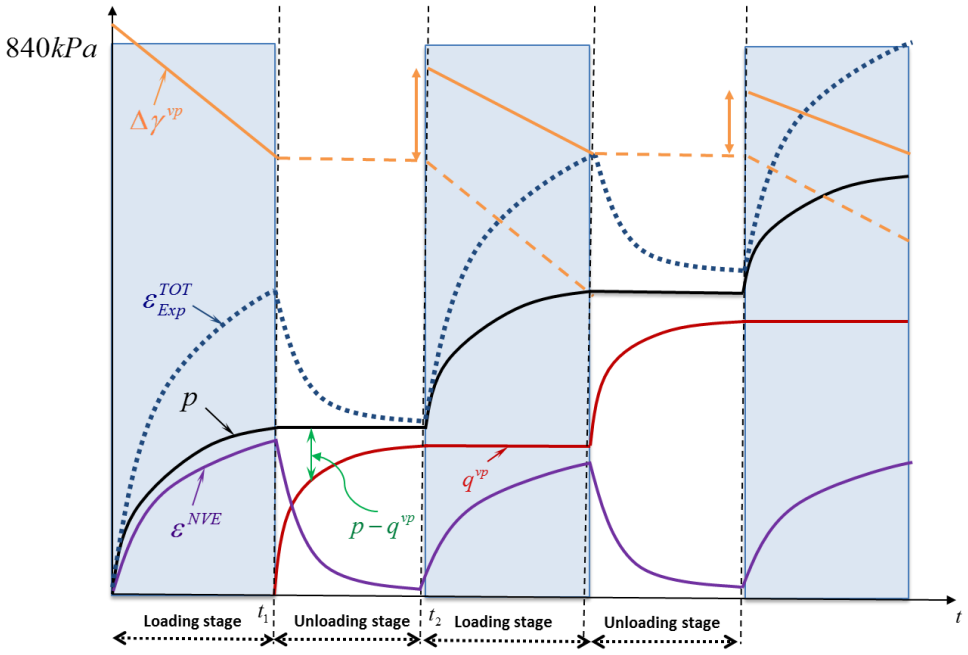

Figure 4-10: Schematic representation of the loading and unloading stages, the evolution of the total strain, the nonlinear viscoelastic strain, the effective VP strain, the hardening-relaxation viscoplastic internal state variable, and VP multiplier function during RCRT-CLR.

From the experimental measurements, calculate the rate of the effective VP strain during different loading cycles using Equation 4-14, as shown in Figure 4-11:

Equation 4-14 $$\dot{p}(t)=\frac{p_2^{Exp}-p_1^{Exp}}{\Delta t}$$

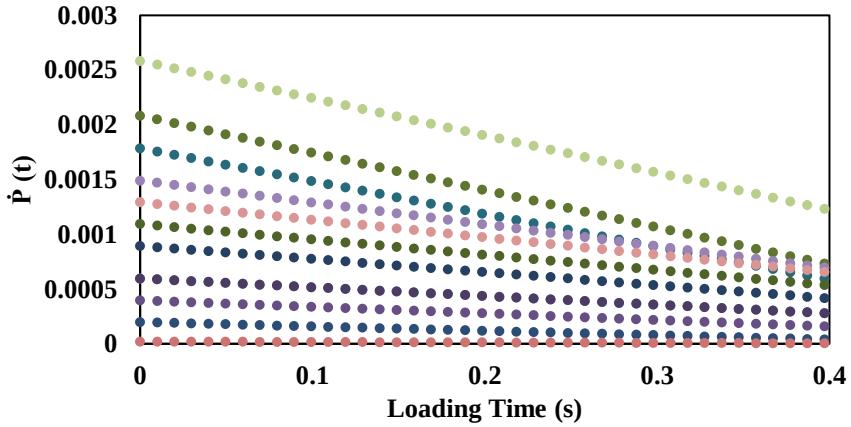

Figure 4-11: Evolution of the rate of the effective VP strain during different loading cycles of RCRT-CLR.

Simplify Equation 4-3 and Equation 4-5 at times t_1 and t_2 two constant part of those equation at any loading cycle are presented as A and B (i.e., Equation 4-15 and Equation 4-16, respectively). Then, by following Equation 4-17 and Equation 4-18, the hardening parameter κ_1 at the end of loading and at the end of the rest period could be obtained, such that:

Equation 4-15 $$A = \frac{\tau - \alpha I_1 - \kappa_0}{\sigma_y^0}$$

Equation 4-16 $$B(t_1) = \frac{1 - \exp(-\kappa_2 p(t_1))}{\sigma_y^0}$$

Equation 4-17 $$\dot{p}(t_1) = \Gamma^{vp}\left[A - \kappa_1(t_1)B(t_1)\right]^N; \quad \dot{p}(t_2) = \Gamma^{vp}\left[A - \kappa_1(t_2)B(t_1)\right]^N$$

Equation 4-18 $$\kappa_1(t_1) = \frac{1}{B(t_1)}\left[A - \left(\frac{\dot{p}(t_1)}{\Gamma^{vp}}\right)^{1/N}\right]; \quad \kappa_1(t_2) = \frac{1}{B(t_1)}\left[A - \left(\frac{\dot{p}(t_2)}{\Gamma^{vp}}\right)^{1/N}\right]$$

Plot $\kappa_1(t_1)$ and $\kappa_1(t_2)$ versus the accumulative loading time t for the all RCRT-CLR as shown in Figure 4-12, respectively. Integrate Equation 4-7 will result in Equation 4-19:

Equation 4-19 $$-\frac{\kappa_1(t) - \kappa_1^{initial}}{S_2} = q^{vp}(t)$$

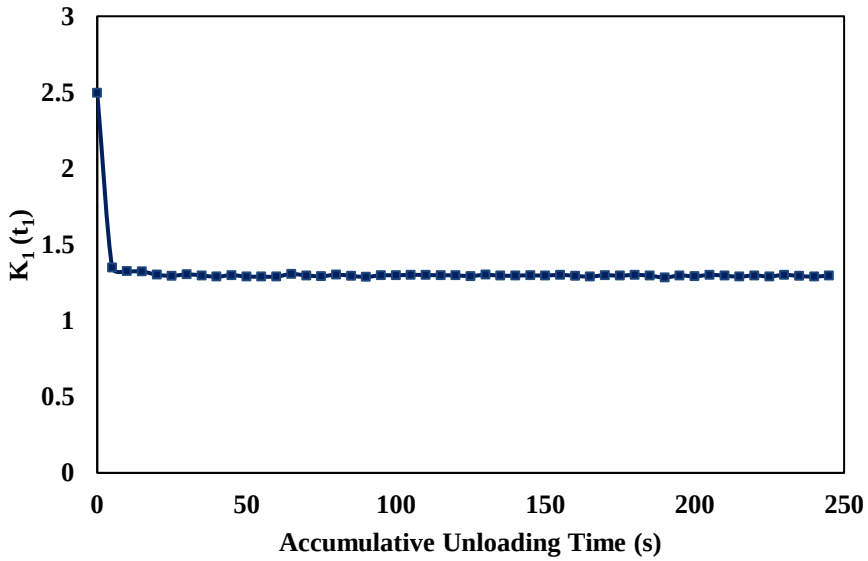

(a)

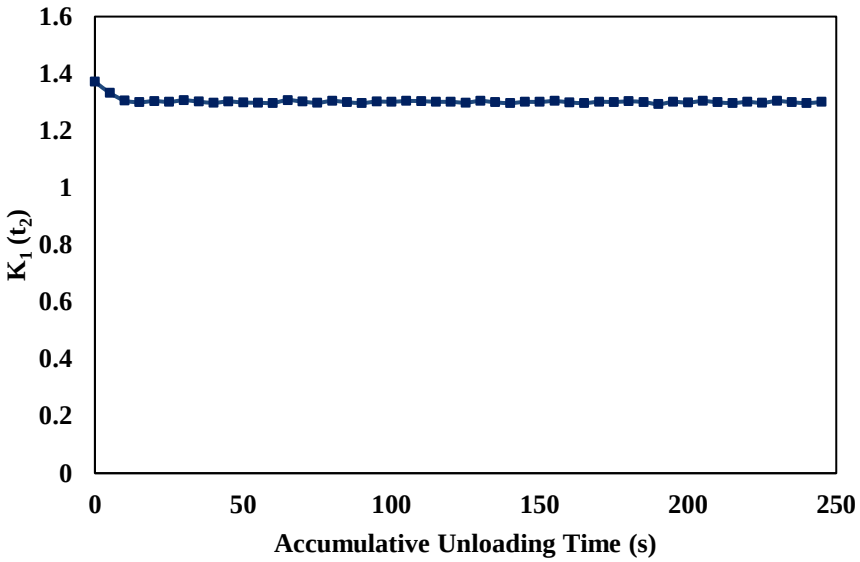

(b)

Figure 4-12: VP material parameter (i.e., κ_1) versus accumulative loading time during loading cycles of RCRT-CLR: (a) $\kappa_1(t_1)$; (b) $\kappa_1(t_2)$.

As presented in Figure 4-13, if enough rest period (i.e., at least three times of loading time) is given to asphalt concrete mixture, the hardening-relaxation viscoplastic internal state variable (i.e., q^{vp}) will evolve to the maximum possible value to become the effective VP strain (i.e., p). Therefore, pick the average values of two replicates during 5 s rest period test of RCRT-CLR for p at the end of the first rest period as the hardening-relaxation viscoplastic internal state variable (i.e. $q^{vp} = p^{final} = p_{Ave}^{Exp}$) and calculate S_2 as shown in Equation 4-20:

Equation 4-20 $$S_2 = \frac{\kappa_1^{initial} - \kappa_1^{final}}{p^{final}}$$

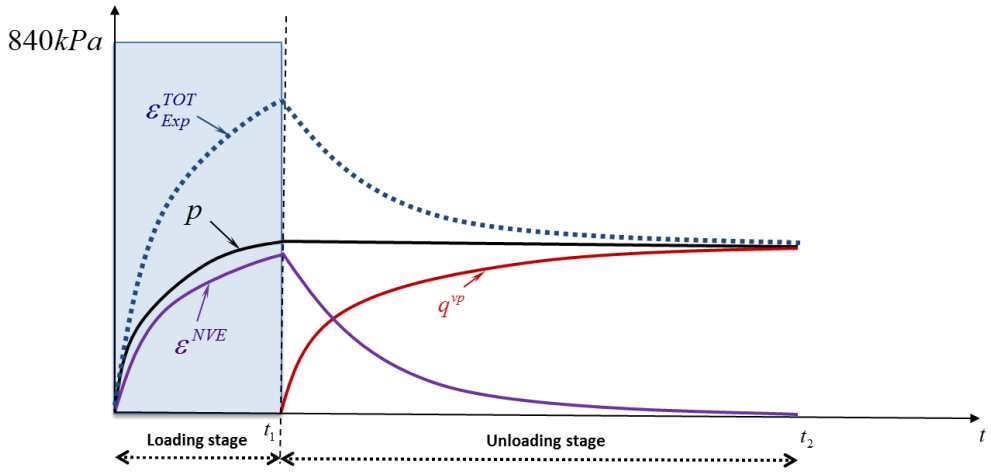

Figure 4-13: Schematic representation of the loading and unloading stage, the evolution of the total strain, the nonlinear viscoelastic strain, the effective VP strain, and the hardening-relaxation viscoplastic internal state variable during a cycle of RCRT-CLR with 5 s rest period.

Calculate $\Delta q^{vp}(t)$ using Equation 4-7 once S_2 is known based on Equation 4-20 by following Equation 4-21 and Equation 4-22:

Equation 4-21 $$\Delta\kappa_1(t) = \kappa_1(t) - \kappa_1^{initial}$$

Equation 4-22 $$\Delta q^{vp}(t) = -\frac{\Delta\kappa_1(t)}{S_2}$$

where t is the accumulative unloading time. Calculate Δq^{vp}, q^{vp}, and p for all cycles of RCRT-CLR from Equation 4-22, Equation 4-23, and experimental measurements, respectively. Figure 4-14 shows the evolution of Δq^{vp} during accumulative unloading time of RCRT-CLR.

Equation 4-23 $$q^{vp}(t) = \sum \Delta q^{vp}(t)$$

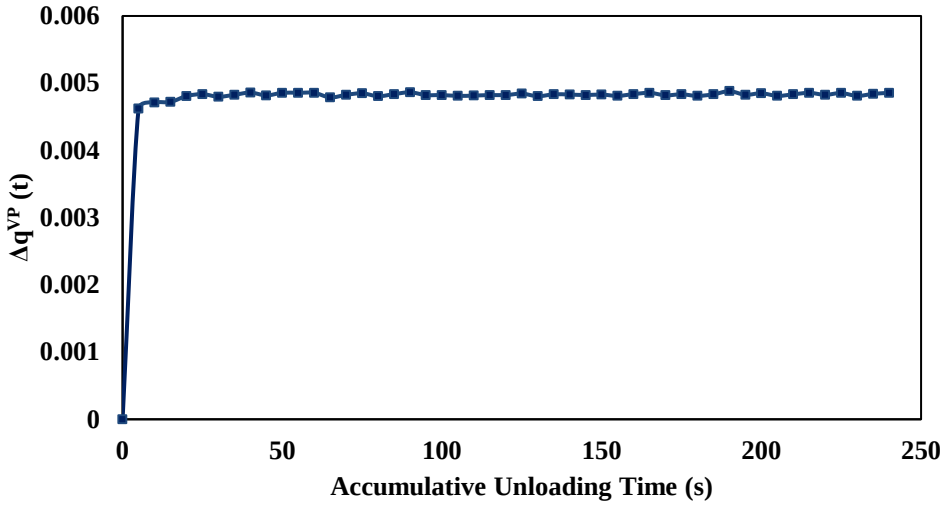

Figure 4-14: The evolution of Δq^{vp} during accumulative unloading time of RCRT-CLR.

Manipulate Equation 4-6 will result in Equation 4-24:

Equation 4-24 $$\frac{\Delta q^{vp}}{\Delta t} = \Gamma^{h-r}\left(p - q^{vp}\right)^{S_1}$$

Plot $\frac{\Delta q^{vp}}{\Delta t}$ versus $p - q^{vp}$ in log-log scale for all available data. Γ^{h-r} is the intersection of $\frac{\Delta q^{vp}}{\Delta t}$-$\left(p - q^{vp}\right)$ curve with Y-axis and S_1 is the slope of the fitted line using the Equation 4-25:

Equation 4-25 $$Ln\left(\frac{\Delta q^{vp}}{\Delta t}\right) = Ln\left(\Gamma^{h-r}\right) + S_1 Ln\left(p - q^{vp}\right)$$

Γ^{h-r} and S_1 could be identified by minimizing the error between left and right hand side of Equation 4-25 by using Equation 4-26 and GAs:

Equation 4-26 $$error = \sum_{i=1}^{K}\left[\left(\frac{Ln\left(\frac{\Delta q^{vp}}{\Delta t}\right)}{Ln\left(\Gamma^{h-r}\right) + S_1 Ln\left(p - q^{vp}\right)} - 1\right)^2\right]$$

4.5.4. Genetic Algorithm Running Parameters

A genetic algorithm maintains a population of candidate solutions for the problem in hand, and makes it evolve by iteratively applying a set of stochastic operators. Stochastic operators include selection, recombination, and mutation. Selection replicates the most successful solutions found in a population at a rate proportional to their relative quality. Recombination decomposes two distinct solutions and then randomly mixes their parts to form novel solutions. Mutation randomly perturbs a candidate solution. Table 4-3 illustrates GAs parameters to extract VP properties of asphalt concrete.

Table 4-3: The GAs parameters to extract VP properties of asphalt concrete materials.

Genetic Algorithm	Nature	Parameters	
Optimization problem	Environment	K_0	Initial yield strength. It has a very low value at high temperatures. Does not affect the results very much. It have a small value between 40-150kPa for most asphalt mixtures.
		K_1	The hardening limit of asphalt mixtures against viscoplastic deformation. It is in the order of compressive strength of asphalt mixtures at 40°C (Saturated Yield Stress (K_0+K_1))
		K_2	Visco-plastic Parameter (Strain Hardening Rate)
		N	Visco-plastic Rate-sensitivity Exponent Parameter
		Γ	Gama (Visco-plastic Fluidity Parameter)
Feasible solutions	Individuals living in that environment	K_0	40-150 (kPa)
		K_1	0-(Saturated Yield Stress minus K_0) (kPa)
		K_2	0-100
		N	0-5
		Γ	0.000001-1 (1/s)
Solutions quality (fitness function)	Individual's degree of adaptation to its surrounding environment (convergence)	0.0001	
A set of feasible solutions	A population of organisms (species or population size)	100	
Stochastic operators	Selection, recombination and mutation in nature's evolutionary process (mutation rate)	0.075	
Iteratively applying a set of stochastic operators on a set of feasible solutions	Evolution of populations to suit their environment (maximum time without improvement)	30	

The computer model introduces simplifications (relative to the real biological mechanisms), but surprisingly complex and interesting structures have emerged out of evolutionary algorithms. Simple GAs produce an initial population of individuals then evaluate the fitness of all individuals, while termination condition not met do; it select fitter individuals for reproduction, recombine between individuals, mutate individuals, evaluate the fitness of the modified individuals, and generate a new population. Figure 4-15 shows the evolutionary cycle.

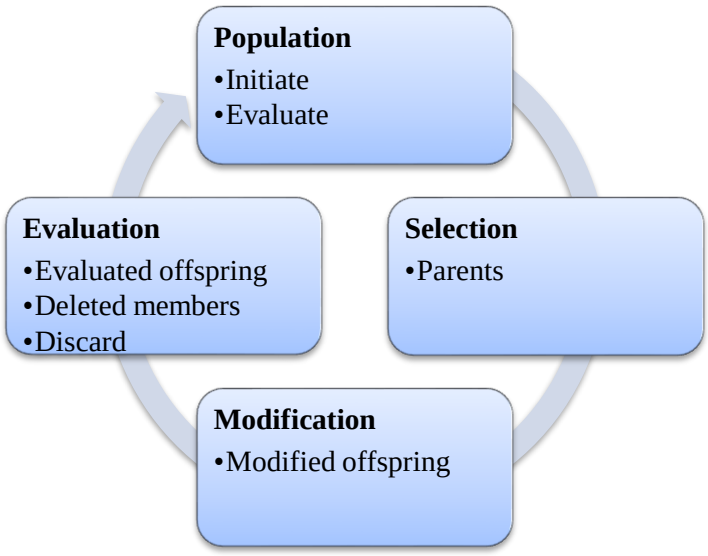

Figure 4-15: The evolutionary cycle.

4.6. Results and Discussion

4.6.1. Saturated Yield Stress

Uniaxial Constant Strain Rate in Compression (UCSR-C) tests are conducted to calculate saturated yield stress of all mixtures. Table 4-4 summarize the average saturated yield stress for four different asphalt mixtures used in FAA's NAPMRC test sections.

Table 4-4: Average saturated yield stress for four different asphalt mixtures used in FAA's NAPMRC test sections.

Mixture	Binder	Average saturated yield stress (kPa)
HMA	PG 76-22	1553
	PG 64-22	1403
WMA	PG 76-22	1452
	PG 64-22	1332

Tests on these binders showed that modified PG 76-22 had the highest viscosity. Furthermore, as Evotherm-M1 added to the virgin binders to produce WMA, the viscosity of binder decreases compare to that of HMA. Based on Witczak's predictive equation (*211*), dynamic modulus of asphalt concrete increases as the bitumen viscosity increases, for the same properties of asphalt concrete materials. Therefore, it is expected that average saturated yield stress of modified PG 76-22 has the highest value. In other words, the mixtures with the bitumen which has the highest viscosity may show the highest saturated yield stress for the same properties of asphalt concrete materials.

4.6.2. Viscoplastic Properties

Repeated Creep-Recovery Test at Variable Stress Levels (RCRT-VS) tests are conducted to calculate VP parameters of all mixtures. Table 4-5 summarize the VP parameters for four different asphalt mixtures used in FAA's NAPMRC test sections.

Table 4-5: Viscoplastic parameters for four different asphalt mixtures used in FAA's NAPMRC test sections.

Mixture	Binder	Initial Yield Strength (kPa)	Compressive Strength of Asphalt Mixture (kPa)	Strain Hardening Rate	Viscoplastic Rate-sensitivity Exponent	Viscoplastic Fluidity (1/s)
		κ_0	κ_1	κ_2	N	Γ^{vp}
HMA	PG 76-22	142	1411	180	1.92	0.008
	PG 64-22	53	1350	170	2.06	0.016
WMA	PG 76-22	57	1395	173	1.98	0.009
	PG 64-22	52	1280	165	2.13	0.023

Viscoplastic fluidity parameter (i.e., Γ^{vp}) controls the amount of plastic strain based on the energy dissipated. As values of Γ^{vp} increases more flow (and therefore smaller stresses) expected. Also, greater values of VP rate-sensitivity exponent (i.e., N) results in more flow. The effect of the hardening function parameters κ_0, κ_1, and κ_2 are best understood by understanding the hardening function κ, as shown in Equation 4-5. The value of the hardening function $\kappa(p)$ varies from κ_0 when $p = 0$ (before viscoplasticity occurs) to $\kappa_0 + \kappa_1$ as $p \to \infty$, and κ approaches the saturated value $\kappa_0 + \kappa_1$ more quickly as κ_2 increases. A decrease in either κ_0 or κ_1 decreases the value of the hardening function κ and results in a more compliant material. Asphalt concrete material has more flow for lower values of κ_2, in other words, asphalt concrete material yields more earlier for lower values of κ_2.

4.6.3. Hardening-relaxation Viscoplastic Properties

Repeated creep-recovery test at constant loading and rest times (RCRT-CLR) tests are conducted to calculate HR viscoplastic parameters of all mixtures. Table 4-6 summarize the HR viscoplastic parameters for four different asphalt mixtures used in FAA's NAPMRC test sections.

Table 4-6: Hardening-relaxation viscoplastic parameters for four different asphalt mixtures used in FAA's NAPMRC test sections.

Mixture	Binder	Hardening-relaxation Exponent	Hardening-relaxation Parameter (kPa)	Hardening-relaxation Fluidity (1/s)
		S_1	S_2	Γ^{h-r}
HMA	PG 76-22	0.332	2.31×10^{5}	2.29×10^{-5}
	PG 64-22	0.347	9.67×10^{4}	3.20×10^{-5}
WMA	PG 76-22	0.301	2.10×10^{5}	2.22×10^{-5}
	PG 64-22	0.336	6.25×10^{4}	3.15×10^{-5}

Hardening-relaxation fluidity parameter (i.e., $\Gamma^{vp,s}$) controls the evolution of the VP softening. The lower HR fluidity parameter results in less softening potential during the rest period for asphalt concrete materials. However, full softening potential of asphalt concrete materials achieves, once a long enough rest period is introduced. Hardening-relaxation exponent (i.e., S_1) only affects the rate of the change in the VP softening. Greater values of HR exponent results in less rate of the change in the VP softening. The softening VP response signifies as the hardening-relaxation parameter (i.e., S_2) increases. In other words, greater values of HR parameter results in faster softening in VP response. Figure 4-16 illustrates the fitting curves for FAA's NAPMRC test sections materials under RCRT-CLR.

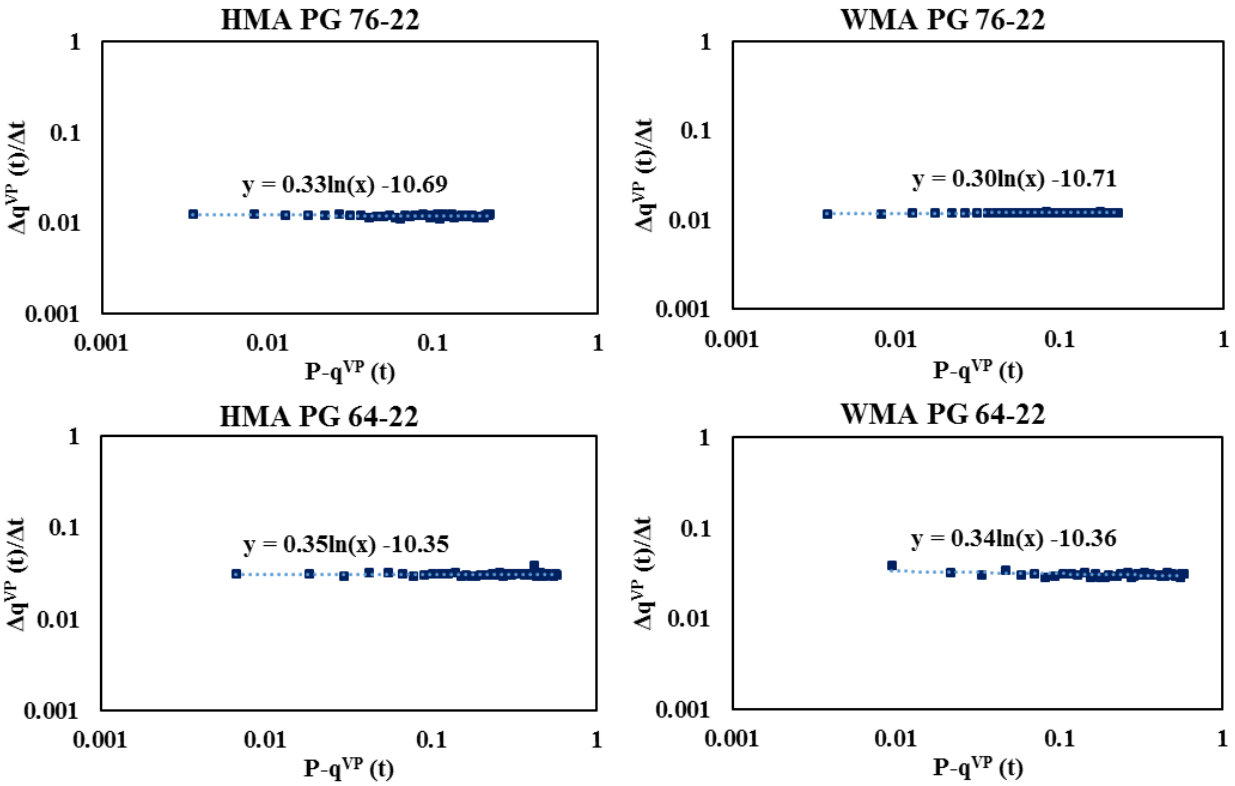

Figure 4-16: The fitting curves for FAA's NAPMRC test sections materials under RCRT-CLR.

4.6.4. Calibration

The model was calibrated by comparing the model predictions and experimental measurements using FAA's NAPMRC test sections materials and RCRT-CLR. Figure 4-17, Figure 4-18, and Figure 4-19 show the HR viscoplastic response of NAPMRC test sections under RCRT-CLR with three different rest times, 0.4, 1, and 5 seconds. Considering the material properties mentioned in previous sections, the model predictions agree well with the experimental data. It should be noted that the HR continues until the rate of the viscoelastic strain reaches a negligible value. Since then on, there is no more softening, because the HR is physically occurred through the rearrangement of the microstructure during the unloading and deformation recovery. Therefore, no more HR is expected once the rate of the recoverable strain during the unloading reaches zero (i.e. full recovery). Asphalt concrete materials show accumulation of the

plastic/viscoplastic strain decreases in each loading cycle even though the applied stress level is constant, which is the effect of HR viscoplastic properties of asphalt concrete materials. In other words, the rate of HR viscoplastic decreases as the viscoplastic strain increases. As shown in Figure 4-17, Figure 4-18, and Figure 4-19, the model predictions are slightly overestimated the viscoplastic strain as the viscoplastic strain increases. This effect might be due to the assumption of the constant pressure-sensitivity parameters α and β. Of course, further investigations are required to resolve this issue and to define a suitable expression for the variation of α and β with the effective viscoplastic strain.

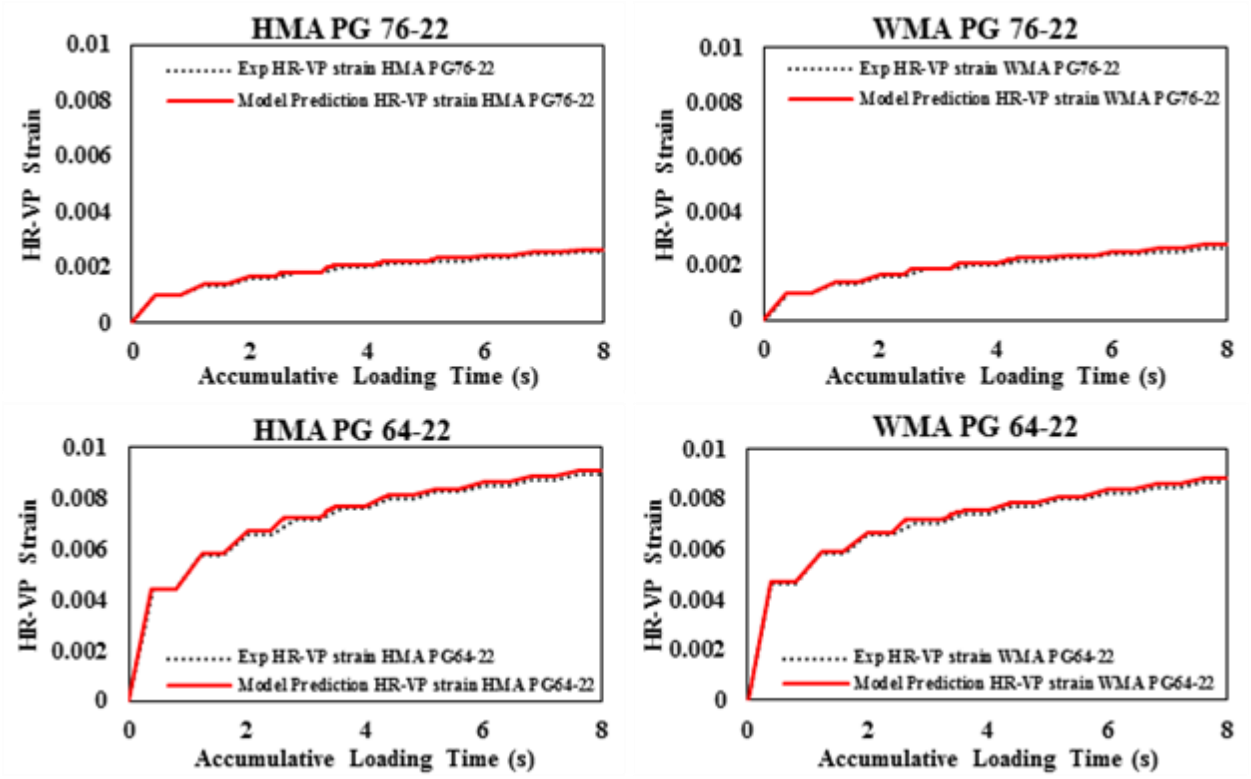

Figure 4-17: The HR viscoplastic response of NAPMRC test sections under RCRT-CLR with 0.4s rest time

As shown in Figure 4-17, Figure 4-18, and Figure 4-19, addition of Evotherm-M1 to both types of modified (i.e., PG 76-22) and unmodified (i.e., PG 64-22) virgin binders used in FAA's

NAPMRC test sections will result in more HR viscoplastic strain. Also, PG 76-22 has shown less HR viscoplastic strain compare to PG 64-22, as expected based on Witzcak (*211*) viscosity equation. Furthermore, the result is consistent with the traffic tests results conducted by FAA on NAPMRC flexible pavement test sections (*131*), both of WMA and HMA PG 64-22 test were found to be the worst performing test in terms of resulting in more VP and HR viscoplastic strain, which will result in more rutting. The HMA PG 76-22 performed slightly better than the respective WMA test. Finally, the more rest time, the more HR viscoplastic strain is observed under cyclic constant stress level as expressed in RCRT-CLR.

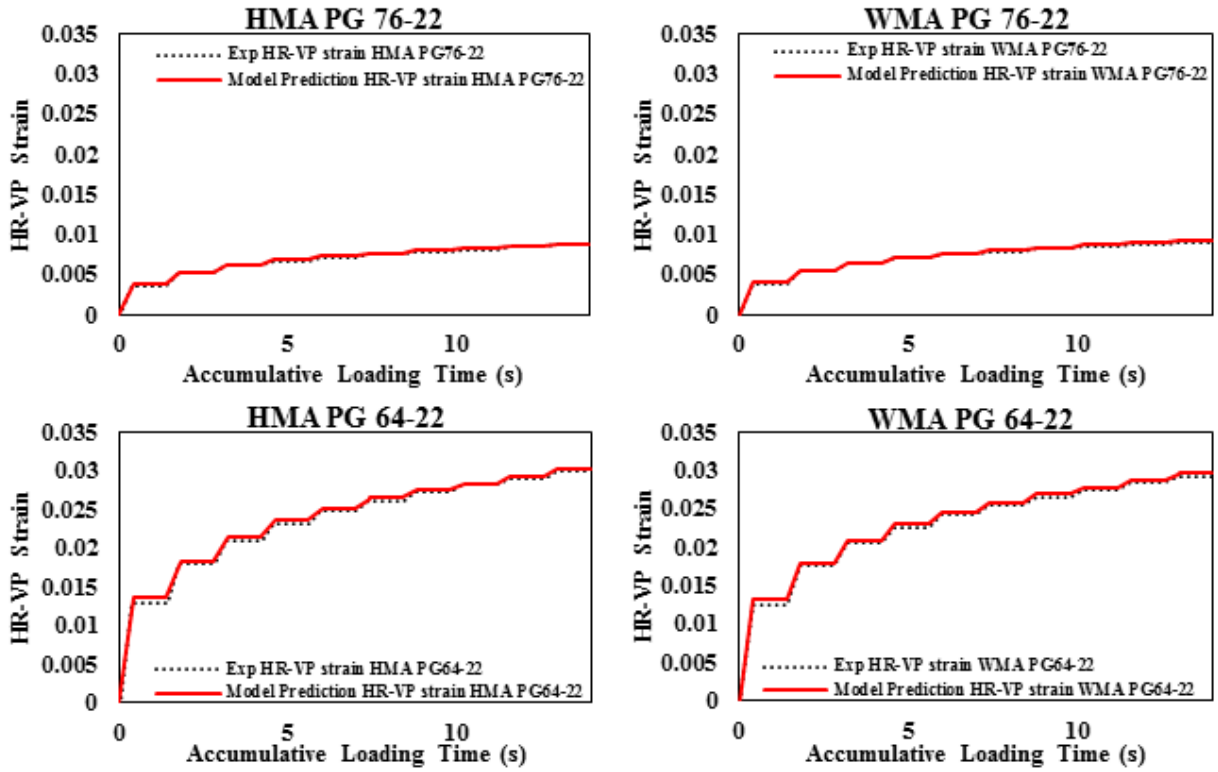

Figure 4-18: The HR viscoplastic response of NAPMRC test sections under RCRT-CLR with 1s rest time

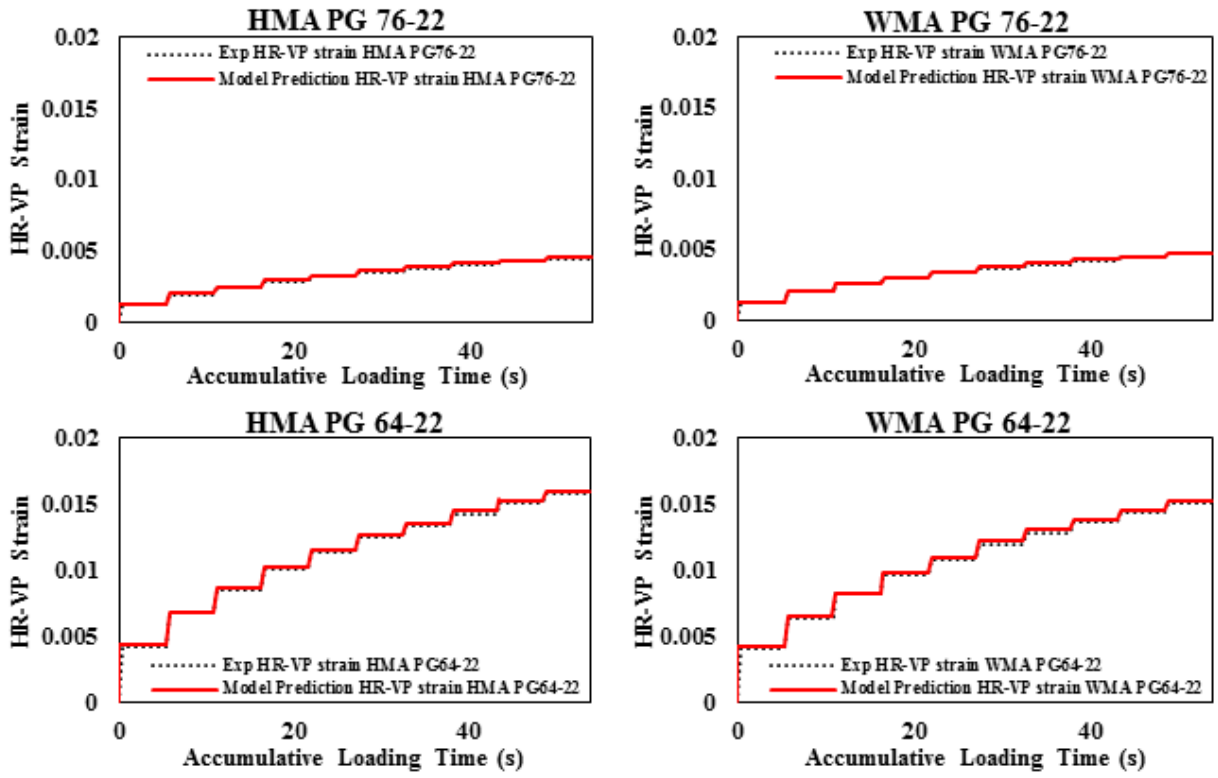

Figure 4-19: The HR viscoplastic response of NAPMRC test sections under RCRT-CLR with 5s rest time

4.6.5. Validations

Once the linear VE properties, nonlinear VE parameters, VP and HR viscoplastic parameters are obtained, these parameters will be employed in a user subroutine UMAT associate with a commercial finite element analysis software ABAQUS to simulate the material response with different loading path. To check the validity of the proposed model, further experimental data have been analyzed according to the test matrix presented in Table 4-7. These tests includes the dynamic modulus test at different temperatures and frequencies; monotonic tests at various strain rates; and repeated creep-recovery tests with various stress levels, loading times, and resting periods were conducted in this study to first calibrate the models and then validate the models against independent experiments, which were not used for calibration purposes. These tests were

conducted at North Carolina State University (NCSU) by Prof. Richard Kim and his research group.

Table 4-7: Test Matrix.

Test		Purposes	Desired properties
Dynamic Modulus Test		Calibration	Linear viselastic properties
Monotonic Test		Calibration	Viscoplastic properrties
Repeated Creep and Recovery Test (RCRT)	*Variable loading test (RCRT-VL)*	Calibration	Nonlinear viscoelastic properties and viscoplastic properties
	Constant loading and time test (RCRT-CLT)	Calibration	Relaxation-Hardening Properties
	Various loading time test (RCRT-VT)	Validation	------
	Reversed various loading time test (RCRT-RVT)	Validation	------
	Various Loading and Time Test (RCRT-VLT)	Validation	------

4.6.5.1. Dynamic Modulus Test

The dynamic modulus test was performed in compression under the confinement level of 140 kPa. The stress levels were determined by controlling the strain amplitudes within 50 to 70 $\mu\varepsilon$ in order to capture the linear viscoelastic response. The test was conducted at temperatures of -10, 10, 35 and 55 ^{o}C with frequencies of 25, 10, 5, 1, 0.5, 0.1, 0.05 and 0.01 Hz. This test will be characterized to obtain the linear viscoelastic properties.

4.6.5.2. Monotonic Test

The monotonic test was conducted at a constant displacement rate. This test was performed at 55ºC for unconfined case and confinement level of 500 kPa. The purpose of this test was to identify the value of α in the viscoplastic model.

4.6.5.3. Repeated Creep and Recovery Test

The repeated creep and recovery tests (RCRT) were conducted at 55 °C with a confinement level of 140 kPa. Five different types of creep and recovery tests were conducted: various loading (VL), constant loading and time (CLT), various loading time (VT), reverse various loading time (RVT), and various loading and time (VLT). The VL and CLT tests were used to calibrate the material properties; while VT, RVT and VLT tests were used for validation purposes. More details of these tests are described in the following sections.

4.6.5.3.1. RCRT- Variable loading test (RCRT-VL)

The RCRT-VL test was conducted with 0.4 sec loading time following 200sec rest period. Within each loading block, 8 stress levels were applied. The first deviatoric stress level in the first loading block was 137.9 kPa and increased by a factor of 1.2 for the next deviatoric stress level. For the next loading block, the first stress level was the same as that of the third loading stress in the preceding loading block. The sketch of RCRT-VL test is shown in Figure 4-20 (a). This test is the main test used to calibrate the NVE and VP models.

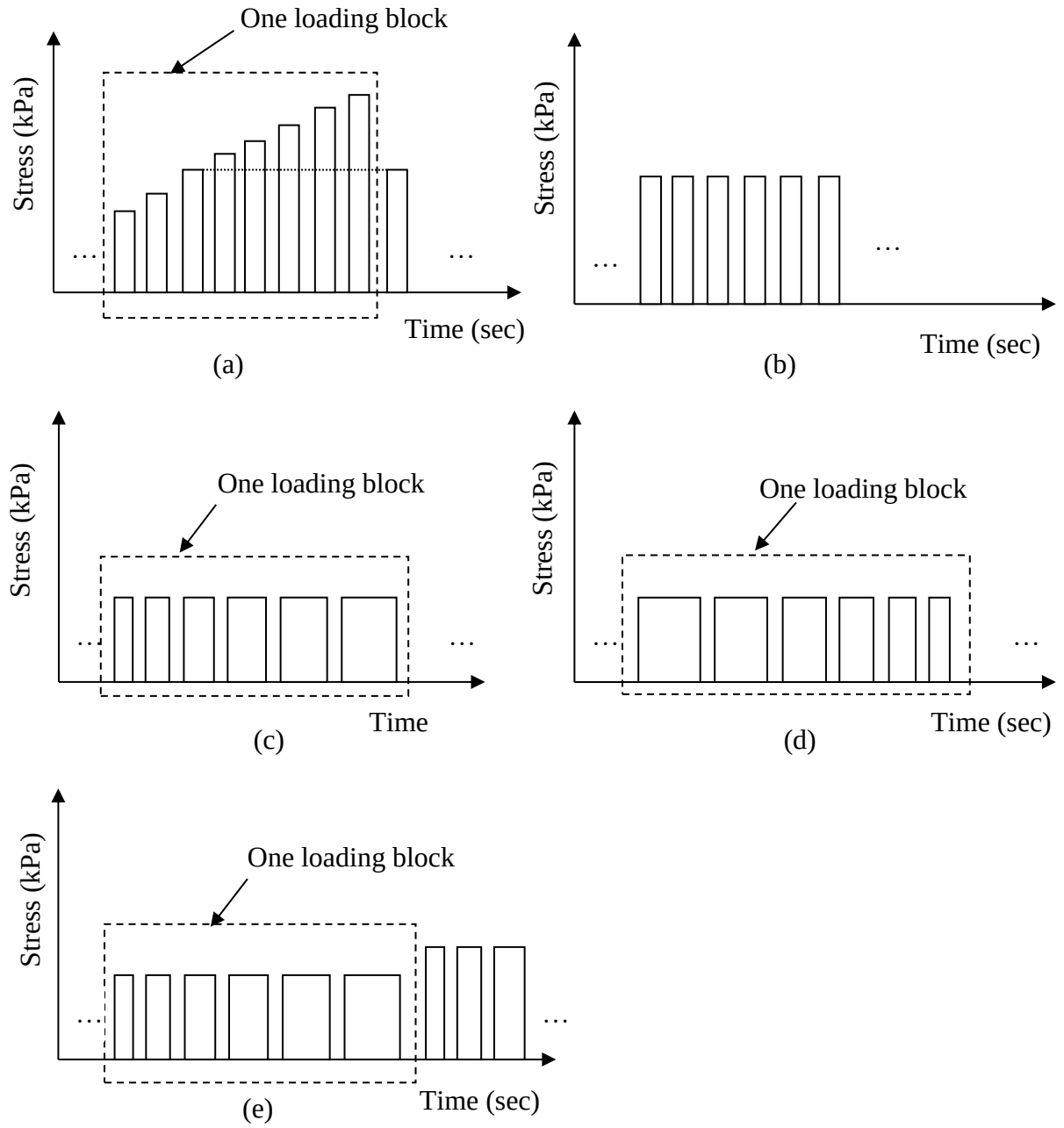

Figure 4-20: The Sketch of (a) RCRT-VL test, (b) RCRT-CLT test, (c) RCRT-VT test, (d) RCRT-RVT test, and (e) RCRT-VLT test.

4.6.5.3.2. RCRT-Constant loading and time test (RCRT-CLT)

In this test, the stress level, loading time and rest period were kept constants over the whole test. The loading periods were considered as 0.1, 0.4, 1.6 and 6.4 sec following the rest period 0.9

sec with a deviatoric stress level of 827 kPa and a confinement stress level of 140 kPa. The sketch of RCRT-CLT test is shown in Figure 4-20 (b). This test was employed to obtain the hardening-relaxation parameters.

4.6.5.3.3. RCRT-Various loading time test (RCRT-VT)

Figure 4-20 (c) illustrates the sketch of RCRT-VT. This test applied the repeated loading blocks and each loading block contains sequence of six different loading periods such as 0.05, 0.1, 0.2, 0.4, 1.6 and 6.4 sec with a constant stress level. Three different rest periods of 200, 1.0 and 0.05 sec were considered.

4.6.5.3.4. RCRT-Reversed various loading time test (RCRT-RVT)

In RCRT-RVT test, the loading conditions were the same as RCRT-VT test except the loading times. Within each loading block, the loading periods were exactly reversed to that in the VT test such as the sequence of loading time were 6.4, 1.6, 0.4, 0.2, 0.1 and 0.05 with a rest period of 200 sec. Figure 4-20 (d) shows the sketch of RCRT-RVT test.

4.6.5.3.5. RCRT-Various Loading and Time Test (RCRT-VLT)

This test combined the RCRT-VT and RCRT-VL tests. In this test, each loading block contains sequence of six loading times such as 0.05, 0.1, 0.2, 0.4, 1.6 and 6.4 sec with a constant deviatoric stress level as shown in Figure 4-20 (e). The devictoric stress level for first loading block was 100 kPa and then the deviatoric stress level increased by 200 kPa with increasing of loading block.

4.6.5.4. Model Calibration and validation

In this section, the systematic analysis procedures are used to calibrate viscoelastic, viscoplastic, and hardening-relaxation models.

4.6.5.4.1. Identification of linear and nonlinear viscoelastic parameters

Following the procedure explained in Chapter 3 the linear and nonlinear viscoelastic properties of asphalt concrete materials are extracted. Figure 4-21 shows the relationship between temperature and time-temperature shift factor, a_T. Then, the long-term linear viscoelastic Prony series coefficients can be obtained by fitting the master curve using Equation 3-3. Figure 4-22 shows the master curve and the fitting results of long-term Prony series model. The long-term Prony series coefficients are shown in Table 4-8. These long-term Prony series coefficients will be employed in the next analysis step to obtain the nonlinear parameters and to separate the irrecoverable and recoverable strain from RCRT-VL test.

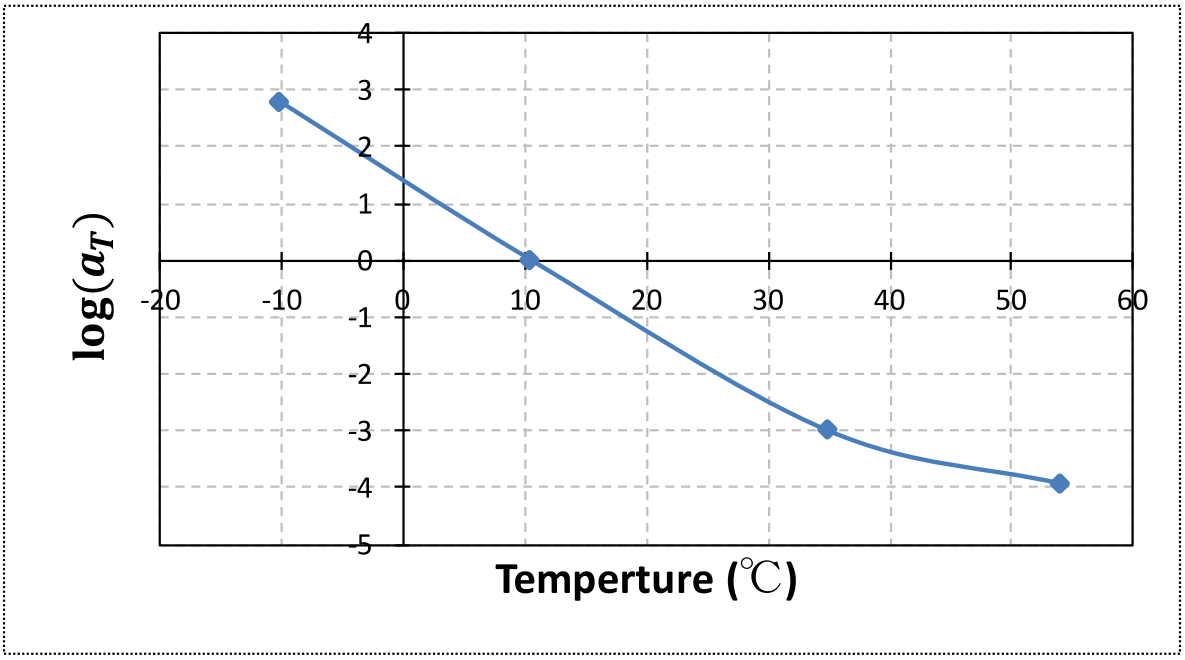

Figure 4-21: The relationship between temperature shifted factors and temperature.

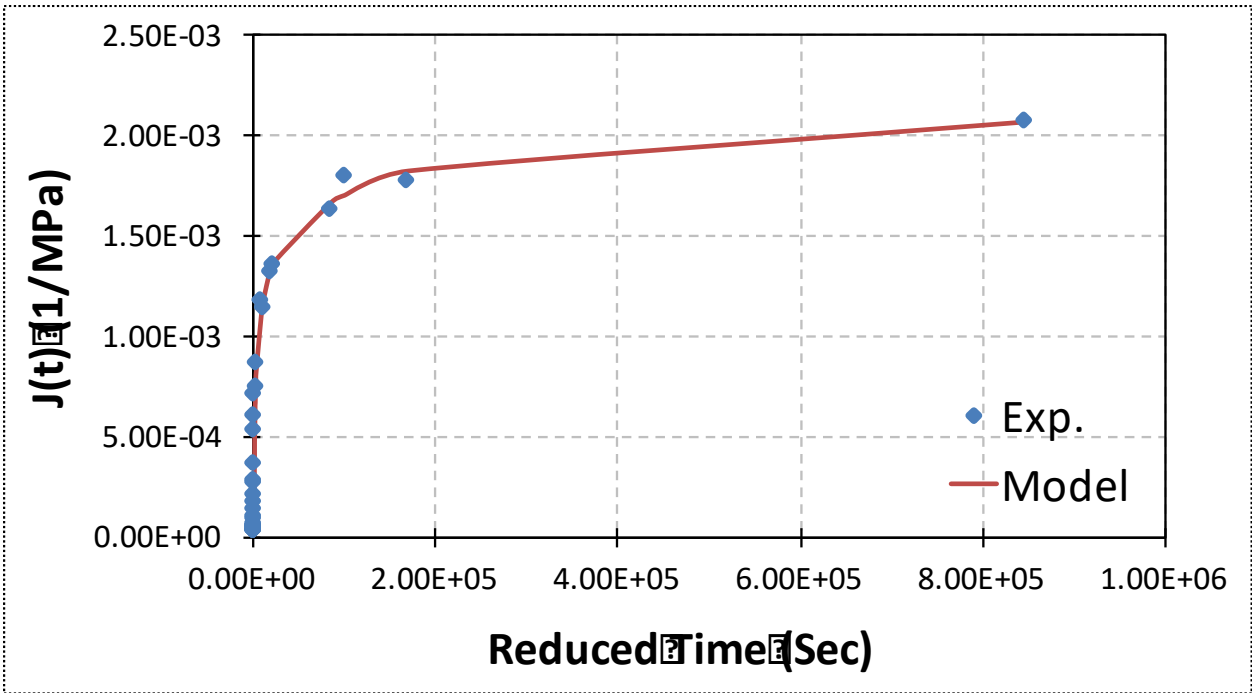

Figure 4-22: The master curve at confinement stress 140 kPa with reference temperature 10ºC.

Table 4-8: The Long-term Linear Viscoelastic Prony Series Coefficients.

n	D_n (MPa^{-1})	λ_n (1/s)
0	3.00×10^{-8}	-
1	3.51×10^{-7}	1.00×10^{-6}
2	3.29×10^{-7}	1.00×10^{-5}
3	5.60×10^{-7}	1.00×10^{-4}
4	4.37×10^{-7}	1.00×10^{-3}
5	2.34×10^{-7}	1.00×10^{-2}
6	5.63×10^{-8}	1.00
7	1.85×10^{-8}	1.00×10^{2}

Once the linear viscoelastic properties (Prony Series coefficients) are obtained from dynamic modulus test, this Prony series are used to characterize the nonlinear parameters (g_1 and

g_2) and decouple the viscoelastic and viscoplastic response through the analysis of recovered response in RCRT-VL test, more details of decoupling recoverable and irrecoverable strain were presented in chapter 3. Figure 4-23 illustrates the decoupled VE and VP strains in the 1st cycle of RCRT-VL test as an example. Figure 4-24 (a) and (b) is the relationship between deviatoric stress and the obtained nonlinear parameters g_1 and g_2 from measurements, respectively. Figure 4-24 (a) shows that the value of nonlinear parameter g_1 is hovering around 1.0, which indicates that the nonlinear parameter g_1 is not highly stress-dependent. Figure 4-24 (b) shows that the nonlinear parameter g_2 is significantly increased with increasing of deviatoric stress level.

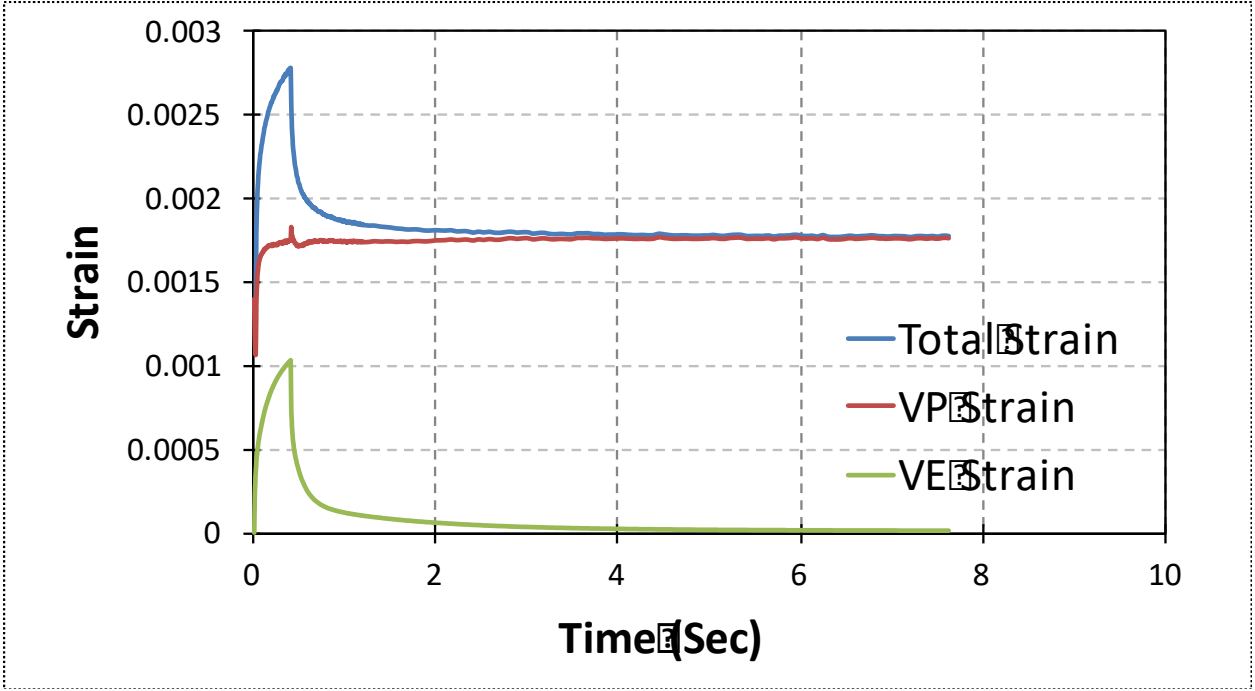

Figure 4-23: The example of decoupled results for 1st cycle of RCRT-VL test.

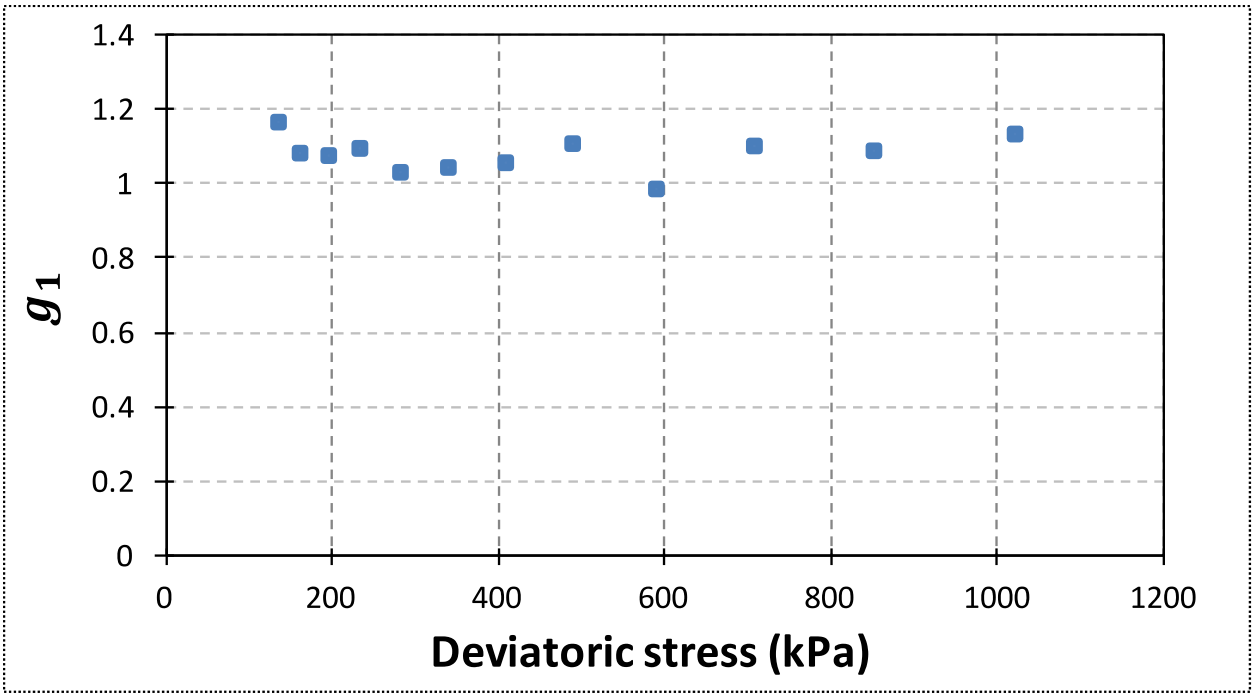

(a) Nonlinear parameter g_1 obtained from experimental measurements

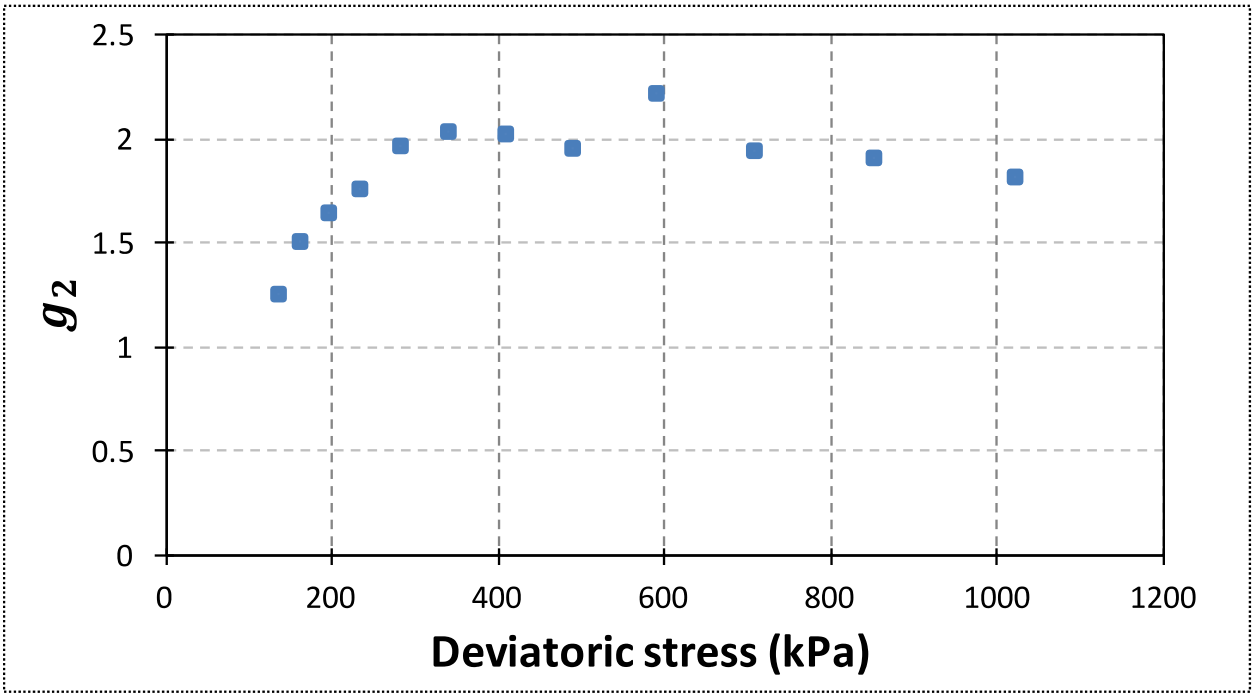

(b) Nonlinear parameter g_2 obtained from experimental measurements

Figure 4-24: The relationship between deviatoric stress and nonlinear viscoelastic parameters.

4.6.5.4.2. Identification of the VP Parameters from RCRT-VL test

Once the VE material properties such as Prony series coefficients and nonlinear viscoelastic parameters are obtained from RCRT-VL test, the recoverable stain during loading can be calculated and then the irrecoverable strain can be decoupled by subtracting the VE strain from total strain as shown in Figure 4-23. This irrecoverable strain is considered as the viscoplastic strain and characterized using Perzyan VP model. The analysis procedure as explained in 4.5.2. Section is applied to identify each VP parameters. The VP parameters are summarized in Table 4-9.

Table 4-9: The VP parameters.

Initial Yield Strength (kPa)	**Compressive Strength of Asphalt Mixture (kPa)**	**Strain Hardening Rate**	**Viscoplastic Rate-sensitivity Exponent**	**Viscoplastic Fluidity (1/s)**
κ_0	κ_1	κ_2	N	Γ^{vp}
50	1800	135	1.00	0.0024

4.6.5.5. Model validations

Figure 4-25 (a), (b), (c) and (d) demonstrate the model predictions of loading time 0.1, 0.4, 1.6 and 6.4 sec, respectively. These figures show that the proposed model has reasonable predictions with experimental measurements for different loading time and the model has the ability to consider the effect of different loading periods.

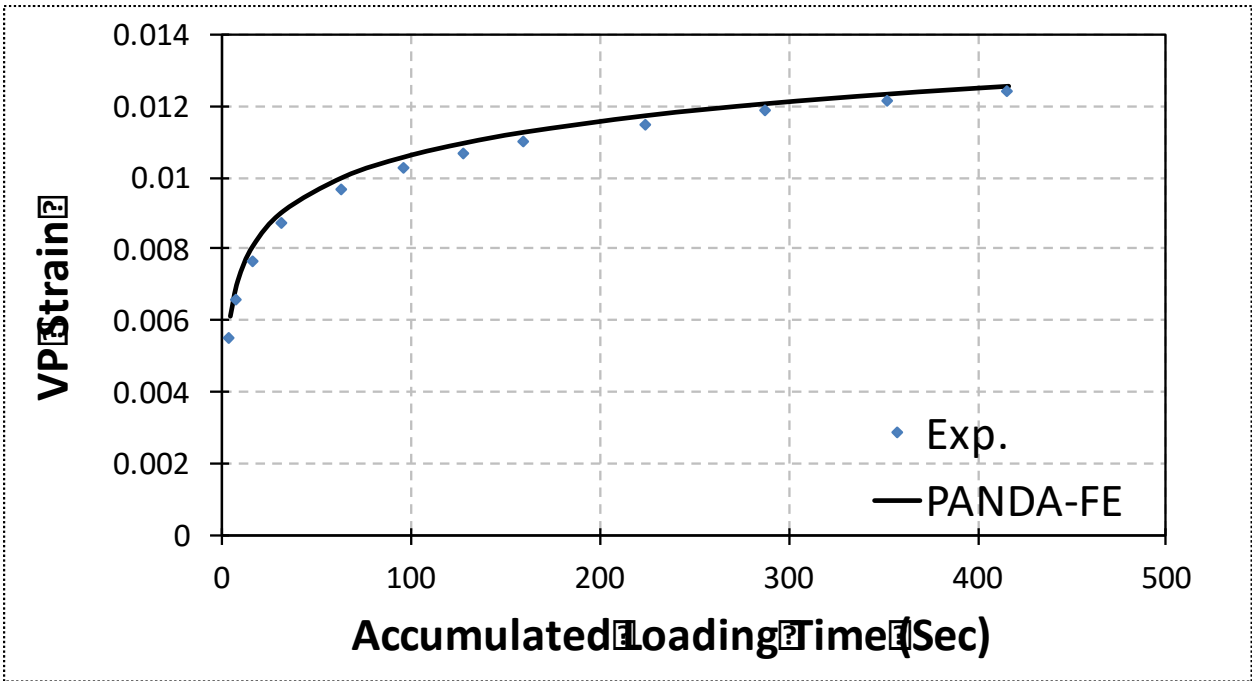

(a) Loading time=0.1 sec.

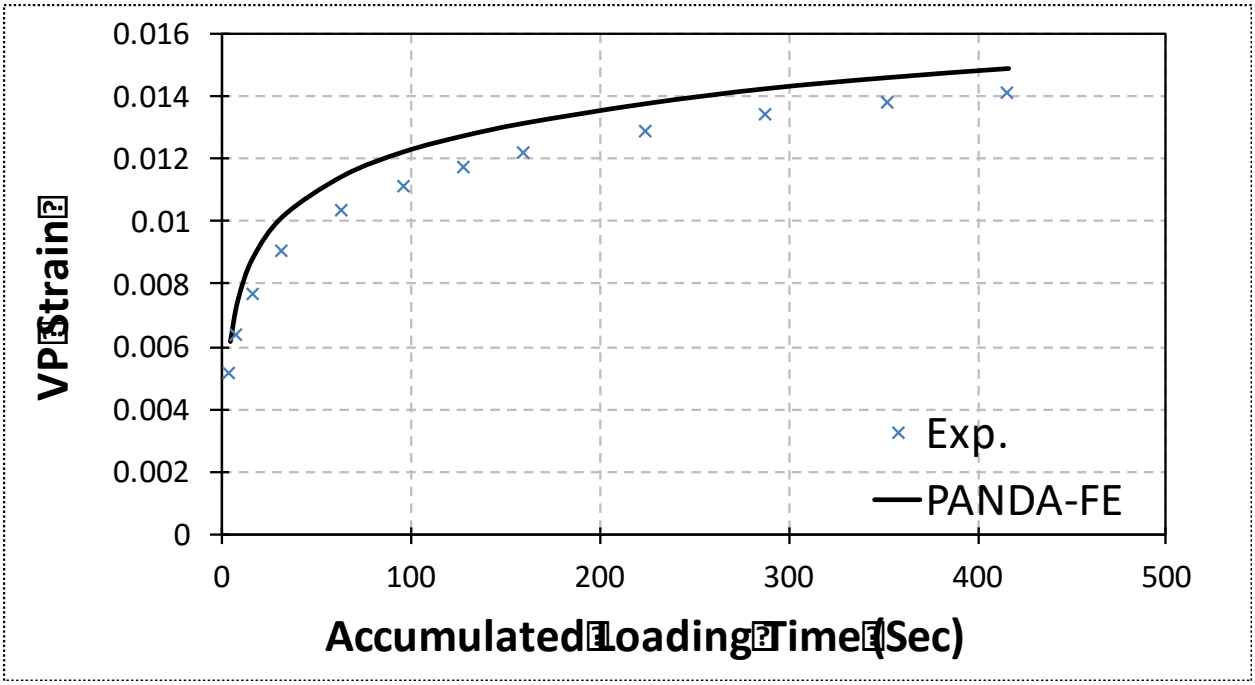

(b) Loading time=0.4 sec.

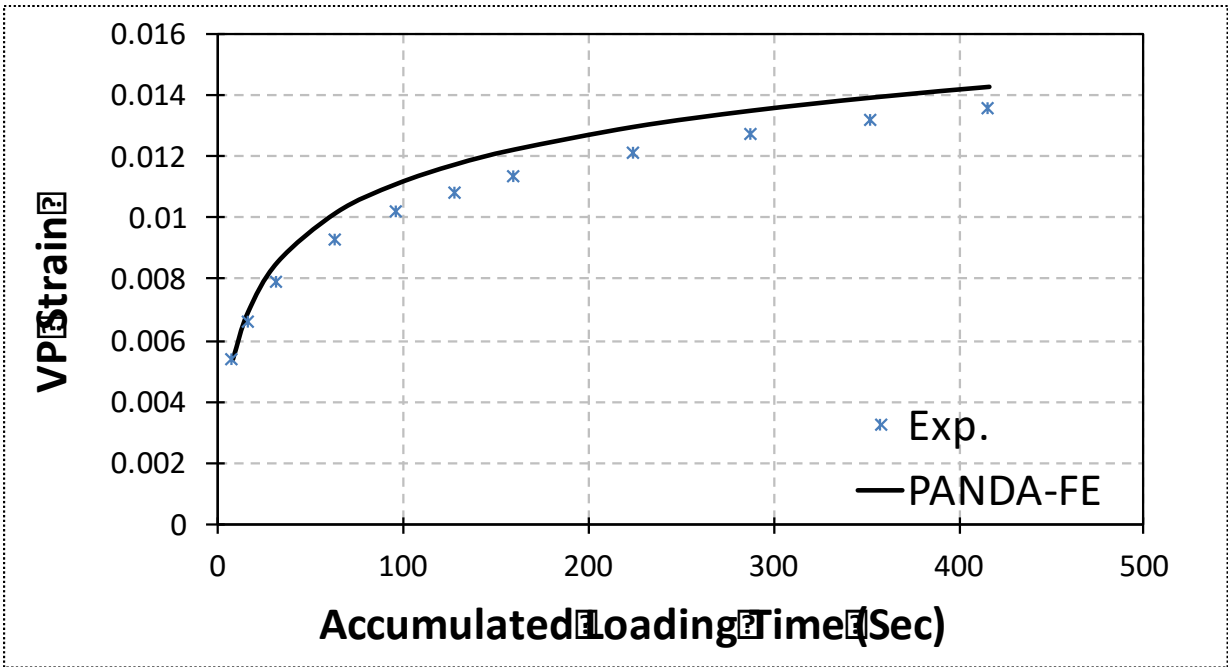

(c) Loading time=1.6 sec.

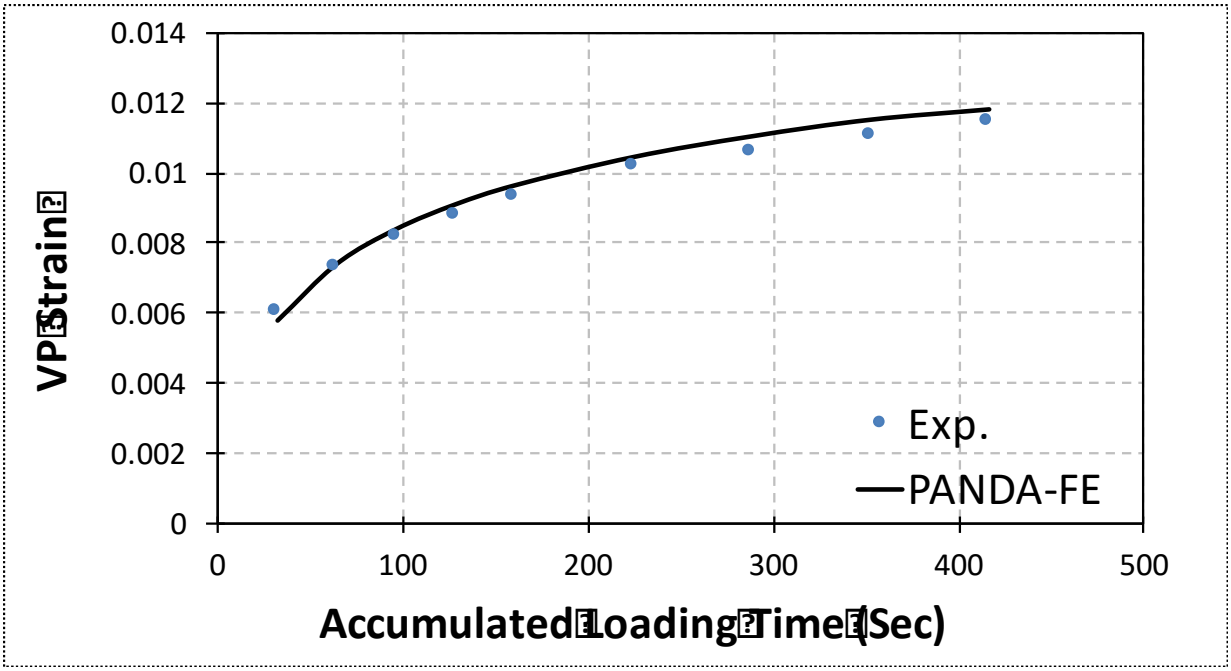

(d) Loading time=6.4 sec.

Figure 4-25: The comparison between model predictions and experimental measurements for RCRT-CLR and different loading time (a) 0.1, (b) 0.4, (c) 1.6 and (d) 6.4 sec.

Figure 4-26 is the model prediction results of RCRT-VL. This figure shows the proposed model has appropriate predictions of experimental measurements.

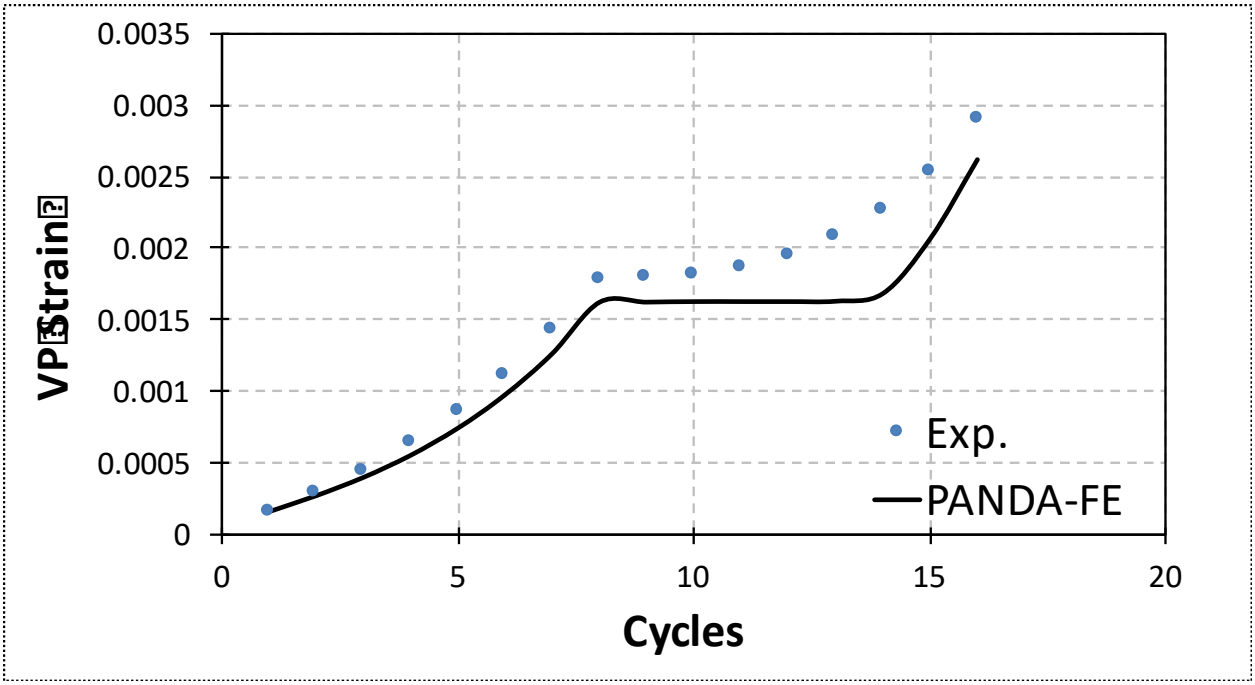

Figure 4-26: The comparison between model predictions and experimental measurements for RCRT-VS.

Figure 4-27 is the comparisons of model predictions of VP strain accumulation with experimental measurements for RCRT-VS test with different rest periods. These figures show that the proposed model has reasonable agreements with experimental measurements and the model can capture the material response for different rest periods.

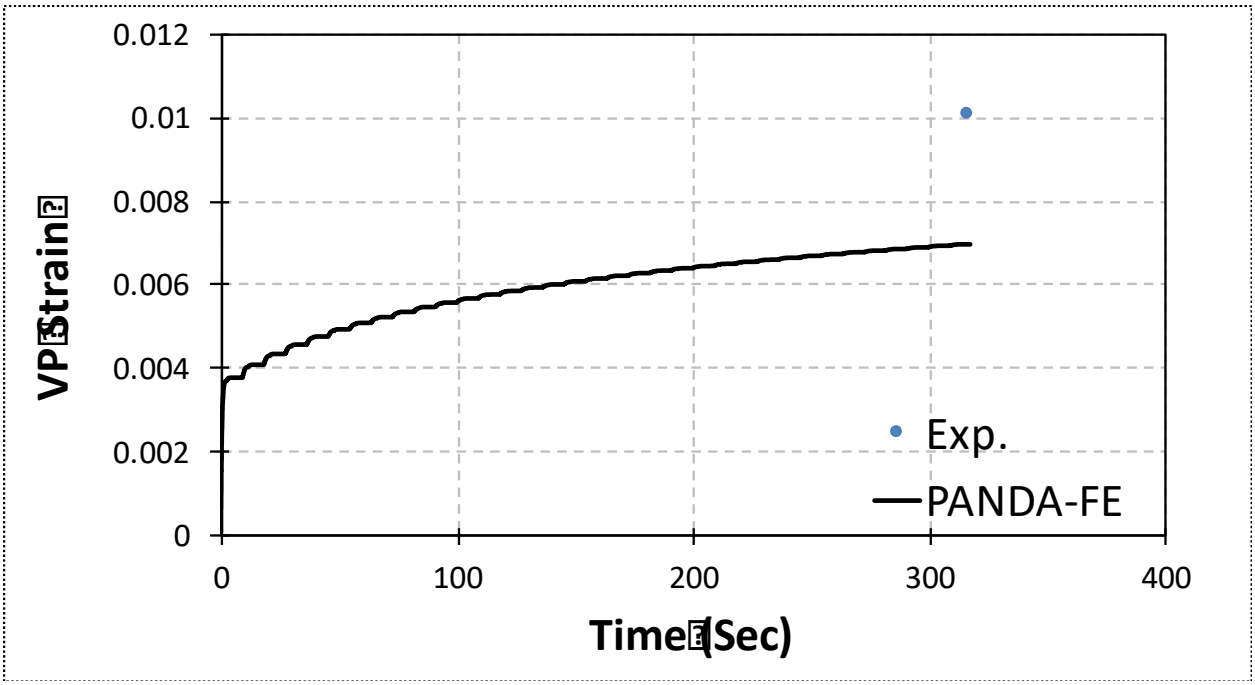

(a) Rest time=0.05 sec.

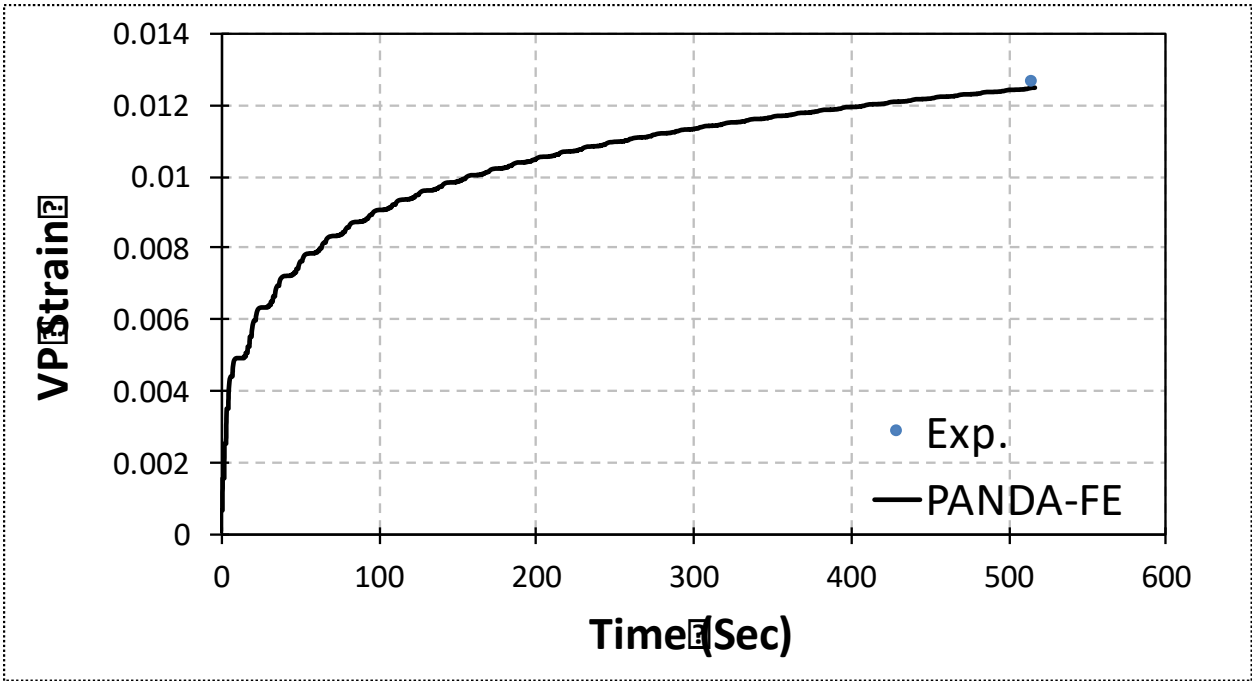

(b) Rest time=1.0 sec.

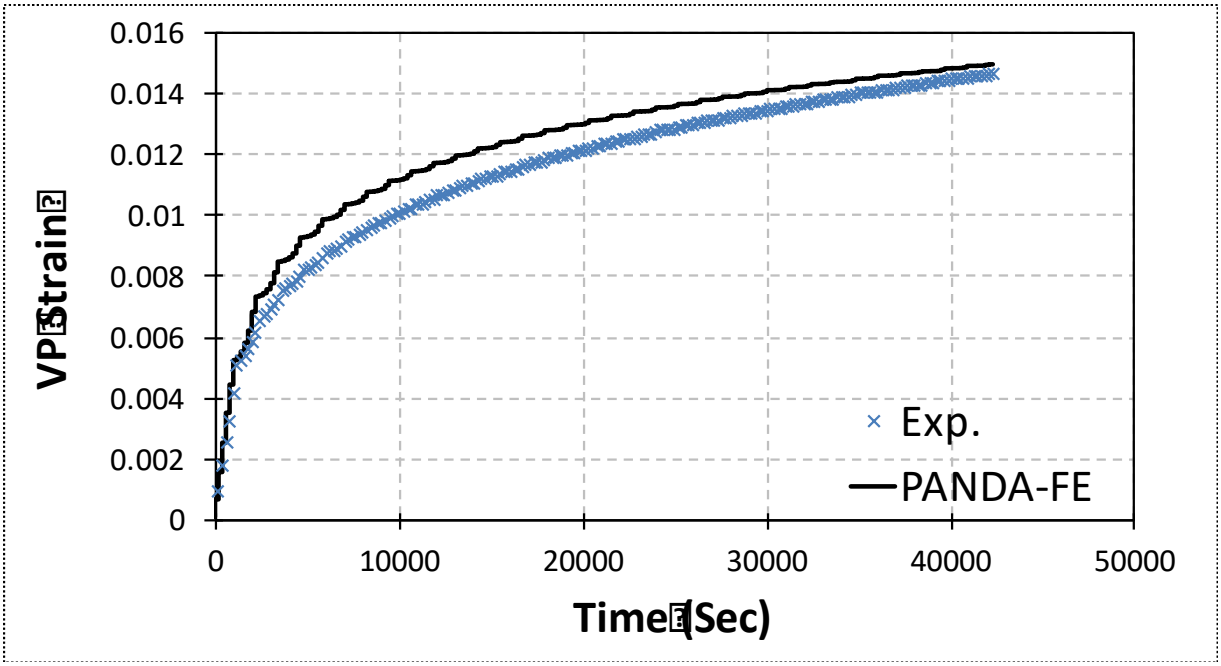

(c) Rest time=200 sec.

Figure 4-27: The comparison between model predictions and experimental measurements for RCRT-VS considering different rest times.

Figure 4-28 is the validation results for RCRT-RVT test and the results also show that a good agreement with experimental measurements.

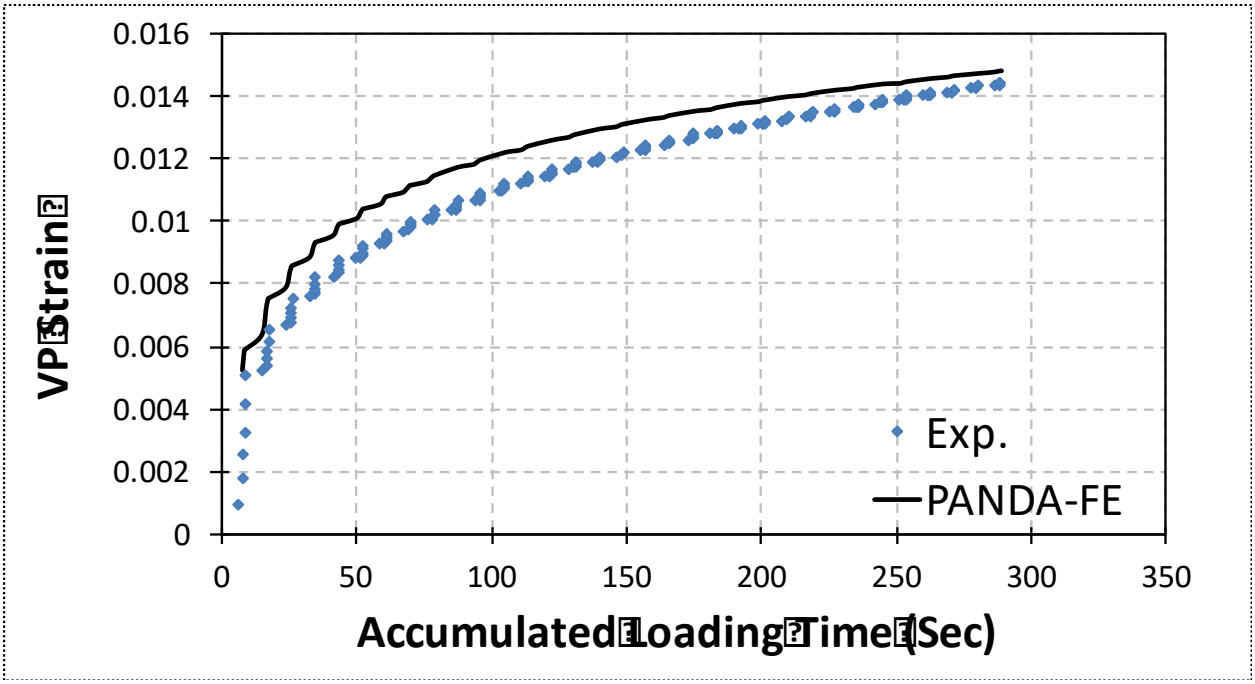

Figure 4-28: The comparison between model predictions and experimental measurements for RCRT-RVT test.

Figure 4-29 is the validation of RCRT-VLT test. This figure illustrates that the model can predict the material response at various stress levels and loading periods.

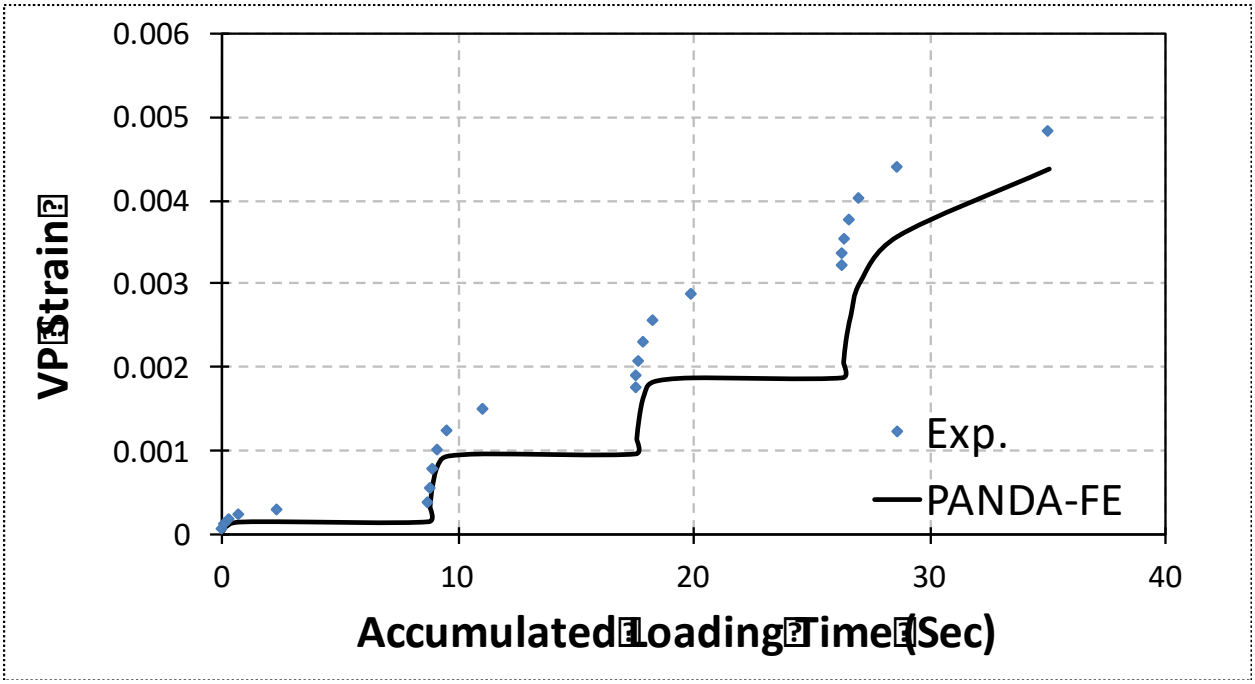

Figure 4-29: The comparison between model predictions and experimental measurements for RCRT-VLT test.

4.6.5.6. Finite element validation

Figure 4-30 represents a 2D axisymmetric finite element (FE) representation one of NAPMRC test section. The symmetric nature of loading and pavement geometry were taken into account while representing the finite element model of the pavement structure. Therefore, only half of the portion of the pavement system was generated by constraining the horizontal direction on the left vertical edge. An extensive mesh sensitivity analysis was carried out to determine the optimum mesh size. At the far right end of the FE model, infinite elements were used for computational convenience and to represent realistic lateral boundary conditions. A tire pressure of 1.75 MPa corresponding to 254 psi tire pressure, was used. Based on the properties of the tire (i.e., contact area) and the speed of applied load, the time required to pass a material point was calculated (i.e., loading time) to be 0.35s. Finite element model was simulated using PANDA.

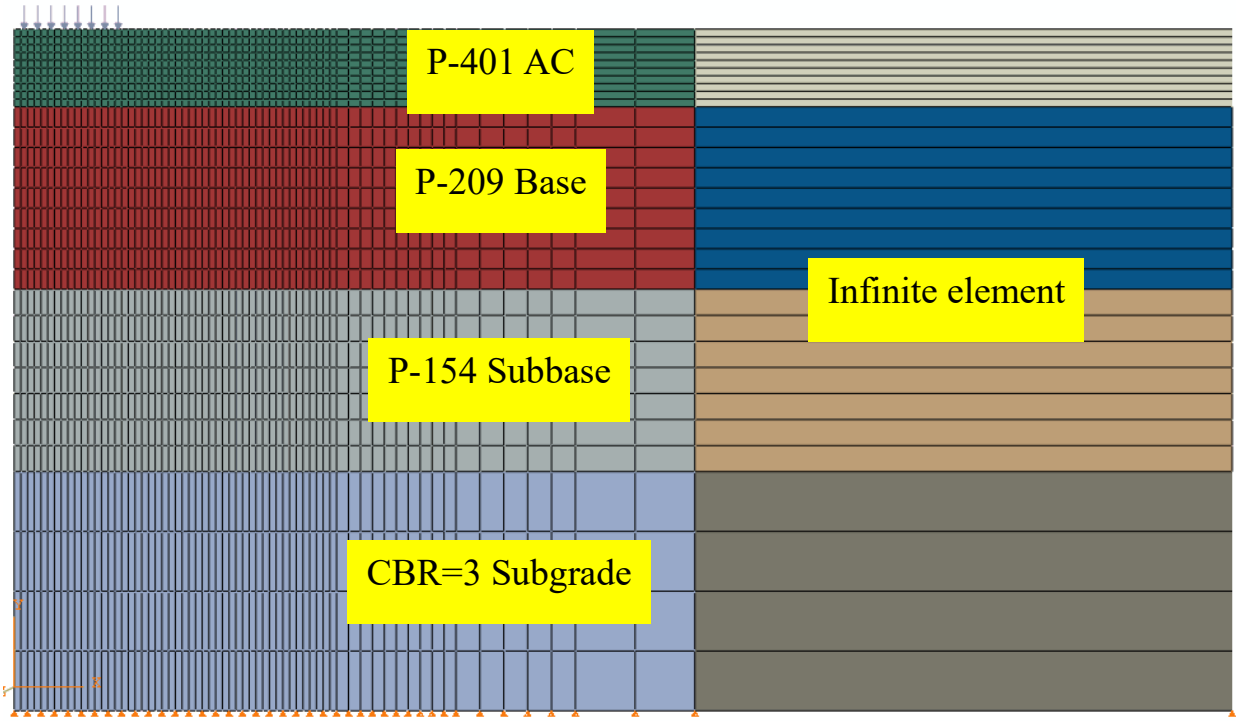

Figure 4-30: The finite element representation of pavement structure.

To investigate the capabilities of PANDA, the rutting results obtained from the FE simulations were compared to the field data from NAPMRC test sections. Figure 4-31 (a) presents the plan view of the designed test sections including asphalt concrete type, test temperature, and test tire pressure. Figure 4-31 (b) shows the design thicknesses for the asphalt concrete (AC), P-209 granular base, and P-154 type granular subbase were selected to be 5, 12 and 12 in. (12.7, 30.5 44 and 30.5 cm), respectively (*131*).

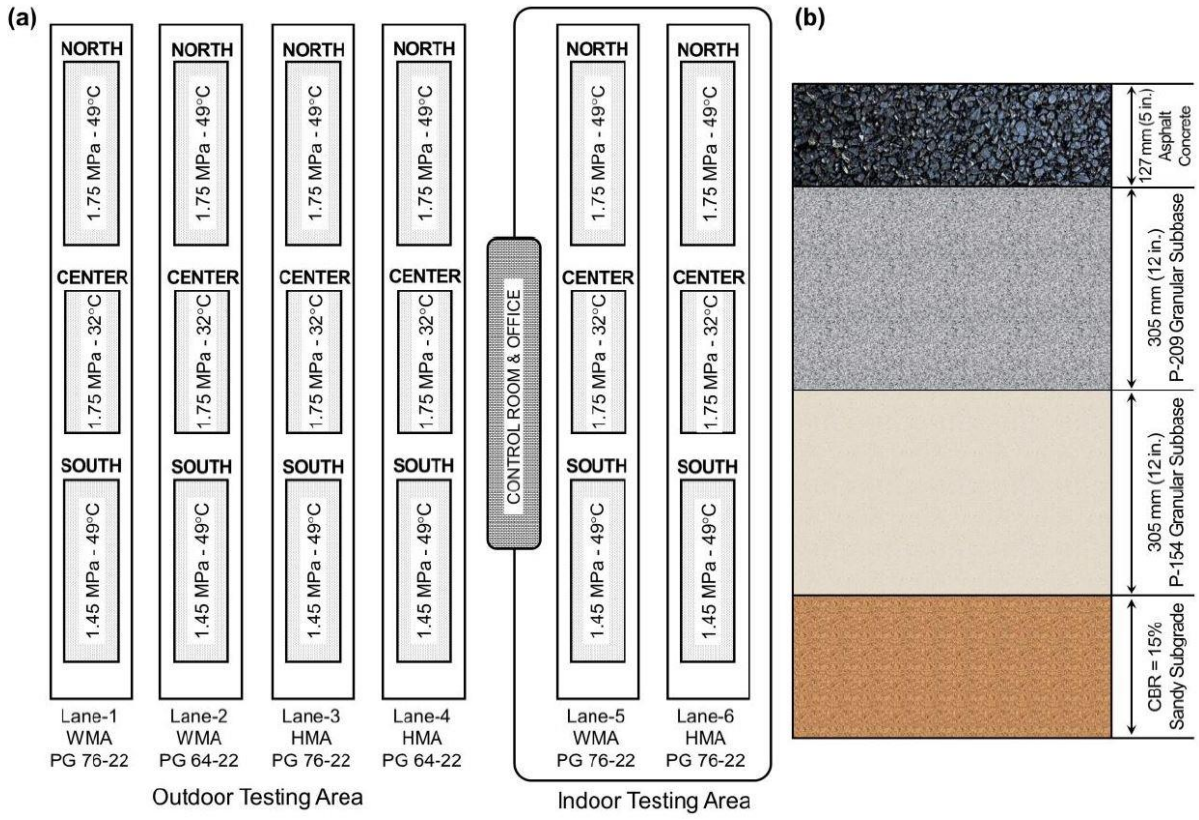

Figure 4-31: (a) Plan view of the full-scale test sections; (b) Cross-sectional view of the designed test sections (*131*).

To validate the extracted material properties associated with the NAPMRC test sections, the FE simulation for the North part of Lane-3 is evaluated. As shown in Figure 4-32 and Table 4-10, the FE model predict less rutting compare to the field observations from NAPMRC. This difference can be attributed to limitations of the FE representation used for these test sections including the facts that 2D instead of 3D simulations were used, shear contact stresses were not considered, wander pattern was not considered, and linear material properties were considered for the sublayers. The FE model was conducted until the failure of asphalt layer on NAPMRC test section, which is 1 in. rutting depth. Figure 4-33 shows the deformed shape of FE simulation.

Table 4-10: The rutting performance comparison of North part of Lane-3 from NAPMRC test section to PANDA FE model.

NAPMRC-Lane-3		
Passes	North	PANDA
	Rut Depth	Rut Depth
0	0	0.0
18	4.1	2.9
48	6.6	4.7
74	5.8	6.0
124	10.8	7.8
186	13.0	9.3
248	14.4	10.4
310	16.4	11.8
372	15.7	13.0
496	19.6	14.1
620	22.4	16.9

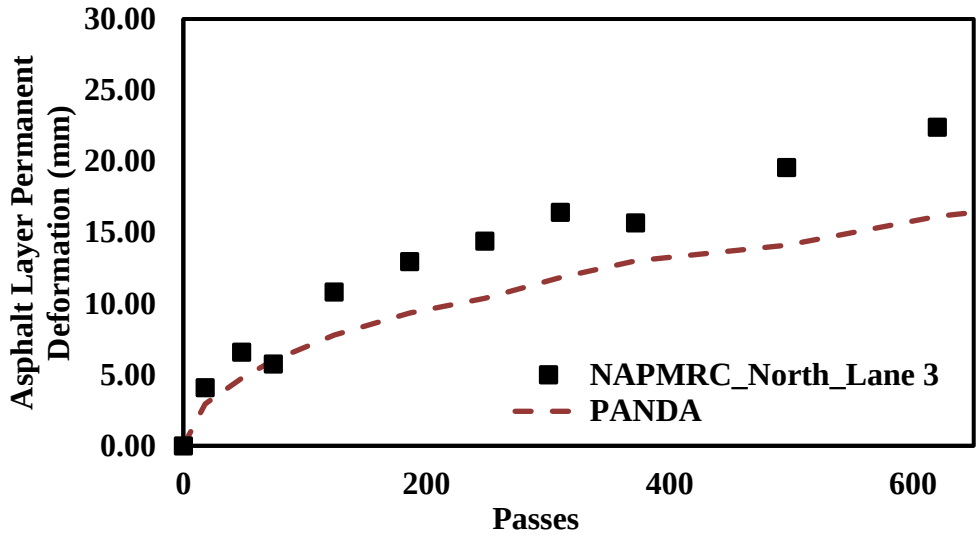

Figure 4-32: The rutting performance comparison of North part of Lane-3 from NAPMRC test section to PANDA FE model.

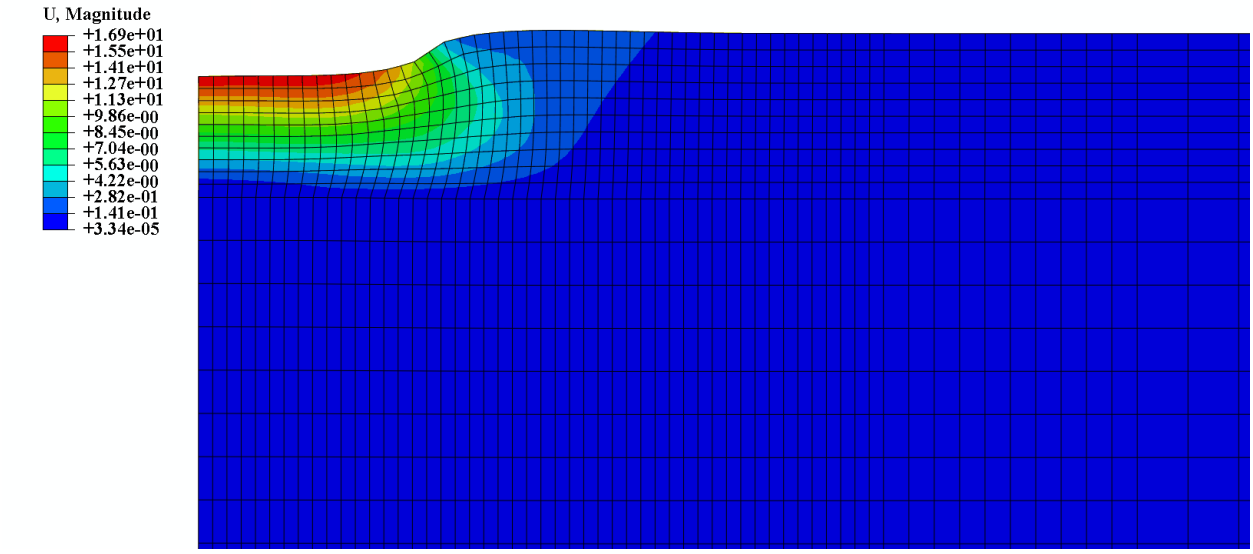

Figure 4-33: The rutting performance of North part of Lane-3 from NAPMRC test section by FE model.

4.6.5.6.1. Finite element validation of confinement level

The confinement pressure induced by the applied load in different elements of asphalt layer as indicated in the Figure 4-34 was determined. The confinement pressure varies from 0 to 1200 kPa due to application of deviatoric stress level, while the second deviatoric invariant varies from 0 to 430 kPa. As we move forward from the applied load (i.e., left to right) the intensity of confinement pressure and second deviatoric stress level are decreases. The initial applied confinement pressure is chosen to be 140 kPa, which were estimated because the joint at longitudinal direction inclines to be less compacted than the center of the pavement, due to the tendency to apply fewer passes at the joints. In addition, the less confinement level at unrestricted/unconfined joints and the higher rate of heat loses at those joints reduce the efficiency of compaction at those joints compared with the pavement center (*212*). The confinement within an asphalt layer cannot exceed the yield surface, which remains linear on the meridian plane for the asphalt concrete materials. The asphalt concrete materials behave more resistible to the applied

axial stress and produce less strain magnitude by increasing the confinement level because the slippage and change of the aggregate orientation during deformation decrease (*88*). Therefore, a far element from applied load consider as representative of initial confinement pressure of 140 kPa as the starting point of the experimental tests.

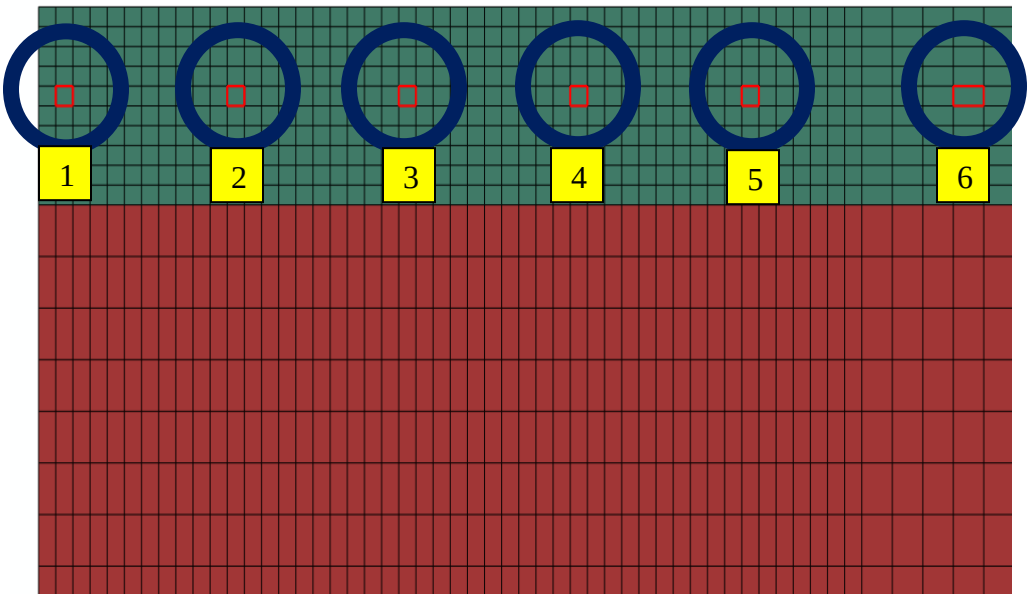

(a)

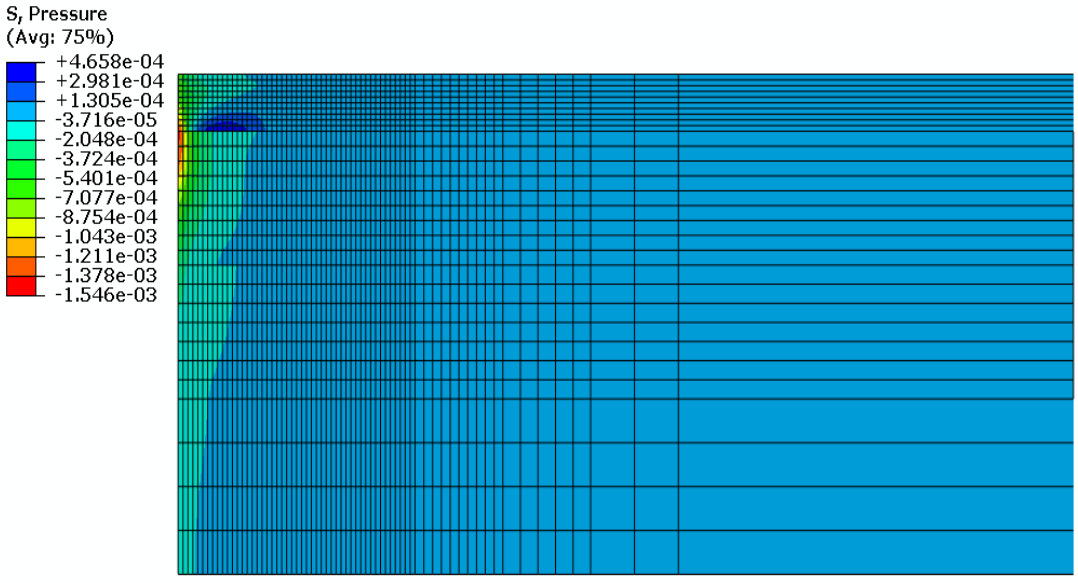

(b)

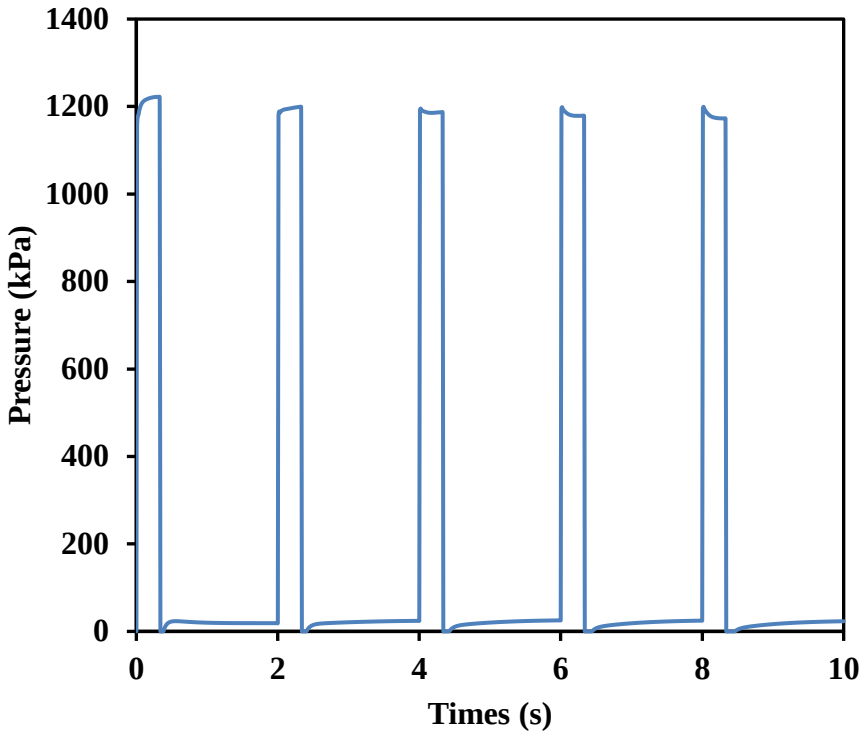
1400
1200
1000
800
600
400
200
0
Pressure (kPa)
0
2
4
6
8
10
Times (s)

(c)

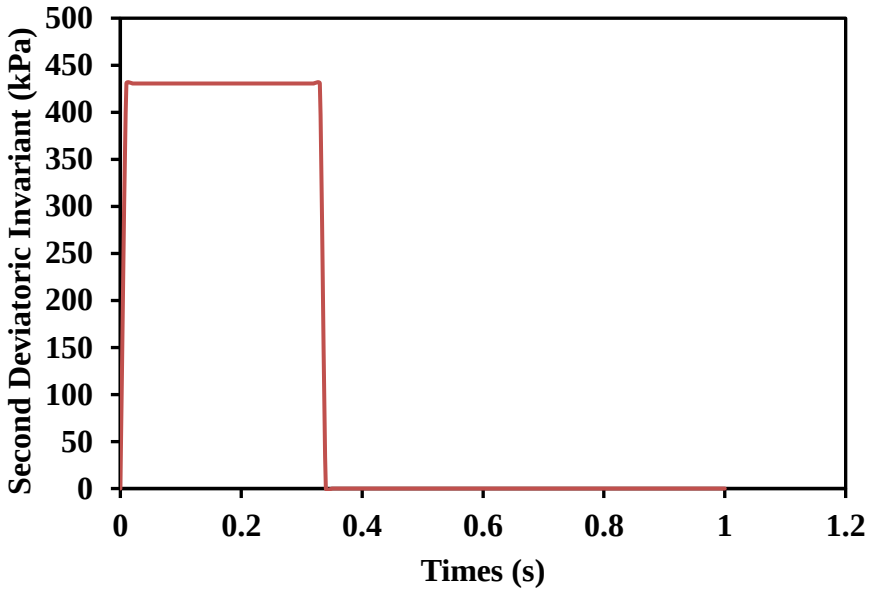
500
450
400
350
300
250
200
150
100
50
0
Second Deviatoric Invariant (kPa)
0
0.2
0.4
0.6
0.8
1
1.2
Times (s)

(d)

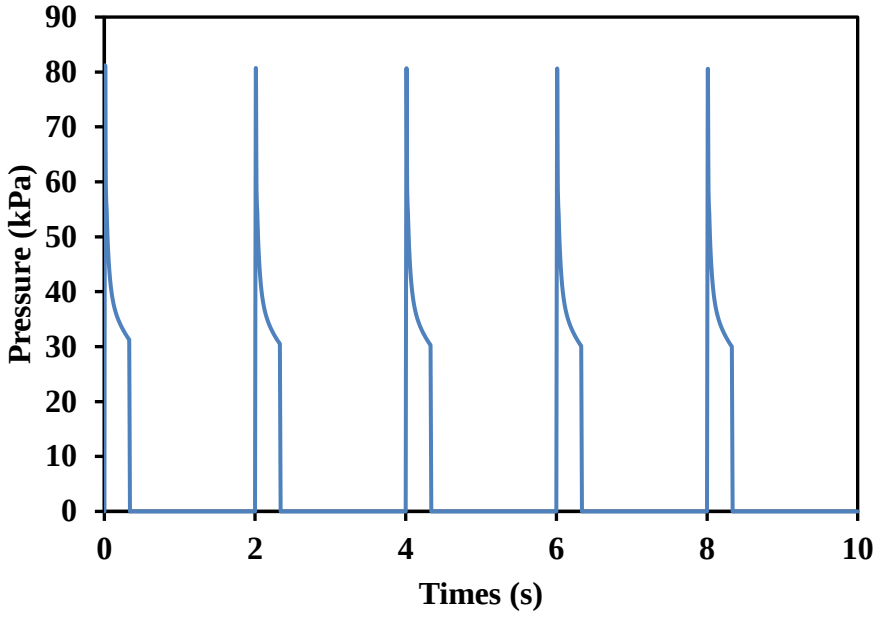

(e)

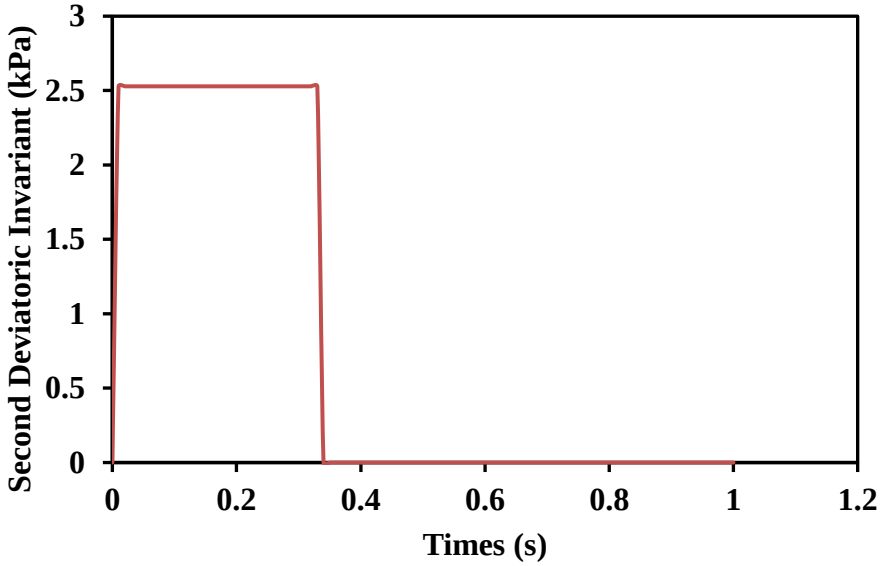

(f)

Figure 4-34: (a) The element locations; (b) The confinement pressure distribution; (c) The changes in confinement levels at element No. 1; (d) The second deviatoric invariant at element No. 2, (e) The changes in confinement levels at element No. 5; (f) The second deviatoric invariant at element No. 5.

4.7. Conclusion

This study, for the first time, implements a GAs analysis procedure to characterize VP and HR viscoplastic properties of asphalt concrete and improve the prediction of the permanent deformation under cyclic loading conditions. The developed procedure is capable of determining VP and HR viscoplastic properties of asphalt concrete considering the effects of deviatoric, confinement, and multi-axial state of stresses. The experimental studies, theoretical developments, and data analysis presented in this paper lead to the following results:

- The proposed GAs procedure along with the dynamic modulus, RCRT-VS, UCSR-C, and RCRT-CLR can be used effectively to characterize VP and HR viscoplastic responses of asphalt concrete materials;
- Model predictions with the VP and HR viscoplastic analysis procedure by GAs show that the proposed procedure significantly improves the accuracy of the model parameters of asphalt concrete at high temperatures subjected to cyclic-compression loading.
- It should be noted that the proposed GAs analysis procedure of VP and HR viscoplastic is general and can be applied to time- and rate-dependent materials which show the viscoplastic-softening (or recovery in the hardening level) behavior during the unloading and rest period.
- Comparisons between the characterized VP and HR viscoplastic model and experimental measurements illustrate the capabilities of the proposed model and GAs characterization procedure in capturing VP and HR viscoplastic response of asphalt concrete materials.

- Addition of Evotherm-M1 to both types of modified (i.e., PG 76-22) and unmodified (i.e., PG 64-22) virgin binders used in FAA's NAPMRC test sections will result in more HR viscoplastic strain.
- The result is consistent with the traffic tests results conducted by FAA on NAPMRC flexible pavement test sections (*131*), both of WMA and HMA PG 64-22 test were found to be the worst performing test in terms of resulting in more VP and HR viscoplastic strain, which will result in more rutting. The HMA PG 76-22 performed slightly better than the respective WMA test.

Finally, the implemented GAs analysis procedure was a promising tool to capture constitutive modeling of the VP and HR viscoplastic responses of asphalt concrete materials, time- and rate-dependent materials, subjected to general loading conditions.

5. Chapter 5: Effect of Evotherm–M1 on Stress-dependent Behavior and Rutting Resistance of Modified/Unmodified Asphalt Binders

5.1. Abstract

Rheological properties has an important role on understanding fundamental behavior of asphalt binders. This paper presents the analysis of laboratory tests conducted at University of Kansas (KU) and Texas A&M University (TAMU) for the federal aviation administration's (FAA) modified/unmodified asphalt binders plus Evotherm-M1 additive. All binder samples have been prepared for multiple stress creep recovery (MSCR) and strain controlled frequency sweep (FS) tests by short-term aged asphalt binder samples using rolling thin film oven (RTFO). The MSCR and FS testing performed using dynamic shear rheometer (DSR), along with the extraction of master curve of all four types of asphalt binders used in FAA's national airport pavement and materials research center (NAPMRC) test sections. Master curve were extracted to characterize phenomenological behavior of asphalt binders under dynamic shear loading in ranges of frequency, temperature and strain of interest. In addition, the nonrecoverable creep compliance (i.e., J_{nr}) and the percentage recovery (i.e., R) values were calculated at each cycle. The average R and J_{nr} values were also calculated at each stress level. The MSCR test results clearly show that polymer modified PG 76-22 is more sensitive to Evotherm-M1 additive as compared to unmodified PG 64-22. Furthermore, asphalt binder materials used in FAA's NAPMRC test sections can be ranked with respect to their resistance to rutting as: polymer modified PG 76-22, polymer modified PG 76-22 plus Evotherm-M1, unmodified PG 64-22, and unmodified PG 64-22 plus Evotherm-M1. It worth mentioning that the results are consistent with the traffic tests results conducted by FAA on NAPMRC flexible pavement test sections (*131*), both modified and

unmodified asphalt binders plus Evotherm-M1 additive test were found to be the less performing test compare to virgin modified and unmodified asphalt binders.

5.2. Introduction

Variety of loads and climate conditions cause various types of distresses on asphalt concretes. Permanent deformation on the wheels path, rutting, is one of the common distress induced by traffic loadings. Several factors cause permanent deformation of asphalt concretes, one of the most important one is reduced viscosity of the binders at high temperatures (*213*). Different types of modifiers were used to enhance resistance of asphalt concretes against rutting by changing properties of asphalt binders (*214-229*) such as styrene-butadienestyrene (SBS) (*230; 231*), ground tire rubber (GTR) (*232; 233*), and polyphosphoric acid (PPA) (*234-236*). Considering rutting, although an appropriate modifier is the one that helps to recover most of the binder's deformation, but modifiers significantly varied with respect to their impact on the time- and temperature-dependent behavior of the modified asphalt (*237; 238*). Polymer modified performance grade (PG) 76-22 asphalt binders used in this study were modified by SBS, which can increase its stiffness, reduce the temperature susceptibility and improve the adhesion and cohesion properties (*217; 218; 239; 240*). Asphalt binders reveal stress-dependent behavior, which is significantly affected by the amount and type of modifiers (*241; 242*). This behavior starts linear at low stress level (i.e., about 100 Pa) and as stress level increases it becomes more non-linear (*243; 244*). This study aims to investigate the effect of Evotherm-M1 on stress-dependent behavior of modified/unmodified asphalt binders used in the FAA's NAPMRC test sections.

Evotherm-M1 is one of the new products which have been developed with the goal of reducing the mixing and compaction temperatures of hot mix asphalt (HMA) without sacrificing

the quality of the resulting pavement, from 30 °C to 50 °C lower than conventional HMA. WMA is the common term for different technologies (e.g., Evotherm-M1) that allows mixing procedure at lower temperatures compare to HMA. WMA technologies were initiated in Europe in 1996, and were used in United States afterward in numerous trial road sections (*245-248*). Although there has been limited information about long-term performance of WMA, but using WMA allows paving benefits, reduces fuel usage and emission, which result in a better working condition (*249-261*). Paving benefits includes improve the compact-ability of mixtures with lower energy consumption, overall reduction in air voids, cold-weather paving, long haul distances, higher percentage of reclaimed asphalt pavements (RAP), less restriction (more production in non-attainment areas), and specific pavement rehabilitations (*250*). However, addition of Evotherm-M1 may affect the resilient modulus of an asphalt mix or may increase the rutting potential of an asphalt mixture. In this study, performance of the Evotherm–M1 as a compaction technology additive to modified/unmodified asphalt binders used in FAA's NAPMRC test sections were evaluated.

To evaluate the performance of modified/unmodified asphalt binders plus Evotherm–M1 additive, rheological properties should be determined. The relationship between load and deformation for viscoelastic materials such as asphalt binders is known as rheological properties. These material properties has an important role on selection and evaluation of asphalt layer on pavement structure. Different rheological modeling of the asphalt materials have been proposed (*262-280*). Considering dynamic loading, although the nonlinearity of asphalt binders has been recognized, effect of strain level has not been considered in modeling (*276-281*). In this study, universal model on a phenomenological basis of modified/unmodified asphalt binders based on Christensen-Anderson mathematical model (*269*) under shear oscillating loading in ranges of

frequency, temperature and strain of interest developed by Zeng et al. (*162*) were used to characterize the dynamic properties of asphalt binders and extract master curve.

5.3. Objectives

The primary objectives of the study presented in this paper are to:

- Investigate rheological properties and stress-dependent behavior of modified/unmodified asphalt binders plus Evotherm–M1 additive.
- Apply multiple stress creep-recovery (MSCR) tests to study the stress-dependent behavior of asphalt binders.
- Use strain controlled Frequency Sweep (FS) tests to characterize phenomenological behavior of asphalt binders under dynamic shear loading in different ranges of interest frequencies, temperatures and strains.
- Evaluate performance of the Evotherm–M1 as a compaction technology additive.
- Observe the trends regarding the recovery of the accumulated strains.

5.4. Rolling Thin-Film Oven Test Results

The test data was analyzed for obtaining the change in sample mass corresponding to heat in an oven for 85 min at 163 °C (325 °F). In addition, the general relationship of change in sample mass obtained. Finally, the standard deviation and acceptable range of two test results are determined based on ASTM C 670 (*282*). Table 5-1 summarize the test results for all four types of asphalt binders used in FAA's NAPMRC test sections.

Table 5-1: RTFO test results for all four types of binders used in FAA's NAPMRC test sections.

Binder types	M_1 (g)	M_2 (g)	M_b (g)	M_s (g)	%ΔM (g)	$\%M_{Loss}$ (g)	X_{avg}	$(1s)^{a,b}$	$(d2s)^{a,b,c}$
	Initial mass	Final mass of bottle and asphalt	Empty weight of bottle	Sample mass	Mass change of the sample as a percentage of the original mass	Mass loss 0.0 to 0.1% OK	average value of two test results	Standard Deviation <0.0079 OK	Acceptable Range of Two Test Results <0.0224 OK
Unmodified PG 64-22	203.1	202.8	169.7	33.4	99.10180	0.00898	0.00911	0.00643	0.01820
	205	204.7	172.5	32.5	99.07692	0.00923		0.00644	
Unmodified PG 64-22 plus Evotherm-M1	205.2	204.9	173.9	31.3	99.04153	0.00958	0.00952	0.00645	0.01824
	203.1	202.8	171.4	31.7	99.05363	0.00946		0.00644	
Polymer modified PG 76-22	206.8	206.5	174	32.8	99.08537	0.00915	0.00904	0.00643	0.01819
	206.5	206.2	172.9	33.6	99.10714	0.00893		0.00642	
Polymer modified PG 76-22 plus Evotherm-M1	210.8	210.5	176.6	34.2	99.12281	0.00877	0.00872	0.00642	0.01816
	207	206.7	172.4	34.6	99.13295	0.00867		0.00641	

5.5. Multiple Stress Creep-Recovery (MSCR) Test Results

The MSCR test was conducted on RTFO-aged (*149; 153*) binders according to AASHTO T 350 (*160*), including polymer modified PG 76-22 with/without Evotherm-M1 and unmodified PG 64-22 with/without Evotherm-M1 binders. This resulted in four binder types, with two replicates (each with standard deviation of less than 10%), amounting to eight acceptable MSCR tests. Based on the MSCR test results indicated in Table 5-2, Figure 5-1, Figure 5-2, and Figure 5-3 the following discussions can be drawn:

- The MSCR test results clearly show that polymer modified PG 76-22 is more sensitive to Evotherm-M1 modification as compared to unmodified PG 64-22. Furthermore, asphalt binder materials used in FAA's NAPMRC test sections can be ranked with respect to their resistance to rutting as followed:
  - Polymer modified PG 76-22,
  - Polymer modified PG 76-22 plus Evotherm-M1,
  - Unmodified PG 64-22, and
  - Unmodified PG 64-22 plus Evotherm-M1.

  considering polymer modified PG 76-22 being the most resistant to rutting and unmodified PG 64-22 plus Evotherm-M1 being the most susceptible to rutting.

- By adding Evotherm-M1 to the modified/unmodified asphalt binders, polymer modified PG 76-22 shows an increase of 23% in J_{nr} at 3.2 kPa. However, the J_{nr} at 3.2 kPa for unmodified PG 64-22 only increases by 9% with Evotherm-M1 addition. Therefore, it is suspected that the difference between rutting performance of polymer modified PG 76-22 and polymer modified PG 76-22 plus Evotherm-M1 will be more significant as that of unmodified PG 64-22 and unmodified PG 64-22 plus Evotherm-M1.
- Polymer modified PG 76-22 and polymer modified PG 76-22 plus Evotherm-M1 are highly nonlinear with respect to the applied stress levels. The percent difference in J_{nr} for polymer modified PG 76-22 and polymer modified PG 76-22 plus Evotherm-M1 are much higher than that of unmodified PG 64-22 and unmodified PG 64-22 plus Evotherm-M1, 55% as compared to 17% respectively. Therefore, it is expected that the asphalt mixtures made with polymer modified PG 76-22 to be more susceptible to the changes in the stress level and tire pressure.
- Polymer modified PG 76-22 and unmodified PG 64-22 can be characterized as heavy binders while polymer modified PG 76-22 plus Evotherm-M1 and unmodified PG 64-22 plus Evotherm-M1 can be regarded as standard binders. MSCR test results show that J_{nr} at 3.2 kPa is less than 2 kPa^{-1} for polymer modified PG 76-22 and unmodified PG 64-22 binders $1 < J_{nr} < 2$ and is higher than 2 kPa^{-1} for polymer modified PG 76-22 plus Evotherm-M1 and unmodified PG 64-22 plus Evotherm-M1. Therefore, the neat binders can be graded as heavy binders and Evotherm-additive binders can be graded as standard binders.
- Polymer modified PG 76-22 with/without Evotherm-M1 binders show higher level of elastic response as compared to unmodified PG 64-22 with/without Evotherm-M1. The

%R values for polymer modified PG 76-22 with/without Evotherm-M1 are much higher than %R for unmodified PG 64-22 with/without Evotherm-M1 (8% as compared to 1% at 3.2 kPa), which is a clear indication that polymer modified PG 76-22 will show more recoverable deformation when subjected to traffic.

Table 5-2: MSCR test results for all four types of binders used in FAA's NAPMRC test sections.

Binder Type	Recovery Portion			Non-Recovered Portion			Indication that the asphalt binder is modified: Load Level 3.2 kPa
	Average Recovery, %		Percent Difference of Recovery, %	Average Non-Recoverable Creep Compliance (J_{nr}), 1/kPa		Percent Difference of J_{nr}, %	
	0.1 kPa	3.2 kPa		0.1 kPa	3.2 kPa		
Unmodified PG 64-22	7.02	0.99	85.94	1.64	1.93	17.65	Probably not modified
Unmodified PG 64-22 plus Evotherm-M1	6.70	0.76	88.61	1.78	2.10	18.02	Probably modified
Polymer modified PG 76-22	32.87	9.75	70.37	1.24	1.92	55.48	Probably not modified
Polymer modified PG 76-22 plus Evotherm-M1	29.62	6.89	76.80	1.51	2.37	57.28	Probably modified

(a)

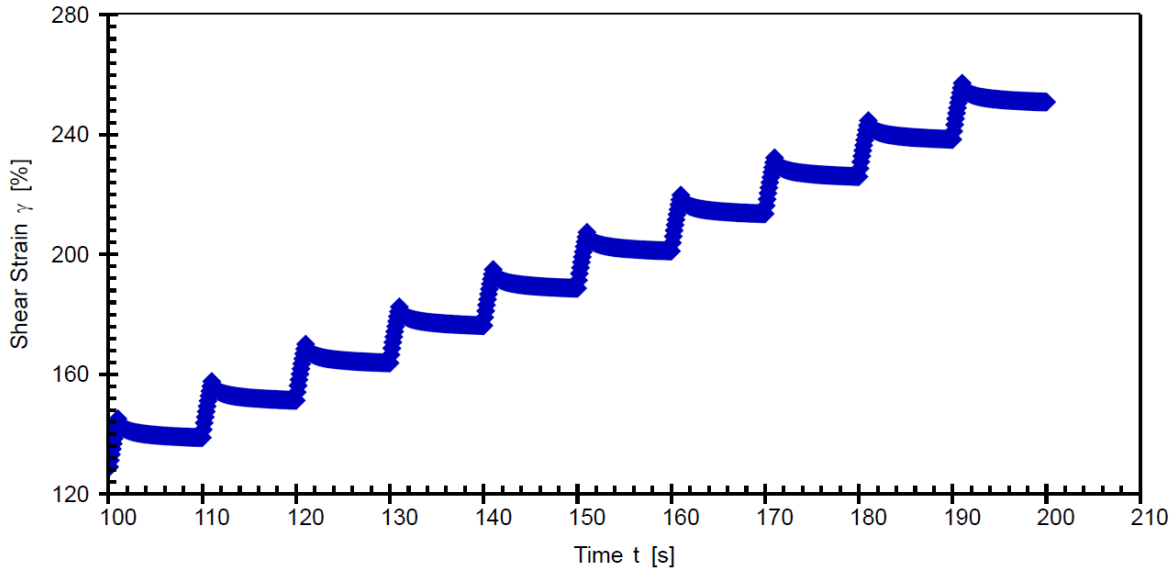
Shear Strain γ [%]
280
240
200
160
120
100
110
120
130
140
150
160
170
180
190
200
210
Time t [s]

(b)

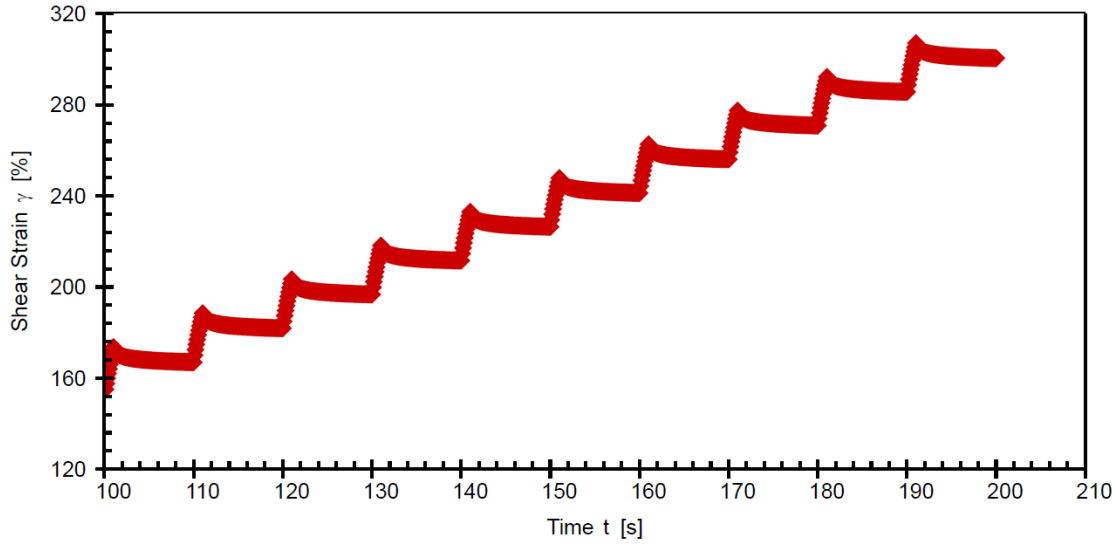
Shear Strain γ [%]
320
280
240
200
160
120
100
110
120
130
140
150
160
170
180
190
200
210
Time t [s]

(c)

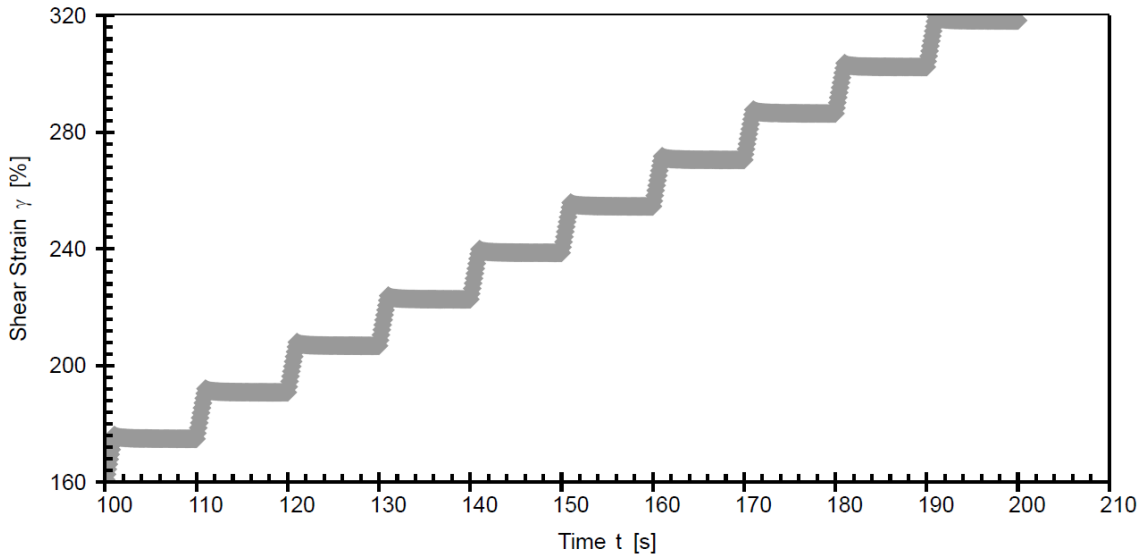

(d)

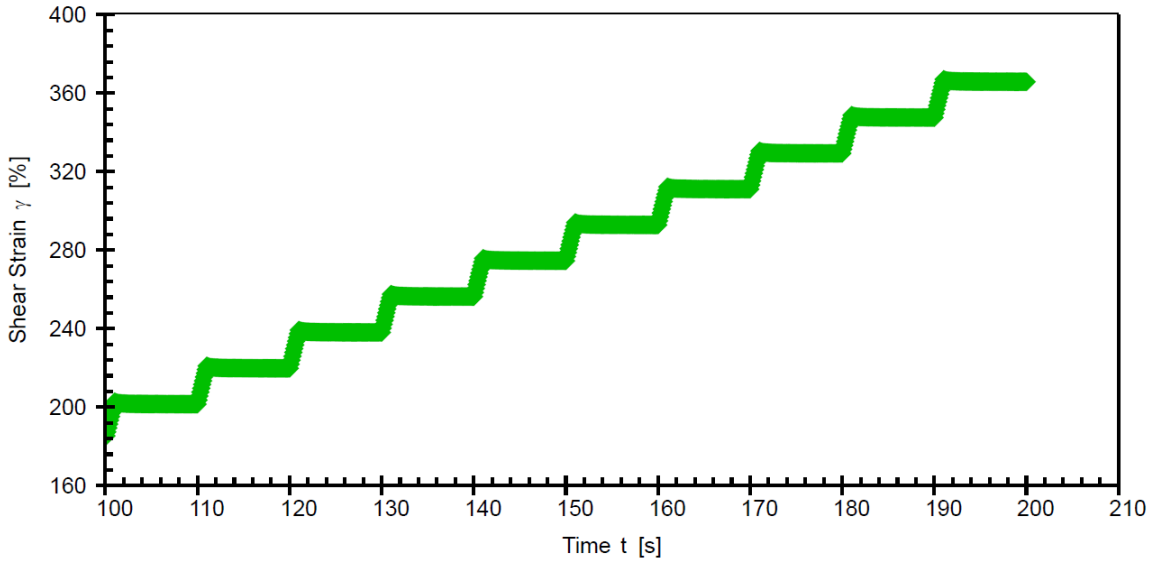

Figure 5-1: MSCR 0.1kPa (conditioning cycles are not shown) (a) Polymer modified PG 76-22; (b) Polymer modified PG 76-22 plus Evotherm-M1; (c) Unmodified PG 64-22; (d) Unmodified PG 64-22 plus Evotherm-M1.

(a)

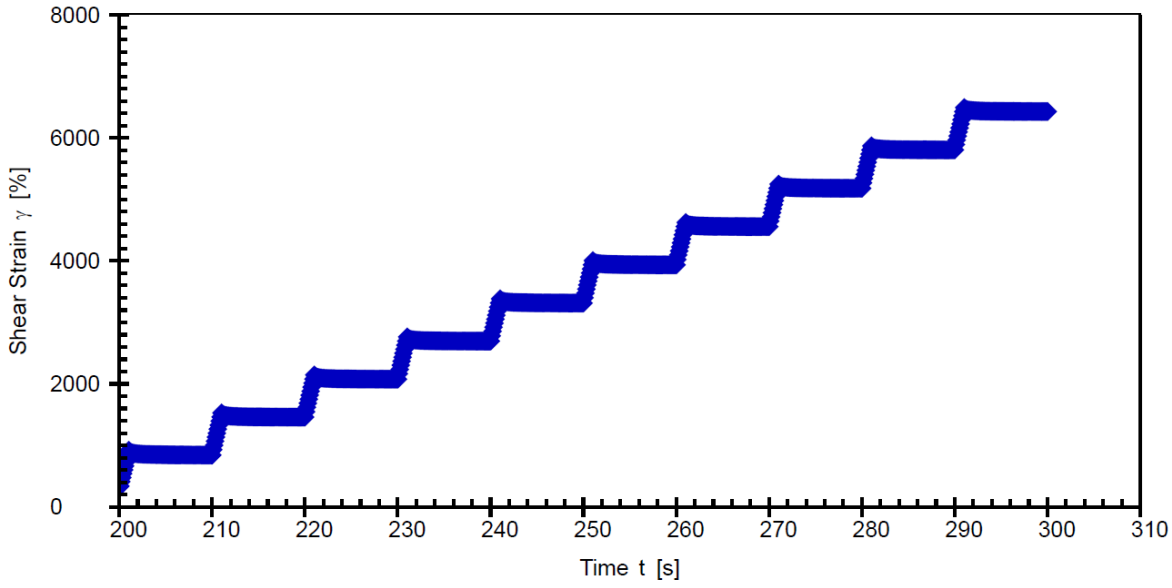
8000
6000
4000
2000
0
Shear Strain γ [%]
200
210
220
230
240
250
260
270
280
290
300
310
Time t [s]

(b)

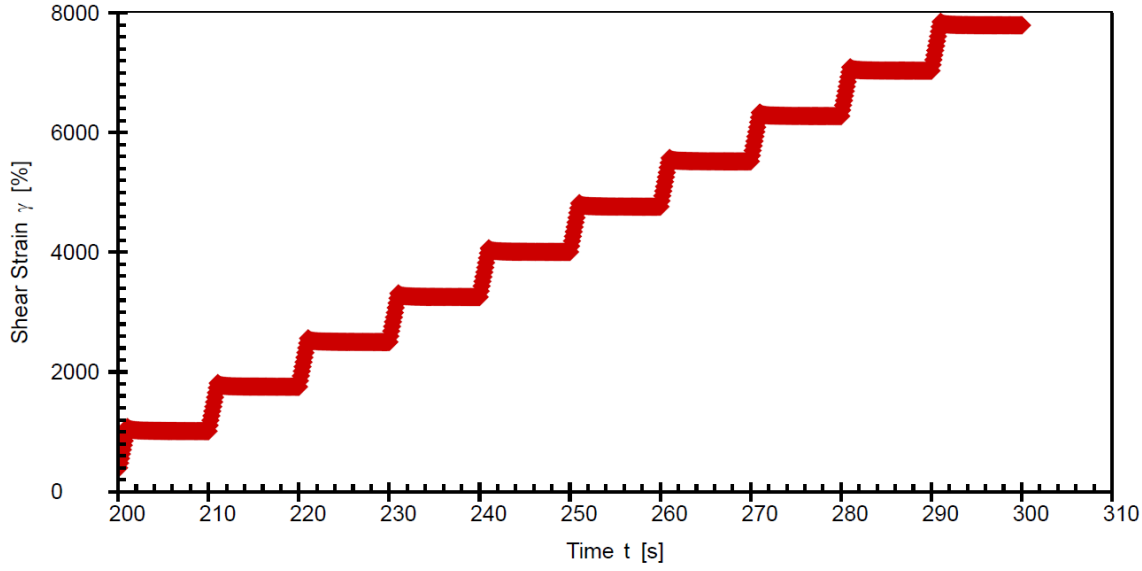
8000
6000
4000
2000
0
Shear Strain γ [%]
200
210
220
230
240
250
260
270
280
290
300
310
Time t [s]

(c)

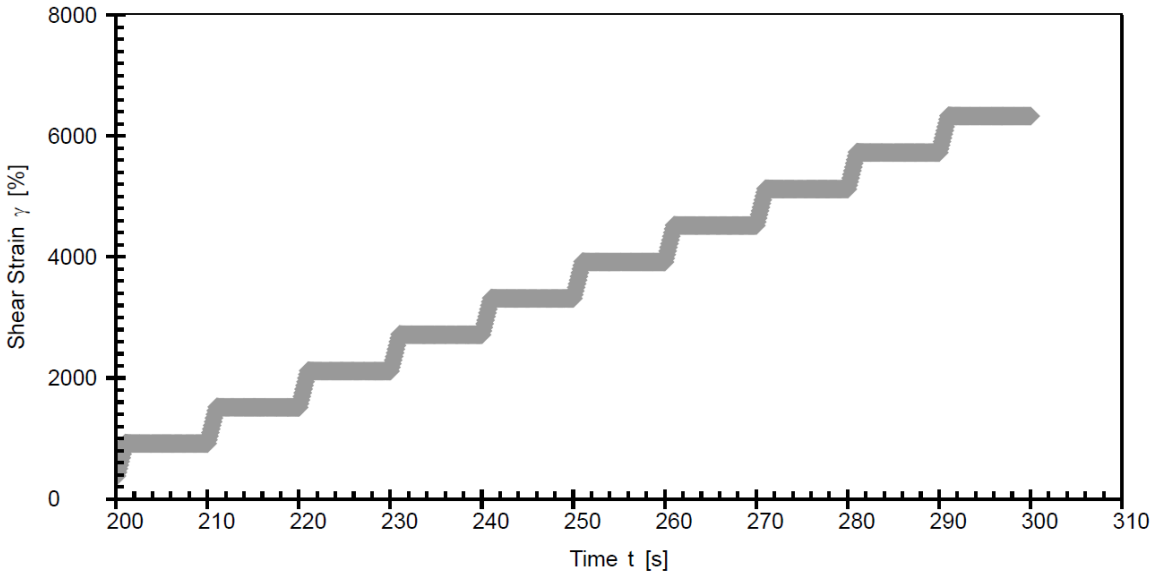

(d)

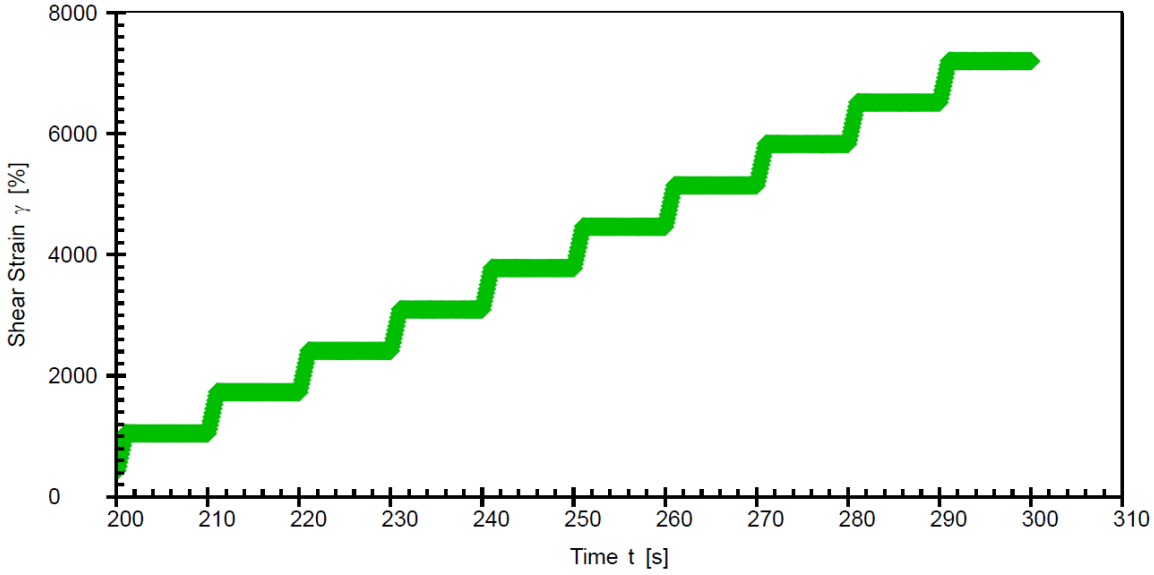

Figure 5-2: MSCR 3.2kPa (a) Polymer modified PG 76-22; (b) Polymer modified PG 76-22 plus Evotherm-M1; (c) Unmodified PG 64-22; (d) Unmodified PG 64-22 plus Evotherm-M1.

(a)

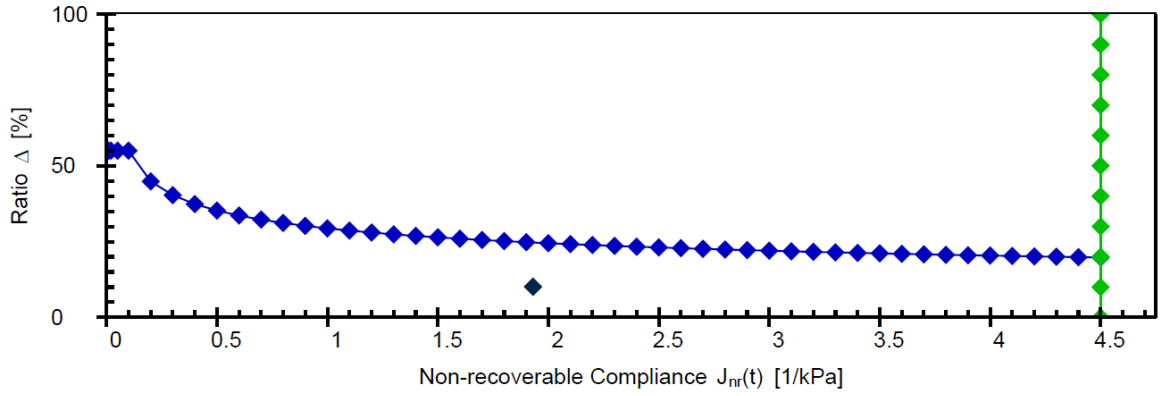
100
50
0
Ratio Δ [%]
0
0.5
1
1.5
2
2.5
3
3.5
4
4.5
Non-recoverable Compliance $J_{nr}(t)$ [1/kPa]

(b)

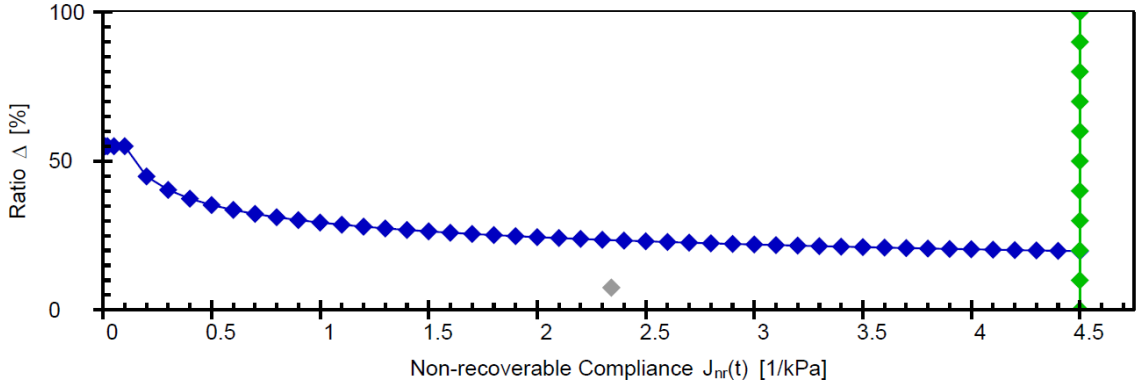
100
50
0
Ratio Δ [%]
0
0.5
1
1.5
2
2.5
3
3.5
4
4.5
Non-recoverable Compliance $J_{nr}(t)$ [1/kPa]

(c)

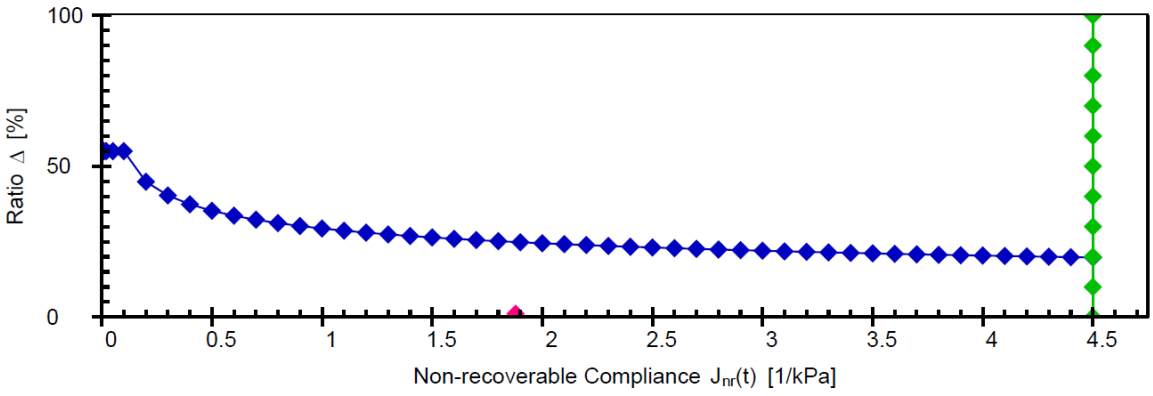
100
50
0
Ratio Δ [%]
0
0.5
1
1.5
2
2.5
3
3.5
4
4.5
Non-recoverable Compliance $J_{nr}(t)$ [1/kPa]

(d)

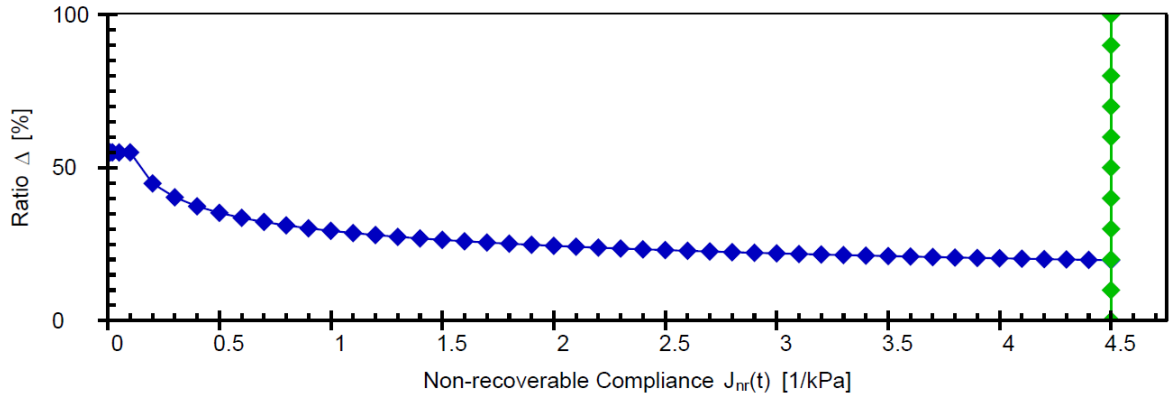

Figure 5-3: J_{nr} vs. percent recovery (at 3.2 kPa). (a) Polymer modified PG 76-22; (b) Polymer modified PG 76-22 plus Evotherm-M1; (c) Unmodified PG 64-22; (d) Unmodified PG 64-22 plus Evotherm-M1.

5.6. Strain Controlled Frequency Sweep (FS) Test Results

The test data was analyzed based on the model presented by Zeng et al. (*162*) to obtain the dynamic shear modulus and phase angle of asphalt binder corresponding to variable temperatures and frequencies as mentioned before. In addition, the general relationship of change in dynamic shear modulus and phase angle obtained. Finally, the percent difference of two test results are determined. The percent difference should not pass 10% for 10, 20, and 30 °C test temperatures and should not pass 15% for 40, 50, 60, and 70°C test temperatures. Figure 5-4, Figure 5-5, Figure 5-6, and Figure 5-7 show the dynamic modulus versus frequency for all four types of asphalt binders used in FAA's NAPMRC test sections.

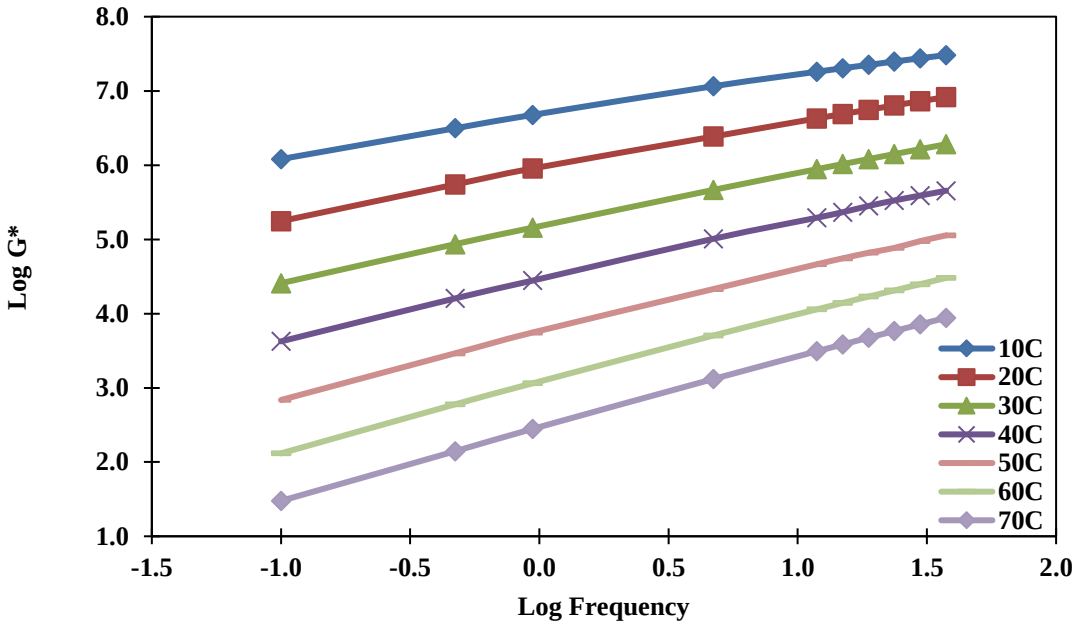

Figure 5-4: Dynamic modulus vs frequency for unmodified PG 64-22 binder

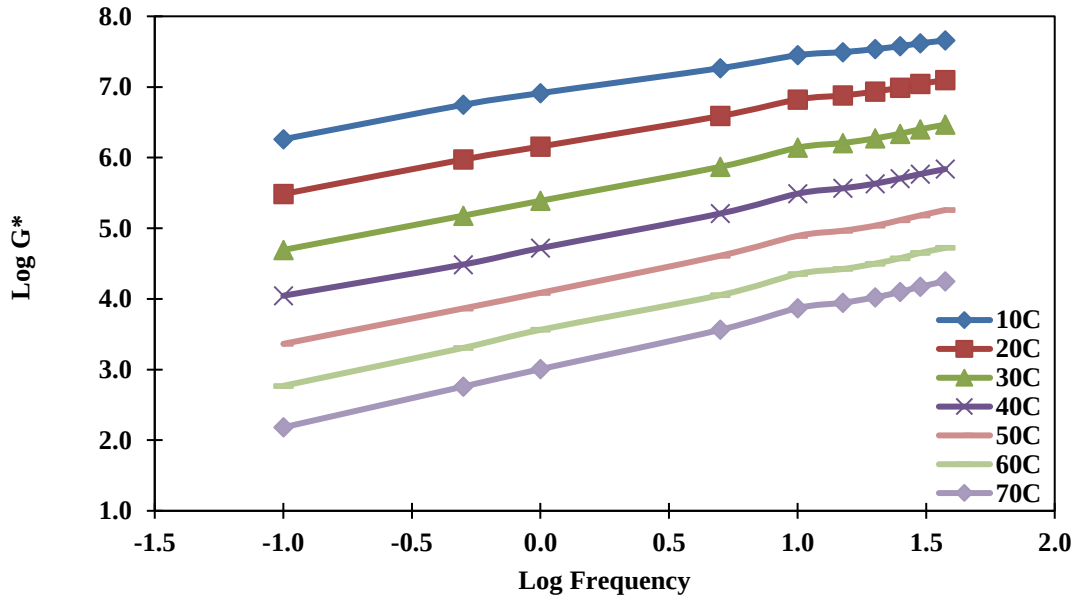

Figure 5-5: Dynamic modulus vs frequency for polymer modified PG 76-22 binder

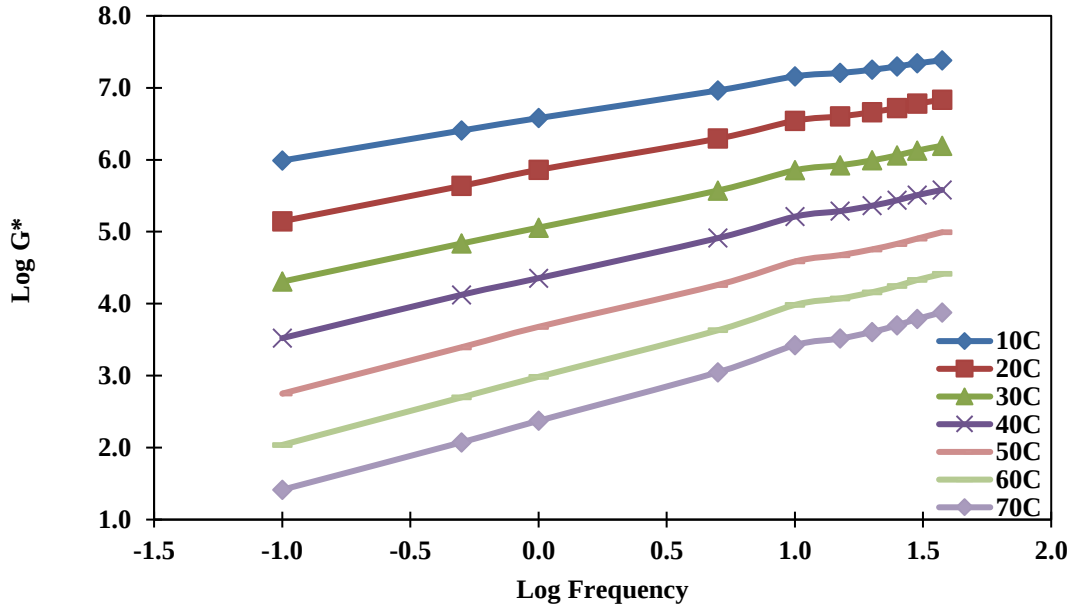

Figure 5-6: Dynamic modulus vs frequency for unmodified PG 64-22 binder plus Evotherm-M1

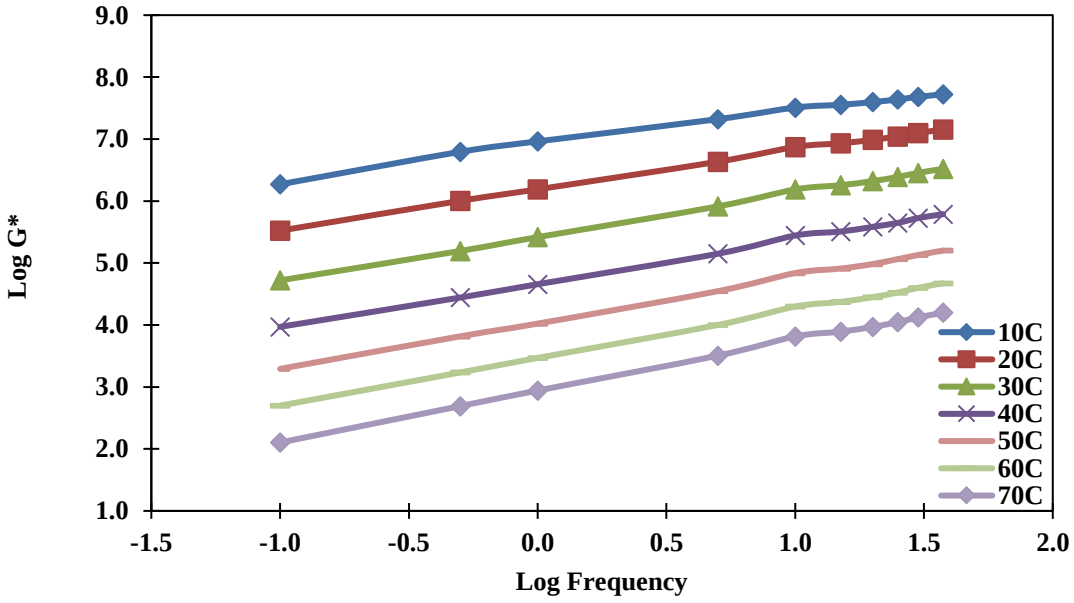

Figure 5-7: Dynamic modulus vs frequency for polymer modified PG 76-22 binder plus Evotherm-M1

The Christensen-Anderson mathematical model (*269*), which can characterize the viscoelastic properties of asphalt binder, was used to construct the master curves of aged binders. This model can be expressed as shown in Equation 5-1:

Equation 5-1 $$G^*(f) = (G^*)_g \left[1 + \left(\frac{f_c}{f_R}\right)^k\right]^{-\frac{m_e}{k}}$$

where $G^*(f)$ is complex shear modulus at the frequency of f, $(G^*)_g$ is glassy modulus (assumed to be equal to 1 GPa), k and m_e are shape parameters and they are dimensionless, f_c is the crossover frequency at the defining temperature, and f_R is the reduced frequency at the defining temperature (i.e., T_R). The f_R is a function of shift factor as shown in Equation 5-2:

Equation 5-2 $$f_R = f \times 10^{\log a_T}$$

where $\log a_T$ is the shift factor as a function of temperature, T is the test temperature (K). The shift factor presents the amount of shifting that is required for data obtained at each test temperature to be shifted to a reference temperature (i.e., T_R). Reference temperature is related to the glass transition temperature, which represents the temperature dependency of the binder. The Williams-Landel-Ferry (WLF) equation, expressed as Equation 5-3, accurately describes the shift factor of asphalt binders (*268; 283*).

Equation 5-3 $$\log a_T = \frac{C_1(T - T_R)}{C_2 + T - T_R}$$

where C_1 and C_2 are constant and temperature constant, respectively. The rheological parameters (k, m_e, f_c, C_1, and C_2) of the Christensen-Anderson model have specific physical significance. Table 5-3 shows the values of the rheological parameters of the studied binders at

reference temperature, which is arbitrarily chosen 20 °C. The value of the crossover frequency (f_c) is related to the overall hardness of the binder. As the crossover frequency increases, the hardness of the binder decreases. Binders plus Evotherm-M1 show higher values of crossover frequency compared to the modified/unmodified virgin binders. In other words, the addition of the Evotherm-M1 decrease the hardness of the modified/unmodified virgin binders. While this decrease in the hardness will have a negative effect on the behavior of the binder at high temperatures (it will decrease the rutting resistance). Similar findings were also reported in the previous studies (*237; 283*).

Table 5-3: Rheological properties of binders used in FAA's NAPMRC test sections.

Binder Type	Constant	Temperature constant	Crossover frequency	Shape parameter	Shape parameter	Reference temperature
	C_1	C_2	f_c	k	m_e	T_R
			(Hz)			(°C)
Unmodified PG 64-22	-15.786	137.610	15.741	0.146	1.119	20
Unmodified PG 64-22 plus Evotherm-M1	-15.512	139.200	16.332	0.143	1.138	
Polymer modified PG 76-22	-16.119	138.387	947.673	0.194	0.815	
Polymer modified PG 76-22 plus Evotherm-M1	-16.029	134.069	1074.838	0.207	0.814	

Figure 5-8, Figure 5-9, Figure 5-10, and Figure 5-11 present the master curve for all four types of asphalt binders used in FAA's NAPMRC test sections. Figure 5-12 shows the master curves for RTFO-aged binders of FAA's NAPMRC test sections. According to the Figure 5-12, dynamic modulus (i.e., G^*) could be rank as polymer modified PG 76-22, polymer modified PG 76-22 plus Evotherm-M1, unmodified PG 64-22, and unmodified PG 64-22 plus Evotherm-M1 at low frequencies, which represent the high temperature properties of asphalt concrete. As dynamic modulus increases, recovered strain decreases. This is also in agreement with to Witczak's

predictive equation (*284*), which developed between the dynamic modulus and mixture properties based on data from more than 200 different asphalt mixes, including a wide range of modified asphalts. Considering the same properties for the asphalt concretes: as bitumen viscosity increases (i.e., η), asphalt concrete dynamic modulus increases (i.e., G^*), which will result in reduction of recovered strain. Bitumen viscosity of polymer modified PG 76-22, polymer modified PG 76-22 plus Evotherm-M1, unmodified PG 64-22, and unmodified PG 64-22 plus Evotherm-M1 are 1.505, 1.215, 0.430 and 0.423 Pa.s, respectively, which extracted based on AASHTO T316 (*285*) and presented at JMF by FAA.

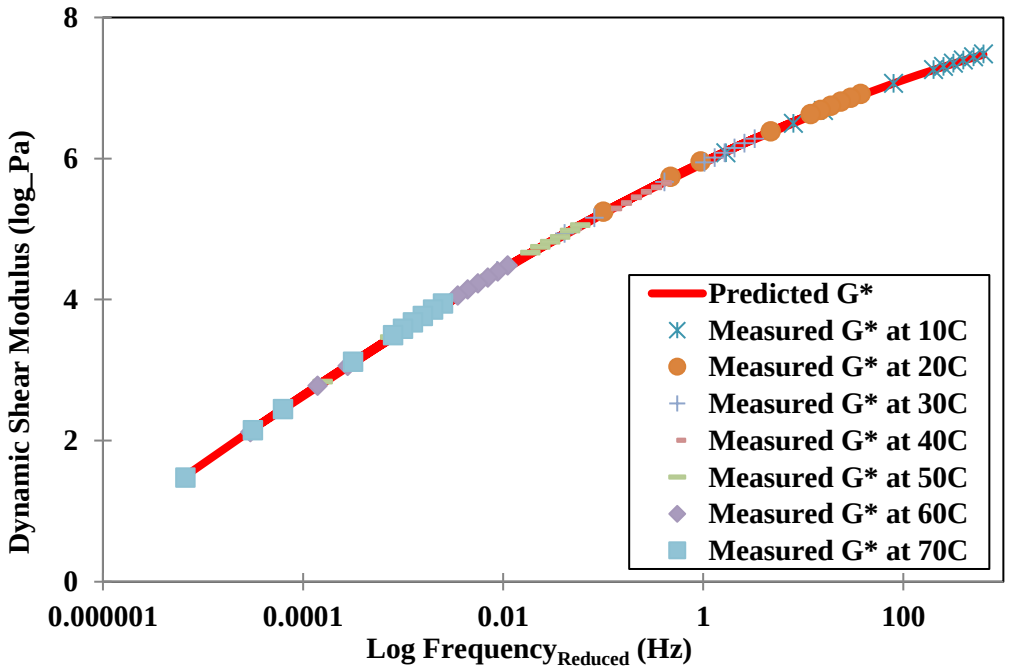

Figure 5-8: Master curve for RTFO-aged unmodified PG 64-22 binder

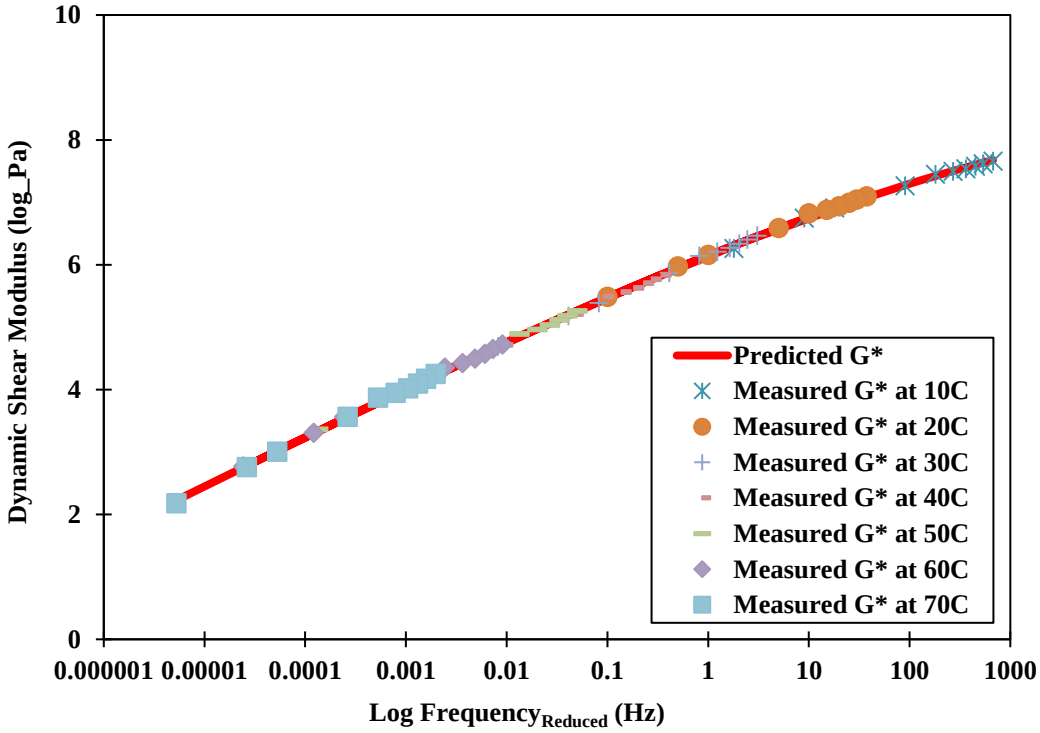

Figure 5-9: Master curve for RTFO-aged polymer modified PG 76-22 binder

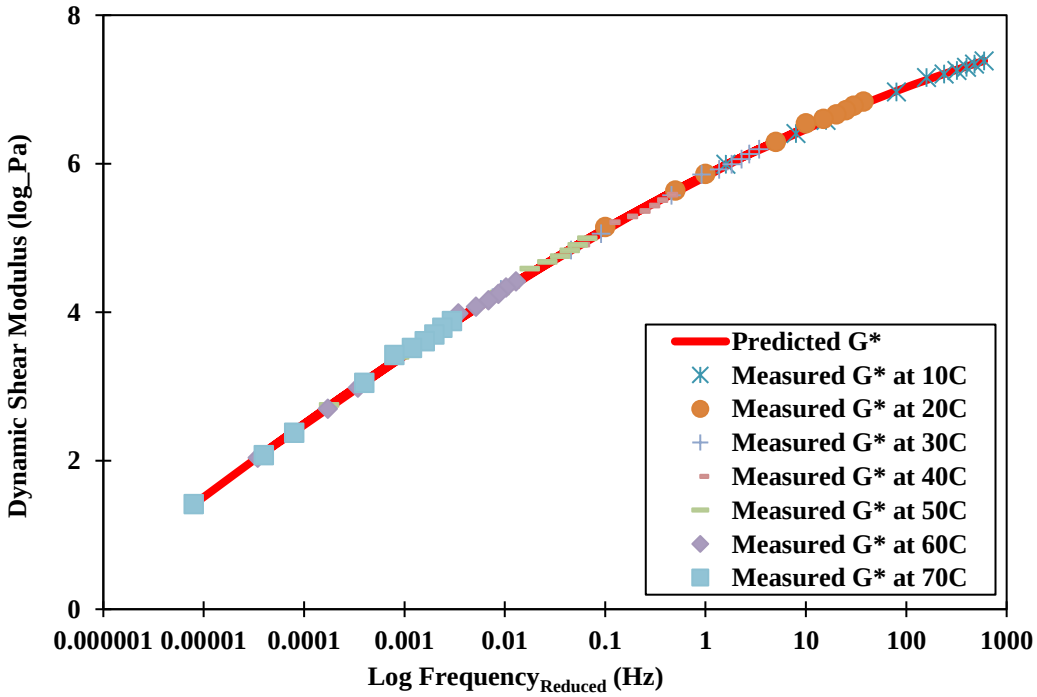

Figure 5-10: Master curve for RTFO-aged unmodified PG 64-22 binder plus Evotherm-M1

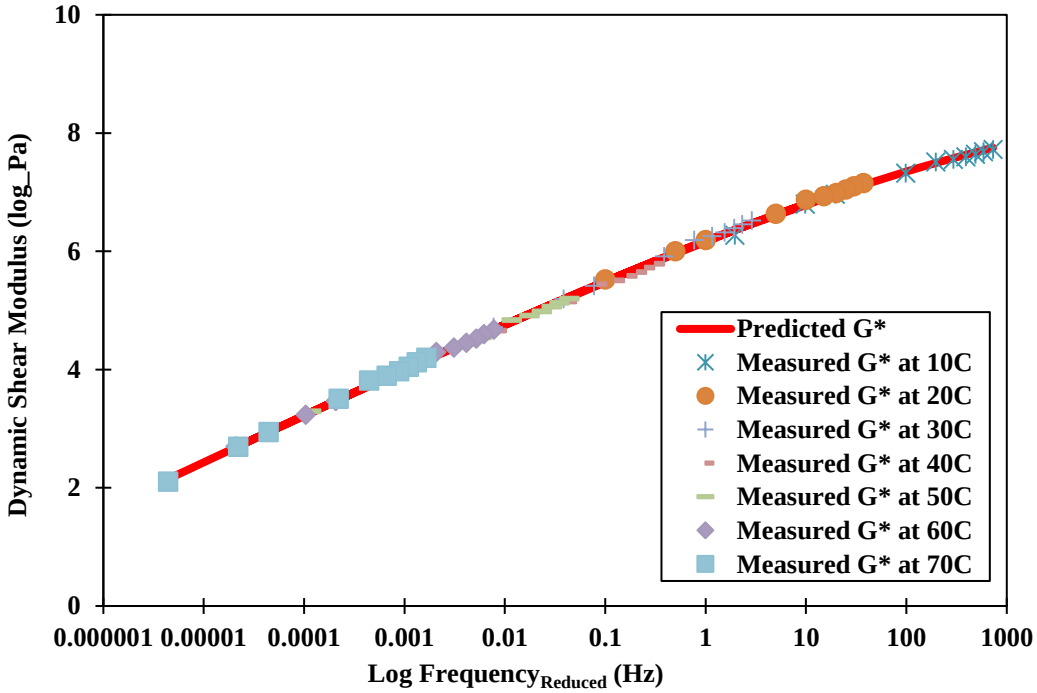

Figure 5-11: Master curve for RTFO-aged polymer modified PG 76-22 binder plus Evotherm-M1

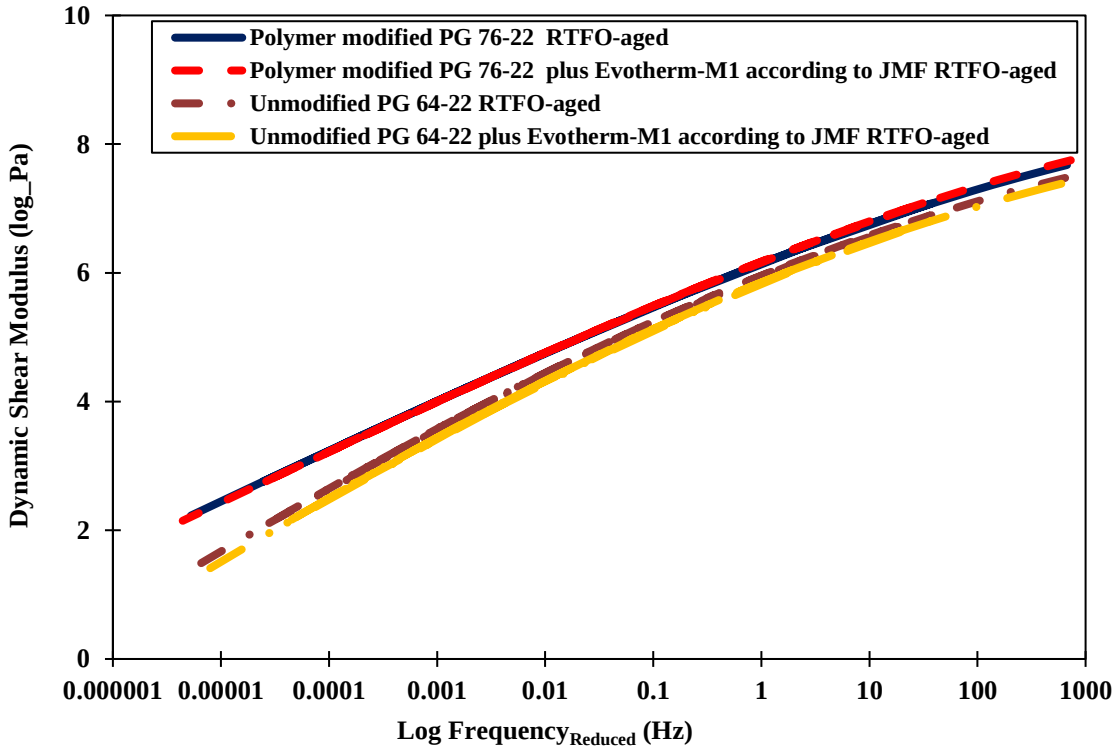

Figure 5-12: Master curves for RTFO-aged binders of NAPMRC test sections

5.7. Conclusions

This study investigates effect of Evotherm-M1 on rheological properties, stress-dependent behavior, and rutting resistance of modified/unmodified asphalt binders used in NAPMRC test sections. The proposed experiments were applied to extract master curve, percent recovery, and nonrecoverable creep compliance of asphalt binders. The DSR was used to grade the original, RTFO-aged and PAV-aged binders based on the conventional PG system. In addition, the DSR was used to grade the RTFO-aged binders based on the MSCR and strain controlled FS tests. The experimental studies and data analysis presented in this paper lead to the following conclusions:

- Polymer modified PG 76-22 is more sensitive to Evotherm-M1 additive as compared to unmodified PG 64-22.
- Addition of Evotherm-M1 cause an increase in the rutting potential with decrease in mixing and compaction temperatures.
- Asphalt binder materials used in FAA's NAPMRC test sections can be ranked with respect to their resistance to rutting as followed:
  - Polymer modified PG 76-22,
  - Polymer modified PG 76-22 plus Evotherm-M1,
  - Unmodified PG 64-22, and
  - Unmodified PG 64-22 plus Evotherm-M1.

  the results are consistent with the traffic tests results conducted by FAA on NAPMRC flexible pavement test sections (*131*), both modified and unmodified asphalt binders plus Evotherm-M1 additive test were found to be the less performing test compare to virgin modified and unmodified asphalt binders.

- Asphalt mixtures made with polymer modified PG 76-22 are more susceptible to the changes in the stress level and tire pressure.
- Modified/unmodified asphalt binders without Evotherm-M1 can be graded as heavy binders and Evotherm-M1 additive asphalt binders can be graded as standard binders.
- Polymer modified PG 76-22 with/without Evotherm-M1 will show more recoverable deformation when subjected to traffic compare to unmodified PG 64-22 with/without Evotherm-M1.
- Considering the same properties for the asphalt concretes: as bitumen viscosity increases, asphalt concrete dynamic modulus increases, which will result in reduction of recovered strain.
- Polymer modified PG 76-22 with/without Evotherm-M1 binders show higher level of elastic response as compared to unmodified PG 64-22 with/without Evotherm-M1.
- Addition of the Evotherm-M1 decrease the hardness of the modified/unmodified virgin binders.

6. Chapter 6: Conclusions and Future Work

6.1. Conclusion

As mentioned in different chapters of this dissertation, flexible pavements clearly show time-, rate-, and temperature-dependent responses. This makes extraction of material properties associated with the constitutive modeling of these materials very challenging and difficult. Therefore, pavement community is reluctant to fully implement this constitutive model due to its complicity. This dissertation aims to provide straightforward experimental and analytical procedures to characterize coupled viscoelastic, viscoplastic, and hardening-relaxation viscoplastic properties of asphalt concrete pavements while maintaining the required level of accuracy by incorporating the important factors affecting this mechanism. The proposed procedures were applied to extract material properties of asphalt mixtures used in FAA's NAPMRC test sections. Finally, model predictions were compared with experimental measurements for validations purposes. The experimental studies, theoretical developments, and data analysis presented in this dissertation lead to the following conclusions:

- PANDA incorporates several material constitutive relationships that define the behavior of asphalt mixtures at a wide range of stress and temperature levels;
- The dynamic modulus and RCRT-VS tests can be used effectively to characterize linear and nonlinear viscoelastic responses of asphalt concrete materials as well as time-temperature shift factors;
- The dynamic modulus, RCRT-VS, UCSR-C, and RCRT-CLR can be used effectively to characterize VP and HR viscoplastic responses of asphalt concrete materials;

- The proposed procedure in the chapter 3 along with the dynamic modulus and RCRT-VS tests can be used effectively to characterize nonlinear viscoelastic responses of asphalt concrete materials;
- The nonlinear viscoelastic response of asphalt concrete strongly depends on confining pressure, deviatoric stress level, and multi-axial state of stresses. Therefore, uniaxial tests such as uniaxial creep-recovery tests cannot be used accurately to characterize nonlinear viscoelastic properties of asphalt concrete.
- The nonlinear viscoelastic properties are highly correlated to the triaxiality ratio that accounts for confinement pressure, deviatoric stress level, and multi-axial stress states;
- The proposed model for nonlinear viscoelastic properties as a function of triaxiality ratio can be used effectively to simulate the nonlinear response of pavements under traffic when specific locations in pavement structures are subjected to general multi-axial state of stresses.
- The nonlinear viscoelastic response of asphalt concrete materials can be effectively expressed as a function of the triaxiality ratio.
- The nonlinear parameter g_1 decreases with the increase in triaxiality ratio leading to less creep strain either as the confinement level increases or the deviatoric stress level decreases.
- The nonlinear parameter g_2 increases with the increase in triaxiality ratio leading to higher recovery of viscoelastic strain during rest period as the confinement level increases and the deviatoric stress level decreases.

- Comparisons between the characterized nonlinear viscoelastic model and experimental measurements illustrate the capabilities of the proposed model and characterization procedure in capturing nonlinear viscoelastic response of asphalt concrete materials.
- The proposed GAs procedure in the chapter 4 along with the dynamic modulus, RCRT-VS, UCSR-C, and RCRT-CLR can be used effectively to characterize VP and HR viscoplastic responses of asphalt concrete materials;
- Model predictions with the VP and HR viscoplastic analysis procedure by GAs show that the proposed procedure significantly improves the accuracy of the model parameters of asphalt concrete at high temperatures subjected to cyclic-compression loading.
- It should be noted that the proposed GAs analysis procedure of VP and HR viscoplastic is general and can be applied to time- and rate-dependent materials which show the viscoplastic-softening (or recovery in the hardening level) behavior during the unloading and rest period.
- Comparisons between the characterized VP and HR viscoplastic model and experimental measurements illustrate the capabilities of the proposed model and GAs characterization procedure in capturing VP and HR viscoplastic response of asphalt concrete materials.
- Addition of Evotherm-M1 to both types of modified (i.e., PG 76-22) and unmodified (i.e., PG 64-22) virgin binders used in FAA's NAPMRC test sections will result in more HR viscoplastic strain.

- The result is consistent with the traffic tests results conducted by FAA on NAPMRC flexible pavement test sections (*131*), both of WMA and HMA PG 64-22 test were found to be the worst performing test in terms of resulting in more VP and HR viscoplastic strain, which will result in more rutting. The HMA PG 76-22 performed slightly better than the respective WMA test.
- The proposed GAs analysis procedure in the chapter 4 was a promising tool to capture constitutive modeling of the VP and HR viscoplastic responses of asphalt concrete materials, time- and rate-dependent materials, subjected to general loading conditions.
- Polymer modified PG 76-22 is more sensitive to Evotherm-M1 additive as compared to unmodified PG 64-22.
- Addition of Evotherm-M1 cause an increase in the rutting potential with decrease in mixing and compaction temperatures.
- Asphalt binder materials used in FAA's NAPMRC test sections can be ranked with respect to their resistance to rutting as followed:
    - Polymer modified PG 76-22,
    - Polymer modified PG 76-22 plus Evotherm-M1,
    - Unmodified PG 64-22, and
    - Unmodified PG 64-22 plus Evotherm-M1.

  the results are consistent with the traffic tests results conducted by FAA on NAPMRC flexible pavement test sections (*131*), both modified and unmodified asphalt binders plus Evotherm-M1 additive test were found to be the less performing test compare to virgin modified and unmodified asphalt binders.

- Asphalt mixtures made with polymer modified PG 76-22 are more susceptible to the changes in the stress level and tire pressure.
- Modified/unmodified asphalt binders without Evotherm-M1 can be graded as heavy binders and Evotherm-M1 additive asphalt binders can be graded as standard binders.
- Polymer modified PG 76-22 with/without Evotherm-M1 will show more recoverable deformation when subjected to traffic compare to unmodified PG 64-22 with/without Evotherm-M1.
- Considering the same properties for the asphalt concretes: as bitumen viscosity increases, asphalt concrete dynamic modulus increases, which will result in reduction of recovered strain.
- Polymer modified PG 76-22 with/without Evotherm-M1 binders show higher level of elastic response as compared to unmodified PG 64-22 with/without Evotherm-M1.
- Addition of the Evotherm-M1 decrease the hardness of the modified/unmodified virgin binders.

6.2. Future Work

- Comparison the difference of Federal Aviation Administration Rigid and Flexible Iterative Elastic Layer Design (FAARFIELD) and Pavement Analysis using Nonlinear Damage Approach for Airfield Pavements (PANDA-AP).

- Calibration of PANDA-AP for airfield pavements. This document will provide, in an FAA standard format, the test methods required to determine the parameters associated with the PANDA-AP material models. This document can be utilized to systematically analyze the laboratory test data in order to extract the PANDA-AP parameters.

- Develop straightforward algorithms to characterize material properties associated with the aging and moisture induced damage. It is extremely important to include more realistic effect of environmental conditions.

- Introduce innovative and more efficient tests for getting material properties of PANDA-AP with applicability to a full range of temperature and loading rate conditions, which may be experienced by a pavement during its lifetime.

- Application of statistical analysis approaches into the constitutive models. It is still in some cases difficult to reduce the variability between two similar samples even in experimentally controlled laboratory situation. The experimental measurements show a range for the material's response. Therefore, the constitutive model will be more realistic if it can predict a range of response under a specific loading condition.

- If successful, improve the design method of pavements.

References

1. Huang, Y. H. Pavement analysis and design. 2004.
2. Authority, E. R., and E. R. AUTHORIT. Pavement Design Manual.In, may, 2004.
3. Officials, T. *AASHTO guide for design of pavement structures, 1993*. AASHTO, 1993.
4. Brill, D. R. *Calibration of FAARFIELD Rigid Pavement Design Procdure*. Federal Aviation Administration William J. Hughes Technical Center, 2010.
5. Hayhoe, G. F., R. D. McQueen, E. H. Guo, and D. R. Brill. LEDFAA, The FAA's New Software for Airport Pavement Design. *US Department of Transportation Report, Office of Aviation Research, Washington, DC, in preparatiuon*, 2002.
6. Brill, D. R., and G. F. Hayhoe. Multiple-gear analysis for flexible pavement design in LEDFAA.In *FAA Worldwide Airport Technology Transfer Conference*, 2004. pp. 1-10.
7. El-Badawy, S., F. Bayomy, and A. Awed. Performance of MEPDG dynamic modulus predictive models for asphalt concrete mixtures: local calibration for Idaho. *Journal of Materials in Civil Engineering*, Vol. 24, No. 11, 2012, pp. 1412-1421.
8. Muthadi, N., and Y. Kim. Local calibration of mechanistic-empirical pavement design guide for flexible pavement design. *Transportation Research Record: Journal of the Transportation Research Board*, No. 2087, 2008, pp. 131-141.
9. Hoegh, K., L. Khazanovich, and M. Jense. Local calibration of Mechanistic-Empirical pavement design guide rutting model: Minnesota road research project test sections. *Transportation Research Record: Journal of the Transportation Research Board*, No. 2180, 2010, pp. 130-141.
10. Darter, M. I., L. Titus-Glover, and H. L. Von Quintus. Implementation of the Mechanistic-Empirical Pavement Design Guide in Utah: validation, calibration, and development of the UDOT MEPDG User's Guide.In, 2009.
11. Muthadi, N. R. Local calibration of the MEPDG for flexible pavement design. 2007.
12. Von Quintus, H. L., and J. S. Moulthrop. Mechanistic-Empirical Pavement Design Guide Flexible Pavement Performance Prediction Models for Montana--Volume I Executive Research Summary.In, 2007.
13. Kim, Y. R., F. M. Jadoun, T. Hou, and N. Muthadi. Local calibration of the MEPDG for flexible pavement design.In, 2011.
14. Souliman, M. I., M. S. Mamlouk, M. M. El-Basyouny, and C. E. Zapata. Calibration of the AASHTO MEPDG for flexible pavement for arizona conditions.In *Proceedings of the Transportation Research Board 89th Annual Meeting*, Transportation Research Board Washington, DC, USA, 2010. p. 22.
15. Tarefder, R., and J. I. Rodriguez-Ruiz. Local calibration of MEPDG for flexible pavements in New Mexico. *Journal of Transportation Engineering*, Vol. 139, No. 10, 2013, pp. 981-991.
16. Caliendo, C. Local calibration and implementation of the mechanistic-empirical pavement design guide for flexible pavement design. *Journal of Transportation Engineering*, Vol. 138, No. 3, 2011, pp. 348-360.
17. Li, J., L. Pierce, and J. Uhlmeyer. Calibration of flexible pavement in mechanistic-empirical pavement design guide for Washington State. *Transportation Research Record: Journal of the Transportation Research Board*, No. 2095, 2009, pp. 73-83.
18. Von Quintus, H. L. Local Calibration of MEPDG-An Overview of Selected Studies (With Discussion). *Journal of the Association of Asphalt Paving Technologists*, Vol. 77, 2008.

19. Hall, K., D. Xiao, and K. Wang. Calibration of the mechanistic-empirical pavement design guide for flexible pavement design in Arkansas. *Transportation Research Record: Journal of the Transportation Research Board*, No. 2226, 2011, pp. 135-141.
20. Kang, M., and T. M. Adams. Local calibration for fatigue cracking models used in the Mechanistic-empirical pavement design guide.In *Proceedings of the 2007 Mid-Continent Transportation Research Symposium*, 2007.
21. Hossain, Z., M. Zaman, C. Doiron, and S. Cross. Development of flexible pavement database for local calibration of MEPDG. *Final Report (Draft), SPR*, Vol. 2209, 2011.
22. Jannat, G. E., X.-X. Yuan, and M. Shehata. Development of regression equations for local calibration of rutting and IRI as predicted by the MEPDG models for flexible pavements using Ontario's long-term PMS data. *International Journal of Pavement Engineering*, Vol. 17, No. 2, 2016.
23. Bayomy, F., S. El-Badawy, and A. Awed. Implementation of the MEPDG for flexible pavements in Idaho.In, Idaho. Transportation Dept., 2012.
24. Guo, X. Local calibration of the MEPDG using test track data.In, 2013.
25. Kim, Y. R. *Implementation plan for the new mechanistic-empirical pavement design guide*. NC Department of Transportation Research and Analysis Group, 2007.
26. Tarefder, R., N. Sumee, G. Agisetti, Y. Huang, R. Sanchez-Silva, and K. Benedict. *Development of a Flexible Pavement Database for Local Calibration of MEPDG*. The Bureau, 2010.
27. Wassem, A. Methodology Development and Local Calibration of MEPDG Permanent Deformation Models for Ontario's Flexible Pavements. *MASc, Ryerson University, Canada*, 2013.
28. Von Quintus, H. L., M. I. Darter, B. Bhattacharya, and L. Titus-Glover. Implementation and Calibration of the MEPDG in Georgia.In, 2016.
29. Johanneck, L., D. Tompkins, T. Clyne, and L. Khazanovich. Minnesota Road Research Data for Evaluation and Local Calibration of the Mechanistic-Empirical Pavement Design Guide's Enhanced Integrated Climatic Model. *Transportation Research Record: Journal of the Transportation Research Board*, No. 2226, 2011, pp. 30-40.
30. Wu, Z., X. Yang, and Z. Zhang. Evaluation of MEPDG flexible pavement design using pavement management system data: Louisiana experience. *International Journal of Pavement Engineering*, Vol. 14, No. 7, 2013, pp. 674-685.
31. Jadoun, F., and Y. Kim. Calibrating Mechanistic-Empirical Pavement Design Guide for North Carolina: Genetic Algorithm and Generalized Reduced Gradient Optimization Methods. *Transportation Research Record: Journal of the Transportation Research Board*, No. 2305, 2012, pp. 131-140.
32. Price, S., Y. Mehta, and L. M. McCarthy. Evaluation and modeling of repeated load test data of asphalt concrete for mechanistic-empirical pavement design. *Journal of Materials in Civil Engineering*, Vol. 19, No. 11, 2007, pp. 993-999.
33. Saxena, P., D. Tompkins, L. Khazanovich, and J. Balbo. Evaluation of characterization and performance modeling of cementitiously stabilized layers in the Mechanistic-Empirical pavement design guide. *Transportation Research Record: Journal of the Transportation Research Board*, No. 2186, 2010, pp. 111-119.
34. Khazanovich, L., I. Yut, S. Husein, C. Turgeon, and T. Burnham. Adaptation of Mechanistic-empirical pavement design guide for design of Minnesota low-volume portland cement concrete pavements. *Transportation Research Record: Journal of the Transportation Research Board*, No. 2087, 2008, pp. 57-67.

35. Veeraragavan, A. Dynamic mechanical characterization of asphalt concrete mixes with modified asphalt binders. *Materials science and engineering: A,* Vol. 528, No. 21, 2011, pp. 6445-6454.
36. Kim, Y.-R., D. Little, and R. Lytton. Fatigue and healing characterization of asphalt mixtures. *Journal of Materials in Civil Engineering,* Vol. 15, No. 1, 2003, pp. 75-83.
37. Thyagarajan, S., L. Tashman, E. Masad, and F. Bayomy. The heterogeneity and mechanical response of hot mix asphalt laboratory specimens. *International Journal of Pavement Engineering,* Vol. 11, No. 2, 2010, pp. 107-121.
38. You, Z., S. Adhikari, and M. E. Kutay. Dynamic modulus simulation of the asphalt concrete using the X-ray computed tomography images. *Materials and Structures,* Vol. 42, No. 5, 2009, pp. 617-630.
39. Romero, P., and E. Masad. Relationship between the representative volume element and mechanical properties of asphalt concrete. *Journal of Materials in Civil Engineering,* Vol. 13, No. 1, 2001, pp. 77-84.
40. Tashman, L. S., E. Masad, B. Peterson, and H. Saleh. Internal structure analysis of asphalt mixes to improve the simulation of superpave gyratory compaction to field conditions.In, Washington State University, 2000.
41. Chehab, G., E. O'Quinn, and Y. Kim. Specimen geometry study for direct tension test based on mechanical tests and air void variation in asphalt concrete specimens compacted by superpave gyratory compactor. *Transportation Research Record: Journal of the Transportation Research Board,* No. 1723, 2000, pp. 125-132.
42. Park, S. W., Y. R. Kim, and R. A. Schapery. A viscoelastic continuum damage model and its application to uniaxial behavior of asphalt concrete. *Mechanics of Materials,* Vol. 24, No. 4, 1996, pp. 241-255.
43. Chang, K.-N. G., and J. N. Meegoda. Micromechanical simulation of hot mix asphalt. *Journal of Engineering Mechanics,* Vol. 123, No. 5, 1997, pp. 495-503.
44. Al-Rub, R. K. A., T. You, E. A. Masad, and D. N. Little. Mesomechanical modeling of the thermo-viscoelastic, thermo-viscoplastic, and thermo-viscodamage response of asphalt concrete. *International Journal of Advances in Engineering Sciences and Applied Mathematics,* Vol. 3, No. 1-4, 2011, pp. 14-33.
45. Kim, Y.-R., D. Allen, and D. Little. Computational constitutive model for predicting nonlinear viscoelastic damage and fracture failure of asphalt concrete mixtures. *International Journal of Geomechanics,* Vol. 7, No. 2, 2007, pp. 102-110.
46. Murali Krishnan, J., and K. Rajagopal. Thermodynamic framework for the constitutive modeling of asphalt concrete: Theory and applications. *Journal of Materials in Civil Engineering,* Vol. 16, No. 2, 2004, pp. 155-166.
47. Masad, E., and N. Somadevan. Microstructural finite-element analysis of influence of localized strain distribution on asphalt mix properties. *Journal of Engineering Mechanics,* Vol. 128, No. 10, 2002, pp. 1105-1114.
48. Saadeh, S., E. Masad, and D. Little. Characterization of asphalt mix response under repeated loading using anisotropic nonlinear viscoelastic-viscoplastic model. *Journal of Materials in Civil Engineering,* Vol. 19, No. 10, 2007, pp. 912-924.
49. Kim, Y.-R., D. Allen, and D. Little. Damage-induced modeling of asphalt mixtures through computational micromechanics and cohesive zone fracture. *Journal of Materials in Civil Engineering,* Vol. 17, No. 5, 2005, pp. 477-484.

50. Huang, C.-W., R. K. Abu Al-Rub, E. A. Masad, D. N. Little, and G. D. Airey. Numerical implementation and validation of a nonlinear viscoelastic and viscoplastic model for asphalt mixes. *International Journal of Pavement Engineering,* Vol. 12, No. 4, 2011, pp. 433-447.
51. Polasik, S., J. Williams, and N. Chawla. Fatigue crack initiation and propagation of binder-treated powder metallurgy steels. *Metallurgical and Materials Transactions A,* Vol. 33, No. 1, 2002, pp. 73-81.
52. Masad, E., N. Somadevan, H. U. Bahia, and S. Kose. Modeling and experimental measurements of strain distribution in asphalt mixes. *Journal of Transportation Engineering,* Vol. 127, No. 6, 2001, pp. 477-485.
53. Davies, M. A., Y. Chou, and C. J. Evans. On chip morphology, tool wear and cutting mechanics in finish hard turning. *CIRP annals,* Vol. 45, No. 1, 1996, pp. 77-82.
54. Cheng, D., D. Little, R. Lytton, and J. Holste. Moisture damage evaluation of asphalt mixtures by considering both moisture diffusion and repeated-load conditions. *Transportation Research Record: Journal of the Transportation Research Board,* No. 1832, 2003, pp. 42-49.
55. Mull, M., K. Stuart, and A. Yehia. Fracture resistance characterization of chemically modified crumb rubber asphalt pavement. *Journal of materials science,* Vol. 37, No. 3, 2002, pp. 557-566.
56. Tayfur, S., H. Ozen, and A. Aksoy. Investigation of rutting performance of asphalt mixtures containing polymer modifiers. *Construction and Building Materials,* Vol. 21, No. 2, 2007, pp. 328-337.
57. Zhang, H. X., C. Feng, Y. C. Zhai, K. L. Jiang, Q. Q. Li, and S. S. Fan. Cross-Stacked Carbon Nanotube Sheets Uniformly Loaded with SnO2 Nanoparticles: A Novel Binder-Free and High-Capacity Anode Material for Lithium-Ion Batteries. *Advanced materials,* Vol. 21, No. 22, 2009, pp. 2299-2304.
58. Liu, G., H. Zheng, X. Song, and V. S. Battaglia. Particles and polymer binder interaction: a controlling factor in lithium-ion electrode performance. *Journal of The Electrochemical Society,* Vol. 159, No. 3, 2012, pp. A214-A221.
59. Alhozaimy, A., P. Soroushian, and F. Mirza. Mechanical properties of polypropylene fiber reinforced concrete and the effects of pozzolanic materials. *Cement and Concrete Composites,* Vol. 18, No. 2, 1996, pp. 85-92.
60. Terrel, R. L., and S. Al-Swailmi. *Water sensitivity of asphalt-aggregate mixes: test selection*. 1994.
61. You, Z., J. Mills-Beale, J. M. Foley, S. Roy, G. M. Odegard, Q. Dai, and S. W. Goh. Nanoclay-modified asphalt materials: Preparation and characterization. *Construction and Building Materials,* Vol. 25, No. 2, 2011, pp. 1072-1078.
62. Little, D. N., J. W. Button, and H. Youssef. *Development of criteria to evaluate uniaxial creep data and asphalt concrete permanent deformation potential*. 1993.
63. Shuler, T. S., J. H. Collins, and J. P. Kirkpatrick. Polymer-modified asphalt properties related to asphalt concrete performance.In *Asphalt Rheology: Relationship to Mixture,* ASTM International, 1987.
64. Tseng, K.-H., and R. L. Lytton. Prediction of permanent deformation in flexible pavement materials.In *Implication of aggregates in the design, construction, and performance of flexible pavements,* ASTM International, 1989.
65. Nobakht, M., M. S. Sakhaeifar, and D. Newcomb. Development of rehabilitation strategies based on structural capacity for composite and flexible pavements. *Journal of Transportation Engineering, Part A: Systems,* Vol. 143, No. 4, 2016, p. 04016016.

66. Nobakht, M., M. S. Sakhaeifar, D. Newcomb, and S. Underwood. Mechanistic-empirical methodology for the selection of cost-effective rehabilitation strategy for flexible pavements. *International Journal of Pavement Engineering,* 2016, pp. 1-10.
67. Abu Al-Rub, R. K. A., M. K. Darabi, S.-M. Kim, D. N. Little, and C. J. Glover. Mechanistic-based constitutive modeling of oxidative aging in aging-susceptible materials and its effect on the damage potential of asphalt concrete. *Construction and Building Materials,* Vol. 41, 2013, pp. 439-454.
68. Darabi, M. K., R. K. Abu Al Rub, E. Masad, C. W. Huang, and D. Little. A Modified Viscoplastic Model to Predict the Permanent Deformation of Asphaltic Materials under Cyclic-Compression Loading at High Temperatures. *International Journal of Plasticity,* Vol. 35, 2012, pp. 100-134.
69. Darabi, M. K., R. K. Abu Al-Rub, E. A. Masad, and D. N. Little. Cyclic hardening-relaxation viscoplasticity model for asphalt concrete materials. *Journal of Engineering Mechanics,* Vol. 139, No. 7, 2012, pp. 832-847.
70. Darabi, M. K., R. K. Abu Al-Rub, E. A. Masad, and D. N. Little. A Thermodynamic Framework for Constitutive Modeling of Time- and Rate-Dependent Materials, Part II: Numerical Aspects and Application to Asphalt Concrete. *International Journal of Plasticity,* Vol. 35, 2012, pp. 67-99.
71. Darabi, M. K., R. K. A. Al-Rub, E. A. Masad, C.-W. Huang, and D. N. Little. A modified viscoplastic model to predict the permanent deformation of asphaltic materials under cyclic-compression loading at high temperatures. *International Journal of Plasticity,* Vol. 35, 2012, pp. 100-134.
72. ---. A thermo-viscoelastic–viscoplastic–viscodamage constitutive model for asphaltic materials. *International Journal of Solids and Structures,* Vol. 48, No. 1, 2011, pp. 191-207.
73. Darabi, M. K., R. K. A. Al-Rub, E. A. Masad, and D. N. Little. A thermodynamic framework for constitutive modeling of time-and rate-dependent materials. Part II: Numerical aspects and application to asphalt concrete. *International Journal of Plasticity,* Vol. 35, 2012, pp. 67-99.
74. ---. Constitutive modeling of fatigue damage response of asphalt concrete materials with consideration of micro-damage healing. *International Journal of Solids and Structures,* Vol. 50, No. 19, 2013, pp. 2901-2913.
75. Rahmani, E., M. K. Darabi, R. K. A. Al-Rub, E. Kassem, E. A. Masad, and D. N. Little. Effect of confinement pressure on the nonlinear-viscoelastic response of asphalt concrete at high temperatures. *Construction and Building Materials,* Vol. 47, 2013, pp. 779-788.
76. Shakiba, M., M. K. Darabi, R. K. A. Al-Rub, E. A. Masad, and D. N. Little. Microstructural modeling of asphalt concrete using a coupled moisture–mechanical constitutive relationship. *International Journal of Solids and Structures,* Vol. 51, No. 25, 2014, pp. 4260-4279.
77. Darabi, M. K. Thermo-viscoelastic-viscoplastic-viscodamagehealing modeling of bituminous materials: Theory and computation.In *Zachry Department of Civil Engineering, No. Doctor of philosophy*, Texas A&M University, Texas, 2011. p. 427.
78. Schapery, R. A. On the characterization of nonlinear viscoelastic materials. *Polymer Engineering & Science,* Vol. 9, No. 4, 1969, pp. 295-310.
79. Perzyna, P. Thermodynamic theory of viscoplasticity. *Advances in applied mechanics,* Vol. 11, 1971, pp. 313-354.

80. Huang, C.-W., E. Masad, A. H. Muliana, and H. Bahia. Nonlinearly viscoelastic analysis of asphalt mixes subjected to shear loading. *Mechanics of time-dependent materials,* Vol. 11, No. 2, 2007, pp. 91-110.
81. Masad, E. A., C.-W. Huang, J. DAngelo, and D. N. Little. Characterization of asphalt binder resistance to permanent deformation based on nonlinear viscoelastic analysis of multiple stress creep recovery (MSCR) test. *Journal of the Association of Asphalt Paving Technologists,* Vol. 78, 2009.
82. Masad, E., C.-W. Huang, G. Airey, and A. Muliana. Nonlinear viscoelastic analysis of unaged and aged asphalt binders. *Construction and Building Materials,* Vol. 22, No. 11, 2008, pp. 2170-2179.
83. Drucker, D. C., and W. Prager. Soil mechanics and plastic analysis or limit design. *Quarterly of applied mathematics,* Vol. 10, No. 2, 1952, pp. 157-165.
84. Simo, J. C., and R. L. Taylor. Consistent tangent operators for rate-independent elastoplasticity. *Computer methods in applied mechanics and engineering,* Vol. 48, No. 1, 1985, pp. 101-118.
85. Masad, E., S. Dessouky, and D. Little. Development of an elastoviscoplastic microstructural-based continuum model to predict permanent deformation in hot mix asphalt. *International Journal of Geomechanics,* Vol. 7, No. 2, 2007, pp. 119-130.
86. Tashman, L., E. Masad, D. Little, and H. Zbib. A microstructure-based viscoplastic model for asphalt concrete. *International Journal of Plasticity,* Vol. 21, No. 9, 2005, pp. 1659-1685.
87. Tashman, L., E. Masad, H. Zbib, D. Little, and K. Kaloush. Anisotropic viscoplastic continuum damage model for asphalt mixes.In *Recent Advances in Materials Characterization and Modeling of Pavement Systems*, 2004. pp. 111-125.
88. Awed, A. M. M. Characteriation of macro scale and meso scale performance of asphalt concrete mixtures under compression.In *Zachry Department of Civil Engineering, No. Doctor of philosophy*, Texas A&M University, Texas, 2016. p. 247.
89. Brown, E. R., P. S. Kandhal, and J. Zhang. Performance testing for hot mix asphalt. *National Center for Asphalt Technology Report*, No. 01-05, 2001.
90. Lemaitre, J. *Handbook of Materials Behavior Models, Three-Volume Set: Nonlinear Models and Properties*. Elsevier, 2001.
91. Findley, W. N., and F. A. Davis. *Creep and relaxation of nonlinear viscoelastic materials*. Courier Corporation, 2013.
92. Haddad, Y. M. *Viscoelasticity of engineering materials*. Chapman & Hall London, 1995.
93. Lakes, R., and R. S. Lakes. *Viscoelastic materials*. Cambridge University Press, 2009.
94. Kim, Y. R., M. N. Guddati, B. S. Underwood, T. Yun, V. Subramanian, and S. Savadatti. Development of a multiaxial viscoelastoplastic continuum damage model for asphalt mixtures.In, Turner-Fairbank Highway Research Center, 2009.
95. Junisbekov, T., V. N. Kestel′man, and N. Malinin. *Stress relaxation in viscoelastic materials*. Science Pub Incorporated, 2003.
96. Liu, C., E. Pineda, and D. Crespo. Mechanical relaxation of metallic glasses: an overview of experimental data and theoretical models. *Metals,* Vol. 5, No. 2, 2015, pp. 1073-1111.
97. Starodubsky, S., I. Blechman, and M. Livneh. Stress-strain relationship for asphalt concrete in compression. *Materials and Structures,* Vol. 27, No. 8, 1994, pp. 474-482.
98. Nguyen, Q. T., H. Di Benedetto, and C. Sauzéat. Linear and nonlinear viscoelastic behaviour of bituminous mixtures. *Materials and Structures,* Vol. 48, No. 7, 2015, pp. 2339-2351.

99. Tanaka, E., and T. van Eijden. Biomechanical behavior of the temporomandibular joint disc. *Critical Reviews in Oral Biology & Medicine,* Vol. 14, No. 2, 2003, pp. 138-150.
100. Detamore, M., and K. Athanasiou. Biomechanical behavior of the temporomandibular joint disc.In *Engineering in Medicine and Biology, 2002. 24th Annual Conference and the Annual Fall Meeting of the Biomedical Engineering Society EMBS/BMES Conference, 2002. Proceedings of the Second Joint, No. 1*, IEEE, 2002. pp. 440-441.
101. Feng, H., M. Pettinari, and H. Stang. Three Different Ways of Calibrating Burger's Contact Model for Viscoelastic Model of Asphalt Mixtures by Discrete Element Method.In *8th RILEM International Symposium on Testing and Characterization of Sustainable and Innovative Bituminous Materials*, Springer, 2016. pp. 423-433.
102. Fwa, T., S. Tan, and L. Zhu. Rutting prediction of asphalt pavement layer using C-ϕ model. *Journal of Transportation Engineering,* Vol. 130, No. 5, 2004, pp. 675-683.
103. Tan, S., B. Low, and T. Fwa. Behavior of asphalt concrete mixtures in triaxial compression. *Journal of Testing and Evaluation,* Vol. 22, No. 3, 1994, pp. 195-203.
104. Chen, W.-F., and X. Liu. *Limit analysis in soil mechanics*. Elsevier, 2012.
105. Chen, W.-F., and E. Mizuno. *Nonlinear analysis in soil mechanics*. Elsevier Amsterdam, 1990.
106. Zhang, Y., M. Bernhardt, G. Biscontin, R. Luo, and R. L. Lytton. A generalized Drucker–Prager viscoplastic yield surface model for asphalt concrete. *Materials and Structures,* Vol. 48, No. 11, 2015, pp. 3585-3601.
107. Seibi, A., M. Sharma, G. Ali, and W. Kenis. Constitutive relations for asphalt concrete under high rates of loading. *Transportation Research Record: Journal of the Transportation Research Board,* No. 1767, 2001, pp. 111-119.
108. Park, D.-W., A. E. Martin, and E. Masad. Effects of nonuniform tire contact stresses on pavement response. *Journal of Transportation Engineering,* Vol. 131, No. 11, 2005, pp. 873-879.
109. Dessouky, S. H., and E. A. Masad. The development of a microstructural-based continuum model for hot mix asphalt.In *Asphalt Concrete: Simulation, Modeling, and Experimental Characterization*, 2006. pp. 44-52.
110. Argyris, J., G. Faust, J. Szimmat, E. Warnke, and K. Willam. Recent developments in the finite element analysis of prestressed concrete reactor vessels. *Nuclear Engineering and Design,* Vol. 28, No. 1, 1974, pp. 42-75.
111. Maiolino, S., and M. P. Luong. Measuring discrepancies between Coulomb and other geotechnical criteria: Drucker-Prager and Matsuoka-Nakai.In *7th Euromech solid mechanics conference, Lisbon, Portugal*, 2009. pp. 09-07.
112. Bardet, J. Lode dependences for isotropic pressure-sensitive elastoplastic materials. *Journal of applied mechanics*, Vol. 57, No. 3, 1990, pp. 498-506.
113. Lin, F.-B., and Z. P. Bažant. Convexity of smooth yield surface of frictional material. *Journal of Engineering Mechanics,* Vol. 112, No. 11, 1986, pp. 1259-1262.
114. Maïolino, S. Proposition of a general yield function in geomechanics. *Comptes Rendus Mecanique*, Vol. 333, 2005, pp. 279-284.
115. Al-Rub, R. K. A., M. K. Darabi, D. N. Little, and E. A. Masad. A micro-damage healing model that improves prediction of fatigue life in asphalt mixes. *International Journal of Engineering Science,* Vol. 48, No. 11, 2010, pp. 966-990.
116. Dessouky, S. H. Multiscale approach for modeling hot mix asphalt.In, Texas A&M University, 2005.

117. Huang, C.-W., R. K. Abu Al-Rub, E. A. Masad, and D. N. Little. Three-dimensional simulations of asphalt pavement permanent deformation using a nonlinear viscoelastic and viscoplastic model. *Journal of Materials in Civil Engineering*, Vol. 23, No. 1, 2010, pp. 56-68.
118. Ara, I. ERES consultants division: guide for mechanistic–empirical design of new and rehabilitated pavement structures. *National Cooperative Highway Research Program, Champaign, Illinois*, 2004.
119. Tashman, L. Microstructural viscoplastic continuum model for asphalt concrete.In, Texas A&M University, 2004.
120. Abdel-Rahman Saadeh, S. Characterization of asphalt concrete using anisotropic damage viscoelastic-viscoplastic model.In, Texas A&M University, 2007.
121. Kim, Y., M. Guddati, B. Underwood, A. Lacroix, C. Baek, M. Eslaminia, and J. Bartucca. Hot-Mix Asphalt Performance-Related Specifications Based on Viscoelastoplastic Continuum Damage (VEPCD) Models. *Quarterly Research Progress Report: October–December*, 2011.
122. Yun, T., and Y. R. Kim. A viscoplastic constitutive model for hot mix asphalt in compression at high confining pressure. *Construction and Building Materials*, Vol. 25, No. 5, 2011, pp. 2733-2740.
123. ---. Experimental investigation of rate-dependent hardening-softening behavior of hot mix asphalt in compression. *Road Materials and Pavement Design*, Vol. 12, No. 1, 2011, pp. 99-114.
124. ---. Modeling of viscoplastic rate-dependent hardening-softening behavior of hot mix asphalt in compression. *Mechanics of Time-Dependent Materials*, Vol. 15, No. 1, 2011, pp. 89-103.
125. Darabi Konartakhteh, M. Thermo-Viscoelastic-Viscoplastic-Viscodamage-Healing Modeling of Bituminous Materials: Theory and Computation.In, 2012.
126. Huang, C. W. Development and numerical implementation of nonlinear viscoelastic-viscoplastic model for asphalt materials. *Ph.D. Dissertation, Texas A&M University*, 2008.
127. Abu Al-Rub, R. K., M. K. Darabi, C.-W. Huang, E. A. Masad, and D. N. Little. Comparing finite element and constitutive modelling techniques for predicting rutting of asphalt pavements. *International Journal of Pavement Engineering*, Vol. 13, No. 4, 2012, pp. 322-338.
128. You, T. Two-and Three-Dimensional Microstructural Modeling of Asphalt Particulate Composite Materials using a Unified Viscoelastic-Viscoplastic-Viscodamage Constitutive Model.In, 2013.
129. Shakiba, M. A Continuum Coupled Moisture-mechanical Constitutive Model for Asphalt Concrete.In, 2013.
130. Rahmani, E. Continuum-Based Constitutive Modeling of Coupled Oxidative Aging-Mechanical Response of Asphalt Concrete.In, 2015.
131. Garg, N., H. Kazmee, L. Ricalde, and T. Parsons. Rutting Evaluation of Hot and Warm Mix Asphalt Concrete Under High Aircraft Tire Pressure and Temperature at National Airport Pavement and Materials Research Center (NAPMRC). *Transportation Research Record (TRR) and Transportation Research Board (TRB) 97th Annual Meeting*, Vol. 2710, No. 18-03566, 2018, p. 21.
132. Standard, A. D3497-79 "Standard test method for dynamic modulus of asphalt mixtures".In *American society for Testing and Materials*, 2003.
133. AASHTO, T. 342 (2011) Standard method of test for determining dynamic modulus of hot-mix asphalt concrete mixtures. *American Association of State Highway and Transportation Officials, Washington, DC*, 2011.

134. ASTM. C136, Standard Test Method for Sieve Analysis of Fine and Coarse Aggregates.In, ASTM, West Conshohocken, PA, 2005.
135. AASHTO, T. 27, Standard Method of Test for Sieve Analysis of Fine and Coarse Aggregates. *Single User Digital Publication, American Association of State Highway and Transportation Officials, Washington, DC*, 2010.
136. AASHTO. T 84-13, Standard Method of Test for Specific Gravity and Absorption of Fine Aggregate.In, American Association of State Highway and Transportation Officials, Washington, DC, 2017.
137. AASHTO, T. 85, Standard method of test for specific gravity and absorption of coarse aggregate.In, American Association of State Highway and Transportation Officials, Washington, DC, 2010b.
138. ---. 176, Standard Method of Test for Plastic Fines in Graded Aggregates and Soils by Use of the Sand Equivalent Test.In, American Association of State Highway and Transportation Officials, Washington, DC, 2008.
139. ASTM, D. D4791, Flat Particles Elongated Particles, or Flat and Elongated Particles in Coarse Aggregate. 2010.
140. AASHTO, T. 304 (2011), Uncompacted void content of fine aggregate. i
In, AASHTO, Washington, DC, 2004.
141. ASTM, D. 5821 Standard Test Method for Determining the Percentage of Fractured Particles in Coarse Aggregate. *American Society for Testing and Materials, Philadelphia, PA*, 2001.
142. AASHTO, M. 320. *Standard Specification for Performance-Graded Asphalt Binder, American Association of State Highway and Transportation Officials*, 2010.
143. ---. 332, 2014. *Standard specification for performance-graded*.
144. Designation, A. D6373-07e1. *Standard Specification for Performance Graded Asphalt Binder*.
145. ASTM, D. 70, Standard Test Method for Specific Gravity and Density of Semi-Solid Bituminous Materials (Pycnometer Method). *Annual Book of ASTM Standards*, Vol. 4, 2003.
146. ASTM. D92-12, Standard Test Method for Flash and Fire Points by Cleveland Open Cup Tester.In, ASTM, West Conshohocken, PA, 2012.
147. AASHTO, T. 316 (2004).". *Viscosity Determination of Asphalt Binder Using Rotational Viscometer." AASHTO Standards, Washington, DC*.
148. ---. 315. *Standard method of test for determining the rheological properties of asphalt binder using a dynamic shear rheometer (DSR)". American Association of State Highway and Transportation Officials, Washington, DC*, 2009.
149. ---. 240-13. *Standard Method of Test for Effect of Heat and Air on a Moving 351 Film of Asphalt (Rolling Thin-Film Oven Test)*, pp. 2872-2804.
150. ---. 313-10, Determining the Flexural Creep Stiffness of Asphalt Binder Using the Bending Beam Rheometer (BBR).In, AASHTO Standard Specifications for Transportation Materials and Methods of Sampling and Testing, Washington, DC, 2011.
151. ---. 312, Standard Method of Test for Preparing and Determining the Density of Hot Mix Asphalt (HMA) Specimens by Means of the Superpave Gyratory Compactor.In, AASHTO, Washington, DC, 2016.
152. ---. 209, Standard method of test for theoretical maximum specific gravity and density of hot-mix asphalt (HMA). .In, American Association of State Highway and Transportation Officials, Washington, DC, 2011.

153. ASTM, D. 2872. *Standard Test Method for Effect of Heat and Air on a Moving Film of Asphalt (Rolling Thin-Film Oven Test)*, 2013.
154. ASTM, A. D6521 (2013). *Standard practice for accelerated aging of asphalt binder using a pressurized aging vessel (PAV). West Conshohocken. PA: American Society Testing & materials*.
155. AASHTO, T. 62-07,(2008).".In *Determining Dynamic Modulus of Hot-Mix Asphalt Concrete Mixtures." Standard Specifications for Transportation and Methods of Sampling and Testing, 28th Edition, and Provisional Standards. America Association of State Transportation and Highway Engineering*.
156. Standard, A. D6648-01. *Standard Test Method for Determining the Flexural Creep Stiffness of Asphalt Binder Using the Bending Beam Rheometer (BBR)*.
157. ---. C136/C136M-14, 2015. *Standard Test Method for Sieve Analysis of Fine and Coarse Aggregates*, 2014.
158. AASHTO. T27, Standard Method of Test for Sieve Analysis of Fine and Coarse Aggregates.In, Standard Specifications for Transportation Materials and Methods of Sampling and Testing, Washington, DC, 2005.
159. AASHTO, T. 269-07, Standard Method of Test for Percent Air Voids in Compacted Dense and Open Asphalt Mixtures.In *Standard Specifications for Transportation Materials and Methods of Sampling and Testing, 27th Edition.* , American Association of State Highway and Transportation Officials (AASHTO), Washington, DC, 2007.
160. AASHTO, T. Standard method of test for multiple stress creep recovery (MSCR) test of asphalt binder using a dynamic shear rheometer (DSR). *American Association of State Highway and Transportation Officials, Washington, DC*, 2014.
161. ASTM, D. 7405. *Standard Test Method for Multiple Stress Creep and Recovery (MSCR) of Asphalt Binder Using a Dynamic Shear Rheometer. American Society for Testing Materials, Washington, DC*, 2010.
162. Zeng, M., H. U. Bahia, H. Zhai, M. R. Anderson, and P. Turner. Rheological modeling of modified asphalt binders and mixtures (with discussion). *Journal of the Association of Asphalt Paving Technologists*, Vol. 70, 2001.
163. ASTM. E4-16, Standard Practices for Force Verification of Testing Machines.In, ASTM, West Conshohocken, PA, 2016.
164. Morrison, G. R., J. K. Lee, and S. A. M. Hesp. Chlorinated Polyolefins for Asphalt Binder Modification. *Journal of Applied Polymer Science*, Vol. 54, No. 2, 1994, pp. 231-240.
165. Uzan, J. Asphalt concrete characterization for pavement performance prediction. *Asphalt Paving Technology*, Vol. 65, 1996, pp. 573-607.
166. Arabali, P., M. Sakhaeifar, T. Freeman, B. Wilson, and J. Borowiec. Decision-making tool for the selection of pavement preservation treatments in general aviation airport pavements.In *International Conference on Transportation and Development 2016*, 2016. pp. 30-41.
167. Arabali, P., M. S. Sakhaeifar, T. J. Freeman, B. T. Wilson, and J. D. Borowiec. Decision-making guideline for preservation of flexible pavements in general aviation airport management. *Journal of Transportation Engineering, Part B: Pavements*, Vol. 143, No. 2, 2017, p. 04017006.
168. Nobakht, M., M. S. Sakhaeifar, and D. E. Newcomb. Selection of Structural Overlays Using Asphalt Mixture Performance. *Journal of Materials in Civil Engineering*, Vol. 29, No. 11, 2017, p. 04017209.
169. Masad, E., L. Tashman, D. Little, and H. Zbib. Viscoplastic modeling of asphalt mixes with the effects of anisotropy, damage and aggregate characteristics. *Mechanics of Materials*, Vol. 37, No. 12, 2005, pp. 1242-1256.

170. Kim, Y. R., and D. N. Little. One-Dimensional Constitutive Modeling of Asphalt Concrete. *Journal of Engineering Mechanics-Asce,* Vol. 116, No. 4, 1990, pp. 751-772.
171. Seibi, A. C., M. G. Sharma, G. A. Ali, and W. J. Kenis. Constitutive relations for asphalt concrete under high rates of loading. *Asphalt Mixtures 2001,* No. 1767, 2001, pp. 111-119.
172. Lee, H. J., J. S. Daniel, and Y. R. Kim. Continuum damage mechanics-based fatigue model of asphalt concrete. *Journal of Materials in Civil Engineering,* Vol. 12, No. 2, 2000, pp. 105-112.
173. Drescher, A., N. Kringos, and T. Scarpas. On the behavior of a parallel elasto-visco-plastic model for asphaltic materials. *Mechanics of materials,* Vol. 42, No. 2, 2010, pp. 109-117.
174. Villani, M. M., C. Kasbergen, A. Scarpas, and D. Lo Presti. Mechanistic procedure for parameter determination of multiplicative decomposition based constitutive models. *International Journal of Pavement Engineering,* Vol. 18, No. 5, 2017, pp. 391-403.
175. Kose, S., M. Guler, H. Bahia, and E. Masad. Distribution of strains within hot-mix asphalt binders: applying imaging and finite-element techniques. *Transportation Research Record: Journal of the Transportation Research Board,* No. 1728, 2000, pp. 21-27.
176. Deshpande, V., and D. Cebon. Steady-state constitutive relationship for idealised asphalt mixes. *Mechanics of materials,* Vol. 31, No. 4, 1999, pp. 271-287.
177. Haj-Ali, R. M., and A. H. Muliana. Numerical finite element formulation of the Schapery non-linear viscoelastic material model. *International Journal for Numerical Methods in Engineering,* Vol. 59, No. 1, 2004, pp. 25-45.
178. Karimi, M. M., N. Tabatabaee, H. Jahanbakhsh, and B. Jahangiri. Development of a stress-mode sensitive viscoelastic constitutive relationship for asphalt concrete: experimental and numerical modeling. *Mechanics of time-dependent materials,* 2016, pp. 1-35.
179. Karimi, M. M., N. Tabatabaee, B. Jahangiri, and M. K. Darabi. Constitutive modeling of hardening-relaxation response of asphalt concrete in cyclic compressive loading. *Construction and Building Materials,* Vol. 137, 2017, pp. 169-184.
180. Schapery, R. Nonlinear viscoelastic solids. *International Journal of Solids and Structures,* Vol. 37, No. 1, 2000, pp. 359-366.
181. Schapery, R. A. *Further development of a thermodynamic constitutive theory: stress formulation*. Purdue University School of Aeronautics, Astronautics and Engineering Sciences, 1969.
182. Christensen, R. M. On obtaining solutions in nonlinear viscoelasticity. *Journal of Applied Mechanics,* Vol. 35, No. 1, 1968, pp. 129-133.
183. Ye, Y., X. Yang, and C. Chen. Modified Schapery's model for asphalt sand. *Journal of Engineering Mechanics,* Vol. 136, No. 4, 2010, pp. 448-454.
184. Motamed, A., A. Bhasin, and K. M. Liechti. Interaction nonlinearity in asphalt binders. *Mechanics of time-dependent materials,* Vol. 16, No. 2, 2012, pp. 145-167.
185. ---. Constitutive modeling of the nonlinearly viscoelastic response of asphalt binders; incorporating three-dimensional effects. *Mechanics of time-dependent materials,* Vol. 17, No. 1, 2013, pp. 83-109.
186. Pellinen, T. K., M. W. Witczak, and R. F. Bonaquist. Asphalt mix master curve construction using sigmoidal fitting function with non-linear least squares optimization.In *Recent advances in materials characterization and modeling of pavement systems,* 2004. pp. 83-101.
187. Glover, C. J., R. R. Davison, and N. Vassiliev. *A new method for simulating hot-mix plant asphalt aging*. Texas Transportation Institute, the Texas A & M University System, 2001.

188. Park, S., and R. Schapery. Methods of interconversion between linear viscoelastic material functions. Part I—A numerical method based on Prony series. *International Journal of Solids and Structures,* Vol. 36, No. 11, 1999, pp. 1653-1675.
189. Pellinen, T., and M. Witczak. Stress dependent master curve construction for dynamic (complex) modulus (with discussion). *Journal of the Association of Asphalt Paving Technologists,* Vol. 71, 2002.
190. Darwin, C. *On the Origin of Species by Means of Natural Selection, Or The Preservation of Favoured Races in the Struggle for Life by Means of Natural Selection, Or, the Preservation of Favored Races in the Struggle for Life And, the Descent of Man, and Selection in Relation to Sex*. Modern library, 1962.
191. Karimi, M. M., N. Tabatabaee, H. Jahanbakhsh, and B. Jahangiri. Development of a stress-mode sensitive viscoelastic constitutive relationship for asphalt concrete: experimental and numerical modeling. *Mechanics of Time-Dependent Materials,* Vol. 21, No. 3, 2017, pp. 383-417.
192. Jahanbakhsh, H., M. M. Karimi, F. M. Nejad, and B. Jahangiri. Viscoelastic-based approach to evaluate low temperature performance of asphalt binders. *Construction and Building Materials,* Vol. 128, 2016, pp. 384-398.
193. Jahangiri, B., M. M. Karimi, and N. Tabatabaee. Relaxation of hardening in asphalt concrete under cyclic compression loading. *Journal of Materials in Civil Engineering,* Vol. 29, No. 5, 2016, p. 04016288.
194. Jahanbakhsh, H., M. M. Karimi, and N. Tabatabaee. Experimental and numerical investigation of low-temperature performance of modified asphalt binders and mixtures. *Road Materials and Pavement Design,* Vol. 18, No. 6, 2017, pp. 1353-1374.
195. Nejad, F. M., H. Sorkhabi, and M. M. Karimi. Experimental investigation of rest time effect on permanent deformation of asphalt concrete. *Journal of Materials in Civil Engineering,* Vol. 28, No. 5, 2015, p. 06015016.
196. Bazzaz, M., M. K. Darabi, D. N. Little, and N. Garg. A Straightforward Procedure to Characterize Nonlinear Viscoelastic Response of Asphalt Concrete at High Temperatures. *Transportation Research Record,* Vol. 0, No. 0, 2018, p. 0361198118782033.
197. Turing, A. M. Intelligent machinery, a heretical theory. *The Turing Test: Verbal Behavior as the Hallmark of Intelligence,* Vol. 105, 1948.
198. Li, H., X. Hu, H. Yang, and L. Li. Anisotropic and asymmetrical yielding and its distorted evolution: Modeling and applications. *International Journal of Plasticity,* Vol. 82, 2016, pp. 127-158.
199. Huang, H., S.-S. Huang, and K. Pilakoutas. Modeling for Assessment of Long-Term Behavior of Prestressed Concrete Box-Girder Bridges. *Journal of Bridge Engineering,* Vol. 23, No. 3, 2018, p. 04018002.
200. Haji Agha Mohammad Zarbaf, S. E., M. Norouzi, R. J. Allemang, V. J. Hunt, and A. Helmicki. Stay Cable Tension Estimation of Cable-Stayed Bridges Using Genetic Algorithm and Particle Swarm Optimization. *Journal of Bridge Engineering,* Vol. 22, No. 10, 2017, p. 05017008.
201. Hunaidi, O. Evolution-based genetic algorithms for analysis of non-destructive surface wave tests on pavements. *NDT & e International,* Vol. 31, No. 4, 1998, pp. 273-280.
202. Tsai, B.-W., V. Kannekanti, and J. Harvey. Application of genetic algorithm in asphalt pavement design. *Transportation Research Record: Journal of the Transportation Research Board,* No. 1891, 2004, pp. 112-120.

203. Mun, S., and Z. W. Geem. Determination of viscoelastic and damage properties of hot mix asphalt concrete using a harmony search algorithm. *Mechanics of Materials,* Vol. 41, No. 3, 2009, pp. 339-353.
204. Gandomi, A. H., A. H. Alavi, M. R. Mirzahosseini, and F. M. Nejad. Nonlinear genetic-based models for prediction of flow number of asphalt mixtures. *Journal of Materials in Civil Engineering,* Vol. 23, No. 3, 2010, pp. 248-263.
205. López Cela, J. J. Material identification procedure for elastoplastic Drucker–Prager model. *Journal of Engineering Mechanics,* Vol. 128, No. 5, 2002, pp. 586-591.
206. Florea, D. Nonassociated elastic/viscoplastic model for bituminous concrete. *International Journal of Engineering Science,* Vol. 32, No. 1, 1994, pp. 87-93.
207. Holland, J. H. Adaptation in natural and artificial systems. 1975. *Ann Arbor, MI: University of Michigan Press and,* 1992.
208. Koza, J. R. *Genetic programming: on the programming of computers by means of natural selection*. MIT press, 1992.
209. Abu Al-Rub, R. K., E. A. Masad, and C. W. Huang. Improving the Sustainability of Asphalt Pavements through Developing a Predictive Model with Fundamental Material Properties. *Southwest University Transportation Center, Texas Transportation Institute, College Station, TX*, 2009, pp. 1-45.
210. Bazzaz, M., M. Darabi, D. Little, and G. Navneet. A Straightforward Procedure to Characterize Nonlinear Viscoelastic Response of Asphalt Concrete at High Temperatures. *Transportation Research Record (TRR): Journal of the Transportation Research Board (TRB) 97th Annual Meeting,* Vol. 2710, No. 03704, 2018, pp. 1-20.
211. Witzcak, M. W. *Simple performance test for superpave mix design*. Transportation Research Board, 2002.
212. Kassem, E. A.-R. *Compaction effects on uniformity, moisture diffusion, and mechanical properties of asphalt pavements*. Texas A&M University, 2008.
213. Özen, H. Rutting evaluation of hydrated lime and SBS modified asphalt mixtures for laboratory and field compacted samples. *Construction and Building Materials,* Vol. 25, No. 2, 2011, pp. 756-765.
214. Dong, F., X. Yu, S. Liu, and J. Wei. Rheological behaviors and microstructure of SBS/CR composite modified hard asphalt. *Construction and Building Materials,* Vol. 115, 2016, pp. 285-293.
215. Modarres, A., and H. Hamedi. Effect of waste plastic bottles on the stiffness and fatigue properties of modified asphalt mixes. *Materials & Design,* Vol. 61, 2014, pp. 8-15.
216. Moreno, F., M. Sol, J. Martín, M. Pérez, and M. Rubio. The effect of crumb rubber modifier on the resistance of asphalt mixes to plastic deformation. *Materials & Design,* Vol. 47, 2013, pp. 274-280.
217. Kök, B. V., and H. Çolak. Laboratory comparison of the crumb-rubber and SBS modified bitumen and hot mix asphalt. *Construction and Building Materials,* Vol. 25, No. 8, 2011, pp. 3204-3212.
218. Behnood, A., A. Shah, R. McDaniel, M. Beeson, and J. Olek. High temperature properties of asphalt binders: statistical and experimental comparison of MSCR and PG grading systems. *Transportation Research Record: Journal of the Transportation Research Board,* Vol. 2574, 2016.
219. Kök, B. V., M. Yılmaz, and M. Akpolat. Evaluation of the conventional and rheological properties of SBS+ Sasobit modified binder. *Construction and Building Materials,* Vol. 63, 2014, pp. 174-179.

220. Kök, B. V., M. Yilmaz, and A. Geçkil. Evaluation of low-temperature and elastic properties of crumb rubber–and SBS-modified bitumen and mixtures. *Journal of Materials in Civil Engineering*, Vol. 25, No. 2, 2012, pp. 257-265.
221. Król, J., P. Radziszewski, and K. J. Kowalski. Influence of microstructural behavior on multiple stress creep recovery (MSCR) in modified bitumen. *Procedia Engineering*, Vol. 111, 2015, pp. 478-484.
222. Behnood, A., M. M. Gharehveran, F. G. Asl, and M. Ameri. Effects of copper slag and recycled concrete aggregate on the properties of CIR mixes with bitumen emulsion, rice husk ash, Portland cement and fly ash. *Construction and Building Materials*, Vol. 96, 2015, pp. 172-180.
223. Ameri, M., and A. Behnood. Laboratory studies to investigate the properties of CIR mixes containing steel slag as a substitute for virgin aggregates. *Construction and Building Materials*, Vol. 26, No. 1, 2012, pp. 475-480.
224. Behnood, A., and M. Ameri. Experimental investigation of stone matrix asphalt mixtures containing steel slag. *Scientia Iranica*, Vol. 19, No. 5, 2012, pp. 1214-1219.
225. Gushgari, S. Y., Y. Zhang, A. Nahvi, H. Ceylan, and S. Kim. Otta Seal Construction for Asphalt Pavement Resurfacing.In *International Conference on Transportation and Development*, 2018. p. 177.
226. Daghighi, A., and A. Nahvi. Effect of different additives on fatigue behaviour of asphalt mixtures.In *Construction Materials and Structures: Proceedings of First International Conference on Construction Materials and Structures*, 2014. pp. 601-607.
227. Rahbar-Rastegar, R., J. Sias Daniel, and G. Reinke. Comparison of asphalt binder and mixture cracking parameters. *Road Materials and Pavement Design*, Vol. 18, No. sup4, 2017, pp. 211-233.
228. Rahbar-Rastegar, R., and E. V. Dave. Evaluation of Viscoelastic and Fracture Properties of Asphalt Mixtures with Long-Term Laboratory Conditioning 2. *Aging*, Vol. 1, 2018, p. 2.
229. Rahbar-Rastegar, R., E. V. Dave, and J. S. Daniel. Fatigue and Thermal Cracking Analysis of Asphalt Mixtures Using Continuum-Damage and Cohesive-Zone Models. *Journal of Transportation Engineering, Part B: Pavements*, Vol. 144, No. 4, 2018, p. 04018040.
230. Lu, X., and U. Isacsson. Rheological characterization of styrene-butadiene-styrene copolymer modified bitumens. *Construction and Building Materials*, Vol. 11, No. 1, 1997, pp. 23-32.
231. Chen, J.-S., M.-C. Liao, and M.-S. Shiah. Asphalt modified by styrene-butadiene-styrene triblock copolymer: Morphology and model. *Journal of Materials in Civil Engineering*, Vol. 14, No. 3, 2002, pp. 224-229.
232. Navarro, F., P. Partal, F. Martınez-Boza, C. Valencia, and C. Gallegos. Rheological characteristics of ground tire rubber-modified bitumens. *Chemical Engineering Journal*, Vol. 89, No. 1, 2002, pp. 53-61.
233. Willis, J. R., C. Plemons, P. Turner, C. Rodezno, and T. Mitchell. Effect of ground tire rubber particle size and grinding method on asphalt binder properties. *National Center for Asphalt Technology. NCAT Report*, 2012, pp. 12-09.
234. Li, X., T. Clyne, G. Reinke, E. Johnson, N. Gibson, and M. Kutay. Laboratory evaluation of asphalt binders and mixtures containing polyphosphoric acid. *Transportation Research Record: Journal of the Transportation Research Board*, No. 2210, 2011, pp. 47-56.
235. Baumgardner, G. L. Why and how of polyphosphoric acid modification–an industry perspective. *Journal of the Association of Asphalt Paving Technologists*, Vol. 79, 2010.

236. Faxina, A., T. Pamplona, F. Sobreiro, and G. Fabbri. Effect of polyphosphoric acid on high-temperature properties of bitumens from different crude sources. *Bituminous Mixtures and Pavements VI*, 2015, p. 127.
237. Behnood, A., and J. Olek. Rheological properties of asphalt binders modified with styrene-butadiene-styrene (SBS), ground tire rubber (GTR), or polyphosphoric acid (PPA). *Construction and Building Materials*, Vol. 151, 2017, pp. 464-478.
238. ---. Stress-dependent behavior and rutting resistance of modified asphalt binders: An MSCR approach. *Construction and Building Materials*, Vol. 157, 2017, pp. 635-646.
239. Kanitpong, K., and H. Bahia. Relating adhesion and cohesion of asphalts to the effect of moisture on laboratory performance of asphalt mixtures. *Transportation Research Record: Journal of the Transportation Research Board*, No. 1901, 2005, pp. 33-43.
240. Behnood, A., A. Shah, R. S. McDaniel, and J. Olek. Analysis of the Multiple Stress Creep Recovery Asphalt Binder Test and Specifications for Use in Indiana. 2016.
241. Isacsson, U., and X. Lu. Laboratory investigations of polymer modified bitumens. *Journal of the Association of Asphalt Paving Technologists*, Vol. 68, 1999.
242. Anderson, M., J. D'Angelo, and D. Walker. MSCR: A better tool for characterizing high temperature performance properties. *Asphalt*, Vol. 25, No. 2, 2010.
243. D'Angelo, J. A. The relationship of the MSCR test to rutting. *Road Materials and Pavement Design*, Vol. 10, No. sup1, 2009, pp. 61-80.
244. Jafari, M., A. Babazadeh, and S. Aflaki. Effects of stress levels on creep and recovery behavior of modified asphalt binders with the same continuous performance grades. *Transportation Research Record: Journal of the Transportation Research Board*, No. 2505, 2015, pp. 15-23.
245. Lee, S.-J., S. N. Amirkhanian, N.-W. Park, and K. W. Kim. Characterization of warm mix asphalt binders containing artificially long-term aged binders. *Construction and Building Materials*, Vol. 23, No. 6, 2009, pp. 2371-2379.
246. Mogawer, W., A. Austerman, and H. Bahia. Evaluating the effect of warm-mix asphalt technologies on moisture characteristics of asphalt binders and mixtures. *Transportation Research Record: Journal of the Transportation Research Board*, No. 2209, 2011, pp. 52-60.
247. Mallick, R., P. Kandhal, and R. Bradbury. Using warm-mix asphalt technology to incorporate high percentage of reclaimed asphalt pavement material in asphalt mixtures. *Transportation Research Record: Journal of the Transportation Research Board*, No. 2051, 2008, pp. 71-79.
248. Moghadas Nejad, F., A. Azarhoosh, G. H. Hamedi, and H. Roshani. Rutting performance prediction of warm mix asphalt containing reclaimed asphalt pavements. *Road Materials and Pavement Design*, Vol. 15, No. 1, 2014, pp. 207-219.
249. Hurley, G. C., and B. D. Prowell. Evaluation of Evotherm for use in warm mix asphalt. *NCAT report*, Vol. 2, No. 06, 2006.
250. Prowell, B. D., G. C. Hurley, and B. Frank. *Warm-mix asphalt: Best practices*. National Asphalt Pavement Association Lanham, Md, USA, 2011.
251. Zhang, Z., L.-p. LIU, and W. Tang. Research on performance of Evotherm warm-mix asphalt. *Journal of Building Materials*, Vol. 12, No. 4, 2009, pp. 438-441.
252. ZHANG, Z., and L.-j. SUN. The Control Indicates Research of Evotherm Warm-Mix Asphalt [J]. *Journal of Wuhan University of Technology*, Vol. 8, 2009, p. 007.
253. Kuang, Y. *Evaluation of Evotherm as a WMA technology compaction and anti-strip additive*. Iowa State University, 2012.

254. ZHANG, Z. LIU Li-ping~ 1, TANG Wen~ 1 (1. Key Laboratory of Road and Traffic Engineering of Ministry of Education, Tongji University, Shanghai 200092, China; 2. Automobile and Transportation School, Qingdao Technological University, Qingdao 266520, China); Research on Performance of Evotherm Warm-Mix Asphalt [J]. *Journal of Building Materials*, Vol. 4, 2009.
255. Yong-chun, Q. HUANG Song-chang~ 2, XU Jian~ 2, LI Feng~ 2, SUN Li-jun~ 1 (1. Key Laboratory of Road and Traffic Engineering of Ministry of Education, Tongji University, Shanghai 200092, China; 2. Key Laboratory of Road Structure & Material (Beijing), Research Institute of Highway, MOC, Beijing 100088, China); Performance of SMA Mixture Based on Evotherm-DAT Warm Mix Asphalt Technology [J]. *Journal of Building Materials*, Vol. 1, 2010.
256. Saleh, M. Laboratory evaluation of warm mix asphalt incorporating high RAP proportion by using evotherm and sylvaroad additives. *Construction and Building Materials*, Vol. 114, 2016, pp. 580-587.
257. Zeng, M.-L., C.-F. Wu, and J.-S. Zhang. Determining mixing and compaction temperatures of Evotherm Warm Mix Asphalt using 100% reclaimed asphalt pavement. *International Journal of Pavement Research and Technology,* Vol. 7, No. 6, 2014, pp. 389-396.
258. Davidson, J. K., C. Lubbers, and K. Takamura. Characterization of Unmodified and SBR Latex-Modified Evotherm® Warm Mix Binder.In *PROCEEDINGS OF THE ANNUAL CONFERENCE-CANADIAN TECHNICAL ASPHALT ASSOCIATION*, *No. 52*, Polyscience Publications; 1998, 2007. p. 297.
259. Arega, Z., A. Bhasin, A. Motamed, and F. Turner. Influence of warm-mix additives and reduced aging on the rheology of asphalt binders with different natural wax contents. *Journal of Materials in Civil Engineering*, Vol. 23, No. 10, 2011, pp. 1453-1459.
260. Prowell, B., G. Hurley, and E. Crews. Field performance of warm-mix asphalt at national center for asphalt technology test track. *Transportation Research Record: Journal of the Transportation Research Board*, No. 1998, 2007, pp. 96-102.
261. Vaitkus, A., V. Vorobjovas, and L. Ziliut. The research on the use of warm mix asphalt for asphalt pavement structures.In *XXVII International Baltic Road Conference*, 2009. pp. 24-26.
262. Poel, V., and C. Der. A general system describing the visco-elastic properties of bitumens and its relation to routine test data. *Journal of Chemical Technology and Biotechnology,* Vol. 4, No. 5, 1954, pp. 221-236.
263. Monismith, C. L., R. L. Alexander, and K. E. Secor. Rheologic behavior of asphalt concrete.In *Assoc Asphalt Paving Technol Proc*, 1966.
264. Jongepier, R., B. Kuilman, R. Schmidt, V. Puzinauskas, and F. Rostler. Characteristics of the rheology of bitumens.In *Association of Asphalt Paving Technologists Proc*, 1969.
265. Dobson, G., C. Monismith, V. Puzinauskas, and H. Busching. The dynamic mechanical properties of bitumen.In *Association of Asphalt Paving Technologists Proc*, 1969.
266. Dobson, G. R. On the development of rational specifications for the rheological properties of bitumens. *Journal of the Institute of Petroleum*, Vol. 58, No. 559, 1972, p. 24.
267. Dickinson, E., and H. Witt. The dynamic shear modulus of paving asphalts as a function of frequency. *Transactions of the Society of Rheology,* Vol. 18, No. 4, 1974, pp. 591-606.
268. Anderson, D. A., D. W. Christensen, and H. Bahia. Physical properties of asphalt cement and the development of performance-related specifications. *Journal of the Association of Asphalt Paving Technologists,* Vol. 60, 1991.

269. Christensen, D. W., and D. A. Anderson. Interpretation of dynamic mechanical test data for paving grade asphalt cements (with discussion). *Journal of the Association of Asphalt Paving Technologists*, Vol. 61, 1992.
270. Lytton, R. L., J. Uzan, E. G. Fernando, R. Roque, D. Hiltunen, and S. M. Stoffels. *Development and validation of performance prediction models and specifications for asphalt binders and paving mixes*. Strategic Highway Research Program Washington, DC, 1993.
271. Anderson, D. A., D. W. Christensen, H. U. Bahia, R. Dongre, M. Sharma, C. E. Antle, and J. Button. Binder characterization and evaluation, volume 3: Physical characterization. *Strategic Highway Research Program, National Research Council, Report No. SHRP-A-369*, 1994.
272. Buttlar, W. G., and R. Roque. Evaluation of empirical and theoretical models to determine asphalt mixture stiffnesses at low temperatures (with discussion). *Journal of the Association of Asphalt Paving Technologists*, Vol. 65, 1996.
273. Marateanu, M., and D. Anderson. TIME-TEMPERATURE DEPENDENCY OF ASPHALT BINDERS--AN IMPROVED MODEL (WITH DISCUSSION). *Journal of the Association of Asphalt Paving Technologists*, Vol. 65, 1996.
274. Uzan, J. ASPHALT CONCRETE CHARACTERIZATION FOR PAVEMENT PERFORMANCE PREDICTION (WITH DISCUSSION). *Journal of the Association of Asphalt Paving Technologists*, Vol. 65, 1996.
275. Stastna, J., L. Zanzotto, and J. Berti. HOW GOOD ARE SOME RHEOLOGICAL MODELS OF DYNAMIC MATERIAL FUNCTIONS OF ASPHALT?(WITH DISCUSSION). *Journal of the Association of Asphalt Paving Technologists*, Vol. 66, 1997.
276. Zeng, M. Nonlinear viscoelastic behaviour of asphalt concrete in stress relaxation. 1997.
277. Christensen, D. Analysis of creep data from indirect tension test on asphalt concrete. *Journal of the Association of Asphalt Paving Technologists*, Vol. 67, 1998, pp. 458-492.
278. Bouldin, M. G., R. Dongre, G. M. Row, M. J. Sharrock, and D. A. Anderson. Predicting thermal cracking of pavements from binder properties: theoretical basis and field validation.In *Association of Asphalt Paving Technologists Proc, No. 69*, 2000.
279. Marasteanu, M., and D. Anderson. Improved model for bitumen rheological characterization.In *Eurobitume workshop on performance related properties for bituminous binders*, European Bitumen Association Brussels, Belgium, 1999.
280. Stroup-Gardiner, M. THE SIGNIFICANCE OF PHASE ANGLE MEASUREMENTS FOR ASPHALT CEMENTS (WITH DISCUSSION). *Journal of the Association of Asphalt Paving Technologists*, Vol. 65, 1996.
281. Bahia, H. U., H. Zhai, K. Bonnetti, and S. Kose. Non-linear viscoelastic and fatigue properties of asphalt binders. *Journal of the Association of Asphalt Paving Technologists*, Vol. 68, 1999, pp. 1-34.
282. ASTM, C. 670. 2003. *Standard Practice for Preparing Precision and Bias Statements for Test Methods for Construction Materials. American Society for Testing and Materials. West Conshohocken, PA.*
283. Booshehrian, A., W. S. Mogawer, and R. Bonaquist. How to construct an asphalt binder master curve and assess the degree of blending between RAP and virgin binders. *Journal of Materials in Civil Engineering*, Vol. 25, No. 12, 2012, pp. 1813-1821.
284. Kim, Y. R., M. King, and M. Momen. Typical dynamic moduli for North Carolina asphalt concrete mixes.In, 2005.
285. AASHTO, R. 28-12, Standard practice for accelerated aging of asphalt binder using a Pressurized Aging Vessel (PAV).In, 2016.

286. AASHTO. XX-XX, Calibration of the Pavement Analysis using Nonlinear Damage Approach (PANDA) Constitutive Relationships In, Texas A&M University College Station, TX, 2013. pp. 1-29.
287. Schapery, R. A. Further development of a thermodynamic constitutive theory: stress formulation. *Purdue University, Purdue Resarch Foundation, Lafayette, IN*, 1969.
288. Masad, E., C. W. Huang, G. Airey, and A. Muliana. Nonlinear viscoelastic analysis of unaged and aged asphalt binders. *Construction and Building Materials,* Vol. 22, No. 11, 2008, pp. 2170-2179.
289. Rahmani, E., M. K. Darabi, R. K. Abu Al-Rub, E. Kassem, E. Masad, and D. Little. Effect of Confinement Pressure on the Nonlinear-Viscoelastic Response of Asphalt Concrete at High Temperatures. *Construction and Building Materials,* Vol. In press, 2013.
290. Perzyna, P. Thermodynamic theory of viscoplastcity. *Advances in Applied Mechanics*, Vol. 11, 1971, pp. 313-354.
291. Darabi, M. K., R. K. Abu Al Rub, E. Masad, and D. Little. Constitutive Modeling of Fatigue Damage Response of Asphalt Concrete Materials with Consideration of Micro-damage Healing *International Journal of Solids and Structures,* Vol. In press, 2013.

Appendix

This appendix presents standard methods and required tests according to AASHTO standards to characterize mechanical properties of asphalt concrete materials. This standard initiated by TAMU researchers during past decade (*286*). The experimental studies, theoretical developments, and data analysis presented in this dissertation led to the modification of the nonlinear viscoelastic, viscoplastic, and hardening-relaxation material properties extraction and analysis procedure, such that:

Standard Methods and Required Tests for

Calibration of the Pavement Analysis using Nonlinear Damage Approach (PANDA) Constitutive Relationships

AASHTO Designation: XX-XX

---

1. SCOPE

1.1. This standard covers the test methods required to determine the material parameters for the Pavement Analysis using Nonlinear Damage Approach (PANDA) constitutive relationships.

1.2. *This standard may involve hazardous material, operations, and equipment. This standard does not support to address all of the safety concerns associated with its use. It is the responsibility of the user of this procedure to establish appropriate safety and health practices and determine the applicability of regulatory limitations prior use.*

---

2. REFERENCED DOCUMENTS

2.1. AASHTO Standards:

- T 342, Determining Dynamic Modulus of Hot Mix Asphalt
- T 166, Bulk Specific Gravity of Compacted Hot Mix Asphalt Using Saturated Surface-Dry Specimens
- T 209, Theoretical Maximum Specific Gravity and Density of Bituminous Paving Mixtures
- T 269, Percent Air Voids in Compacted Dense and Open Asphalt Mixtures

- T 307, Determining the Resilient Modulus of Soils and Aggregate Materials
- T 312, Preparing and Determining the Density of the Hot Mix Asphalt (HMA) Specimens by Means of the Superpave Gyratory Compactor

2.2. ASTM Standards:

- E 4, Standard Practices for Force Verification of Testing Machines

3. SIGNIFICANCE AND USE

3.1. The material parameters or constants determined using this standard are used in the constitutive relationships of Pavement Analysis using Nonlinear Damage Approach (PANDA) in order to predict the performance of asphalt pavements. PANDA incorporates several material constitutive relationships to define the behavior (viscoelastic, viscoplastic, mechanical damage, fatigue damage, and fracture) of an asphalt mixture.

3.2. PANDA is used in asphalt pavement performance analysis.

4. SUMMARY OF TEST METHODS

4.1. This standard consists of several test methods required to determine the material parameters needed for the calibration of different components of PANDA. The dynamic modulus test is used to identify the linear viscoelastic parameters and the time-temperature shift factors. The repeated creep-recovery test at variable stress level (RCRT-VS) conducted at 55^{o}C is used to identify the viscoplastic parameters. The repeated creep-recovery test at constant loading and rest times (RCRT-CLR) is used to identify the hardening-relaxation viscoplastic parameters. The uniaxial constant strain rate test in both compression and tension is used to determine the viscodamage parameters. Table 1 summarizes the test methods required to determine parameters associated with PANDA constitutive relationships.

Table 1. Summary of the Test Methods Required for Calibration of PANDA Constitutive Relationships.

Test Mode	*Total No. of Specimens*	*Test Method*	*Temperature (°C)*	*Level*	*Loading Time/Resting Time (sec)*	*Confining Pressure (kPa)*
Compression	2	AASHTO T 342	Varies	80-110 με	N/A	0
	2	RCRT-VS	55	Varies	0.4/5	140
	6	RCRT-CLR	55	840 kPa	0.4/0.4, 1, 5	140
	4	Uniaxial Constant Strain Rate	55	0.021 mm/sec	N/A	140, 380
Tension	6	Uniaxial Constant Strain Rate	5	5×10^{-6}, 1×10^{-5}, 5×10^{-5} 1/sec	N/A	0

5. APPARATUS

5.1. *Dynamic Modulus Test System*—The system should be capable of conducting the Dynamic Modulus Test at specified temperatures and frequencies in accordance with AASHTO Standard T 342.

5.2. *Universal Materials Testing System*—The machine should be capable of producing controlled load in both compression and tension. It shall be equipped with ±22 kN (5,000 lb) load cell. The load cell should be calibrated in accordance with ASTM E 4. The system shall be fully computer controlled capable of measuring and recording the time, load, deformation, and confining pressure.

5.3. *Environmental Chamber*—The chamber is required to control the temperature of the test specimens at the desired temperatures. It should be capable of controlling the temperature of the test specimens over a temperature range of -10°C to 55°C. The chamber should accommodate the triaxial cell, which is shown schematicallyin Figure 1.

5.4. *Triaxial Cell*—A triaxial is required for applying a confining pressure on the test specimens. The cell should stand a working pressure up to 400 kPa (air). The cell should accommodate test specimens, with each has the dimensions of 101.6 mm diameter by 152.4 mm height. The cell shall facilitate up to three “through-the-wall” radial strain transducers. Figure 1 shows a schematic for a triaxial.

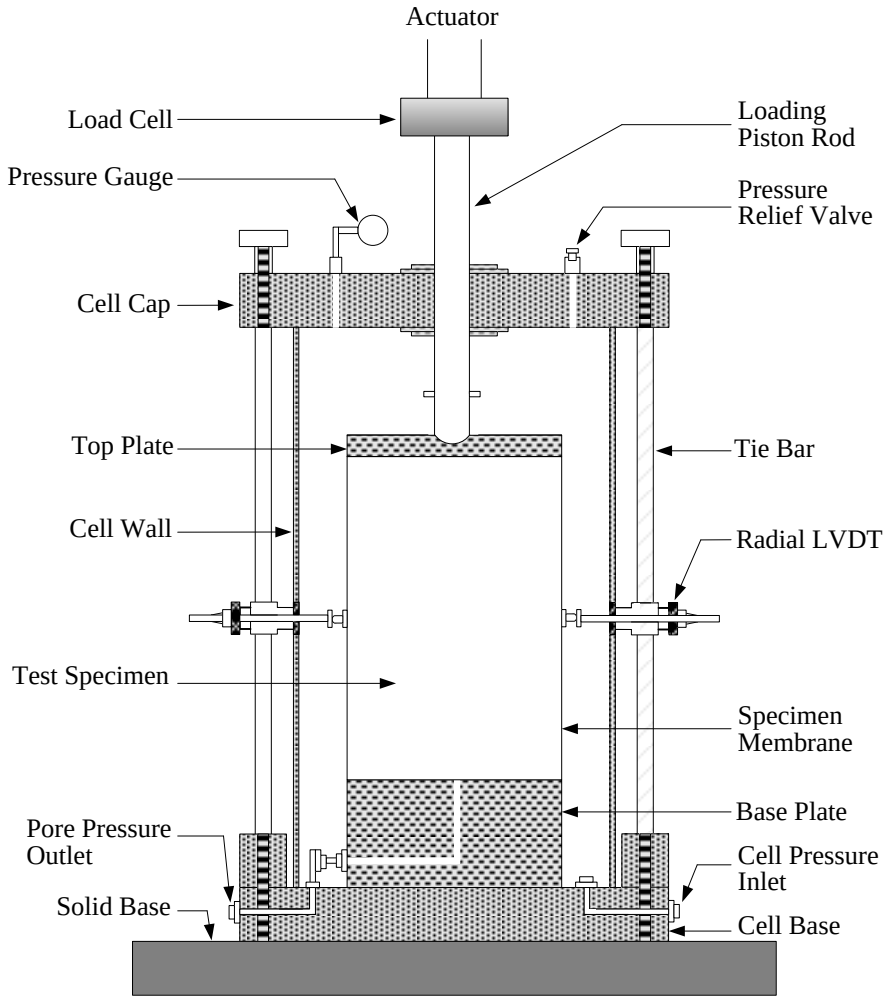

Figure 1. Schematic View of Typical Triaxial Cell with through-the-wall Radial LVDTs

5.5. *Pressure gauge*—The pressure inside the triaxial cell shall be monitored using a conventional pressure gauge with working pressure of up to 600 kPa and minimum accuracy of 0.7kPa.

5.6. *Strain Transducers*—The axial and radial deformations shall be measured using linear variable differential transformers (LVDTs). Three axial LVDTs shall be used to measure axial deformation. The LVDTs shall be placed on the test specimens at 120 degree apart. A schematic view of the test setup with mounted axial LVDTs is given in Figure 2. Three LVDTs shall be used to measure the radial deformation at the center of the test specimens. Figure 1 shows a tri-axial with "through-the-wall" radial LVDTs. The LVDTs shall have a linear range of ±2.50 mm and meet the following minimum specifications: linearity, ±0.15 percent of full scale; sensitivity, 156.43mV/V/mm; and repeatability, ±1 percent of full scale.
Note 1—The specifications of the LVDTs used in the dynamic modulus test shall comply with the T 342 specifications.

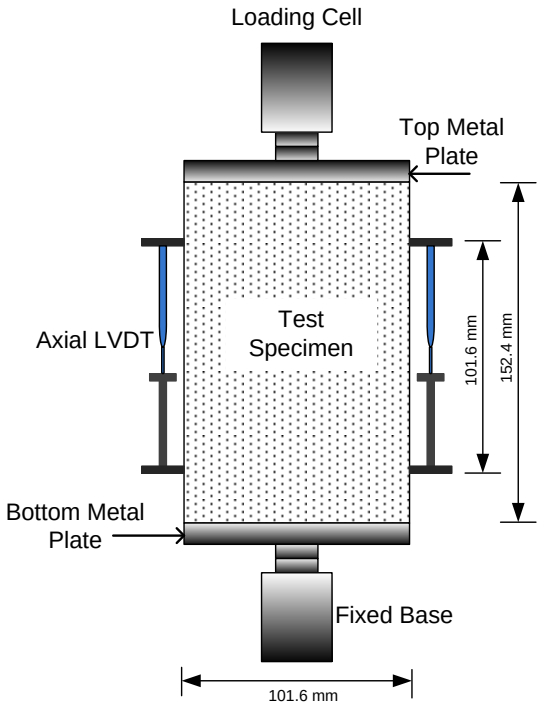

Figure 2. Schematic View of Test Setup with Mounted Axial LVDTs

5.7. *Loading platens*—The loading platens should be made of stainless steel or high-strength aluminum. The size of the loading platens (104.5±0.5 mm) should be slightly larger than diameter of the test specimens.

5.8. Pressurized air supply—A compressed air supply that is capable of supplying clean, dry, oil-free air up to 400 kPa

5.9. *Calipers*—Digital or analog calipers with an accuracy of ±0.01 mm.

5.10. Glue—must be able to withstand force applied to the sample by a machine and must bond well to the test specimen and loading platens.

5.11. *Superpave Gyratory Compactor*—A compactor and associated equipment needed to compact 152.4-mm diameter and 170-mm height specimens in accordance with the AASHTO T 312 Standard.

5.12. *Core Drill*—A coring machine with a diamond coring bit should be able to cut 101.6-mm diameter specimens out of 152.4-mm diameter SGC specimens.

5.13. *Saw*—Single or double saw with diamond cutting edge should be capable of trimming 170-mm height SGC specimens to 152.4-mm height specimens.

5.14. *Balance*—A balance shall meet the requirements of AASHTO M 231 Standard.

5.15. *Thermometers*—A thermometer should be able to measure the temperature of test specimens over the range of -10º C to 55º C.

5.16. *Latex Membrane*—71.1 mm diameter by 0.3mm thick rubber membrane is used when confining pressure is required.

5.17. *End-Friction Reducer*—Greased double latex is placed between the specimen and loading platen.

5.18. *Other apparatus*—other apparatus required to perform the procedures described in this document include a recipient for the applied vacuum saturation.

6. HAZARDS

6.1. Observe and practice standard laboratory safety precautions when preparing, handling, and testing hot mix asphalt (HMA) specimens. Caution should be taken when applying confining pressure on test specimens. The confining pressure must not exceed the limit specified by the manufacturer of the tri-axial cell.

7. TEST SPECIMENS FABRICATION AND INSTRUMENTATION

7.1. HMA specimens are prepared in accordance with T 312. A SGC is used to compact cylindrical 170±1-mm tall and 152.4±1-mm diameter specimens.

7.2. The SGC specimens are cored to 101.6±1-mm diameter, and trimmed using a double or single saw cut to 152.4±1-mm tall. The sides and ends of test specimens shall be smooth and parallel.

7.3. The ends of the test specimens should be perpendicular to axis of the specimens. Each specimen shall be checked using a machinist's square.

7.4. The air void content of test specimens shall be determined in accordance with T 269. A tolerance of 0.5 percent from the target percent air voids is allowed. Any specimen that exceeds this tolerance shall be discarded.

7.5. At least two specimens shall be tested at each test condition.

7.6. Three axial LVDTs shall be mounted to the sides of the test specimens at 120 degree apart. Figure 2 presents a schematic view of the test setup with mounted axial LVDTs. The gauge length of the axial LVDTs shall be 101.6±1 mm. The metal studs are mounted at a distance of 25.4 mm from the top and bottom of the test specimens. The mounting studs for axial LVDTS should be glued directly to test specimens.
Note 2—Quick setting epoxy and glue accelerator such as E-Z BOND and MAXI-CURE exhibit satisfactory performance.

7.7. Three metal studs for the radial LVDTs shall be mounted in the center of the test specimens at 120 degree apart and 60 degree from the axial LVDTs. The gauge length of the radial LVDTs shall be equal to the radius of the test specimens (50.8±0.5 mm). The mounting studs for radial LVDTS should be glued directly to test specimens.

7.8. When confining pressure is required, a latex membrane should be stretched over the test specimen. O-rings should are used to seal the membrane to the top and bottom plates.

8. TEST PROTOCOLS

8.1. Dynamic Modulus Test According to AASHTO TP-62

The dynamic modulus test is used to identify the linear viscoelastic parameters and time-temperature shift factors. This test is conducted in accordance with the AASHTO TP 62. This test is conducted at five different temperatures (−10 °C, 4.4 °C, 21.1 °C, 37.8 °C, and 54.4 °C) and six loading frequencies (0.1, 0.5, 1.0, 5, 10, and 25 Hz) at each temperature. A sinusoidal loading is applied and adjusted to obtain axial strain between 80 to 110 microstrain. Testing starts from the lowest to highest temperature and from highest to lowest frequency. The applied stress and recorded strain are used to calculate the dynamic modulus and phase angle.

8.2. *Repeated Creep*-Recovery *Test at Variable Stress Levels (RCRT-VS)*

The repeated creep-recovery test at variable stress level (RCRT-VS) is conducted at 55^{o}C to identify the viscoplastic parameters. The test includes six loading blocks. Each loading block consists of eight creep-recovery cycles with increasing applied deviatoric stress level. The loading and unloading times of each loading cycle remain constant through the entire test. The loading time is 0.4 sec while the unloading time is 30 sec. The deviatoric stress of the first loading cycle of the first loading block is 140 kPa and it increases by a factor of $1.2^{(n-1)}$; where n is the number of loading cycle in a specific loading block; for the next loading cycles until the 8th loading cycle. The first deviatoric stress of the subsequent loading blocks equals to the third stress level in the previous loading block, and it increases by the same factor of $1.2^{(n-1)}$ for the next loading cycles until the 8th loading cycle of that loading block. A confining pressure of 140 kPa is maintained during the entire test. Figure 3 shows an example of the first three loading blocks of the RCRT-VS.

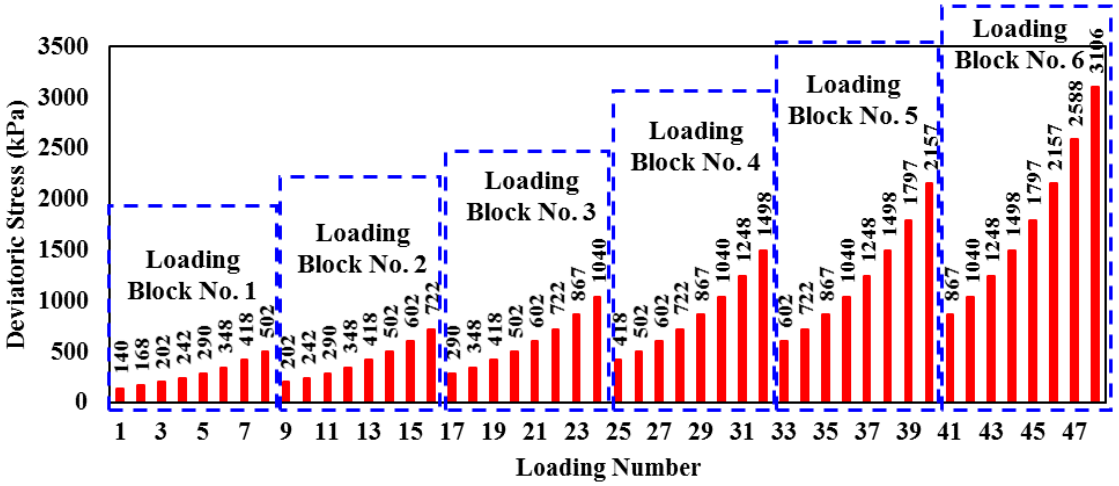

Figure 3. Applied Deviatoric Stress in the First Three Loading Blocks of the RCRT-VS

8.3. ***Repeated Creep-Recovery Test at Constant Loading and Rest Times (RCRT-CLR)***

The creep-recovery test at constant loading and rest times (RCRT-CLR) is performed to identify the hardening-relaxation viscoplastic parameters. The RCRT-CLR consists of repeated creep-recovery loading cycles. The applied confinement and deviatoric stresses in the RCRT-CLR test are 140 kPa and 840 kPa, respectively. The loading time and rest period of all loading cycles are maintained constant throughout the test. A loading time of 0.4 sec and rest periods of 0.4, 1, and 5 sec are used. Two specimens are tested at each rest period as given in Table 1. Figure 4 illustrates a schematic for the RCRT-CLR test.

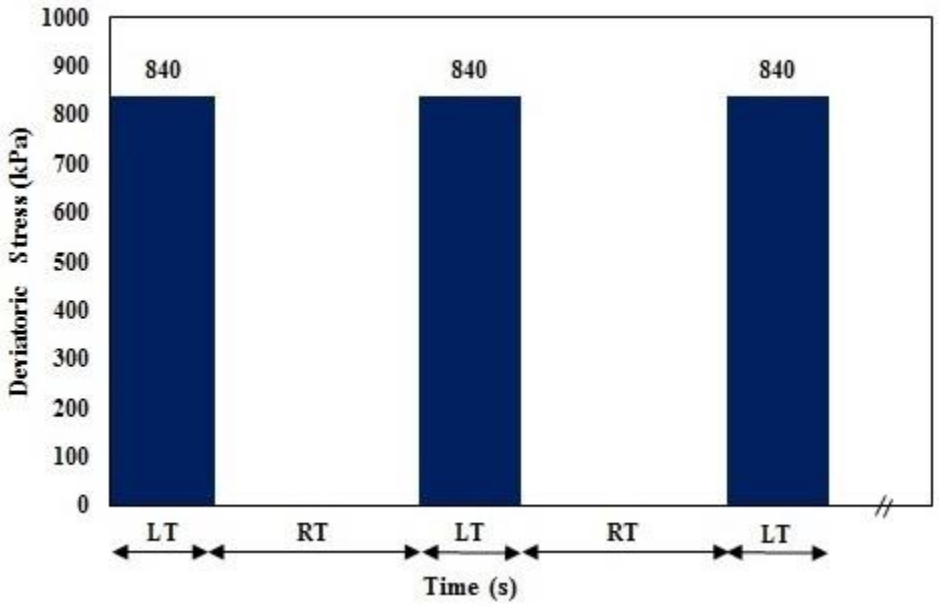

Figure 4. Schematic for loading cycles of the RCRT-CLR

Note: LT is loading time and RT is rest time

8.4. ***Uniaxial Constant Strain Rate Compression Test***

A constant uniaxial strain rate of 0.021 mm/sec is applied on test specimens in compression until failure. This test is conducted at 55^{o}C and two levels of confining pressure; 140 kPa and 380 kPa are required. Two specimens are tested at each confining level as given in Table 1.

8.5. ***Uniaxial Constant Strain Rate Tension Test***

This test is conducted in tension at 5^{o}C to determine the viscodamage parameter. The test is performed without confining pressure at three different constant strain rates of 5×10^{-6}, 1×10^{-5} , and 5×10^{-5}/sec until failure. Two specimens are tested at each strain rate as given in Table 1.

Note 3: The uniaxial constant strain rate in tension can be performed without using the tri-axial cell since no confining pressure is required. In this test the test specimen must be glued to the top and bottom plates. The used glue shall be able to withstand force applied to the sample by a machine and must bond well to the test specimen and loading platens. The J-B WELD steel reinforced epoxy is found to provide satisfied adhesion between specimen surface and end plates, and it stands the tensile force. A schematic of the test specimen for the uniaxial constant strain rate in tension is illustrated in Figure 2.

9. TEST PROCEDURE

9.1. Attach the mounting metal studs of the radial and axial LVDTs to the test specimens as described in Sections 7.6. and 7.7.

9.2. Stretch the rubber membrane over the test specimen described in Section 7.8., and fix the fixtures of the LVDTs.

9.3. Place friction reducers between the test specimen and loading platens, and seal the rubber membrane to the top and bottom platens using O-rings as discussed in Section 7.8. When applying confining pressure, the bottom friction reducer should have a hole to allow a passage for specimen's entrapped air to pass to the atmospheric pressure through the base plate as shown in Figure 1.

9.4. Set the temperature of the environmental chamber to the desired test temperature.

9.5. Place the test specimen inside the triaxial cell and adjust the position of the specimen so that the loading piston rod is right in the middle of the top loading platen as shown in Figure 1.

9.6. Install the axial LVDTs, and ensure that the deformation of each axial LVDT is within the calibrated linear range.

9.7. Close the triaxial test and tighten the tie bars.

9.8. Adjust the through-the-wall radial LVDTs and ensure that the deformation of each radial LVDT is within the calibrated linear range.

9.9. Open the pore pressure outlet valve of the triaxial cell (Figure 1).

9.10. Place a dummy specimen inside the environmental chamber and monitor the temperature of this specimen.

9.11. Open the software select pre-programmed testing protocol as described in details in Section 8.
Note 4: The dynamic modulus test should be conducted in accordance AASHTO TP 62.

9.12. Start the test when the temperature of the dummy specimen reaches the desired value. When applying confining pressure, a conditioning period of 2 hours is required after applying the required confining pressure and before loading. This conditioning time is found sufficient to ensure that the bulk creep occurred before loading.

9.13. The RCRT tests are performed until a test specimen fails.

9.14. Perform data quality check on axial deformation measurements. Ensure that the average coefficient of variation of the three axial LVDTs readings, throughout the test and before test specimen fails, is less than 20 percent.

10. CALIBRATION PROTOCOL FOR PANDA CONSTITUTIVE RELATIONSHIPS

10.1. Calibration of Linear Viscoelastic Constitutive Relationship using Dynamic Modulus Test

This section presents a systematic procedure to identify time-temperature shift factors as well as the linear viscoelastic parameters based on dynamic modulus test data.

10.1.1 Linear viscoelastic constitutive relationship and its associated parameters

Schapery's (*287*) nonlinear viscoelasticity is implemented in PANDA. The nonlinear viscoelastic constitutive relationship can be written as follows:

$$\varepsilon_{ij}^{ve} = g_0 D_0 \bar{\sigma}_{ij}^{t} + g_1 \int_0^t \Delta D^{\left(\psi^t - \psi^\tau\right)} \frac{d\left(g_2 \bar{\sigma}_{ij}^{\tau}\right)}{d\tau} d\tau \tag{1}$$

where

$$D^{\psi^t} = \sum_{n=1}^{N} D_n \left[1 - \exp\left(-\lambda_n \psi^t\right)\right]; \qquad \psi^t = \int_0^t \frac{d\xi}{a_T} \tag{2}$$

where ε_{ij}^{ve} is the viscoelastic strain tensor; $\bar{\sigma}_{ij}$ is the stress tensor; D_0 is the instantaneous compliance; ΔD is the transient compliance; D_n and λ_n are the

Prony series coefficients; N is the number of Prony series; a_T is the time-temperature shift factor; and g_0, g_1, and g_2 are the nonlinear viscoelastic parameters. For the linear viscoelasticity $g_0 = g_1 = g_2 = 1$ is assumed. The procedure for identification of nonlinear parameters will be presented in the next section. Table 2 lists the parameters associated with the linear viscoelastic constitutive relationship and their physical significance.

Table 2. List of linear viscoelastic parameters and their physical significance

Parameter	Physical meaning
a_T	Time-temperature shift factor. Captures the response at different temperatures.
D_0	Instantaneous compliance. Related to the instantaneous viscoelastic response.
D_n	n^{th} Prony series coefficient related to transient compliance.
λ_n	n^{th} Retardation time associated with the n^{th} transient compliance D_n.
N	Number of Prony series to acquire desired accuracy. $N = 9$ is recommended. No need to be determined. It should be assumed.

10.1.2 Obtaining time-temperature shift factor

- Dynamic modulus $\left|E^*\right|$ and the phase angle θ at each frequency and temperature are the outputs of the dynamic modulus test. Values of dynamic compliance $\left|D^*\right|$ is determined, such that:

$$\log\left|D^*\right| = -\log\left|E^*\right| \tag{3}$$

- A sigmoidal-type function is used to fit the experimental data and to obtain the time-temperature shift factors. The sigmoidal function for the complex compliance can be written as:

$$-\log\left|D^*\right| = \delta + \frac{\alpha}{1+\exp\left[\beta+\gamma\log\left(\omega_r\right)\right]} \tag{4}$$

where ω_r is the reduced frequency, δ is the maximum value of the dynamic compliance, $\delta+\alpha$ is the minimum value of the dynamic compliance, and β and γ are parameters describing the shape of the sigmoidal function. Time-temperature shift factor is defined as:

$$a_T = \frac{\omega_r}{\omega} \tag{5}$$

where ω is the angular frequency. The term a_T is the time-temperature shift factor at each temperature. Eqs. (4) and (5) introduce $4+(n_T-1)$ unknowns which should be determined ($\alpha, \beta, \delta, \gamma, a_T(n_1), a_T(n_2) \ldots a_T(n_T-1)$); n_T is the number of temperatures at which the test is conducted. It should be noted that

number of unknown time-temperature shift factors are $(n_T - 1)$ since a_T is known at the selected reference temperature T_r (i.e. $a_T(T_r) = 1$).

- The error function is defined as:

$$R^2 = 1 - \frac{SSE}{SST} \tag{6}$$

where

$$SSE = \sum_{i=1}^{M} \left(\log D_{\exp} - \log D_{fit} \right)^2 \tag{7}$$

$$SST = \sum_{i=1}^{M} \left(\log D_{\exp} - \overline{\log D} \right)^2 \tag{8}$$

where M is the number of data points obtained from dynamic modulus test, $\log D_{\exp}$ is the experimentally measured compliance, $\log D_{fit}$ is the compliance fitted using Eq. (4), $\overline{\log D}$ is the mean value of the measured compliance.

- The $4 + (n_T - 1)$ unknown variables are determined by minimizing the error function R^2 using Generalized Reduced Gradient (GRG) algorithm which is also available in the excel solver. Initial values for the unknown variables will be set in Excel solver by selecting the corresponding cells for each variable. The objective cell would be the calculated value of R^2. The sigmoidal function parameters and the time-temperature shift factors will be identified by minimizing R^2.
- Excel solver or other optimization algorithms available in other software such as Matlab can be used to obtain the $4 + (n_T - 1)$ parameters.

10.1.3 Identification of Linear Viscoelastic Parameters of PANDA

- Once the time-temperature shift factors are identified, the linear viscoelastic parameters can be identified.
- Using the experimental data, storage compliance D' and loss compliance D'' can be calculated using the values of the complex compliance and phase angle, such that:

$$D' = \left| D^* \right| \cos\theta; \qquad D'' = \left| D^* \right| \sin\theta \tag{9}$$

- The loss and storage compliances are related to the Prony series coefficients and angular frequencies, such that:

$$D'(\omega) = D_0 + \sum_{i=1}^{N} \frac{D_i}{\omega^2 / \lambda_i^2 + 1}; \qquad D''(\omega) = \sum_{i=1}^{N} \frac{\omega / (\lambda_i D_i)}{\omega^2 / \lambda_i^2 + 1} \tag{10}$$

where N is the number of Prony series coefficients, D_0 is the instantaneous compliance, D_i is the i^{th} transient compliance associated with the i^{th} retardation time λ_i.

- The error function is defined as:

$$error = \frac{1}{M}\sum_{i=1}^{N}\left[\left(\frac{D'_{fit}}{D'_{\exp}}-1\right)^2+\left(\frac{D''_{fit}}{D''_{\exp}}-1\right)^2\right] \quad (11)$$

where M is the number of data points. D'_{fit} and D''_{fit} are based on Eq. (10) while $D'_{\exp}$ and $D''_{\exp}$ are calculated experimentally.

- The linear viscoelastic PANDA model parameters (i.e. Prony series coefficients) will be identified by minimizing the error function presented in Eq. (11). Eq. (11) can be minimized using excel solver or using other commercial software such as Matlab.
- There is no need to identify N. Based on the desired accuracy, N can be assumed between 5 and 9. $N=9$ is recommended.

10.2. Calibration of Nonlinear Viscoelastic PANDA Model Parameters using Repeated Creep-Recovery Test at Various Stress levels (RCRT-VS)

This section outlines the procedure for identification of the nonlinear viscoelastic parameters using repeated creep-recovery test at various stress levels (RCRT-VS), refer to Masad et al. (*288*), Rahmani et al. (*289*), and Bazzaz et al. (*210*) for more details on identification of nonlinear viscoelastic parameters. To accurately represent the stress states in the pavements, it is recommended to conduct this test at a confinement level of 140-250 kPa. Based on RCRT-VS, three nonlinear parameters g_0, g_1, and g_2 should be determined. It is assumed that $g_0=1$. The viscoelastic nonlinearity will be captured through parameters g_1 and g_2. Tables 3 and 4 list the parameters that are fixed and the parameters that should be identified along with their physical significances.

Table 3. List of nonlinear viscoelastic parameters that are fixed and can be assumed. No need to identify these parameters.

Parameter	Recommended value	Physical significance
g_0	1.0	Affects the instantaneous response. It is recommended to assume $g_0=1$ since it is very difficult to measure the instantaneous response of asphalt mixtures. The nonlinear viscoelastic response will be captured through nonlinear parameters g_1 and g_2 Time-temperature shift factor. Captures the response at different temperatures

Table 4. List of nonlinear viscoelastic parameters that should be identified.

Parameter	Physical meaning
g_1	Controls the nonlinearity in the transient compliance. Affects the viscoelastic nonlinearity mostly during the loading stages.
g_2	Controls the nonlinear response during the recovery and at different loading rates.

10.2.1 Viscoelastic strain decomposition

- To capture the effect of multi-axial state of stresses on nonlinear viscoelastic response of asphalt mixes, the total nonlinear viscoelastic strain tensor ε_{ij}^{nve} is decomposed into deviatoric strain tensor e_{ij}^{nve} and volumetric component ε_{kk}^{nve}, such that:

$$\varepsilon_{ij}^{nve} = e_{ij}^{nve} + \frac{1}{3}\varepsilon_{kk}^{nve}\delta_{ij} \tag{12}$$

- Deviatoric and volumetric components of the viscoelastic strain can be expressed as:

$$e_{ij}^{nve,t} = \frac{1}{2}g_0 J_0 \bar{S}_{ij}^{t} + \frac{1}{2}g_1 \int_0^t \Delta J\left(\psi^t - \psi^\tau\right)\frac{d\left(g_2 \bar{S}_{ij}^{\tau}\right)}{d\tau}d\tau \tag{13}$$

$$\varepsilon_{kk}^{t} = \frac{1}{3}g_0 B_0 \bar{\sigma}_{kk}^{t} + \frac{1}{3}g_1 \int_0^t \Delta B\left(\psi^t - \psi^\tau\right)\frac{d\left(g_2 \bar{\sigma}_{kk}^{\tau}\right)}{d\tau}d\tau \tag{14}$$

where $\bar{S}_{ij}$ are the components of the deviatoric stress tensor and $\bar{\sigma}_{kk}$ is the volumetric stress.

- Shear and bulk instantaneous (i.e. J_0 and B_0) and transient (i.e. ΔJ and ΔB) compliances are calculated based on the identified linear viscoelastic parameters and using the following equations:

$$J_0 = 2\left(1+\nu\right)D_0; \qquad \Delta J\left(\psi\right) = 2\left(1+\nu\right)\Delta D\left(\psi\right) \tag{15}$$

$$B_0 = 3\left(1-2\nu\right)D_0; \qquad \Delta B\left(\psi\right) = 3\left(1-2\nu\right)\Delta D\left(\psi\right) \tag{16}$$

- Assume the Poisson's ratio to be 0.35, $\nu = 0.35$.
- Deviatoric and volumetric components of the stress for RCRT-VS under confinement stress $\bar{\sigma}_c$ and additional axial stress of $\Delta\bar{\sigma}$ are calculated as follows:

$$\frac{1}{3}\bar{\sigma}_{kk}\delta_{ij} = \left(\sigma_c + \frac{\Delta\sigma}{3}\right)\delta_{ij} \quad , \; \bar{S}_{ij} = \begin{bmatrix} \frac{2}{3}\Delta\sigma & 0 & 0 \\ 0 & -\frac{1}{3}\Delta\sigma & 0 \\ 0 & 0 & -\frac{1}{3}\Delta\sigma \end{bmatrix} \tag{17}$$

10.2.2 Parameter g_0

- Assume nonlinear parameter g_0 to be unity, $g_0 = 1.0$.

10.2.3 Parameter g_2

Figure 5 schematically represents the strain response during a cycle of RCRT-VS test.

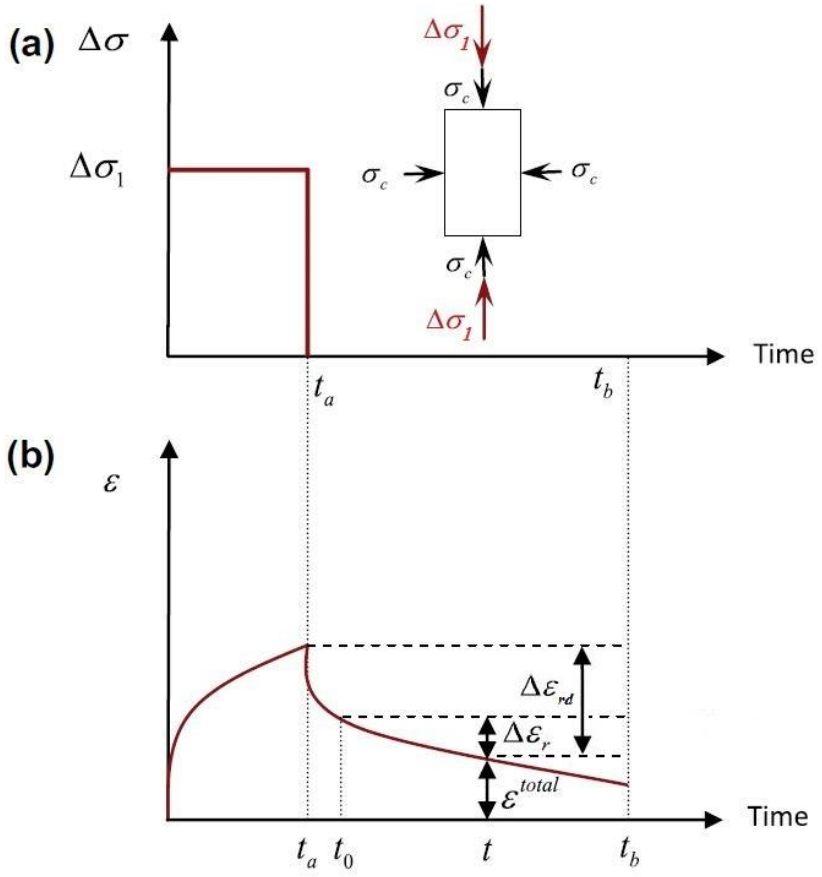

Figure 5. Schematic representation of the strain response during a cycle of RCRT-VS test.

- Select an arbitrary point during the recovery (e.g. t_0). It is recommended to assume t_0 such that $t_0 - t_a$ is $\frac{1}{40}$ of the rest period.
- Calculate the recovered strain $\Delta\varepsilon_r$ for every point after t_0 during the rest period. $\Delta\varepsilon_r$ can easily be calculated using experimental data, such that:

$$\Delta\varepsilon_r^{Exp} = \varepsilon^{total,r}(t_0) - \varepsilon^{total,r}(t) = \left[\varepsilon_{11}^{NVE}(t_0) + \varepsilon_{11}^{vp}(t_0)\right] - \left[\varepsilon_{11}^{NVE}(t) + \varepsilon_{11}^{vp}(t)\right] \quad (18)$$

- Using Eqs. (13)-(17) and assuming that the viscoelastic response under pure confinement to be linear (i.e. $\varepsilon_{11}^{vp}(t_0) = \varepsilon_{11}^{vp}(t)$) yields the following relations for viscoelastic strain during the recovery:

$$\Delta\varepsilon_r = \varepsilon_{11}^{NVE}\left(t_0\right) - \varepsilon_{11}^{NVE}\left(t\right) = g_2\left[\Delta D\left(\psi^{t_0}\right) - \Delta D\left(\psi^{t_0} - \psi^{t_a}\right)\right]\Delta\sigma_1 - g_2\left[\Delta D\left(\psi^{t}\right) - \Delta D\left(\psi^{t} - \psi^{t_a}\right)\right]\Delta\sigma_1; \quad t_o \le t \le t_b \tag{19}$$

Eq. (19) shows that the only unknown to analytically calculate viscoelastic strain is g_2.

- Calculate g_2 by minimizing the error between experimental measurements (i.e. Eq. (18)) and model predictions (i.e. Eq. (19)) for viscoelastic recovery strain (i.e., $\Delta\varepsilon_r^{Exp}$ and $\Delta\varepsilon_r$, respectively).

10.2.4 Parameter g_1

Once the parameter g_2 is defined, the parameter g_1 can be identified as follows:

- Calculate the total recovered viscoelastic strain $\Delta\varepsilon_{rd}^{Exp}$ at any time t during the rest period based on the experimental measurements. The term $\Delta\varepsilon_{rd}^{Exp}$ is the difference between the total strain a tat before the end of the loading and the strain at an arbitrary point during the rest period, as proposed in Eq. (20), see Figure 5.

$$\Delta\varepsilon_{rd}^{Exp} = \varepsilon_{11}^{total}\left(t_a^-\right) - \varepsilon_{11}^{total}\left(t\right); \qquad t_a \le t \le t_b \tag{20}$$

- Calculate $\Delta\varepsilon_{rd}$ using the nonlinear viscoelastic constitutive relationship, such that:

$$\Delta\varepsilon_{rd} = \varepsilon_{11}^{NVE}\left(t_a^-\right) - \varepsilon_{11}^{NVE}\left(t\right) = \left[\left(D_0 + g_1 g_2 \Delta D\left(\psi^{t_a}\right)\right)\Delta\sigma_1\right] - \left[g_2\left(\Delta D\left(\psi^{t}\right) - \Delta D\left(\psi^{t} - \psi^{t_a}\right)\right)\Delta\sigma_1\right]; \qquad t_a \le t \le t_b \tag{21}$$

- Identify g_1 by minimizing the error between the experimentally measured (i.e. Eq. (20)) and calculated values (i.e. Eq. (21)) of $\Delta\varepsilon_{rd}$.

10.3. Calibration of Viscoplastic PANDA Model using Repeated Creep-Recovery Test at Various Stress levels (RCRT-VS)

10.3.1 Viscoplastic constitutive relationship and its associated parameters

Perzyna's (*290*) viscoplastic constitutive relationship with modified Drucker-Prager yield surface has been implemented in PANDA. The viscoplastic flow rule can be written as:

$$\dot{\varepsilon}_{ij}^{vp} = \dot{\gamma}^{vp} \frac{\partial F}{\partial \bar{\sigma}_{ij}}; \qquad \dot{\gamma}^{vp} = \Gamma^{vp} \left\langle \frac{f}{\sigma_y^0} \right\rangle^N \tag{22}$$

where $\dot{\varepsilon}_{ij}^{vp}$ is the viscoplastic strain tensor, $\dot{\gamma}^{vp}$ is the viscoplastic multiplier, N is the viscoplastic rate-sensitivity exponent parameter, $\langle\ \rangle$ is the Macaulay brackets defined by $\langle \mathrm{X} \rangle = (\mathrm{X} + |\mathrm{X}|)/2$, and σ_y^0 is a yield stress quantity which is used to normalized the yield surface and can be assumed as unity. Functions f and F are yield surface and plastic potential functions, respectively, such that:

$$f = \tau - \alpha I_1 - \kappa(p); \qquad F = \tau - \beta I_1; \qquad \tau = \frac{\sqrt{3J_2}}{2}\left[1 + \frac{1}{d^{vp}} + \left(1 - \frac{1}{d^{vp}}\right)\frac{3J_3}{\sqrt{3J_2^3}}\right] \tag{23}$$

where α and β are the pressure-sensitivity material parameters; $I_1 = \bar{\sigma}_{kk}$ is the first stress invariant; τ is the deviatoric effective shear stress; $J_2 = \frac{1}{2}\bar{S}_{ij}\bar{S}_{ij}$ and $J_3 = \frac{1}{2}\bar{S}_{ij}\bar{S}_{jk}\bar{S}_{ki}$ are second and third deviatoric stress invariants, respectively; d^{vp} is the parameter that distinguishes the viscoplastic responses during extension and contraction mode of loadings; and κ is the hardening function expressed as:

$$\kappa(p) = \kappa_0 + \kappa_1\left[1 - \exp(-\kappa_2 p)\right]; \qquad \dot{p} = \left[1 + 2\left(\frac{0.5 + \beta/3}{1 - \beta/3}\right)\right]^{-0.5}\sqrt{\dot{\varepsilon}_{ij}^{vp}\dot{\varepsilon}_{ij}^{vp}} \tag{24}$$

where p is the effective viscoplastic strain.

10.3.2 Assumed Viscoplastic parameters

Several of viscoplastic parameters are assumed because they do not vary significantly from one asphalt mixture to the other and can be assumed constant with reasonable accuracy. These parameters, their physical meaning and the recommended values are listed in Table 5, please refer to Huang (*126*), Abu Al-Rub et al. (*209*), and Darabi et al. (*70*) for more details on the identification of viscoplastic parameters.

Table 5. List of viscoplastic parameters that are fixed and can be assumed. No need to identify these parameters.

Parameter	Recommended value	Physical significance
α	0.15-0.3	Related to the angle of friction of the asphalt mixtures.
β	$\alpha - 0.05$	Related to the angle of friction and the dilation characteristics of asphalt mixtures.
d^{vp}	0.78	Ratio of yield strength in tension to that in compression. Fixed for most asphalt mixes.
σ_y^0	100 kPa	Yield stress quantity

10.3.3 Extraction of viscoplastic strain during the creep part of RCRT-VS

- Use Eq. (1) to calculate the viscoelastic strain response during the loading stage of RCRT-VS once linear and nonlinear viscoelastic parameters are identified.
- Subtract the viscoelastic strain from the total strain to obtain the viscoplastic strain response during the creep part of RCRT-VS.
- Figure 6 schematically illustrates the extraction of the viscoelastic and viscoplastic strain responses from the total measured strain. The viscoplastic parameters will be identified by analyzing the extracted viscoplastic strain response.

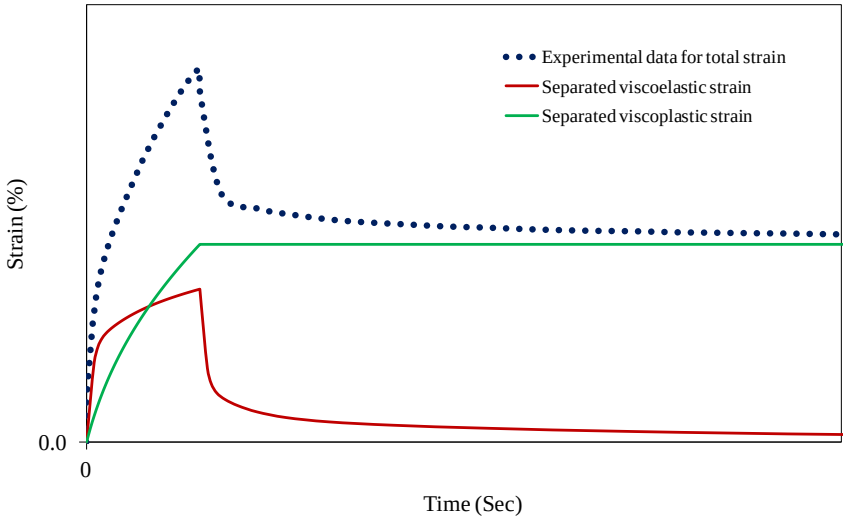

Figure 6. Schematic illustration of the extraction of the viscoelastic and viscoplastic components of the strain.

10.3.4 Identification of viscoplastic parameters

- Calculate effective viscoplastic strain p^{Exp} using extracted a (i.e. ε_1^{vp} and ε_2^{vp}) , such that:

$$p^{Exp} = \left[1+2\left(\frac{0.5+\beta/3}{1-\beta/3}\right)\right]^{-0.5} \sqrt{\left(\varepsilon_1^{vp}\right)^2 + 2\left(\varepsilon_2^{vp}\right)^2} \tag{25}$$

- If the radial viscoplastic strain measurements are not available, Eq. (26) may be used to estimate radial viscoplastic strain.

$$\varepsilon_2^{vp} = \left(\frac{0.5+\beta/3}{1-\beta/3}\right)\varepsilon_1^{vp} \tag{26}$$

- Manipulating Eqs. (22) and (23) yields:

$$\frac{\Delta\gamma^{vp}}{\Delta t}=\Gamma^{h-r}\left[\frac{\left\{\tau-\alpha I_1-\left[\kappa_0+\kappa_1\left(1-\exp\left(-\kappa_2 p\right)\right)\right]\right\}}{\sigma_y^0}\right]^N \tag{27}$$

- Calculate $\Delta\gamma^{vp}$ using the extracted axial viscoplastic strain $\Delta\varepsilon_1^{vp}$, such that:

$$\Delta\gamma^{vp}=\Delta\varepsilon_1^{vp}/\left(1-\beta/3\right) \tag{28}$$

- Pick values for $\Delta\gamma^{vp}$ at different stress levels of RCRT-VS test at constant Δt (i.e., approximately 0.05s), the recommended time intervals are 0.05, 0.1, 0.15, 0.2, 0.25, 0.3, 0.35, and 0.4 second. Rearrange Eq. (27) to calculate p^{Model}, such that:

$$p^{Model}=-\frac{1}{\kappa_2}ln\left(1-\frac{\tau-\alpha I_1-\left(\sigma_y^0\left(\frac{\Delta\gamma^{vp}}{\Gamma^{h-r}\Delta t}\right)^{1/N}+\kappa_0\right)}{\kappa_1}\right) \tag{29}$$

- The parameters κ_0, κ_1, κ_2, N, and Γ^{h-r} are unknowns in Eq. (29), which can be extracted by minimizing the error, i.e. Eq. (30), between the experiments, i.e. Eq. (25), and analysis, i.e. Eq. (29), using Genetic Algorithms.

$$error=\sum_{i=1}^{K}\left[\left(\frac{p^{Model}}{p^{Exp}}-1\right)^2\right] \tag{30}$$

- Genetic Algorithm maintains a population of candidate solutions for the problem in hand, and makes it evolve by iteratively applying a set of stochastic operators. Stochastic operators include selection, recombination, and mutation. Selection replicates the most successful solutions found in a population at a rate proportional to their relative quality. Recombination decomposes two distinct solutions and then randomly mixes their parts to form novel solutions. Mutation randomly perturbs a candidate solution. Table 6 illustrates Genetic Algorithms parameters to extract viscoplastic properties of asphalt concrete.

Table 6. The Genetic Algorithms parameters to extract viscoplastic properties of asphalt concrete materials.

Genetic Algorithm	Nature	Parameters	
Optimization problem	Environment	K_0	Initial yield strength. It has a very low value at high temperatures. Does not affect the results very much. It have a small value between 40-150kPa for most asphalt mixtures.
		K_1	The hardening limit of asphalt mixtures against viscoplastic deformation. It is in the order of compressive strength of asphalt mixtures at 40°C (Saturated Yield Stress (K_0+K_1))
		K_2	Visco-plastic Parameter (Strain Hardening Rate)
		N	Visco-plastic Rate-sensitivity Exponent Parameter
		Γ	Gama (Visco-plastic Fluidity Parameter)
Feasible solutions	Individuals living in that environment	K_0	40-150 (kPa)
		K_1	0-(Saturated Yield Stress minus K_0) (kPa)
		K_2	0-100
		N	0-5
		Γ	0.000001-1 (1/s)
Solutions quality (fitness function)	Individual's degree of adaptation to its surrounding environment (convergence)	0.0001	
A set of feasible solutions	A population of organisms (species or population size)	100	
Stochastic operators	Selection, recombination and mutation in nature's evolutionary process (mutation rate)	0.075	
Iteratively applying a set of stochastic operators on a set of feasible solutions	Evolution of populations to suit their environment (maximum time without improvement)	30	

10.4. Calibration of Hardening-Relaxation Viscoplastic PANDA Model using Repeated Creep-Recovery Test at Constant Loading and Rest times (RCRT-CLR)

10.4.1. Hardening-relaxation constitutive relationship and its associated parameters

When subjected to cyclic creep loading with rest periods between the loading cycles, the viscoplastic behavior of asphalt concrete materials changes such that the rate of accumulation of the viscoplastic strain at the beginning of a loading cycle increases comparing to that at the end of the preceding loading cycle. This phenomenon is referred to as the *hardening-relaxation* and is a key element in predicting the permanent deformation (rutting) of asphalt pavements. The hardening relaxation phenomenon is modeled using the hardening-relaxation memory concept (*68*). To model the hardening-relaxation, static and dynamic hardening-relaxation memory surfaces are defines as:

$$f^{h-r} = p - q^{vp} \le 0\,; \qquad \chi^{h-r} = p - q^{vp} - \left(\frac{\dot{q}^{vp}}{\Gamma^{h-r}}\right)^{\frac{1}{S_1}} \le 0 \tag{31}$$

where f^{h-r} and χ^{h-r} are static and dynamic hardening-relaxation memory surfaces, respectively. The term q^{vp} is the hardening-relaxation internal state variable that memorizes the maximum experienced viscoplastic strain for which the hardening-relaxation has occurred while p is the effective viscoplastic strain. Parameters Γ^{h-r} and S_1 are hardening-relaxation parameters. The rate of relaxation in the hardening parameter is calculated, such that:

$$\dot{\kappa}_1 = -S_2 \dot{q}^{vp} \tag{32}$$

where S_2 is another parameter associated with the hardening-relaxation constitutive relationship. Table 7 lists the parameters associated with the hardening-relaxation constitutive relationship and their physical significance. Repeated creep-recovery test at constant loading and rest times (RCRT-CLR) will be used to identify the hardening-relaxation parameters.

Table 7. List of hardening-relaxation viscoplastic parameters.

Parameter	Physical meaning
Γ^{h-r}	Hardening-relaxation fluidity parameter controlling the rate of evolution of the hardening-relaxation state variable.
S_1	Hardening-relaxation exponent controlling the time-dependency of the hardening-relaxation state variable.
S_2	Hardening-relaxation parameter controlling the rate at which the hardening parameter relaxes.

10.4.2. Identification of hardening-relaxation parameters

Figure 7 schematically shows the evolution of the effective viscoplastic strain p and the hardening-relaxation state variable q^{vp} during a cycle of RCRT-CLR.

- From the experimental measurements, calculate the rate of the effective viscoplastic strain during different loading cycles using Eq. (33):

$$\dot{p}(t) = \frac{p_2^{Exp} - p_1^{Exp}}{\Delta t} \tag{33}$$

- To simplify Eqs. (22) and (23) at times t_1 and t_2 two constant part of those equation at any loading cycle are presented as A and B (i.e., Equations (34) and (35), respectively).

$$A = \frac{\tau - \alpha I_1 - \kappa_0}{\sigma_y^0} \tag{34}$$

$$B(t_1) = \frac{1 - \exp\left(-\kappa_2 p(t_1)\right)}{\sigma_y^0} \tag{35}$$

- Then, by following Eqs. (36) and (37), the hardening parameter κ_1 at the end of loading and at the end of the rest period could be obtained, such that:

$$\dot{p}(t_1) = \Gamma^{h-r}\left[A - \kappa_1(t_1)B(t_1)\right]^N; \qquad \dot{p}(t_2) = \Gamma^{h-r}\left[A - \kappa_1(t_2)B(t_2)\right]^N \tag{36}$$

$$\kappa_1(t_1) = \frac{1}{B(t_1)}\left[A - \left(\frac{\dot{p}(t_1)}{\Gamma^{h-r}}\right)^{1/N}\right]; \qquad \kappa_1(t_2) = \frac{1}{B(t_2)}\left[A - \left(\frac{\dot{p}(t_2)}{\Gamma^{h-r}}\right)^{1/N}\right] \tag{37}$$

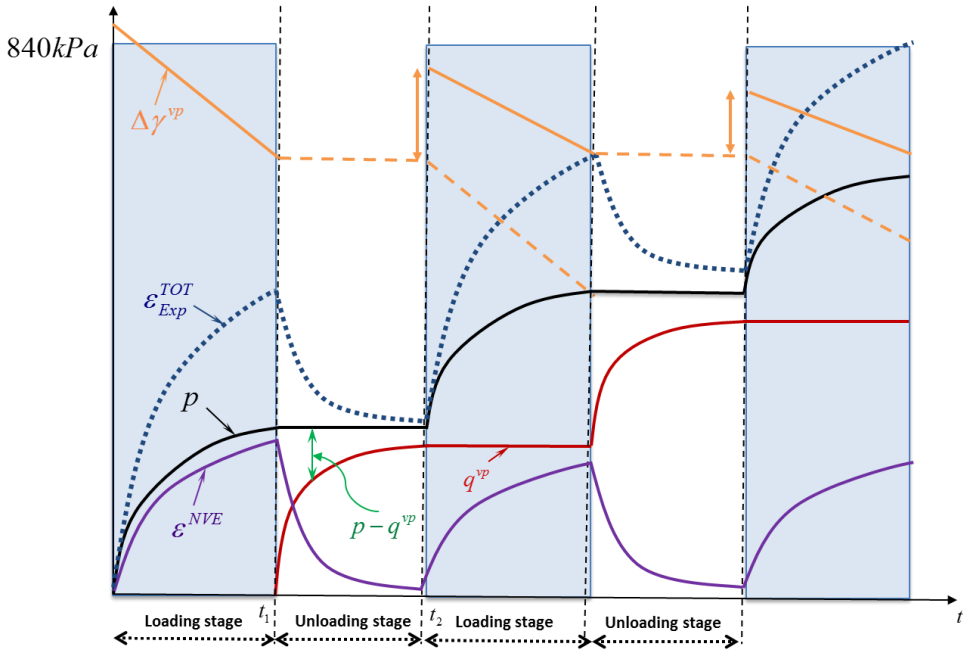

Figure 7. Schematic representation of the loading and unloading stages, the evolution of the total strain, the nonlinear viscoelastic strain, the effective viscoplastic strain, the hardening-relaxation viscoplastic internal state variable, and viscoplastic multiplier function during RCRT-CLR.

- Plot $\kappa_1(t_1)$ and $\kappa_1(t_2)$ versus the accumulative resting time t for the all RCRT-CLR tests.
- Integrate Eq. (32), such that:

$$-\frac{\kappa_1(t)-\kappa_1^{initial}}{S_2}=q^{vp}(t) \tag{38}$$

- As presented in Figure 8, if enough rest period (i.e., at least three times of loading time) is given to asphalt concrete mixture, the hardening-relaxation viscoplastic internal state variable (i.e., q^{vp}) will evolve to the maximum possible value to become the effective viscoplastic strain (i.e., p). Therefore, pick the average values of two replicates during 5 s rest period test of RCRT-CLR for p at the end of the first rest period as the hardening-relaxation viscoplastic internal state variable (i.e. $q^{vp}=p^{final}=p_{Ave}^{Exp}$) and calculate S_2, such that:

$$S_2=\frac{\kappa_1^{initial}-\kappa_1^{final}}{p^{final}} \tag{39}$$

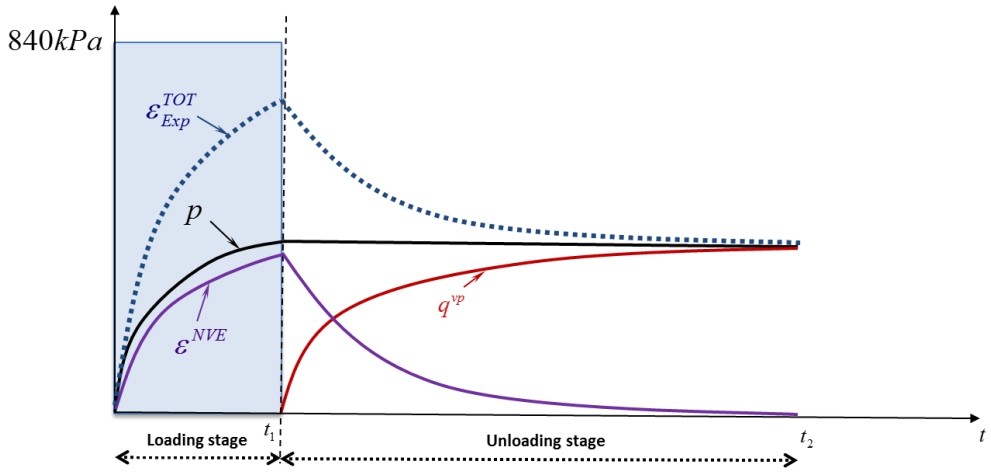

Figure 8. Schematic representation of the loading and unloading stage, the evolution of the total strain, the nonlinear viscoelastic strain, the effective viscoplastic strain, and the hardening-relaxation viscoplastic internal state variable during a cycle of RCRT-CLR with 5 s rest period.

- Calculate $\Delta q^{vp}(t)$ using Eq. (32) once S_2 is known based on Eq. (39) by following Eqs. (40) and (41), such that:

$$\Delta\kappa_1(t) = \kappa_1(t) - \kappa_1^{initial} \tag{40}$$

$$\Delta q^{vp}(t) = -\frac{\Delta\kappa_1(t)}{S_2} \tag{41}$$

where t is the accumulative unloading time.

- Calculate Δq^{vp}, q^{vp}, and p for all cycles of RCRT-CLR tests from experimental measurements Eq. (41) and model prediction Eq. (42).

$$q^{vp}(t) = \sum \Delta q^{vp}(t) \tag{42}$$

- Manipulate Eq. (31), such that:

$$\frac{\Delta q^{vp}}{\Delta t} = \Gamma^{h-r}\left(p - q^{vp}\right)^{S_1} \tag{43}$$

- Plot $\frac{\Delta q^{vp}}{\Delta t}$ versus $p - q^{vp}$ in log-log scale for all available data.

- Calculate Γ^{h-r} as the intersection of $\frac{\Delta q^{vp}}{\Delta t}$-$\left(p-q^{vp}\right)$ curve with Y-axis and S_1 as the slope of the fitted line using the following equation:

$$Ln\left(\frac{\Delta q^{vp}}{\Delta t}\right)=Ln\left(\Gamma^{h-r}\right)+S_1 Ln\left(p-q^{vp}\right) \tag{44}$$

- Γ^{h-r} and S_1 could be identified by minimizing the error between left and right hand side of Equation (44) by using Equation (45) and Genetic Algorithms:

$$error=\sum_{i=1}^{K}\left[\left(\frac{Ln\left(\frac{\Delta q^{vp}}{\Delta t}\right)}{Ln\left(\Gamma^{h-r}\right)+S_1 Ln\left(p-q^{vp}\right)}-1\right)^2\right] \tag{45}$$

10.5. Calibration of Viscodamage PANDA Model using Uniaxial Constant Strain Rate Tests

10.5.1. Viscodamage constitutive relationship and its associated parameters

The viscoelastic-viscoplastic constitutive relationships are coupled with damage within the context of continuum damage mechanics using the damage density variable ϕ, such that:

$$\sigma_{ij}=\left(1-\phi\right)\bar{\sigma}_{ij} \tag{46}$$

where σ_{ij} is the stress tensor in the nominal configuration which is identical to the experimentally measured stresses while $\bar{\sigma}_{ij}$ is the true stress tensor in the undamaged configuration which is the resulting stress if the damage density ϕ is assumed to be zero. The evolution function for damage density is expressed as (*291*):

$$\dot{\phi}=\Gamma^{vd}\left(\frac{\bar{Y}}{Y_0}\right)^q\left(\varepsilon_{eff}\right)^k;\qquad \bar{Y}=\tau-\alpha I_1;\qquad \varepsilon_{eff}=\sqrt{\varepsilon_{ij}\varepsilon_{ij}} \tag{47}$$

where $\bar{Y}$ is the damage force and ε_{eff} is the total effective strain. The term Y_0 is the reference damage force which is used for dimensional consistency and can be assumed to be unity.

Table 8 lists the parameters associated with the viscodamage evolution function and their physical significance.

Table 8. List of viscodamage parameters that should be identified.

Parameter	Physical meaning
Γ^{vd}	Viscodamage fluidity parameter controlling the rate of damage evolution.
q	Stress sensitivity parameter. Controls the effect of stress level on damage evolution and growth.
k	Strain sensitivity parameter. Controls the effect of total strain level on damage evolution and growth.

10.5.2. Calculation of damage density during uniaxial constant strain rate test

The first step in calibrating the damage evolution function is to calculate the damage density variable during the uniaxial constant strain rate test. The constant strain rate test should be conducted at minimum of three strain rates at low temperatures (e.g. 5°C).

- Select the constant strain rate tests at a low temperature (5°C is recommended) where the viscoplastic strain can be neglected. The strain input for constant strain rate test can be expressed as:

$$\varepsilon(t) = Ct \tag{48}$$

where C is the strain rate.

- Calculate the induced stress in the undamaged configuration, such that:

$$\bar{\sigma}(t) = C\int_0^t E(\tau)\,d\tau \tag{49}$$

where $E(t)$ is the relaxation modulus which is known from the dynamic modulus test.

- Calculate the damage density using the calculated stress in the undamaged configuration and the experimentally measured stress, such that:

$$\phi(t) = 1 - \frac{\sigma(t)}{\bar{\sigma}(t)} \tag{50}$$

- Calculate the rate of the damage density using the calculated damage density, such that:

$$\dot{\phi} = \frac{\Delta\phi}{\Delta t} = \frac{\phi(t+\Delta t) - \phi(t)}{\Delta t} \tag{51}$$

10.5.3. Identification of q parameter

- Select four arbitrary strain levels.

- Plot $\bar{Y}/Y_0$ versus rate of the damage density at different strain rates for each selected strain level in logarithmic scale.
- Figure 8 schematically shows the procedure to select and plot $\bar{Y}/Y_0$ versus $\dot{\phi}$

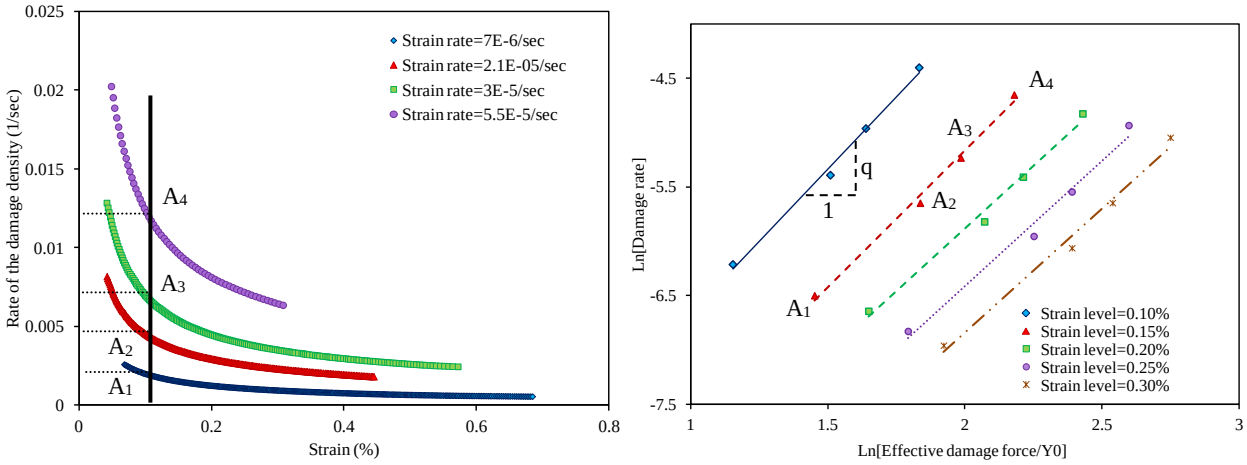

(a) (b)

Figure 8. Schematic presentation of: (a) Rate of the damage density versus the effective strain plotted at different strain rates for the uniaxial constant strain rate tests; (b) Plot of the damage density rate versus the normalized effective damage force which is used to identify q.

- Calculate the slope of the fitted lines in the $\bar{Y} / Y_0$ versus $\dot{\phi}$ plot at each strain level.
- The parameter q is the average of the measured slopes.

10.5.4. Identification of k parameter

- Select four arbitrary calculated stress levels at undamaged configuration, $\bar{\sigma}$.
- Calculate $\bar{Y} / Y_0$ for each selected stress level.
- Plot ε_{eff} versus rate of the damage density at different stress levels in logarithmic scale.
- Figure 9 schematically shows the procedure to select and plot ε_{eff} versus $\dot{\phi}$.

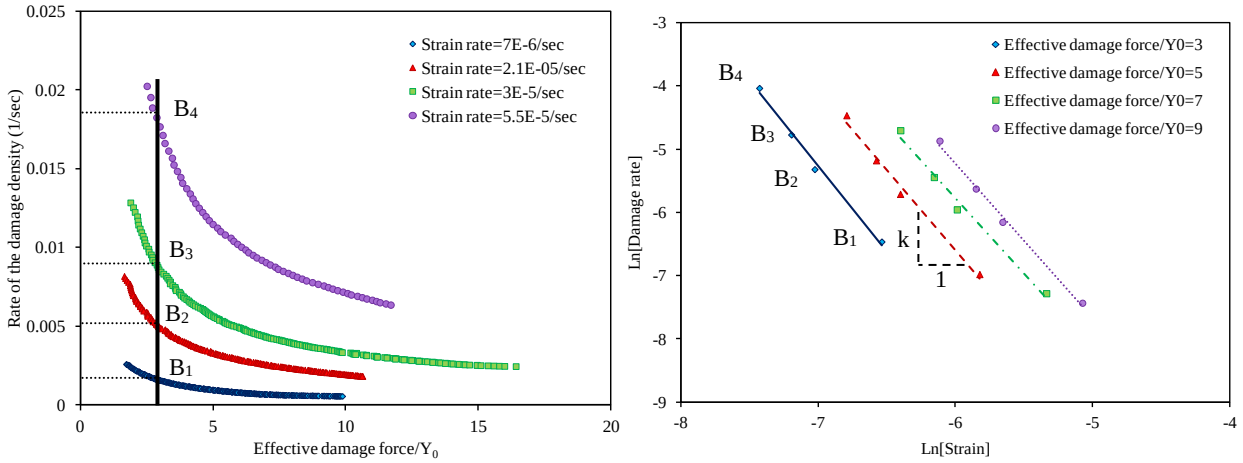

Figure 9. Schematic presentation of: (a) Rate of the damage density versus the dimensionless effective damage force (i.e. $\bar{Y} / Y_0$) plotted at different strain rates for the uniaxial constant strain rate tests; (b) Plot of the damage density rate versus the effective strain which will is used to identify k.

- Calculate the slope of the fitted lines in the ε_{eff} versus $\dot{\phi}$ plot at each strain level.
- The parameter k is the average of the measured slope.

10.5.5. Identification of Γ^{vd}

- Select the data points used to identify q and k.
- Calculate $\bar{Y} / Y_0$ and ε_{eff} for the selected data points.
- Calculate $qLn\left(\frac{\bar{Y}}{Y_0}\right)$ and $kLn\left(\varepsilon_{eff}\right)$ once q and k are identified.
- Record rate of the damage density for the selected data points.
- Calculate $Ln\left(\dot{\phi}\right) - qLn\left(\frac{\bar{Y}}{Y_0}\right) - kLn\left(\varepsilon_{eff}\right)$.
- Calculate Γ^{vd} for each data point as: $Ln\left(\Gamma^{vd}\right) = Ln\left(\dot{\phi}\right) - qLn\left(\frac{\bar{Y}}{Y_0}\right) - kLn\left(\varepsilon_{eff}\right)$.
- Identify the parameter Γ^{vd} by averaging the calculated Γ^{vd} for each data point.

11. KEYWORDS

Asphalt Mixtures, Performance, PANDA, Mechanical Damage, Viscoelastic, Viscoplastic, Hardening-Relaxation.

12. REFERENCES

Abu Al-Rub, R.K., Masad, E.A., Huang, C.W., 2009. Improving the sustainability of asphalt pavements through developing a predictive model with fundamental material properties. Southwest University Transportation Center, Texas Transportation Institute, College Station, TX, 1-45.

Bazzaz, M., Darabi, M. K., Little, D. N., & Garg, N., 2018. A straightforward procedure to characterize nonlinear viscoelastic response of asphalt concrete at high temperatures. *Transportation Research Record*.

Darabi, M.K., Abu Al-Rub, R.K., Masad, E.A., Little, D.N., 2012. A thermodynamic framework for constitutive modeling of time- and rate-dependent materials, part ii: Numerical aspects and application to asphalt concrete. International Journal of Plasticity 35, 67-99.

Darabi, M.K., Abu Al Rub, R.K., Masad, E., Huang, C.W., Little, D., 2012. A modified viscoplastic model to predict the permanent deformation of asphaltic materials under cyclic-compression loading at high temperatures. International Journal of Plasticity 35, 100-134.

Darabi, M. K., Al-Rub, R. K. A., Masad, E. A., & Little, D. N., 2013. Constitutive modeling of fatigue damage response of asphalt concrete materials with consideration of micro-damage healing. *International Journal of Solids and Structures*, *50*(19), 2901-2913.

Huang, C.W., 2008. Development and numerical implementation of nonlinear viscoelastic-viscoplastic model for asphalt materials. Ph.D. Dissertation, Texas A&M University.

Masad, E., Huang, C.W., Airey, G., Muliana, A., 2008. Nonlinear viscoelastic analysis of unaged and aged asphalt binders. Construction and Building Materials 22, 2170-2179.

Perzyna, P., 1971. Thermodynamic theory of viscoplastcity. Advances in Applied Mechanics 11, 313-354.

Rahmani, E., Darabi, M. K., Al-Rub, R. K. A., Kassem, E., Masad, E. A., & Little, D. N., 2013. Effect of confinement pressure on the nonlinear-viscoelastic response of asphalt concrete at high temperatures. *Construction and Building Materials*, *47*, 779-788.

Schapery, R.A., 1969. Further development of a thermodynamic constitutive theory: Stress formulation. Purdue University, Purdue Resarch Foundation, Lafayette, IN.